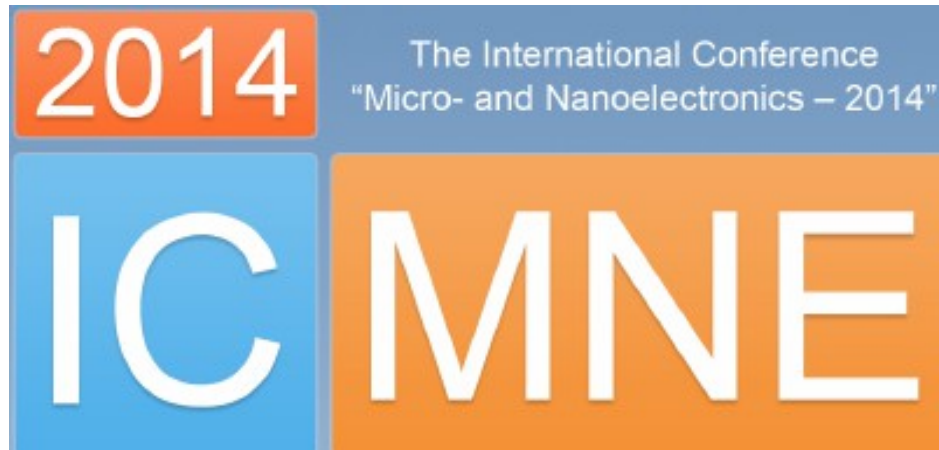


International Conference “Micro- and Nanoelectronics – 2014”



with the Extended Session



Quantum Informatics

Book of **ABSTRACTS**

October 6th – 10th, 2014
Moscow – Zvenigorod, Russia

Травление, напыление и выращивание микро и нано структур

**OXFORD
INSTRUMENTS**

Компания **Oxford Instruments Plasma Technology** является мировым лидером в области производства плазмохимического оборудования для модификации материалов, выращивания наноструктур и создания микроэлектронных и оптоэлектронных компонентов.



Плазменное травление и осаждение

Атомно-слоевое осаждение

Ионно-лучевое травление и осаждение

Выращивание наноструктур

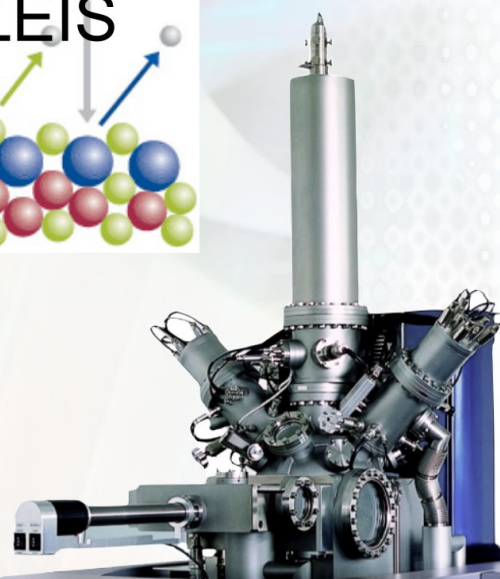
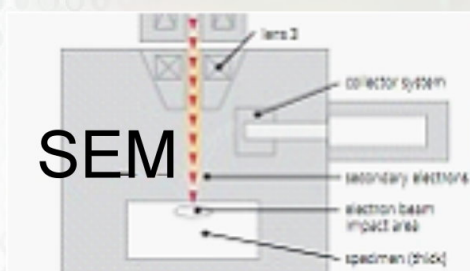
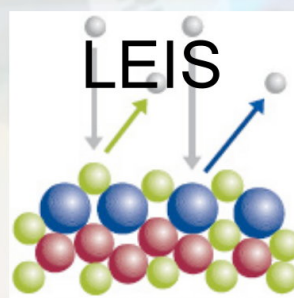
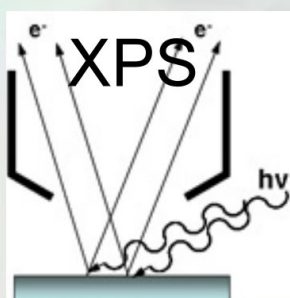
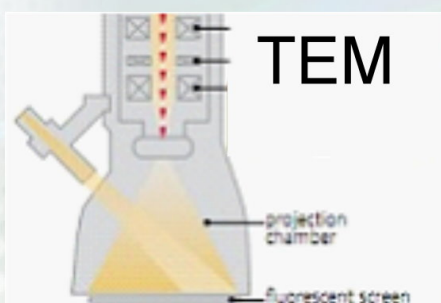
Гидридная эпитаксия

Магнетронное напыление

Анализ поверхности

При использовании одного метода невозможно получить всю необходимую информацию, однако, для решения определенных задач редко требуется применение всех доступных методов.

XPS, Auger, TOF SIMS, LEIS, UPS, SEM, TEM, EDX, EELS, FIB, EBSD....





НИКС КОМПЬЮТЕРЫ



БИЗНЕС, ОСНОВАННЫЙ НА НАУЧНОМ ПОДХОДЕ

**Спонсор конференций ICMNE2003, Qi2004,
ICMNE2005, 2007, 2009, 2012**

Год основания:.....1991

Профиль:.....компьютеры,
- комплектующие,
- программное обеспечение,
- бизнес-анализ

Учредители:.....выпускники МФТИ

Сотрудники:.....600 человек,
- из них 20% выпускников МФТИ и других
физико-математических вузов России

Годовой оборот:.....\$80млн

Сайт:.....www.nix.ru

- 150 тыс. уникальных посетителей в день

Компьютерный супермаркет НИКС в рамках собственного проекта NANOSOFT® занимается всесторонней поддержкой российской науки и образования, исследований в области квантовой информатики. На гранты нашей компании многие талантливые студенты, преподаватели и российские учёные смогли успешно развивать свою научную деятельность.

NANOSOFT.RU

ваш шанс на прорыв в будущее

Nanosoft® - собственная программа Компьютерного супермаркета НИКС по поддержке российских ученых, занимающихся теоретическими и экспериментальными исследованиями квантовых приборов и нанотехнологий.

<http://www.nanosoft.ru>, science@nix.ru

Анализаторы цепей НОВОГО ПОКОЛЕНИЯ от Rohde & Schwarz

Векторные анализаторы цепей R&S®ZNC / R&S®ZNB

R&S®ZNC: для пассивных компонентов, диапазон частот до 3 ГГц, двухпортовый прибор
R&S®ZNB: для компонентов со сложной структурой, приборы с 2 или 4 портами до 20 ГГц,
приборы с 2 портами до 40 ГГц

Высокие эксплуатационные характеристики

- Малое время измерения для обеспечения высокой производительности
- Динамический диапазон до 140 дБ — для фильтров с высоким коэффициентом подавления
- Возможность работы с высокими мощностями для измерения усилителей
- Широкий выбор методов калибровки для волноводных измерений и измерений на подложках

Убедительные практические свойства

- Долгие межкалибровочные интервалы за счет высокой долговременной стабильности
- Компактность, бесшумность работы, низкое энергопотребление
- Гибкость в модернизации благодаря модульной аппаратной части

www.rohde-schwarz.ru



Обновленный модельный ряд
планарного оборудования
SemiTEq



ОТ ЗАМЫСЛА
ДО ВОПЛОЩЕНИЯ

Закрытое акционерное общество
«Научное и технологическое оборудование»

STE ICP

Технологическая платформа нового поколения для проведения процессов плазмохимического травления и осаждения в индуктивно-связанной плазме



- Оптимальная конфигурация для прецизионного и глубокого травления полупроводников и диэлектриков
- Осаждение высококачественных диэлектриков с возможностью программирования начальных режимов техпроцесса

Новая универсальная система магнетронного напыления для осаждения многокомпонентных покрытий в вакууме на групповую партию пластин

STE MS



- Загрузка в одном процессе:
24 шт. – 60×48 мм с возможностью двустороннего напыления
34 шт. – 60×48 мм с односторонним напылением
- Прецизионный нагрев до 500°C и ионная очистка

ЗАО «НТО»

пр. Энгельса, 27 Санкт-Петербург, 194156, Россия.
Тел.: +7 812 601 06 05, Факс: +7 812 313 54 29
sales@semiteq.ru

ЗАО «Предприятие Остек»

Официальный дистрибьютор линейки планарного оборудования SemiTEq® в РФ и СНГ

www.semiteq.ru

TABLE OF CONTENTS

Monday, October, 6th	Special Session: S1-01 – S1-07
Tuesday, October, 7th	Invited Papers: L1-01 – L1-03 qL1-01 – qL1-04 Oral Papers: O1-01 – O1-25 q1-01 – q1-05
Wednesday, October, 8th	Invited Papers: L2-01 – L2-05 Oral Papers: O2-01 – O2-11 q2-01 – q2-09 Posters: P1-01 – P1-37
Thursday, October, 9th	Oral Papers: O3-01 – O3-17 q3-01 – q3-10 Posters: P2-01 – P2-39

How to search for necessary abstract?

Every Abstract has its own identification number (for instance, L1-04, O1-07, P2-28, and so on), which is printed at the page bottom. This number corresponds to the one in the *Conference Programme*. If you do not know the number of the paper, but know at least one of the authors it is possible to find the Abstract using the *Author Index* located in the end of the *Book of Abstracts*.

Как отыскать интересующие Вас тезисы доклада?

Каждый доклад имеет собственный идентификационный номер (например, L1-04, O1-07, P2-28 и т.д.), который указан внизу страницы. Этот номер совпадает с номером, присвоенным докладу в *Программе Конференции*. Если Вы не знаете номера доклада, но Вам известен хотя бы один из авторов, вы можете воспользоваться *Авторским Указателем*, расположенным в конце *Сборника Тезисов*.

Oxford Instruments Plasma Technology equipment for the micro- and nano-engineering of materials for semiconductor, optoelectronics, MEMS and other applications

A. Krynin

Technoinfo Limited, Moscow, kryninalex@technoinfo.ru

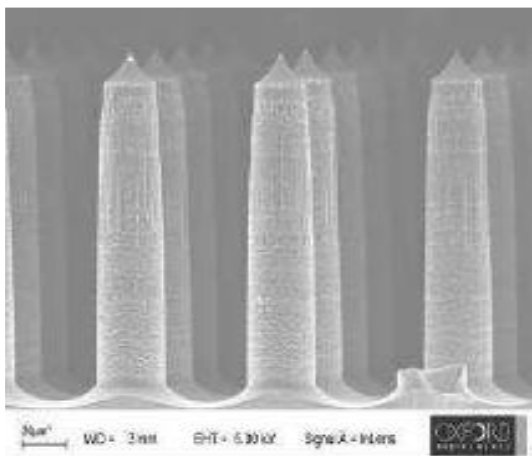
Oxford Instruments Plasma Technology (OIPT) provides a range of high performance, flexible tools to semiconductor and electronic processing customers in both R&D and production. Today the company offers equipment and technology for Plasma Etch and Deposition, Atomic Layer Deposition, Ion Beam Etch and Deposition, Nanoscale Growth and Hydride Vapour Phase Epitaxy. With a 30-year history of high performance tools production and process development, OIPT has great experience in this area and good worldwide reputation. More than 2.500 systems were installed around the world.

Oxford Instruments has a process library of over 6,000 recipes developed in our process laboratories. Our processes are backed by process guarantees for key parameters and repeatability such as rate and uniformity to ensure rapid start-up during installation. Oxford Instruments' process tools offer a powerful range of stand-alone and clusterable process modules to enable the widest range of applications: Plasma Etch (ICP, RIE, RIE/PE, DRIE), Plasma Deposition (PECVD and ICP CVD, ALD (PE & thermal), DLC, PVD).

ALD systems have next features: Plasma and thermal ALD in one tool, possibility to be clustered to other modules using hex handler with robot and 25 wafer cassette for 4", 6", or 8" wafers, 100% conformal coatings of up to 200mm wafers handling and pieces on carrier plate.

Nanoscale features can be formed by growth techniques ('bottom up') and etching ('top down'). The NanofabTM Systems are aimed to satisfy the nanotechnology market. Nanoscale growth processes encompass: Nanotubes/nanowires, Nanoscale thin films. Nanofab700 and Nanofab800Agile: can accommodate variable sample sizes up to 200 mm wafer with excellent temperature uniformity, can provide growth of nanotubes and nanowires with a flexible temperature range up to 700°C and 800°C respectively.

Oxford Instruments' Ion Beam technology offers unique abilities in etch and deposition. OIPT Ion Beam tools have next benefits: Etch and Deposition tools, Versatile tool for a wide range of applications, Flexible system configuration to match specific process applications, easy optimisation for repeatable process results. Next processes can be started: Ion Beam Etch (IBE), Reactive Ion Beam Etch (RIBE), Chemical Assisted Ion Beam Etch (CAIBE), Ion Beam Deposition (IBD), Reactive Ion Beam Deposition (RIBD).

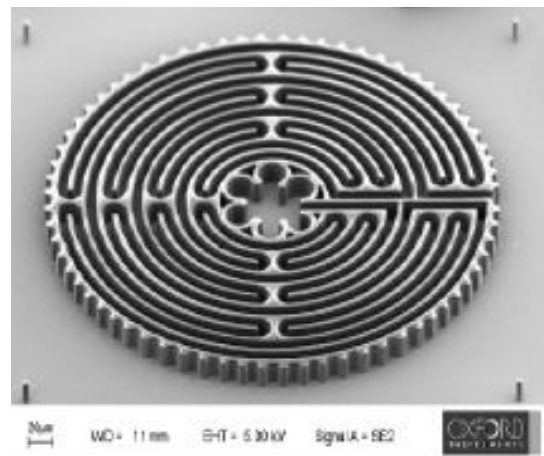


Left Image

Microneedles (Bosch-process) for Bio-medical application

Right Image

Micro-mould (Cryo etching) for Micromachines/Actuators



Application of ION-TOF equipment for microelectronics development and process control

V. Sudin

Technoinfo Limited, Moscow, sudin.vlad@technoinfo.ru

ION-TOF GmbH produces equipment on the base of ion optics and time of flight mass separation devices for both R&D and in-process monitoring. The company's general product line includes innovative instruments for surface analysis, like secondary ion mass-spectrometers (SIMS) and high-sensitivity low-energy ion scattering (HS LEIS). More than 200 hi-end installed systems and more than 30 years of experience allow company produce very high performance equipment and to solve a customer's problems successfully.

The most useful device is secondary ion mass-spectrometer TOF.SIMS 5. This product is the result of more than 25 years of investigations. The device gives the opportunity to analyze the surface of samples with unique sensitivity like 5×10^{-14} at/sm³ for As in silicone, reconstruct a depth profile for ion implantation and make a 3D vision of objects as a result of using separate etching ion column. Recent developments improve lateral resolution to less than 80 nm and mass resolution to high, than 18000 m/dm on ²⁹Si line. Powerful capabilities allow to use this device in many microelectronics applications like failure analysis, quality control and others.

High interest concerns the HS LEIS system named Qtac 100. It has extremely sensitive surface and provides elemental and structural characterization of the top atomic layer. This new generation instrument has been developed to include small spot analysis, surface imaging, and both static and dynamic depth profiling. Its unique surface sensitivity makes the Qtac the perfect tool to study surface processes. General application of the tool is quantitative analysis of the top atomic layer, but one more specific application is static depth profiling. This method give information about subsurface atoms and applicable for study of diffusion thru barriers and control ALD processes. Usage of the second high energy ion gun allows to construct depth profiles and to make a quantitative 3D analysis.

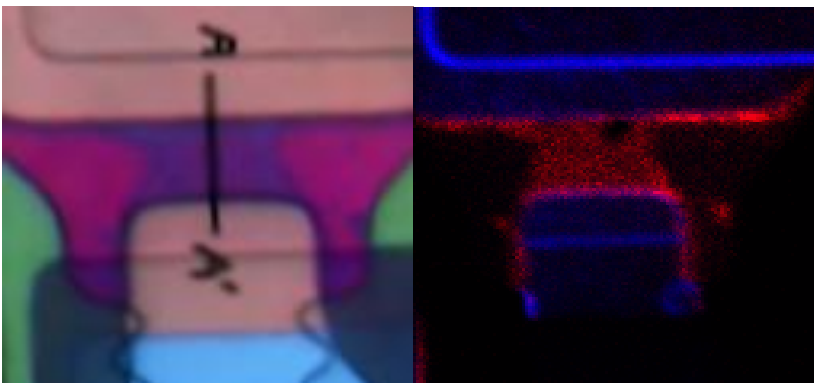


Image 1. Cerium contamination in thin film transistor, founded by TOF.SIMS 5.

Measurements of permittivity and permeability at radio frequencies. Matching active devices during radio modules design

E. Suchkov
Rohde&Schwarz Russia

Wide use of magnetic and dielectric materials in electronics and microelectronics causes need to measure according parameters. Quality and parameters of dielectrics used in capacitors, delay lines, substrates and fill of coaxial waveguides determinates quality and efficiency of designed and produced systems. Same could be told about magnetic materials used in transformers, phaseshifters, etc.

Rohde&Schwarz company provides systems to measure permittivity and permeability for radiofrequencies from megahertz to hundreds of gigahertz. Such systems are based on vector network analysers, supplied with coaxial probes, coaxial-waveguide adapters or other adapters to connect measurement equipment with tested sample. Calculating and interacting software is also included, which is made by companies makes according parts of systems. Such measurement methods are based on reflection and transmission coefficients measure, which are then used to calculate permittivity and permeability by NIST, Nicholson-Ross-Weir and other methods.



Pic.1. SPEAG probe with Rohde&Schwarz VNA for permittivity measurements

During radio modules design there is also tasks appear to match output impedance of active element (transistor) with next stages in module. Low impedance of transistors ($0,5 \div 2$ Ohm) is totally mismatched with 50Ohm circuits. Therefore, design of matching networks is significant part of modules design. To solve this problem Rohde&Schwarz and Focus Microwaves offer vector network analysers with impedance tuners. Such way one can measure radio parameters of future module with different impedances at the output of transistor.

Measurement systems designed by Rohde&Schwarz are used at Russian production lines and during research engineering.

1. <http://www.speag.com/products/dak/dielectric-measurements/>
2. <http://www.focus-microwaves.com/>

Hitachi HD-2700 STEM with automated Cs-corrector

E. Kremer^{1,2}

1. Interlab JSC, Moscow, Russia, kremer@interlab.ru

2. Hitachi High Technologies, Tokyo, Japan, web@nst.hitachi-hitec.com

Hitachi High-Technologies Corporation is presenting HD-2700, a scanning transmission electron microscope (STEM) equipped with a spherical aberration corrector developed by Hitachi High-Tech. The associated automatic aberration correction function facilitates the use of the corrector and significantly reduces the time needed for aberration correction.

In the fields ranging from R&D of advanced nano materials and semiconductor devices to quality control, there have been increased demands in recent years for improving spatial resolution and analytical performance for electron microscopes. Aberration correction provides a prominent solution to these demands. Hitachi High-Tech had previously commercialized electron microscopes equipped with spherical aberration correction capability, since then the continuous efforts concentrated on the concept of providing both high throughput and high performance benefited from aberration correction. The newly developed spherical aberration corrector by Hitachi High-Tech on the HD-2700 STEM realized this concept successfully.

The Hitachi-made spherical aberration corrector is software-controlled, the fully automatic aberration correction process can be executed simply by one mouse-click, user's pre-experience and intensive operation training for aberration correction are not required. Moreover, the time needed for high-order aberration correction is cut down to about 20% compared with other comparable Hitachi High-Tech instruments therefore dramatically improves the total throughput. For those experienced users, step-by-step involvement in the aberration correction process is also possible.

Along with the newly developed Hitachi spherical aberration corrector, the HD-2700 is also powered by another two well-known technologies of the Hitachi High-Tech-cold field-emission electron gun and high-resolution objective lens, both are included as standard components. The synergy of all these technologies guarantees routinely obtainable specified high spatial resolution as well as high-quality chemical analysis with high throughput. This latest HD-2700 model preserves secondary electron (SE) imaging, EDX elemental mapping and EELS mapping, all three done with atomic level resolution.

SemiTEq technological equipment set for micro- and nanoelectronics

S.I. Petrov¹, A.N. Alexeev¹, D.M. Krasovitsky², V.P. Chaly², V.V. Mamaev^{1,3}

1. *SemiTEq JSC, Saint-Petersburg, Russia, petrov@semiteq.ru*

2. *Svetlana-Rost JSC, Saint-Petersburg, Russia*

3. *State Polytechnical University, Saint-Petersburg, Russia*

Progress in modern microelectronics and nanoelectronics is directly related to the production of new materials and devices. This requires the simultaneous development of both technology and corresponding technological equipment. This primarily relates to growth methods and following wafer processing for fabrication of new types of devices.

SemiTEq is the Russian brand which covers wide range of HV and UHV equipment meeting all modern semiconductor technology requirements. State-of the art design of both molecular beam epitaxy systems (for growth of different material systems such as InAlGa_N, InAlGa_{As}, wideband A²B⁶ etc) and vacuum wafer processing equipment lines (for electron-beam and magnetron sputtering, thermal annealing, plasma etching and deposition etc) ensure high quality of epiwafer growth and its further processing under R&D and pilot production in the field of opto-, micro-, and nanoelectronics. These products are the base for fully equipped compact Nanolaboratory which intended for creating the wide range of semiconductor devices.

Complete set of Nanolab's technological equipment includes: compact MBE system STE75 in two configurations: for A³B⁵/A²B⁶ and A³N compounds; electron-beam evaporation system STE EB71; magnetron sputtering system with load lock chamber; plasma etching and plasma enhanced chemical vapour deposition system (PE & PECVD) with inductively coupled (ICP) and capacitive matched plasma sources; RTA and RTP systems; complex of required analytical tools; equipment for chemical process and photolithography; basic technology processes documentation; extensive modern training program, including video-training, 3D-visualization of technological route and specialized training software.

Equipment is oriented to R&D on substrates of 2 inches (Ø50.8 mm) or 3 inches (Ø76.2 mm), with the possible upgrade of equipment components to increase the maximum diameter of the substrates up to 100 mm. Systems are unified of substrate holders type. Systems technological reactors are equipped with viewports for maximum process visualization. Graphical interface of process control is realized to simplify the process of specialists training to perform various technological operations.

One of the main advantages for the design and production of equipment is the use of own technological experience in the SemiTEq Application lab. Basic technological processes are developed for each system to demonstrate equipment capabilities together with new processes which are developing for prospective directions.

Using of SemiTEq technological equipment set is shown in example of a closed cycle of basic technological operations for production of high-power field microwave transistors based on GaN and GaAs in the "Svetlana-Rost" JSC. Basic technological operations are shown: MBE growth of heterostructures, metal deposition of contacts using electron-beam evaporation system, thermal annealing of Ohmic contacts, mesa-isolation plasma-chemical etching and dielectric plasma deposition. The main problems during the technological route as well as ways to solve are discussed. In particular, ways to reduce the dislocation density in the active region of the transistor heterostructures based on GaN grown on the mismatched substrates are described in detail. Special attention is given to the uniformity and reproducibility both after some operations and regarding to the whole technological route.

New possibilities of scanning probe microscopy for studying the local properties of the samples

V.A. Bykov¹, S.M. Magonov², S.Y. Krasnoborodko¹

1. NT-MDT Co, Zelenograd, Moscow, Russia, E-mail: serg@ntmdt.ru

2. NT-MDT Development Inc., Tempe AZ USA, E-mail: info@ntmdt.us

Scanning probe microscopy as a family of characterization techniques applied for studies of materials at small scales has originated from tunneling microscopy. In STM current between a sharp tip and sample surface is employed for profiling atomic-scale surface topography and local variations of the partial electron density related to the electron transfer. A detection of local current became also one of features of atomic force microscopy with the latter having a large variety of other modes and techniques focused on local measurements of surface potential, dielectric response, capacity variations, piezoelectric phenomena, etc. Recent developments of these techniques and their applications to different materials realized with NT-MDT microscopes is the subject of this article: AFM-Based Electric Modes & Quantitative Analysis, Probing and Mapping of Electrostatic Force Response & Surface Potential (Kelvin Force Microscopy), Towards Local Quantitative Dielectric Measurements, Piezoresponse Force Studies.

Practically, scanning probe microscopes of all kinds, which are manufactured by NT-MDT under such platforms as TITANIUM, NTEGRA, SOLVER have the capabilities of current sensing, electric force microscopy, Kelvin force microscopy, piezo response measurements. Furthermore they are empowered by multi-frequency approaches, single and double pass procedures, as well as by broadband frequency detection.

The electric measurements are realized in the main AFM modes: contact modes and 2 oscillatory modes: resonant amplitude modulation and non-resonant Hybrid mode (1). The long-distance nature of electrostatic and magnetic forces can be utilized in electric force microscopy and magnetic force microscopy measurements in Hybrid mode. The non-resonance character of the probe oscillations allows the assignment of the probe deflections to the electrostatic and magnetic force. It is important that in these measurements the probe and sample are separated therefore there is no non-desirable cross-talk between the electrostatic and magnetic force response and mechanical tip-sample force interactions.

Progress in micromechanics manufacturing resulted in significant increase of the cantilever yield rate (to practically 100%) with repeatability of resonant characteristics at 10% level, thus preconditioning implementation of the concept of multi-probe cartridges for AFM. A cartridge of this type is a multi-probe contour-type sensor with 38 cantilevers. A cantilever to operate is selected by a control program using optical feedback. The cantilevers can be either of the same type or "colored" with predefined coverings and rigidities. A cartridge can be exchanged manually through a simple procedure. The cartridges operate in dedicated measuring heads, which are designed for integration in the latest instruments by the Company.

NTEGRA platform has been designed as the special base for the constantly developing options of Scanning Probe Microscopy that combines them with various other modern research methods. This platform allows to integrate of SPM and optical techniques such as confocal microscopy / luminescence / Raman scattering spectroscopy. Owing to the effect of giant amplification of Raman scattering (TERS – Tip Enhances Raman Scattering) it allows carrying out spectroscopy studies and obtaining images with resolution less than 50nm.

Development of modes for scanning spectroscopy combined with SPM in the instruments NTEGRA-SPECTRA and SPECTRUM provides new options of confocal laser luminescence spectroscopy and Raman spectroscopy as well as higher reliability of detection for TERS and high resolution magnetic resonance probe-optical spectroscopy. Probes with diamond nanocrystals containing N-V defects are capable to detect magnetic states as microscopic as single spins and so they are promising for studies of surface catalytic activity and for detection of free radicals, including applications in biology and medicine.

1 J. Alexander, S. Magonov, and M. Moeller. *JVST B* **27** (2), pp. 903-911, 2009.

CAMECA Magnetic Sector SIMS instruments for Semiconductor applications and Materials Sciences

E. Norman, P. Peres, A. Merkulov

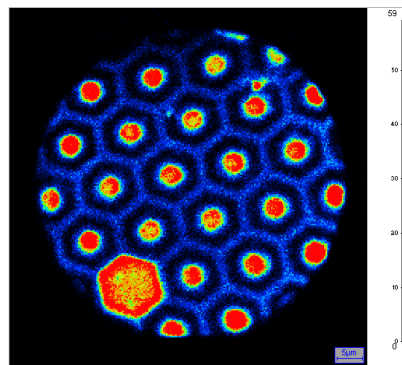
Cameca, 29 Quai des Grésillons, 92622 Gennevilliers Cedex, France

The advantages of **Magnetic Sector SIMS** are well established: extreme sensitivity (down to ppb detection limit), high depth resolution depth profiling (sub-nm), high lateral resolution elemental and isotope mapping (tens of nm), high precision (e.g. tenth per mil for isotope ratios) together with high throughput.

CAMECA has developed different high-end Magnetic Sector SIMS instruments in order to achieve the highest specific performance for different applications. This presentation will focus on two product line: IMS7f-Auto and IMS Wf/SC Ultra

The latest model **IMS 7f-Auto** is the most automated SIMS tool offering 2D and 3D imaging with sub- μm resolution, high sensitivity depth profiling including for atmospheric elements with benchmark throughput, high depth resolution, and precise isotope analysis.

The IMS7f-Auto has new **motorized storage chamber** allowing to keep under vacuum up to six sample holders. The holder exchange between the storage chamber and analysis chamber is fully motorized and computer controlled, allowing a set of analyses to be performed in **automated, unattended or remote mode on multiple sample holders**. This significantly improves the **throughput** of the tool, since up to 24 samples (assuming 4 samples per holder) can be analyzed in chained mode. It includes a **redesigned, in-line primary column** allowing easier operation and faster primary beam tuning. For high efficiency operation, auto-tuning routines have been specifically developed in order to increase the ease of use, and enhance the reproducibility of the instrument by minimizing operator-related biases.



2D Aluminum mapping in a honeycomb SiC structure at the sample surface. Image field of view: 60 μm in \varnothing .

The **IMS Wf/SC Ultra line** has been developed to meet the analytical requirements for advanced microelectronics developments.

Today, new processes used in semiconductor device manufacturing scale the junction depths below the 10nm range with profile steepness below 1 nanometer per decade. At such scale, the SIMS technique can be used to monitor in-depth distributions of dopants, provided that SIMS profiles can be measured with depth resolution better than nanometer per decade. In order to face with the analytical challenge, an Extremely Low Impact Energy approach has been developed. An extremely low impact energy (EXLIE) recipe offers sub-nm depth resolution, and under some conditions minimizes near surface (depth <5nm) artifacts associated with sputter and ion yields variation.

The IMS Wf has the capability to perform analysis on full patterned 300mm wafers with a high degree of automation.

Alternative Metals for Advanced Interconnects

C. Adelmann¹, L.G. Wen¹, A. Premkumar Peter¹, Y. K. Siew¹, S. Dutta^{1,2}, K. Croes¹, J. Swerts¹, M. Popovici¹, K. Sankaran¹, G. Pourtois^{1,3}, Sven Van Elshocht¹, J. Bömmels¹, and Zsolt Tókei¹

1. Imec, B-3001 Leuven, Belgium, email address: christoph.adelmann@imec.be

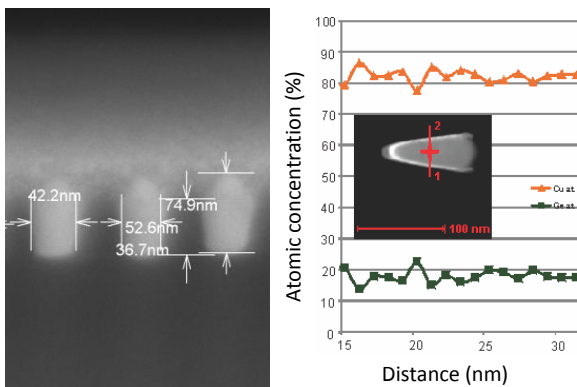
2. Department of Physics and Astronomy, KU Leuven, B-3001 Leuven, Belgium

3. PLASMANT, Department of Chemistry, University of Antwerp, 2610 Antwerpen, Belgium

The aggressive scaling of the dimension of CMOS transistors following Moore's law entails the scaling of the interconnects. In future technology nodes, the half pitch of local interconnects will reach values of 10 nm within the next decade. This will lead to several issues for the currently used Cu-based metallization. Small interconnect dimensions will lead to strong increase of the resistivity of Cu due to increasing grain boundary and surface scattering [1], as well as negatively impact electromigration [2]. Moreover, the scaling of Cu barriers to the required dimensions of the order of 1 nm and less [3] will become extremely challenging and alternative barrierless metallization technologies may become highly preferable.

These limitations may be overcome by replacing the conventional Cu- (or W-) based metallization by alternative metals with, ideally, better reliability and lower line resistance. Although it has been argued that *e.g.* Al may have lower resistivity in narrow interconnect lines than Cu [1], this has never been experimentally observed. Key criteria for the selection of alternative metals are their resistivity and reliability in small dimensions. However, for many metals, this is not yet well known. While this statement is already true for elemental metals, the situation is even worse for intermetallics and alloys where very little data are available even for binary systems. Since the integration of alternative metals in scaled interconnect lines is challenging, it is therefore important to find proxies for the expected behavior to select the most promising materials. We will discuss the usage of the bulk resistivity and the melting temperature as such proxies for the resistivity and electromigration of alternative metals in scaled interconnects and compare them to results of *ab initio* calculations. This allows us to obtain a shortlist of potential alternative metals for scaled interconnects and discuss the prospects of these materials for the different technology nodes.

Alternative metals, in particular more complex alloys or intermetallics will require alternative metallization schemes since the conventional bottom-up electroplating, as used for Cu-based metallization may be difficult to adapt to new materials. We will discuss metallization schemes for complex materials, such as transition metal germanides (Cu_3Ge , see Figure below, NiGe , CoGe_2) and silicides, as well as the usage of CoAl alloys as alternative metallization in scaled interconnects. In addition, the prospects of ALD for conformal metallization will be assessed.



Left: Cross-sectional SEM image of 40 nm half-pitch trench structures filled by Cu_3Ge . Right: Atomic concentration profile measured by EDS across a trench indicating that Cu_3Ge composition is uniform.

1. P. Kapur, J.P. McVittie, K.C. Saraswat, "Technology and Reliability Constrained Future Copper Interconnects—Part I: Resistance Modeling", *IEEE Trans. Electr. Dev.*, **4**, pp. 590–597, 2002.
2. C.K. Hu, D. Canaperi, S.T. Chen, L.M. Gignac, B. Herbst, S. Kaldor, M. Krishnan, E. Liniger, D.L. Rath, D. Restaino, R. Rosenberg, J. Rubino, S.-C. Seo, A. Simon, S. Smith, W.T. Tseng, "Effects of overlayers on electromigration reliability improvement for Cu/low K interconnects", *Proc. 42nd IEEE Annual Intl. Reliability Physics Symp.* pp. 222–228, 2004.
3. ITRS roadmap, 2011 edition, available at www.itrs.net.

Ultra low-k integration into sub 100 nm technologies: Challenges of plasma processing

S. Zimmermann^{1,*}, N. Lang², N. Köhler³, M. Haase³, M. Hübner², J. Röpcke, and S.E. Schulz

1. Fraunhofer ENAS, Department Back-end of Line, D-09126 Chemnitz, Germany

2. Leibnitz Institute for Plasma Science and Technologie, D-17489 Greifswald, Germany

3. Technische Universität Chemnitz, Center for Microtechnologies, D-09107 Chemnitz, Germany

* Corresponding author: Phone: (+49) 371 531 33671, e-Mail: sven.zimmermann@enas.fraunhofer.de

The integration of the porous ultra low-k material SiCOH results in special challenges concerning the further scaling of interconnects dimensions. Usually such materials will be structured using reactive ion etching (RIE) with fluorocarbon plasmas [1]. During such processes the SiCOH material will be damaged with the result of deep carbon depletion in combination with an undesirable increase in its k-value [2]. Especially in the sidewalls of the etched trenches, see Fig. 1, this effect causes a serious increase of the line to line capacitances and therewith an enhanced crosstalk noise. Consequently a lot of papers in the last years deal with the minimization of low-k and sidewall damage during RIE and plasma assisted photoresist removal. However, the exact physical and chemical damage mechanism are not completely understood up to now. In this work fluorocarbon based etch plasmas for porous SiCOH materials were analyzed using quantum cascade laser absorption spectroscopy (QCLAS). We successfully correlate sidewall damage, undercut and etch profile quality with the concentration of different species inside the etch plasma, e.g. CF₄, COF₂, SiF₄ and CF₂. The CF₂ radical, which shall be understood as main polymer precursor inside the process chamber, shows a direct influence on the sidewall damage.

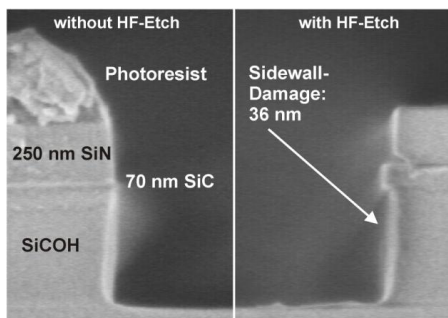


Fig. 1. Visualization of the sidewall damage after trench RIE using diluted HF solution

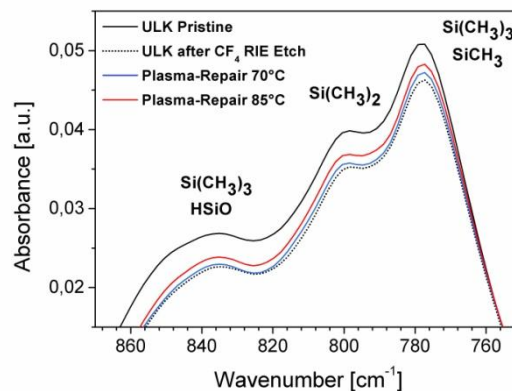


Fig. 2. SiMe_x absorption bands in the FTIR spectra for repair processes in organosilicon containing plasmas

Aside from the etch process, the repair of the damaged regions by the reintegration of methyl groups into the damaged areas is another way for sidewall damage reduction. In this work a completely new repair process was developed, which bases on the plasma fragmentation of liquid repair chemicals. The process uses the mechanism of silylation [3], which is provided by the reaction between polar silanol groups inside the damaged areas and fragments of the repair liquid. Different organosilicon compounds were injected into a downstream microwave plasma and fragmented to small parts with a high reactivity and enhanced diffusion behavior. Using this process the successful reintegration of carbon containing Si(CH₃)_x groups into the damaged material was realized, see Fig. 2. After process optimization a sidewall restoration effect of nearly 25 percent was reached.

- [1] S. Zimmermann et al.: Microelectronic Engineering, **87**, p. 337, 2010.
- [2] T. Tatsumi, Appl. Surf. Sci.: **253**, pp. 6716-6737, 2007.
- [3] N.R.E.N. Impens et. al.: Microporous and Mesoporous Mater. **28**, p. 217, 1999.

NEMS/MEMS generators, thermoelectric devices, and pumps

L. Montes

Grenoble INP/PHELM/IMEP-LAHC, Minatec, Grenoble, France

Ultimate communication rates of phase-insensitive quantum channels

A.S. Holevo

Steklov Mathematical Institute, Moscow, Russia

This talk reports recent progress in the solution of a long-standing problem in Quantum Communications presented in [1].

1. V. Giovannetti, R. Garcia-Patron, N.J. Cerf, and A.S. Holevo, DOI:10.1038/NPHOTON.2014.216.

Conception of quantum hashing and its possible applications

F. Ablayev, M. Ablayev

Kazan Federal University, Kazan, Russia, E-mail address fablayev@gmail.com, mablayev@gmail.com

Quantum computing is inherently a very mathematical subject, and the discussions of how quantum computers can be more efficient than classical computers in breaking encryption algorithms started since Shor invented his famous quantum algorithm. The answer of the cryptography community is "Post-quantum cryptography", which refers to research on problems (usually public-key cryptosystems) that are no more efficiently breakable using quantum computers than by classical computer architectures. Currently post-quantum cryptography includes several approaches, in particular, hash-based signature schemes such as Lamport signatures and Merkle signature schemes.

Hashing itself is an important basic concept for the organization transformation and reliable transmission of information. The concept known as " ε -universal hashing" was invented by Carter and Wegman [1] in 1979. In 1994 a relationship was discovered between ε -universal hash families and error-correcting codes [2]. In [3] Wigderson characterizes ε -universal hashing as being a tool which "should belong to the fundamental bag of tricks of every computer scientist".

Gottesman and Chuang proposed a quantum digital system [4], based on quantum mechanics. Their results are based on quantum a fingerprinting technique and add "quantum direction" for post-quantum cryptography. Gavinsky and Ito [5] viewed quantum fingerprints as cryptographic primitives.

In [6, 7] we considered quantum fingerprinting as a construction for binary hash functions and introduced a non-binary hash function. For more introductory information we refer to [6].

In this work we define the concept of a quantum hash generator and offer a design, which allows one to build different quantum hash functions. The construction is based on the composition of classical ε -universal hash family with a given family of functions - quantum hash generator.

The construction proposed combines the properties of robust presentation of information by classical error-correcting codes together with the possibility of highly compressed presentation of information by quantum systems.

In particularly, using the relationship between ε -universal hash families and error-correcting codes, we presented quantum hash function based on Reed-Solomon code, and we proved that this construction is optimal in the sense of number of qubits needed for the construction. Next, using the relationship between ε -universal hash families and Freivalds' fingerprinting schemas we present an explicit quantum hash function and prove that this construction is optimal with respect to of number of qubits needed for the construction.

1. J. Carter, M. Wegman. *Universal Classes of Hash Functions*. J. Computer and System Sciences **18**, 143-154, 1979.
2. J. Bierbrauer, T. Johansson, G. Kabatianskii, B. Smeets. *On Families of Hash Functions via Geometric Codes and Concatenation*. Advances in Cryptology — CRYPTO' 93, Lecture Notes in Computer Science Volume 773, pp 331-342, 1994.
3. A. Wigderson, *Lectures on the Fusion Method and Derandomization*. Technical Report SOCS-95. 2, School of Computer Science, McGill University (file /pub/tech-reports/library/reports/95/TR95.2.ps.gz at the anonymousftpsiteftp.cs.mcgill.ca) 1995.
4. D. Gottesman, I. Chuang. *Quantum digital signatures*, <http://arxiv.org/abs/quant-ph/0105032>, 2001.
5. D. Gavinsky, T. Ito. *Quantum fingerprints that keep secrets*. Quantum Information and Computation Volume 13 Issue 7-8, 583—606, 2013.
6. F. Ablayev, A. Vasiliev. *Quantum Hashing*, 2013, arXiv:1310.4922 [quant-ph], 2013.
7. F. Ablayev, A. Vasiliev. *Cryptographic quantum hashing*, Laser Physics Letters, **11**, p. 025202, 2014.

Multi-qubit quantum random access memory

E.S. Moiseev¹, and S.A. Moiseev^{2,3}

1. *Institute for Quantum Science and Technology, University of Calgary, Canada,*

2. *Quantum Center, Kazan National Research Technical University, Russia,*

3. *Kazan E.L. Zavoisky Physical-Technical Institute of KSC RAS, Russia*

e-mail: samoi@yandex.ru

We propose protocol for quantum random access memory (QRAM) based on the coupled multi-qubit photon echo quantum memory and three-level atom situated in two interacted QED cavities. We have found the conditions for deterministic quantum control of the storage (retrieval) of single photon qubits by using the quantum transport via three-level atom. Based on this finding we have also demonstrated the quantum addressing in the QRAM scheme by using the photonic time bin state for control of the three-level atom. Finally we have discussed important advantages of the proposed QRAM scheme in terms of the possibility to work with multi-qubit states and its practical realized with current quantum technologies in optical and microwave domain.

Experimental adaptive Bayesian tomography: From qubits towards ququarts

K.S. Kravtsov^{1,2}, I.V. Radchenko^{1,2}, S.S. Straupe², G.I. Struchalin², and S.P. Kulik²

1. A.M. Prokhorov General Physics Institute, Moscow, Russia.

2. Faculty of Physics, M.V. Lomonosov Moscow State University, Moscow, Russia.

We discuss an experimental realization of an adaptive quantum state tomography protocol. The method we suggested and tested takes advantage of a Bayesian approach to statistical inference and is naturally tailored for adaptive strategies. For pure states we observe close to $1/N$ scaling of infidelity with overall number of registered events N , while best non-adaptive protocols allow for $1/\sqrt{N}$ scaling only. This is the theoretical limit for any tomographic protocol, and further improvement may only affect pre-factors in this power law. Also we consider particular strategies of the state reconstruction based on adequate and inadequate models and compare their scaling.

Experiments have been performed for polarization qubits and ququarts, but the approach is readily adapted to any dimension. Our method does not take into account systematic errors caused, for example, by inaccuracies in retardant plates rotation. However for the reached values of infidelities of on the order of 10^{-4} – 10^{-3} we did not observe any deviations from expected behavior and were not able to identify the influence of systematic errors.

DC Magnetron Sputtered Silicon Thin Films on Dielectric Substrates

D. Mitin, A. Markin, A. Serdobintsev, S. Venig
Chernyshevsky Saratov State University, Saratov, Russia, mitindm@mail.ru

Scientific and technical progress is inconceivable without electronics. Intensive development of electronics is connected with the appearance of new various semiconductor devices and integrated microcircuits which find wide application in IT equipment, automatics, measuring techniques, medicine, biology etc. Therefore synthesis and investigation of silicon thin films is actual task.

As it is known, synthesis of silicon thin films on nonconductive substrates is a difficult task. In this regard the special DC magnetron sputtering system for synthesis of silicon thin films has been developed.

Silicon thin films have been synthesized by DC magnetron sputtering method with following parameters: discharge current – 100 mA, sputtering time – 5-20 min., synthesis voltage range $\approx 350\div 500$ V. Glass, glass-ceramics, Al_2O_3 and single crystal Si plates were used as substrates. Pressure of gas in working chamber (argon) which changed ranging from $7\cdot 10^{-5}$ to 10^{-3} Torr was the varied parameter.

Synthesized silicon films were subjected to a number of researches for study of different properties. Atomic-force microscopy was used for study of surface morphology; the profilometer was used for study of films deposition rate, research of current-voltage characteristics allowed to define conductivity of films [1]. X-ray diffraction method and the Raman spectroscopy were carried out for determination of crystalline structure of the films.

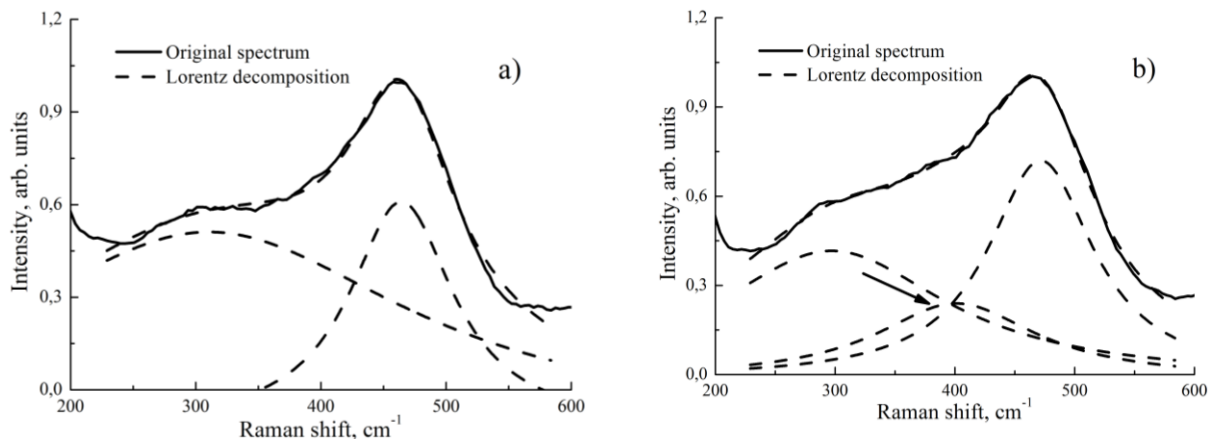


Fig. 1 Raman spectra of silicon thin films synthesized at pressure of 10^{-3} Torr (a) and $7\cdot 10^{-5}$ Torr (b)

Raman spectroscopy is one of the well-known techniques allowing to distinguish different phases in crystalline structure of silicon thin films. Raman spectra of silicon thin films synthesized at different pressure are presented on Fig. 1. The difference in profiles of amorphous silicon spectra in area from 200 to 480 cm^{-1} shows difference between samples of amorphous silicon films. Lorentz decomposition of initial spectra was done for more detailed analysis. It was found that 400 cm^{-1} peak is present at spectrum at pressure of $7\cdot 10^{-5}$ Torr and no peak in this region was detected for 10^{-3} Torr sample. It can be explained by a bigger degree of crystallinity of film deposited at lower pressure.

Now using of polycrystalline and crystalline silicon on dielectric substrates is of great interest. Especially, the poly-Si can be used in high resolution and integrated active-matrix liquid-crystal displays and active-matrix organic light-emitting diodes because of its high mobility compared to hydrogenated amorphous silicon [2]. In this connection a further stage of work is aimed to crystallization of amorphous silicon thin films.

This study was supported in part by the Russian Foundation for Basic Research, project no. 14-02-31089.

1. D.M. Mitin, A.A. Serdobintsev. "Properties of silicon films grown under different pressures in a plasma-forming system". *Semiconductors*, **47**, pp. 1264-1266, 2013.
2. S.Y. Yoon, S.J. Park, K.H. Kim, J. Jang "Metal-induced crystallization of amorphous silicon". *Thin Solid Films*, **383**, pp. 34-38, 2001.

Reversible and non-reversible changes in nanostructured Si in humid atmosphere

V. Zhigalov, O. Pyatlova, S. Timoshenkov, S. Gavrilov

National Research University of Electronic Technology (MIET), Zelenograd, Moscow, Russia

E-mail: zhigalov@gmail.com

Silicon based nanostructures are actively investigated due to its original properties in many application areas, in particular in cold emitters. It is known that air humidity affects work function (ϕ) of nanostructured Si, due to sorption of the H₂O by the surface [1]. Objective of our investigation was to research the work function changes of nanostructured Si in humid atmosphere in long-time (month) and short-time scale and investigate the mechanisms leading to these changes.

Two types of nanostructured layers: porous and nanowires arrays were prepared on the double side polished silicon wafers (boron doped, 1 Ohm-cm). Porous Si was prepared by anode etching process in solutions contained HF and C₂H₅OH with current density $j = 7 \text{ mA/cm}^2$. Silicon nanowires arrays were prepared by metal-assisted chemical etching with Ag thin films as catalyst in solutions contained HF and H₂O₂. The analysis of the microstructure of the samples was performed by scanning electron microscopy (SEM).

Samples were exposed to the air with 100%, 0% humidity (H) in exsiccator and ~50% humidity in laboratory. The value ϕ of samples was measured by static capacitor method with ionizing gap. Long-term curves of ϕ was recorded at 100% humidity, also short-term dynamics of ϕ by the rapid humidity changes was investigated.

Two components in dynamics of ϕ were found. The first component is reversible and appears as anti-correlation of ϕ and H (Fig. 1). The second component is non-reversible and appears as long-term descending trend of ϕ (0.1 eV per month). This component also appears as changes in transition curve of ϕ by rapid H changes.

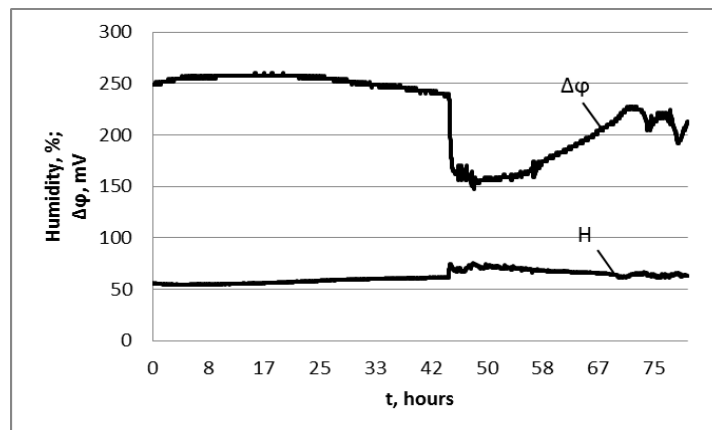


Figure 1. Work function changes ($\Delta\phi$) anti-correlate with humidity (H) ($r_{\Delta\phi H} = -0.94$).

Fourier transform infrared transmission (FT-IR) spectra of samples were recorded for studying mechanisms of ϕ changes. Non-reversible changes of FT-IR spectra of both samples: porous Si and silicon nanowires were observed. Peak intensity in the range 1050-1100 cm^{-1} (Si-O binding) was increased as samples were exposed to the humid air, what is in good accordance to [2]. Dynamics of non-reversible processes in humid air was estimated. Non-reversible aging of samples due to chemisorption with oxidizing of surface starts from first days even in 50% humidity atmosphere. As FT-IR spectra show, in 100% humidity aging of samples is finished during one month.

Effect of correlation between ϕ and H has perspective to use in the new type of humidity sensors.

1. S.N. Novikov et al. "Investigating impact of nanorelief of Si surface and technological conditions of holding Si-wafers on the state of sorbed humid media". Izv. Vuzov. Electronica, **2**, pp. 22-30. 2014 (in Russian).
2. T. Maruyama, S. Ohtani "Photoluminescence of porous silicon exposed to ambient air". Applied Physics Letters, **65** (11), pp. 1346-1348, 1994.

High-temperature surface morphologies of Ge layers on Si

A.A. ShklyaeV

Rzhanov Institute of Semiconductor Physics SB RAS, Novosibirsk, 630090, Russia, E-mail: shklyaeV@isp.nsc.ru

Multiple component structures, which contain inhomogeneous strain distributions, may have a tendency to phase separation depending on the strain relaxation mechanism. The phase separation is the dominating effect in the formation of Ge layers on Si surfaces. It commonly consists in the segregation of Ge and SiGe into three-dimensional islands during Ge or SiGe depositions on Si substrates. The Ge layer growth on Si is usually studied for thicknesses up to several nanometers. The thicker Ge layers have a complicated surface relief of the nanometer scale which makes difficult its imaging with scanning probe techniques. The other fields that appear worthy of investigations are the growth of Ge layers on Si or their annealing at temperatures above 500 °C. This arises from the fact that high temperatures initiate radical Ge layer modification due to the simultaneous action of several physical processes including Ge-Si intermixing, introduction of misfit dislocations and their motion, and significant mass transfer caused by the strain relaxation and by the surface energy minimization.

We use scanning tunneling microscopy and scanning electron microscopy (SEM) to study the surface morphologies obtained by the growth or by post-growth annealing at temperatures above 700 °C of Ge layers with thickness up to 100 nm on pure and on oxidized Si surfaces. The Ge layers were grown using a molecular beam epitaxy technique. The experimental data for the relatively thick Ge layers grown at lower temperatures are published in [1, 2].

The phase separation, which is usually described by the spinodal decomposition theory, is considered by us from the view-point of microscopic factors. The phase separation occurs by means of extensive transformation of the grown Ge layer with the surface covered with relatively low-sloped facets to islands and continuous ridges with steep facets under annealing at 700-850 °C. In the case of Si(111) substrates, the annealing also forms atomically flat areas between the islands and ridges with (5×5) reconstruction indicative of Ge wetting layers on Si(111). The dominating strain relaxation mechanism is associated with Ge amount reduction at the Ge/Si interface. This leads to the surface morphology with the aspect ratio up to about 0.41 and, hence, to the increase in surface energy. The role of surface energy minimization, being nonessential in the phase separation, consists in the formation of energetically preferable facets on sidewalls of ridges and in their configuration.

Growth and annealing of Ge layers on Si at high temperatures provide the formation of different surface morphologies such as island arrays, nets of continuous ridges, patterns of re-crystallization, and atomically smooth continuous thin films. Ge layers on Si with such surface morphologies are interesting for the single-crystal graphene growth, as well as a basis for Ge lasers and new Ge/Si hetero- and nanostructure fabrication.

1. A.A. ShklyaeV, K.N. Romanyuk, and A.V. Latyshev, *JSEMAT*, **3**, pp. 195-204, 2013.
2. A.A. ShklyaeV, K.N. Romanyuk, and S.S. Kosolobov, *Surf. Sci.*, **625**, pp. 50-56, 2014.

Investigation of the two-dimensional electron gas optic excitation in nanoheterostructures InAlAs/InGaAs/InAlAs

D.V. Lavrukhin, S.S. Pushkarev, V.S. Lopotov, A.N. Aleshin, G.B. Galiev
 Institute of Ultrahigh Frequency Semiconductor Electronics, RAS, 117105, Moscow, Russia

Research of charge carrier recombination in quantum heterostructures, on the one hand, is fundamentally interesting, and, on the other hand, is profitable for perspective semiconductor materials development. Epitaxially grown high electron mobility transistor (HEMT) heterostructures (further referred to as “samples”) containing 10–20 nm quantum well $\text{In}_{0.7}\text{Al}_{0.3}\text{As}/\text{In}_{0.7}\text{Ga}_{0.3}\text{As}/\text{In}_{0.7}\text{Al}_{0.3}\text{As}$ with two-dimensional electron gas are considered in present work.

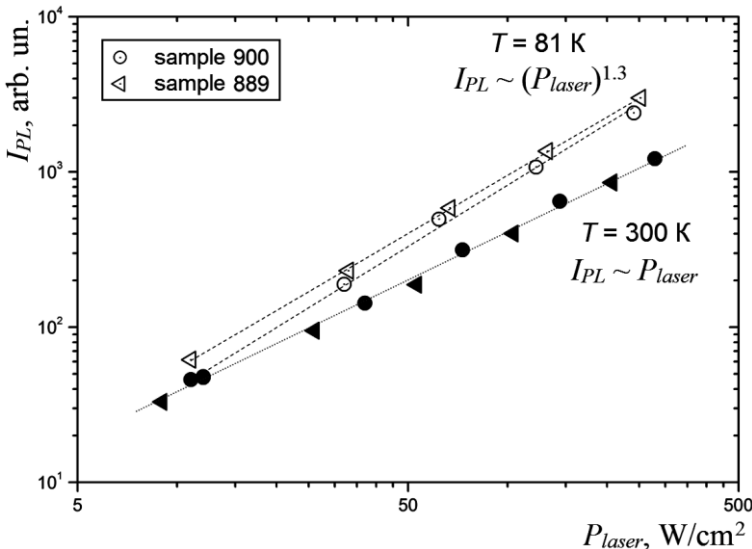
Hall electron mobility and two-dimensional electron density in samples were measured by means of the Hall effect at room temperature and liquid nitrogen temperature (77 K). The experimental setup includes high-power light emitting diode with photon energy 2.16 eV (green) to irradiate samples. 2D electron density appears to increase under illumination and at $T = 77$ K the augmentation is essentially larger than at room temperature. Measured values for two samples involved are shown in the table 1. At $T = 77$ K, after light emitting diode was turned off, the increased electron density gradually dropped down to the initial “dark” value during several tens of seconds. However, at room temperature the electron disturbance vanished practically immediately. It means that in samples under chilling the recombination of photoexcited electrons and holes is significantly suppressed.

Table 1. Hall electron mobility μ_e , 2D electron concentration n_s , and optic electron excitement Δn_s .

Sample	$\mu_e, \text{cm}^2/(\text{V}\cdot\text{s})$				$n_s, 10^{12} \text{cm}^{-2}$			
	300 K		77 K		300 K		77 K	
	darkness	light	darkness	light	darkness	light	darkness	light
830	11600	11400	40300	40600	1.72	1.74	1.65	2.16
842	6100	6300	12800	14600	1.98	2.01	1.95	2.38

To get more information about recombination mechanisms, HEMT samples also were investigated by means of photoluminescence (PL) spectroscopy in optical cryostat at room temperature and at $T = 81$ K. The radiation of He-Ne laser with photon energy 1.96 eV was used for charge carriers optical excitation. Radiation power density P_{laser} on a sample surface varied within the range of 40–480 W/cm^2 with the help of neutral filters set.

PL signal at the photon energy range 0.6–0.8 eV was related to the emission from quantum well. PL intensity integrated in this range I_{PL} (proportional to count of emitted photons) and laser radiation power



P_{laser} are found to be connected by the empirical relationship

$$I_{PL} \sim (P_{laser})^\alpha,$$

where $\alpha = 1$ at room temperature and $\alpha = 1.3$ at $T = 81$ K as shown in the fig. 1. We can conclude that $\alpha = 1$ correspond to low electron gas excitement, and in chilled samples due to suppressed non-radiative recombination the disturbance of charge carrier concentration can't be considered as low.

This work is supported by the Ministry of Education and Science of the Russian Federation under contract No 14.604.21.0003 (unique identifier RFMEFI57614X0009).

Fig. 1. Relation between laser radiation power P_{laser} and integrated PL intensity I_{PL}

Low dislocation density and high mobility GaN based HEMT heterostructures grown by plasma-assisted and high temperature ammonia MBE

S.I. Petrov¹, A.N. Alexeev¹, D.M. Krasovitsky², V.P. Chaly², V.V. Mamaev^{1,3}

1. *SemiTEq JSC, Saint-Petersburg, Russia, petrov@semiteq.ru.*

2. *Svetlana-Rost JSC, Saint-Petersburg, Russia*

3. *State Polytechnical University, Saint-Petersburg, Russia.*

One of the main problems in manufacturing GaN-based devices up to date is the lack of low cost lattice-matched substrates. Growth of III-Nitrides on mismatched substrates using different buffer layers usually yields high dislocation density, in the range of 10^9 - 10^{10} cm⁻² for MBE and 10^7 cm⁻² for MOCVD using ELOG, which affect the device quality and reliability. Moreover, typical growth temperatures in MBE are much lower as compared with MOCVD. It leads to insufficient surface mobility of adatoms, worse coalescence of nucleation blocks, and, as a result, high dislocation density which limits carrier mobility. Typical values of room temperature electron mobility in GaN grown on sapphire are in the range 250-350 cm²/V's for MBE and 500-700 cm²/V's for MOCVD. On the other hand, MBE has several advantages: in-situ RHEED monitoring, sharper heterojunctions, higher purity etc. At present time, an increasing number of researchers choose plasma-assisted (PA) MBE as it is simpler in service and has its own benefits: possibility of low-temperature growth and absence of hydrogen on the growing surface. However unlike to ammonia MBE, this method does not allow noticeable increase of the growth temperature, which usually improves the material quality.

In this paper we present the results of employing both types of MBE (plasma-assisted and ammonia), obtained in STE3N MBE System (SemiTEq). It is shown that the use of high-temperature buffer layers AlN/AlGa_xN grown by NH₃-MBE at extremely high temperatures (up to 1150 °C) allows one to improve drastically GaN structural quality. The dislocation density in GaN grown by NH₃-MBE or PA-MBE on such buffer layer was reduced down to $(9-10) \times 10^8$ cm⁻² that resulted in substantial increase in electron mobility up to 600-650 cm²/V's in a 1.5-μm-thick GaN:Si ($n = (3-5) \times 10^{16}$ cm⁻³) [1]. This result is comparable with a good quality MOCVD GaN and several times better than in conventional MBE. Importantly, growth of AlN at 1150 °C is difficult to realize in PA-MBE since Al-rich mode is necessary for 2D-growth, while desorption of Al becomes significant at $T > 900$ °C.

Employing such a GaN layer in a double heterostructure (DH) with the cap Al_xGa_{1-x}N barrier layer ($x = 0.25-0.4$) allowed us to vary the electron sheet density and mobility in a two dimensional electron gas (2DEG) in the range of $(1.0-1.8) \times 10^{13}$ cm⁻² and 1300-1700 cm²/V's, respectively, providing control of a 2DEG channel sheet resistance in the range of 230-400 Ω/□.

Application of this technology and DH design for structures grown on SiC substrates enabled one to manufacture a DHFET with a gate length of 0.5 μm for 0.03-4.0 GHz extra-broadband power amplifiers having $P_{out} = 2.5$ W, gain 17-25 dB, and efficiency 30%. During aging tests all the devices have shown reliable operation for more than 3500 hours under 85 °C. These device parameters confirm the high quality of the heterostructure and chosen technological approaches.

On the other hand, unlike the NH₃-MBE which is difficult to use at $T < 500$ °C (because of low decomposition efficiency of ammonia), PA MBE growth is very effective at low temperatures, for example for InAlN layers lattice-matched to GaN. However, the results of the growth of InAlN lattice-matched to GaN by NH₃-MBE at extremely high flux of ammonia were published recently [2]. In this paper we show the results of growth of high quality GaN/InAlN heterostructures (electron sheet density and mobility in the range $(2.2-2.4) \times 10^{13}$ cm⁻² and 1200-1300 cm²/V's, respectively) using both PA-MBE and NH₃-MBE.

1. Petrov, S. I., et al. "Growth of high quality III-N heterostructures using specialized MBE system." *Physica Status Solidi (c)*, **9**, pp. 562-563, 2012.

2. Wong, Man Hoi, et al. "Molecular beam epitaxy of InAlN lattice-matched to GaN with homogeneous composition using ammonia as nitrogen source." *Applied Physics Letters*, **100**, pp. 072107, 2012.

Electron transport and magnetic properties of ferromagnetic-antiferromagnetic planar junctions

A. Chernikh, L. Fomin, I. Malikov, V. Vinnichenko, and G. Mikhailov

Institute of Microelectronics Technology and High Purity Materials RAS, Chernogolovka, Russia, E-mail: mikhailo@iptm.ru

It is well known that spin polarized current is often used for switching of magnetic junctions consisted of ferromagnetic contacts of definite magnetization. Unfortunately, a switching demands the current of high enough density that restrict further developing. One of the reasons is in application of ferromagnetic metals (FM) that possess nonzero total magnetization. In this connection, application of antiferromagnetic metals (AFM) with, as it is known, zero total magnetization may have some advantages. However, for a long time AFMs are only used to fix magnetization of FM layer in magnetoelectronics through by exchange interaction at FM-AFM interface resulted also in exchange bias of FM magnetization reversal.

Only recently [1], it was experimentally found that an AFM layer may serve also as an active element in FM-AFM/MgO/Ta junction, in which the AFM magnetic state directly effects on the tunneling magnetoresistance termed a tunneling anisotropic magnetoresistance. Modification of the FM magnetization coupled at FM-AFM interface with an AFM magnetic state causes the violation of spatial distribution of AFM magnetic sublattices because of the effect of exchange spring. Due to spin-orbit interaction it also results in modification of the wave-function spatial part of electrons participating in tunneling. These first results show that a new alternative based on application of AFMs as an active elements in magnetoelectronics may appear [2]. At the same time, theoretical results [3,4] predicted that AFM layers under spin-polarized current incline their magnetic sublattices at the current density lower than those for FM layer switching. This motivates more deep both investigation of FM-AFM junction under current state and developing of the methods of their fabrication.

The investigation was provided of FM-AFM (Fe-FeMn) junctions that fabricated on a- or r-plane single-crystalline sapphire. The magnetic junction was a magnetic meta-material, consisted of continuous FeMn layer of 30 nm thickness with imbedded Fe inlands of 15 nm height and 10-s nm in a diameter. The junction was prepared as a layered structure, in which the first layer of nonpercolated Fe-inlands is covered by the second continuous FeMn layer. It was found that for each definite thickness of the first layer there is some minimal growth temperature termed percolating temperature, at which isolated Fe-inlands grow. The first layer grown at the percolating temperature or at higher temperature is not electrically conductive. A percolating temperature logarithmically depends on the layer thickness and increases with it.

The magnetoresistance of FM-AFM junction shaped as a planar bridge was investigated. It is sensitive to the current density flowing through the bridge that explained by the influence of AFM magnetic state modification due to flowing current. The spins of conductive electrons passing the Fe-inlands become polarized along inlands magnetization. These spin-polarized electrons after entering the AFM part of the junction exhibit sd-interaction and cause inclination of AFM magnetic sublattices. Inclination angle increases with the current. As the result, sd scattering and current dissipation yields of conducting electrons start to depend on the flowing current. Magnetic properties of FM-AFM junction was also investigated by micromagnetic simulations.

1. B.G. Park et al. "A spin-valve-like magnetoresistance of an antiferromagnet-based tunnel junction". *Nature Mater.* **10**, pp. 347–351, 2011.
2. R. Duine. "Spintronics: An alternating alternative". *Nature Materials* **10**, pp. 344–345, 2011.
3. Yu.V. Gulyaev, P.E. Zil'berman, and E.M. Epshtein. "The Influence of the Current on the Magnetization Dynamics in a Ferromagnet–Antiferromagnet Structure: Simulation", **57**, pp. 558-564, 2012.
4. A.S. Núñez et al. "Theory of spin torques and giant magnetoresistance in antiferromagnetic metals", *Phys. Rev. B* **73**, pp. 214426, 2006.

Evaluation of a new MgO barrier based on CoFeB/MgO/CoFeB structure for advanced MRAM applications

E. Smirnov¹, M. Genkin¹, C. Portemont², C. Ducruet², J. Alvarez-Hérault², E. Danilkin¹,
D. Choutov¹, K. Mackay²

1. Crocus Nanoelectronics, Moscow, Russia, e.smirnov@crocusnano.com. 2. Crocus Technology, 5 Place Robert Schumann, BP 1510, 38025 Grenoble Cedex 1 France, cportemont@crocus-technology.com

Magnetoresistive memory (MRAM) is one of the types of nanotechnology enabled memories which is going to replace the traditional memories such as DRAM, SRAM and Flash because of its non-volatility and ability to very fast write/read operations [1]. Magnetic Tunnel Junctions (MTJs) based on CoFeB/MgO/CoFeB structures are very promising for future spintronics, especially in MRAM memory operation due to its high tunnel magnetoresistance (TMR) and reasonable range of resistance area product (RA).

The deposition process of MgO barrier in such structures is one of the most difficult challenges to achieve good parameters of MTJs and it strongly affects on the barrier roughness, especially on the low RA region because of insufficient crystallization of thin MgO on an amorphous CoFeB [2]. Ordinary MgO barrier creation takes a long time due to obligatory steps of Mg oxidation in different module that makes process complicated. It will be shown that the new approach of barrier formation directly in deposition module is less difficult, takes less time and show better ratio of TMR vs RA which is very important for good MTJs performance. Several groups of samples were deposited on 200mm wafers using advanced cluster PVD tool:

- (1) CoFeB/MgO wedge RF, 1 mTorr/CoFeB,
- (2) CoFeB/Mg/MgO wedge RF, 1 mTorr/Mg/CoFeB,
- (3) CoFeB/Mg/MgO wedge RF, 5 mTorr/Mg/CoFeB.

In this study the insulating MgO layer was deposited by the RF-sputtering directly from MgO target in deposition module. The applied working RF power to MgO target during deposition was fixed at 4 kW. All the metallic layers including Mg insertions were deposited by using DC-sputtering with constant parameters. The Ar partial pressure was fixed for 1st and 2nd groups at 1 mTorr. For 3rd group the Ar partial pressure was fixed at 5 mTorr in order to see the influence of higher pressure. All samples have additional seed and capping layers with following placement: seed layer/CoFeB/MgO/CoFeB/capping layer annealed after the deposition in a high-vacuum furnace and measured by current in plane tunneling (CIPT) technique directly from blanket wafers [3].

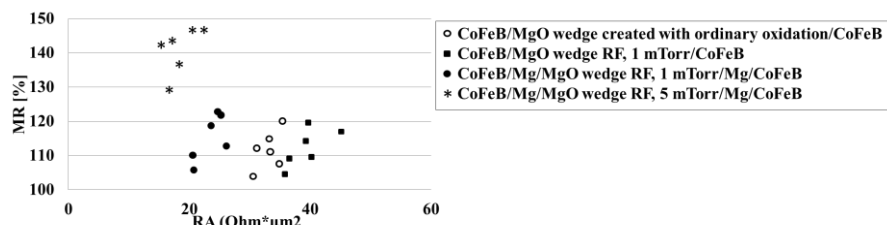


Fig. 1. TMR versus RA for 3 different groups of samples.

It is shown that the group of samples with CoFeB/MgO wedge RF 1 mTorr /CoFeB structure have the lowest TMR comparable to ordinary oxidized MgO with highest RA distribution (Fig. 1). Second group with thin Mg insertions provides lower RA and similar TMR in comparison to the second group. The increasing of Ar partial pressure in the third group to 5 mTorr reduces the RA distribution and significantly increases the TMR. As a result, the last barrier composition with Mg insertions and higher Ar partial pressure shows very promising ratio of TMR vs RA which can be used in MTJs required for low “read” and “write” currents having a big delta between R_{min} and R_{max} in the most advanced MRAM applications.

1. Ricardo C. Sousa, I. Lucian Prejbeanu. "Non-volatile magnetic random access memories (MRAM)", *Comptes Rendus Physique*, **6** (9), pp. 1013-1021, 2005.
2. J. Wrona et al. "Low resistance magnetic tunnel junctions with MgO wedge barrier", *J. Phys.: Conf. Ser.*, **200**, 052032, 2010.
3. D.C Worledge and P.L. Trouilloud. "Magnetoresistance measurement of unpatterned magnetic tunnel junction wafers by current-in-plane tunneling", *Appl. Phys. Lett.* **83**, p. 84, 2003.

Prospective sensors of ultra weak magnetic fields for medical applications

L.P. Ichkitidze¹, R.Y. Preobrazhensky¹, M.L. Gavrushina²

1. National Research University of Electronic Technology (MIET), Moscow, e-mail: leo852@inbox.ru

2. Bazovye Technologii JSC, Ivana Franko str., 4, Moscow

Biomagnetic fields generated by human body organs lay mainly within the range 10 pT÷1 fT, i.e., are ultra weak and can be detected by super-high-sensitivity magnetic field sensors (MFSs). In this study, we consider MFSs with the highest medicine application potential, which are divided in two types: operating at room temperature (**Type I**) and operating under cryogenic cooling conditions (**Type II**). We report some calculated and experimental characteristics: magnetic field resolution δB , magnetic flux resolution $\delta\phi$, energy resolution ε , dynamic measurement range D_r , and others.

Type I. 1.1. In the beginning of this century, commercial production of laser-pumped atomic magnetometers (LPMs) with a working cell volume of about 1 cm³ was started. For a LPMs with the cell 4×19×40 mm³ in size containing potassium ions, in which circularly polarized laser diodes are used, the following parameters were attained: the resolution at the intrinsic magnetic noise level $B_n \sim 7 \text{ fT/Hz}^{1/2}$ and $\varepsilon \approx 7 \cdot 10^{-29} \text{ J/Hz}$ in the magnetometer configuration and $B_n \sim 0.54 \text{ fT/Hz}^{1/2}$ and $\varepsilon \approx 7 \cdot 10^{-31} \text{ J/Hz}$ in the gradiometer configuration.

1.2. The values $\delta B \sim 100 \text{ pT}$ and $D_r \sim 70 \text{ dB}$ are attained in ferroprobe MFSs with a magnetosensitive element (MSE) made of single-domain single-crystal permalloy. Such MFSs directly measure the absolute values of the magnetic field projection and allow detecting agglomerates of ferromagnetic particles in biomedical objects. The drawbacks of these sensors are the large size and limited dynamic range.

1.3. Various MFSs have been developed and produced that are based on the magnetoresistive effects, such as giant magnetoresistance (GMR), anisotropic magnetoresistance, tunnel magnetoresistance, and extraordinary magnetoresistance (EMR). The EMR was demonstrated the only main noise is the Johnson noise.

Type II. 2.1. In SQUIDs based on high-temperature superconductors (HTS) (Y-Ba-Cu-O system) with the working temperature $T_w \sim 77 \text{ K}$, the parameters $\delta\phi \sim 10^{-5} \div 10^{-6} \phi_0$ ($\phi_0 \approx 2 \cdot 10^{-15} \text{ Wb}$ is the quant of magnetic flux), $\delta B \sim 10^{-14} \div 10^{-13} \text{ T}$, and $\varepsilon \sim 10^{-27} \text{ J/Hz}$ were implemented, which are worse than the values for the SQUIDs based on low-temperature superconductors (LTS). In particular, for the Nb-based SQUID with the working temperature $T_w \sim 4 \text{ K}$, the resolutions are $\delta\phi \sim 10^{-6} \div 10^{-7} \phi_0$, $\delta B \sim 10^{-15} \text{ T}$, $D_r \geq 140 \text{ dB}$, and $\varepsilon \sim 10^{-30} \text{ J/Hz}$ [1]. The HTS SQUIDs are usually much more expensive than LTS SQUIDs, which is important for the systems containing hundreds of SQUIDs (Elekta Neuromag magnetoencephalograph with over 300 SQUIDs).

2.2. Magnetomodulation magnetometers (MMMs) are similar to ferroprobe sensors, but contain HTS ceramic rods of the Josephson medium type as MSEs. At the working temperature $T_w \sim 77 \text{ K}$, they demonstrate the acceptable absolute magnetic-field sensitivity (no less than 10^5 V/T) and the resolutions $\delta B \geq 10^{-13} \text{ T}$ and $\delta\phi \geq 10^{-4} \phi_0$. However, the MMMs are much cheaper and, in contrast to SQUIDs, can directly measure the absolute value of a magnetic field. Further development of the technology for fabrication of Josephson media and the MMM parameters closer to the SQUID characteristics.

2.3. In recent time, combined MFSs based on the superconductor magnetic field concentrator (MFCs)/nonsuperconductor MSE structures have been intensively developed (HTS/GMR, LTS/GMR, etc). Nanostructuring of MFCs superconducting film active strips in an MFS was proposed. Fragmentation of an MFC active strip into parallel superconducting branches and cuts with widths of 20–1400 nm significantly improves the parameters of the combined MFS [2]. In particular, δB decreases by more than an order of magnitude and D_r broadens in several times as compared with the MFSs with nonstructured MFCs. Thus, the parameters comparable with those of HTS SQUIDs ($\varepsilon \sim 10^{-27} \text{ J/Hz}$) and LTS SQUIDs ($B_n \sim 1 \text{ fT/Hz}^{1/2}$).

We have demonstrated that the LPMs (type I) are applicable in magnetocardiography and SQUIDs (type II) can be used both in magnetocardiography and magnetoencephalography. The occurrence of commercial combined MFSs with nanostructured elements are expected, the parameters of which will be no worse than those of HTS SQUIDs at much lower const.

1. D. Robbes. "Highly sensitive magnetometers—a review". *Sensors and Actuators*, **A 129**, pp. 86-93, 2006.

2. L.P. Ichkitidze, A.N. Mironyuk. "Superconducting film flux transformer for a sensor of magnetic field". *Physica C*, **472** (1), pp. 57-59, 2012.

Study the interface through “isolated 3D silicon tensoframe on silicon” heterostructure of MEMS-SOIMT pressure sensor

L. Sokolov

Institute of Aircraft Equipment, Zhukovsky, Russia, sokol@niiao.com

At present the causes are not investigated enough that produce insertion and residual mechanical stresses as a transducer instability factor [1] during the manufacturing process of MEMS-SOI strain transducers.

The study object is experimental samples of MEMS-SOIMT pressure sensor based on “isolated 3D silicon tensoframe on silicon” heterostructure where a monolithic tensoresistive frame (MT) is both a functional component and a structural component of the MEMS at the same time [2].

The investigated results through the interface layer images are shown in the proposed work.

The results of an experimental batch manufacturing have formed the basis for the analysis of possible causes that contribute to the generation of mechanical stresses local centers in the process of forming a micromechanical structure for a MEMS-SOIMT sensor and bonding the sensor with a support glass component in the electrostatic field, as well as the process of SOI wafer production and improvement.

The investigations were performed with the SEM technique using TM-3000 and Carl Zeiss SMT microscopes, and AFM Veeco.

The MEMS-SOIMT sensors were micromachined by the two sides anisotropic chemical etching (ACE) of SOI wafers with a “silicon-glass-silicon” heterostructure 100 mm in diameter, which were produced using the direct thermocompression bonding technology. The tensomodule was formed with the technique of thermoelectric-assisted bonding in the electrostatic field.

The investigations have found the diffusion of glass components into the silicon at the transition layer of the silicon-glass interfaces and local formations as glass nanoclusters in the silicon near-surface layer.

In addition, the SEM images of the glass surface morphology distinctly shows multiple formations as nanobubbles, whose occurrence can be caused by the humidity effects during the high-temperature process of thermocompression bonding of silicon wafers onto a SOI structure, that conforms with the conclusions made in [3].

During the analysis of the silicon (100) surface morphology at the silicon-glass dielectric interface the end face dents from a contact component of the anode bonding machine and the crack initiation centers around the dents have been found. A crack microprofile has been measured.

The SEM image of the local face area (111) of the 3D tensoframe clearly shows etching steps as a feature of the well-known layer-by-layer silicon ACE mechanism.

Thus, the analysis of possible causes which initiate the generation of mechanical stress local centers during the micromachining process of the MEMS-SOIMT micromechanical structure and a tensomodule formation process, as well as the manufacturing process of wafers with a SOI heterostructure, have been performed using the investigation results. The enhancement of the production technology based on minimum insertion stresses is planned with consideration for obtained results.

1. L. Sokolov, V. Shkolnikov. “About the Problem of Temporary Instability of Integral Sensors and Basic Methods of Instability Decrease”. *Measurement Techniques*, **10**, pp. 27-29, 2002.

2. L.V. Sokolov. “Conceptual Basis for Creating New-Generation High-Stable High-Temperature Microelectromechanical Sensors Based on a Silicon-On-Isolator Heterostructure with a Monolithic Integral Tensoframe for Intelligent Transducers”. *Proceedings of 9th International Symposium on Measurement Technology and Intelligent Instruments*. Vol. 3, D.S. Rozhdestvensky Optical Society, St.-Petersburg, pp. 248-251, 2009.

3. A.Y. Usenko. “Humidity Effects on Substrate Bonding for Silicon-on-Glass”. *219th ECS Meeting Transactions. Advanced Semiconductor-on-Insulator Technology and Related Physics 15*. Edited by Y. Omura, F. Gamiz, H. Ishii, J. Martino, B. Nguyen, J. Raskin, S. Selberherr. Vol. 35, Issue 5, The Electrochemical Society, Pennington, New Jersey, USA, pp. 111-115, 2011.

Development of driving setup for micromechanical friction vacuum gauge

A. Boyko, A. Shalimov, S. Timoshenkov, P. Kovyркиn, D. Kuznetsov

National Research University of Electronic Technology (MIET), Zelenograd, Moscow, Russia, ant_nico@mail.ru

Micromechanical vacuum gauges are small-sized and compatible to industrial scale fabrication, so are promising in a wide range of applications including vacuum technique, electronics and MEMS-based devices for internal pressure monitoring [1]. This work describes micromechanical friction vacuum gauge sensible to viscous damping of moving resonator in the surrounding gas [2]. Such gauges allow to measure vacuum pressure up to 10^{-5} mbar [2, 3].

Micromechanical transducer or resonator consists of a torsion silicon proof mass, made by bulk micromachining using wet and dry etching processes and static glass substrate; the gap between moving mass and parallel substrate is in the range from 5 to 20 microns. Gas film sandwiched between moving plate and static substrate acts the part of a spring and it is one of the most dominating energy loss mechanisms in MEMS resonators. Movement amplitude and a magnitude of output electric signal are reducing exponentially due to the squeeze film damping; decay time of the oscillation is proportional to the surrounding pressure. Electrostatic capacitive driving and reading are implemented; displacement between movable electrode of the proof mass and fixed electrode of the substrate is measured with the help of capacitance-to-voltage converter, which allows to transduce changing of capacitance between electrodes to equivalent voltage signal. Several sequential steps have to be done for pressure measuring: excitation of moving mass; an output data reading and recording; the pressure computation using dedicated program. RMS-DC conversion is applied for data stream reducing and processing of the envelope curve, digitized data are sent to computer with universal serial bus for final processing and analyzing. The use of PC allows to optimize data processing, storage and visualization.

Of high interest is how to push the proof mass for free oscillation appearance, but it's not a trivial task. The form of silicon plate vibration is multiplex and represents itself as a complex sum of motions with different eigenfrequencies. So the drive pulse has to provide stable noise-eliminating oscillations and good repeatability of measurements. Various signal waveforms have been analyzed and a saw-tooth signal is preferred as a most satisfying the defined claims.

Specialized electric circuit providing saw-tooth driving pulse has been created for implementation of proposed processing algorithm. The driving pulse of small fixed amplitude is generated with microcontroller, required amplitude of the signal is provided with high-voltage amplifier. Triggered with PC control command the circuit generates single saw-tooth pulse directed to actuating plate of micromechanical transducer. Damped vibration of activated silicon plate results in registered changes of differential capacitance. The measuring circuit allows to control the oscillations with an oscillograph. Experimental observation of proposed driving setup exhibits encouraging behavior of micromechanical transducers in the surrounding low-pressure atmosphere, good response of silicon resonators on driving pulse was demonstrated. The results can be applied for creation of micromechanical friction vacuum gauges.

1. A. Gorecka-Drzazga. "Miniature and MEMS-type vacuum sensors and pumps". *Vacuum*, **83**, pp. 1419–1426, 2009.
2. D. Tenholte, S. Kurth, T. Geßner, W. Dotzel. "A MEMS friction vacuum gauge suitable for high temperature environment". *Sensors and Actuators, A* **142**, pp. 166–172, 2008.
3. S.P. Timoshenkov, A.N. Boiko, B.M. Simonov. "Parameter estimation technique for sensitive elements of microaccelerometers and micromirrors". *Semiconductors*, **42** (13), pp. 1564-1568, 2008.

The chemistry screening for ultra low-k dielectrics plasma etching

A. Zotovich^{1,2}, M. Krishtab¹, F. Lazzarino¹, M.R. Baklanov¹

1. IMEC, Leuven, Belgium

2. Lomonosov Moscow State University, Moscow, Russia, Zotovich@physics.msu.ru

Scaling of ULSI devices brings new challenges to semiconductor industry. One of the important problems is related to interconnect delay, dynamic power consumption and crosstalk [1, 2]. This compels introduction and integration of new materials with low dielectric permittivity (low-k materials) as insulator in interconnects. One of such materials under consideration for sub 10 nm technology node is a spin-coated organosilicate glass layer with ordered porosity (37-40%) and a k-value of 2.2 (OSG 2.2). High porosity of this material leads to significant challenges during the integration and one of them is a dielectric material degradation during the plasma etching step [1, 3, 4]. Exposing to etching plasma induces losing material hydrophobicity, subsequent moisture adsorption, and dramatic increase of the k-value and degradation of reliability. To be able to step down to 10 nm and 7 nm technology nodes the thickness of the damaged layer of low-k film must be in order of few nanometers. One way to solve this problem is to find the less-damaging etching chemistry.

The low-k samples have been etched in a CCP double frequency plasma chamber from TEL. Several etching chemistries with fluorocarbon gases have been evaluated under different plasma conditions. Standard recipes developed for microporous materials with $k > 2.5$ and based on mixture of C_4F_8 and CF_4 with N_2 , O_2 , and Ar were found significantly damaging ULK materials and the degree of damage increases with pore size. In this work, the standard etch recipe was compared with oxygen free etch chemistries based on mixture CF_4 with CH_2F_2 and Ar assuming that the presence of oxygen in the first recipe will have significant negative impact in high porous ULK materials.

The film damage (loss of methyl groups and moisture uptake) has been analyzed using FTIR spectroscopy [5] and the k-value has been extracted by capacitance CV-measurements. Three plasma components can cause low-k damage: radicals, ions and photons. In this study, it is shown that chemistry of use and hence radicals doesn't play a significant role for low-k damage, even when oxygen presents in a recipe, but plasma conditions such as applied power and chamber pressure mainly control it. Etching at varying low-frequency power, which controls the ion energy within certain recipe, shows that ion bombardment impact on low-k degradation to be quite small. There is also an indirect evidence that vacuum ultraviolet photons cause the main damage of low-k, whereas radicals and ions are not so harmful.

Except of the low damage, a good structure profile and low roughness are demanded. Structure profile quality becomes very important at small scales and sufficiently small surface roughness is needed for a desirable quality of a barrier deposition. To evaluate the patterning capability of this recipes trench structures have been etched in low-k film with two samples for every recipe. After the etching one sample underwent HF dipping and then both were examined by cross-SEM. HF dipping had an aim to remove the damaged part of low-k and visualize the sidewall damage. It was shown that recipes with addition of polymer formed fluorocarbon gases passivate sidewalls and top of the structure with polymer that provides a good profile by reducing of hardmask faceting and isotropic etching. As was expected and verified with AFM, decreasing of energy at low frequency helps one to improve the surface smoothness after the etching step, which can be very important for further integration. The results of the research allowed to optimize the patterning process for dual damascene integration.

1. M.R. Baklanov, P.S. Ho, E. Zschech. *Advanced interconnects for ULSI technology*. Ch. 1, John Wiley and Sons, Chichester, 2012.
2. K. Maex, M.R. Baklanov et al. *J. Appl. Phys.*, **93**, 8793 (2003).
3. R.J.O.M. Hoofman, G.J.A.M. Verheijden et al. *Microelectronic Engineering*, **80**, 337 (2005).
4. M.R. Baklanov, J-F. de Marneffe et al. **113**, 041101 (2013).
5. A. Grill and D.A. Neumayer. *J. Appl. Phys.* **94**, 6697 (2003).

Comparative analysis of the factors leading to low-k degradation during the integration process

A. Zotovich^{1,2}, M. Krishtab¹, F. Lazzarino¹, M.R. Baklanov¹

1. IMEC, Leuven, Belgium

2. Lomonosov Moscow State University, Moscow, Russia, Zotovich@physics.msu.ru

Following the Moore's law forces one to constantly decrease the node size of ULSI devices that gives rise to a lot of new challenges in semiconductor production. New interconnect materials with low dielectric permittivity (low-k materials) have to be designed and integrated to solve the problems of interconnect delay, dynamic power consumption and crosstalk [1]. Organosilicate glass layer with ordered porosity (37-40%) and a k-value of 2.2 (OSG 2.2) is one of the candidate for sub 10 nm technology node.

Different steps during the integration process can lead to low-k degradation caused by loosing of hydrophobicity, subsequent moisture uptake and increasing of k-value [1, 3]. These steps include hardmask deposition, low-k etching, barrier layer deposition, metal filling and chemical mechanical polishing (CMP). 7-10 nm node technology demands integrated k-value to be less than 2.4 and that is why different sources of damage should be examined.

To improve selectivity of photoresist etching over the low-k, hardmask is deposited over the dielectric surface. The hardmask is a multilayer stack and its first layer is a thin oxide that is used to provide low-k surface sealing and protection during the rest of the hardmask deposition. It was shown by FTIR analysis and ellipsometric porosimetry, that 10nm of the first hardmask layer is enough to reach this goals.

The next step of integration is a low-k etching. This step can seriously degrade low-k material [1, 3, 4] and the etching recipe screening and hardmask modifications are demanded to reduce the etching step damage. Except of the low damage, etching recipe should provide smooth structure bottom necessary for appropriate quality of metal barrier deposition. High roughness of low-k surface after the etching can lead to low quality of barrier deposition and subsequent barrier and Cu penetration into the low-k, that seriously deteriorates dielectric properties by increasing leakage current and decreasing breakdown voltage. Two etching recipes were chosen to etch the low-k layer and TEM analysis was performed on integrated structures to reveal quality of metallization step. The TEM results were compared with AFM data of surface roughness measurements and improvement of barrier deposition by decreasing of surface roughness after the etching was proved.

CMP was the last step of integration under the consideration [1, 2]. Alkaline slurries that are usually used for CMP can lead to loosing of material hydrophobicity and k-value increasing. Wafers coated with low-k layer with and without sealing layer experienced CMP process. FTIR data and k-value C-V measurements showed CMP process modify only the thin top layer of low-k, which can be restored then by thermal annealing.

Among the all integration steps considered in this study, vacuum ultraviolet (VUV) photons from the etch plasma bring most of the damage. To reduce this damage, hardmasks with different thicknesses of oxide layer were tried. The samples were exposed to VUV light from Ar ($\lambda = 106$ nm) and Xe ($\lambda = 147$ nm) plasmas. According to FTIR data, 30 nm of oxide sealing layer and 50 nm of amorphous carbon can significantly reduce VUV-caused damage in case of Ar plasma, but not Xe plasma that emits light in the most damageable for low-k region of VUV. The recipe for low-k etching should provide a tradeoff between VUV light intensity reduction and sufficiently high etch rate that is needed for radical damage reduction. All the observed findings were proven by direct measurement of dielectric constant and generated recommendations have been introduced into integration lots.

1. Mikhail R. Baklanov, Paul S. Ho, Ehrenfried Zschech. *Advanced Interconnects for ULSI Technology*, John Wiley and Sons, Chichester, 2012.

2. Parshuram B. Zantye, Ashok Kumar, A.K. Sikder. *Materials Science and Engineering* **R 45**, pp.89–220, 2004.

3. R.J.O. M. Hoofman, G.J.A.M. Verheijden et al., **80**, p. 337, 2005.

4. A. Zotovich, M. Krishtab, F. Lazzarino, M.R. Baklanov. "The chemistry screening for ultra low-k dielectrics room temperature plasma etching". ICMNE-2014.

Impact of structural changes in e-beam negative resist hydrogen silsesquioxane (HSQ) to etch-resistance at different doses of exposure

I.P. Ivanenko, V.A. Kalnov, A.V. Miakonkikh, N.A. Orlikovsky, A.A. Tatarintsev
Institute of Physics and Technology of Russian Academy of Science, Moscow, Russia.
E-mail: tatarintsevandrew@gmail.com

Hydrogen silsesquioxane (HSQ) resist is a negative electron beam resist with good etch-resistance and high mechanical stability. Therefore this resist has become a material of considerable interest for nanolithography. The fully-condensed HSQ structure has the formula $(\text{HSiO}_{3/2})_n$ [1]. For $n = 8$, the proposed structure of HSQ is cubic, with silicon and hydrogen atoms at the vertices and oxygen atom forming the edges.

Lines with width of 1 μm were made on Si-wafer by electron beam lithography. The exposure doses of lines varied from 500 to 2000 $\mu\text{C}/\text{cm}^2$. As was shown in [2], changes in Si-H₂ peak at $\sim 2000 \text{ cm}^{-1}$ in the Raman spectra and release of SiH_x products in EBID demonstrate, that electron-beam-exposed material crosslinks via a redistribution reaction. In this paper also release of significantly more H₂ than SiH₂ during EBID was observed, which indicate additional reaction mechanism. As shown in fig. 1, these redistributions influence on the HSQ-resistance for plasma etching.

Samples with resist were annealed at atmosphere for 30 min at 400 °C, which significantly improves selectivity of silicon etching respectively to resist. Longer annealing did not show any improvements. Etching was performed in RIE tool PlasmaLab 100 from Oxford Instruments Plasma Technology in mix of SF₆ and C₄F₈ called Pseudo Bosch. By changing the ratio SF₆:C₄F₈, the sidewall profile angle can be controlled. Increasing the ratio improves the etch rate, reduces the selectivity, and decrease profile angle. Increasing the forward power again reduces the selectivity with a slight improvement in etching rates.

Forward ICP power was 1200 W, with electrode power in range 25-35 W, which lead to DC bias 168-208 V respectively. Pressure was 10 mTorr, chuck temperature 20 °C. Gas mixture composition was optimized in separate experiment to obtain vertical profile of sidewalls for low aspect ratio trenches with 0.3-1 micrometer depth, and was 25 sccm for SF₆ and 45 sccm for C₄F₈. Etching time varied from 30 sec to 3 minutes. For comparison of resist etch rate with etch rate of silicon oxide, unpatterned samples of thermal SiO₂ were etched in the same processes and thickness of initial and remaining oxide were measured by spectroscopic ellipsometry. Thickness of remaining resist and silicon profile was measured by SEM.

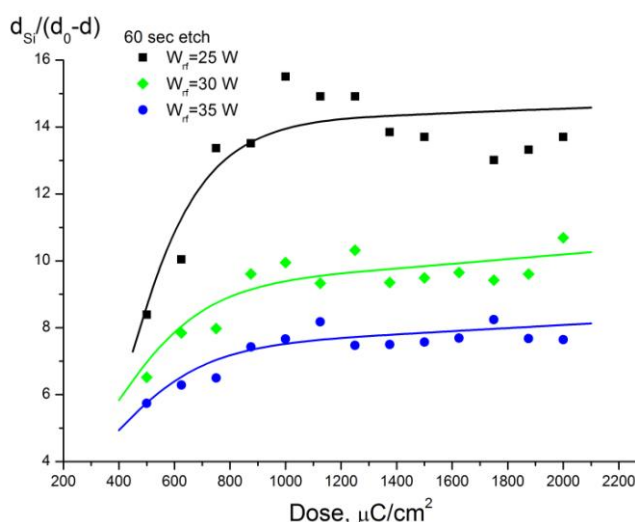


Fig. 1. Dependence of selectivity hydrogen silsesquioxane (HSQ) relative to Si on the dose of exposure for different electrode power. Etching time is 60 sec. Samples annealed at 400 °C for 30 min.

1. G. Li, L. Wang, H. Ni, C. U. Pittman. *J. Inorg. Organomet. Polym.*, **11**, p. 123, 2001.
2. D.L. Olynick, B. Cord, A. Schipotin, D.F. Ogletree, P.J. Schuck. *J. Vac. Sci. Technol. B.*, **28**, pp. 581-587, 2010.

Properties of HfO₂/Si interface layer formed by H₂ and NH₃ plasma pretreatments in PEALD reactor

A. Rogozhin, A. Miakonkikh, K. Rudenko

Institute of Physics and Technology of RAS, Moscow, Russia, rogozhin@fian.ru.

High-k dielectrics with metal gates (HKMG) appeared in high performance MOSFETs in 2007 [1]. Hf-based material is used as gate dielectric. It is well known that SiO₂-based interfacial layer (IL) is formed at the HfO₂/Si interface [2]. Modern plasma-enhanced atomic layer deposition (PEALD) systems open new ways for *in situ* pretreatment of substrates before gate dielectric deposition. Particularly the properties of IL can be modified by preliminary annealing or plasma treatment. In this work impact of *in situ* H₂ and NH₃ plasma pretreatment on the properties of IL has been investigated.

Hafnium dioxide was deposited on Si (100) wafers (B-doped, $1.1 \cdot 10^{15} \text{ cm}^{-3}$) by PEALD. All substrates were RCA-cleaned (SC1 and SC2) followed by HF treatment. Then some substrates were processed in H₂ or NH₃ plasma (10 min, 200 mTorr of H₂ or NH₃, 500 W ICP) in the FlexAl ALD-system. After HfO₂ deposition in same chamber, tungsten electrode was formed by DC magnetron sputtering. Contact areas were defined using standard litho process, followed by wet etching in 5% hydrogen peroxide (H₂O₂). The post-metallization annealing (PMA) was performed at 425 °C for 30 min.

The high-k layers have ~ 9 nm thickness to minimize the leakage influence on electrical measurements. Before W deposition dielectric stacks were investigated by spectroscopic ellipsometry. It was found that plasma pretreatment leads to higher thicknesses of ALD grown layer.

High (100 kHz) and low (1 Hz) frequency capacitance-voltage (CV) and current voltage (IV) characteristics were measured. PMA resulted in shift of CV characteristics toward zero and substantial decrease of hysteresis. Also 45% increase in oxide capacitance has been observed for HF-last (without plasma treatment) samples and 10% increase – for plasma treated samples (fig. 1, left) but leakage current through dielectric in HF-last samples is two orders higher than in plasma treated ones.

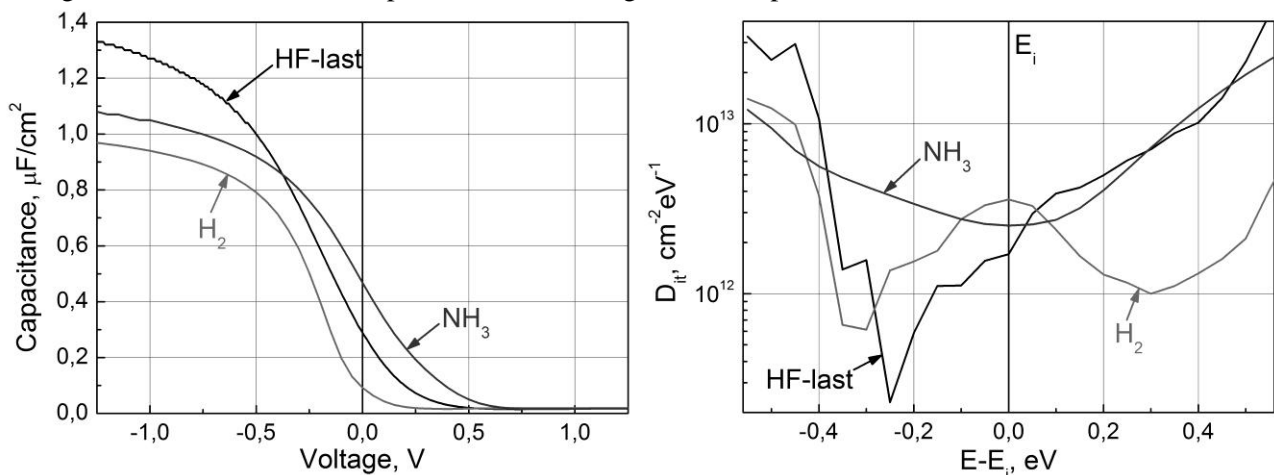


Fig. 1. CV characteristics (left) and interface trap density (right) for samples processed in HF and plasmas of H₂ or NH₃.

Interface trap density values were estimated for annealed samples (fig. 1, right) by high-low frequency method. Interface trap density in all samples is quite high (about $(1-5) \cdot 10^{12} \text{ cm}^{-2} \text{ eV}^{-1}$). We believe that lower D_{it} values for HF-last with H₂-plasma pre-treated samples are due to SiO₂ interfacial layer formation and hydrogen passivation of the interface traps. High D_{it} and flat-band voltage shift in NH₃-plasma treated sample can be explained by nitrogen diffusion to the interface and high density of fixed charges in dielectric stack. Thus plasma pretreatments can lead to lower interface trap densities but increase equivalent oxide thickness. This work was supported by RFBR, research project №14-07-00844 A.

1. K. Mistry et al., IEDM Tech. Digest, p. 247, 2007.
2. T. Ando, Materials, **5**, p. 478, 2012.

Conformal Deposition of HfO₂ by Plasma Enhanced ALD Process on Silicon Fin and Trench Structures

A. Miakonkikh, K. Rudenko, and A. Orlikovsky

Institute of Physics and Technology (FTIAN), Moscow, Russia, miakonkikh@ftian.ru.

Decrease of the gate dielectric electrical thickness providing physical thickness which is enough for suppressing tunneling current lead to implementation of high-k metal oxides as the gate dielectric, for example HfO₂[1]. Hafnium oxide is also promising for high density DRAM structures. Promising 3D FET nanotransistor (for instance FinFET or nanowire based transistors) will definitely need gate dielectric deposition technology with high degree of conformity. Even more challenges appear for technology of growth of conformal dielectric layer in nano-trenches of capacitive structures DRAM.

It is known that, ALD technique allows to produce ultrathin films with atomic level control of film thickness (only monatomic layer is deposited in each ALD-cycle of process), and excellent conformal coverage.

In present work we study dependence of film thickness conformality on ALD cycle parameters (duration of precursor dosage) and temperature. Fin and trench structures with 70nm-5μm width and aspect ratio of 5-50 were formed by ICP RIE in SF₆+C₄H₈ plasma which allows producing features with vertical walls and extended aspect ratio.

The films were deposited in plasma enhanced ALD process with TEMAH (Hf(N(C₂H₅)(CH₃))₄) as metal precursor and O₂ as non-metal plasma precursor at FlexAl ALD System. This process is truly self limited and hence process dependence on external parameters (stage temperature, duration of the process, pressure) is flat in significant interval. That provides “process window”, in which stable and reproducible film properties can be achieved [2]. Thickness of films was measured by SEM.

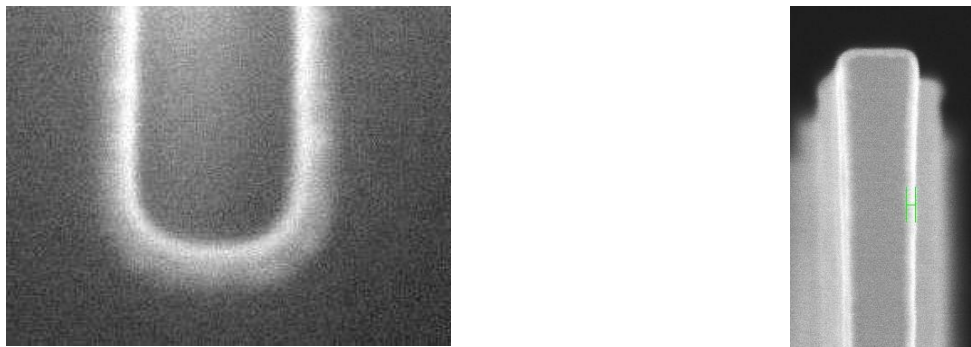


Fig. 1. PE-ALD conformal deposition of 10 nm HfO₂ on silicon 70 nm / 350 nm trench (left) and 70 nm wide silicon fin structure (right)

It was revealed that film thickness on the walls of trench decrease linearly with depth, with increased thickness on horizontal part of bottom of the trench. This effect become pronounced for aspect ratio higher than 10. For example in 2.4 μm wide trench with 27.5 nm depth, covered with 36 nm layer of HfO₂ (measured on open surface), thickness of film on the sidewall decreases from 36 nm on the upper part to 16 nm on the bottom part, with 22 nm thickness on horizontal part of bottom. Thickness of film on sidewall of fin does not depend on its height or width (ideal step coverage) for sparsely located fins. Simple theoretical model was proposed for film thickness on sidewalls of trench and the ways for enhancing conformality of ALD process for sub-100 nm trenches have been proposed. Degree of conformality of deposited film was compared with that for aluminum oxide process (TMA+O₂-plasma) at the same conditions.

1. J.H. Choi, Y. Mao, J.P. Chang, “Development of hafnium based high-k materials. A review”, *Materials Science and Engineering*, R **72**, pp. 97–136, 2011.
2. A. Miakonkikh, A. Rogozhin, K. Rudenko, and A. Orlikovsky, Properties of thin HfO₂ gate dielectric formed in Atomic Layer Deposition process, ICMNE Book of abstracts, Zvenigorod, Russia, 1-5 October 2012.

Superconductor – ferromagnetic control unit for superconducting memory compatible with RSFQ logic circuits

M.Yu. Kupriyanov^{1,4}, C.B. Bakurskiy^{2,4}, A.A. Golubov^{3,4}, T.Yu. Karminskaya¹, N.V. Klenov²,
I.I. Soloviev¹, N.G. Pugach¹, and S.L. Prischepa⁵

1. Skobeltsyn Institute of Nuclear Physics, Lomonosov Moscow State University, Moscow, Russia,
E-mail address (mkupr@pn.sinp.msu.ru).

2. Physics Department, Lomonosov Moscow State University, Moscow, Russia.

3. Faculty of Science and Technology and MESA+ Institute for Nanotechnology, University of Twente, The Netherlands.

4. Moscow Institute of Physics and Technology, State University, Dolgoprudny, Moscow region, Russia.

5. Belarusian State University of Informatics and RadioElectronics, Minsk, Belarus.

We overview the current status of theoretical understanding and experimental realizations of superconducting spin valves, which can be used as control units for superconducting memory compatible with RSFQ logic circuits.

The interest to this problem is motivated by the recent developments, which clearly demonstrated that the achieved background in this field provides the opportunity for finding solutions for elaboration of superconducting memory cells, which can be integrated with RSFQ logic circuits. These cells are based on heterostructures, which consist of superconducting (S) materials, insulator (I), ferromagnetic (F) and normal (N) metals. Fabrication and study of such heterostructures is one of the components of the new U.S. program, providing for the next 4 years the establishment of production for the manufacture of working model of a prototype superconducting computer [1].

We start with the brief discussion of peculiarities of proximity effect in SF and SFF multilayers and their manifestation in spin valve devices controlling critical temperature of S film or conductance of one of the F layers in SFF structures.

The recent status of experimental and theoretical achievements in developing SISFS and SFFS Josephson control units of superconducting memory cell will be discussed. Special attention will be given to the effect of formation of domain walls and normal phase inclusions in the F films on the junction critical current.

Support by RFBR grants 14-02-90018, 14-02-31002_mol_a, Ministry of Education and Science of the Russian Federation, President grant MK-1841.2014.2, and BFBR grant F14R-020 is acknowledged.

1. D.S. Holmes, A.L. Ripple, and M.A. Manheimer, *IEEE Trans. on Appl. Supercond.*, **23**, 1701610, 2013; http://www.iarpa.gov/Programs/sso/C3/solicitation_c3.html

Soliton scattering in Josephson vortex interferometer as a basis of low level measurements

I.I. Soloviev^{1,2}, N.V. Klenov^{3,2}, S.V. Bakurskiy^{3,4,5}, A.L. Pankratov^{6,7}, E. Il'ichev⁸,
and L.S. Kuzmin^{9,6,1}

1. Lomonosov Moscow State University Skobel'syn Institute of Nuclear Physics, 119991 Moscow, Russia

2. Lukin Scientific Research Institute of Physical Problems, Zelenograd, 124460 Moscow, Russia

3. Physics Department, Lomonosov Moscow State University, 119991 Moscow, Russia

4. Moscow Institute of Physics and Technology, State University, Dolgoprudniy, Moscow region, Russia

5. Faculty of Science and Technology and MESA+, Institute for Nanotechnology, University of Twente, 7500 AE Enschede, The Netherlands

6. Laboratory of Cryogenic Nanoelectronics, Nizhny Novgorod State Technical University, 603950 Nizhny Novgorod, Russia

7. Institute for Physics of Microstructures of RAS, 603950 Nizhny Novgorod, Russia

8. Leibniz Institute of Photonic Technology, D-07702 Jena, Germany

9. Chalmers University of Technology, SE-41296 Goteborg, Sweden

Using of solitons for information receiving and processing can be very attractive due to their inherent particle-like stability joint with a wave nature. In superconducting electronic devices (e.g. all-digital-RF receiver systems [1], read-out systems for superconducting single photon detectors [2]) based on Josephson junctions, magnetic flux quantum vortices representing data bits are solitons, also called fluxons. In ballistic detectors that are widely used for mesoscopic quantum measurements, a measured system controls a transport of solitons via Josephson transmission (JTLs) lines by creating a scattering potential [3]. The detector scheme can be organized in an interferometer manner (see Fig. 1a).

We examine the numerical and analytical approaches for calculation of the soliton scattering at point-like successive inhomogeneities of the driving force in a presence of thermal fluctuations. Considering the scattering as a measurement tool, we argue that the accelerated soliton propagation leads to an enhancement of the signal-to-noise ratio of the detector scheme due to a relativistic dependence of a soliton mass on its velocity.

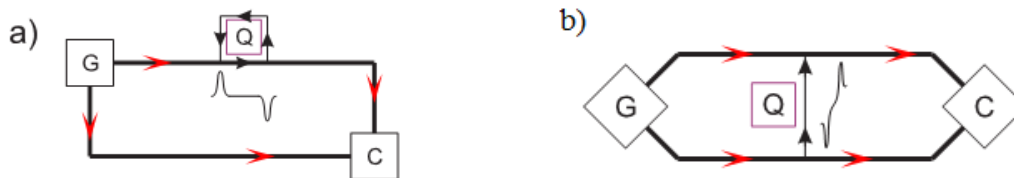


Fig. 1. a) Ballistic Josephson vortex interferometer scheme. G box represents a fluxon generator, Q box is a qubit and C box is a comparator. b) The detector scheme in which the coupling loop is connected symmetrically to the both JTLs.

We propose an approach to symmetrize the detector scheme and explore arising advantages in the signal-to-noise ratio (SNR) and in the back-action on a measured object (see Fig. 1b). We show that symmetrization of the scheme leads to significant SNR increase due to the involvement of the both fluxons in the scattering events and effective increase of the scattering potential amplitude. At the same time, the back-action is drastically reduced because of differential origin of the backaction flux. The SNR estimation for the both cases of utilization the continuous and the discrete JTLs, for experimentally relevant parameters, is well above 100. This opens the opportunity of using the considered detector in practical applications including implementation of a unified interface circuit on the basis of RSFQ digital cells for linking the room temperature electronics and its quantum superconducting counterparts.

This work was supported by RFBR-BFBR grants no. 14-02-90018, 14-02-31002-mol_a, Ministry of Education and Science of the Russian Federation, grant no. 14Y26.31.0007, 14.604.21.0005 Russian President grant MK-1841.2014.2, Scholarship of the President of the Russian Federation and Dynasty Foundation

1. D. Gupta et al., IEEE Trans. Appl. Supercond. **21**, 1EB01, 2011.

2. H. Terai, T. Yamashita, S. Miki, K. Makise, and Z. Wang, Opt. Express **20** (18), 20115, 2012.

3. K.G. Fedorov, A.V. Shcherbakova, R. Schlafer, and A.V. Ustinov, Appl. Phys. Lett. **102**, 132602, 2013.

Josephson magnetic rotary valve

I.I. Soloviev^{1,5}, N.V. Klenov^{2,5}, S.V. Bakurskiy^{2,3}, M.Yu. Kupriyanov^{1,3}, A.A. Golubov^{3,4}

1. Skobeltsyn Institute of Nuclear Physics, Lomonosov Moscow State University, Moscow, Russian Federation

2. Physics Department, Lomonosov Moscow State University, Moscow, Russian Federation.

3. Moscow Institute of Physics and Technology, State University, Dolgoprudniy, Moscow region, Russian Federation

4. Faculty of Science and Technology and MESA+ Institute for Nanotech., University of Twente, The Netherlands

5. Lukin Scientific Research Institute of Physical Problems, Zelenograd, Moscow, 124460 Russia

Superconducting digital circuits based on Josephson junctions underwent significant progress in the last decades offering high frequency data receiving and processing (e.g. all-digital RF receiver with clock frequency of up to 30 GHz [1]). Magnetic flux quantization in a superconducting loop allowing representation of information bit as a flux quantum is one of the key features providing the superconducting technology advantages. Unfortunately, the reverse side of using this feature is a requirement to store the flux quantum in superconducting valves and memory cells that naturally limits possibilities of their miniaturization restraining progress of the technology.

Magnetic devices, which rely on manipulation of the local magnetizations, are well known for their applications in random access memory and recording heads. Recent advances in understanding of hybrid S-F structures operating at the interplay of generally mutually exclusive phenomena of superconductivity (S) and ferromagnetism (F) opened exciting opportunities to develop the new tunable Josephson junctions which characteristics are defined by properties of the F-layer(s) placed in the weak link area. For example, the junction ground-state phase difference can be π -shifted in comparison with that of conventional junction or even arbitrary φ -shifted ($0 < \varphi < \pi$) and doubly degenerated ($\varphi_0 = \pm\varphi$) by implementation of spatially inhomogeneous $0-\pi$ junction. A number of approaches were proposed for development of the Josephson valves relying on control of the induced superconducting pair states in the weak link area by directly changing the F-layer exchange field or changing the mutual orientation of magnetizations of multiple F-layers, or making use of the mentioned φ -junction ground-state bistability. However, experimental realizations revealed the drawbacks that depending on the used approach can be as follows: 1) the junction critical current is modulated in a very narrow range; 2) characteristic frequency of the junction is highly suppressed; 3) the critical current modulation requires application of strong magnetic fields; 4) the junction size cannot be reduced well below the Josephson penetration length which is larger by an order than characteristic dimension of modern junctions.

To circumvent the drawbacks we propose an approach that combines the advantages of some known Josephson valves in a single structure. We restrict ourselves by the single F-layer introducing a spatial $0-\pi$ inhomogeneity of the junction. Since the stable states of the 0 - and π -parts are shifted in phase, their coupling provides the leveling of the phase across the junction (if the junction is small enough) corresponding to nearly unstable state that manifests itself via significant reduction of the total critical current I_c . The F-layer's magnetic field oriented parallel to the $0-\pi$ boundary can perform an "effective decoupling" providing the phase gradient across the junction, spreading the phase in the parts close to their initial ground states, and thus restoring the I_c . If the F-layer's magnetization is rotated perpendicularly to the junction's spatial inhomogeneity, the field is vice versa enhances the critical current suppression. We show that the $0-\pi$ inhomogeneity can be formed by introducing an additional thin normal (N) layer above some part of the F-layer. To provide the required high-frequency characteristics of the junction, the proposed S-F/FN-S valve can be used as a control element in the SISFS junction which we proposed earlier [2]. In this case the $I_c R_n$ product which is proportional to characteristic frequency of a Josephson junction is determined by the SIS part while modulation of the junction critical current in a wide range corresponds to rotation of the F-layer magnetization in the s-F/FN-S part used instead of the sFS one. This rotation can be easily provided by application of reasonable mutually orthogonal magnetic fields. The using of the magnetization orientation for the critical current control provides non-volatility of the element and the ability of non-destructive read-out.

This work was supported by RFBR-BFBR grants no. 14-02-90018, 14-02-31002-mol_a, Ministry of Education and Science of the Russian Federation, grant no. 14Y26.31.0007, Russian President grant MK-1841.2014.2, Scholarship of the President of the Russian Federation and Dynasty Foundation.

1. D. Gupta et al., IEEE Trans. Appl. Supercond., **21**, 1EB01, 2011.

2. S.V. Bakurskiy, N.V. Klenov, I.I. Soloviev, M.Yu. Kupriyanov, and A.A. Golubov, Phys. Rev. B, **88**, 144519, 2013.

Theory of charge transport in contacts with multiband unconventional and topological superconductors

I.A. Devyatov¹, A.V. Burmistrova²

1. Lomonosov Moscow State University Sobel'sin Institute of Nuclear Physics, 1(2), Leninskie gory, GSP-1, Moscow 119991, Russian Federation, igor-devyatov@yandex.ru

2. Lomonosov Moscow State University Faculty of Physics, Leninskie gory, Moscow 119991, Russian Federation, burangelina@yandex.ru

We present the theory of charge transport in contacts with multiband unconventional and topological superconductors. This theory based on recently proposed microscopic tight-binding approach [1, 2]. This approach [1, 2] takes into account the complex excitation spectrum of these superconductors, their multiband Fermi surface, the anisotropy of the superconducting order parameter as well as interband and intervalley scattering at the boundaries. We have considered theoretically break junctions of multiband Fe-based superconductor (FeBS) and contacts between usual single-band s-wave superconductor and FeBS (S-S_p junctions). We also calculated current-voltage characteristics of contacts between doped superconducting insulators Cu_xBi₂Se₃ and normal metal, based on microscopic approach [1, 2].

We have demonstrated that investigation of current-voltage characteristics of FeBS break junctions provides the possibility to distinguish possible s₊₊ and s₊ symmetries of the order parameter in FeBS only in the case of tunneling in a-b plane of FeBS. The investigation of c-oriented FeBS break junctions provides the information about magnitudes of gaps in FeBS and about the anisotropy of gaps. We also have calculated phase dependencies of the Josephson current and temperature dependencies of critical Josephson current across S-S_p junctions for different directions of current relative to the crystallographic axes of FeBS and different lengths of an insulator layer. We have demonstrated the relatively large contribution of the second harmonic to Josephson current-phase relation of a-b oriented S-S_p junctions. We have confirmed microscopically the recently proposed experimental scheme to determine the symmetry of the order parameter in FeBS [3] for c-oriented FeBS Josephson junctions.

Based on our microscopic approach [1, 2] we have calculated current-voltage characteristics of contacts between doped superconducting insulators Cu_xBi₂Se₃ and normal metal and compare our results with previous phenomenological calculations, presented in [4].

Support by the Russian Foundation for Basic Research, projects N 13-02-01085-a, 14-02-31366-mol_a and by the Ministry of Education and Science of the Russian Federation is acknowledged.

1. A.V. Burmistrova and I.A. Devyatov, "Boundary Conditions for the Junction of a Normal Metal with Multiband Superconductors with Unusual Types of superconducting Pairing", JETP Letters, **96**, pp.391-396, 2012.
2. A.V. Burmistrova, I.A. Devyatov, A.A. Golubov, K. Yada, and Y. Tanaka, "Theory of Tunneling Spectroscopy of Multi-Band Superconductors", J. Phys. Soc. Jpn., **82**, pp.034716-1-034716-13, 2013.
3. A.A. Golubov and I.I. Mazin, "Designing phase-sensitive tests for Fe-based superconductors", Appl. Phys. Lett., **102**, pp. 032601, 2013.
4. A. Yamakage, K. Yada, M. Sato, and Y. Tanaka, "Theory of tunneling conductance and surface-state transition in superconducting topological insulators", Phys. Rev. B. **85**, pp. 180509(R), 2012.

Magnetic field oscillation phenomena in multiple asymmetric superconducting rings of 1 μm diameter

V.L. Gurtovoi¹, M. Exarchos², R. Shaikhaidarov², V.N. Antonov², A.V. Nikulov¹, and V.A. Tulin¹

1. Institute of Microelectronics Technology, Russian Academy of Sciences, 142432 Chernogolovka, Moscow Region, Russia. E-mail: nikulov@iptm.ru

2. Physics Department, Royal Holloway University of London, Egham, Surrey TW20 0EX, UK

Measurements [1-4] of transport properties of superconducting asymmetric ring structures have discovered new phenomena: rectification of alternating current or noise [1-3] and a paradoxical shift of the critical current oscillations in magnetic field [3-4]. The phenomena have both fundamental and practical importance. Systems of superconducting asymmetric rings may be used as a quantum detector of noise [5] and a power source [6]. These applications depend on rectification efficiency of the rings. Rectification efficiency was determined to be a function of temperature, magnetic field, amplitude of external bias current and geometrical ring parameters such as ring diameter, superconductor film thickness and asymmetry degree (width ratio of different ring arms). Some of these parameters have been investigated in details [1-6]. It has been shown that series ring connection in multiple ring structures results in synchronous and additive rectification of individual rings and increase of rectified voltage which was proportional to the number of rings [2,6]. This allows drastic sensitivity improvement by increasing the number of rings when these structures are used as noise detectors. In this work results of measurements of a structure with 667 asymmetric 1 μm in diameter rings will be presented, Fig.1.

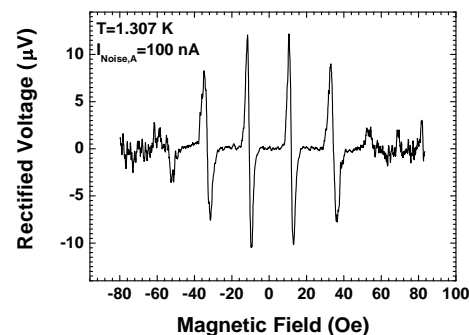
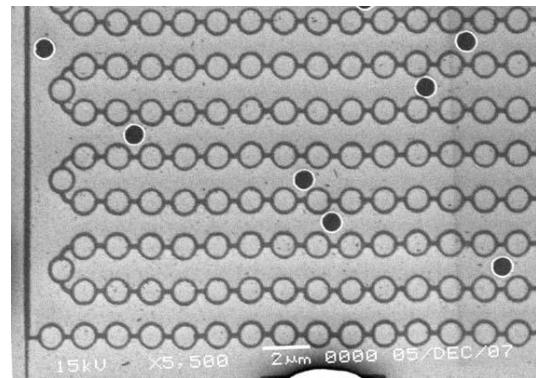


Fig.1. A fragment of structure consisting of 667 asymmetric rings with diameter of 1 μm (upwardly) and typical rectified voltage oscillations in magnetic field when white noise current is applied (below).

1. S.V. Dubonos, V.I. Kuznetsov, I.N. Zhilyaev, A.V. Nikulov, and A.A. Firsov, "Observation of the External-ac-Current-Induced dc Voltage Proportional to the Steady Current in Superconducting Loops". *JETP Letters*, **77**, pp. 371–375, 2003.
2. A.A. Burlakov, V.L. Gurtovoi, S.V. Dubonos, A.V. Nikulov, and V.A. Tulin, "Little–Parks Effect in a System of Asymmetric Superconducting Rings". *JETP Letters*, **86**, pp. 517–521, 2007.
3. V.L. Gurtovoi, S.V. Dubonos, A.V. Nikulov, N.N. Osipov and V.A. Tulin, "Dependence of the magnitude and direction of the persistent current on the magnetic flux in superconducting rings". *JETP*, **105**, pp. 1157–1173, 2007.
4. V.L. Gurtovoi, S.V. Dubonos, S.V. Karpi, A.V. Nikulov, V.A. Tulin, "Contradiction between the Results of Observations of Resistance and Critical Current Quantum Oscillations in Asymmetric Superconducting Rings". *JETP*, **105**, pp. 257–262, 2007.
5. V.L. Gurtovoi, S.V. Dubonos, A.V. Nikulov, N.N. Osipov and V.A. Tulin, "Calibration of quantum detector of noise based on a system of asymmetric superconducting loops", the *Proceedings of SPIE Vol. 6260, Micro- and nanoelectronics – 2005*, edited by Kamil A. Valiev and Alexander A. Oplikovskii, pp. 62600T1–62600T8, 2006.
6. A.A. Burlakov, V.L. Gurtovoi, A.I. Ilin, A.V. Nikulov, V.A. Tulin, Possibility of persistent voltage observation in a system of asymmetric superconducting rings. *Phys. Lett. A* **376**, pp. 2325–2329, 2012.

Magnetic dependencies of critical current of aluminium and tantalum ring with asymmetric link-up of current leads

A.V. Burlakov, A.V. Chernykh, V.L. Gurtovoi, A.I. Ilin, G.M. Mikhailov, A.V. Nikulov, and V.A. Tulin

Institute of Microelectronics Technology, Russian Academy of Sciences, 142432 Chernogolovka, Moscow Region, Russia. E-mail: nikulov@iptm.ru

A superconducting quantum interference device (SQUID) has provided the highest sensitivity of magnetic flux for several decades. It is based on a closed superconducting loop with one (rf SQUID) or two (dc SQUID) Josephson junctions [1]. Since the supercurrent through a Josephson junction is $I = I_c \sin \Delta\varphi$ and $\Delta\varphi + 2\pi\Phi/\Phi_0 = 2\pi n$ [2], measurable quantities vary from minimum to maximum values on a scale of $\Phi_0/2$. Here $\Delta\varphi$ is the phase difference at the Josephson junctions; Φ is the magnetic flux through the loop; $\Phi_0 = 2\pi\hbar/q$ is the flux quantum; $q = 2e$ is the charge of electron pair; n is the quantum number. Recently a idea of a SQUID without Josephson junctions and with a more sharp dependence of measurable parameters on the magnetic flux was proposed [3]. The idea is based on the effect discovered by V.A. Little and R.D. Parks [4]. The Little-Parks oscillations are observed because of the change of the velocity of the Cooper pairs

$$\oint dl v = \frac{2\pi\hbar}{m} \left(n - \frac{\Phi}{\Phi_0} \right) \quad (1)$$

and the persistent current $I_p = sqn_s v$.

The critical current of superconducting ring equals

$$I_{ext,c} = I_{c0} + \frac{l}{l_{long}} I_p \quad (2)$$

at asymmetric link-up of current leads, when $(l_{long} - l_{sh})l_{long}/l^2 \geq I_{p,A}/I_{c0}$ [3]. Here I_{c0} is the critical current when the persistent current $I_p = I_{p,A}2(n - \Phi/\Phi_0)$ equals zero; $I_{p,A}$ is the absolute value $|I_p| = I_{p,A}$ of the persistent current at $|n - \Phi/\Phi_0| = 0.5$; l_{long} and l_{sh} is

the length of the long and short segments of the ring with the total length $l_{long} + l_{sh} = l = 2\pi r$. The critical current should change by jump on $(l/l_{long})2I_{p,A}$ with n at $\Phi \approx (n + 0.5)\Phi_0$ because the quantum number n is integer. The idea of the new type of SQUID is based on this unquestionable prediction of quantum theory. But even unquestionable prediction should be verified experimentally. First results of the verification will be presented in this work, see typical magnetic dependence of the critical current on Fig.1.

1. B.B. Schwartz and S. Foner (Ed.), *Superconductor Applications: SQUIDs and Machines*, Plenum, New York, 1977.
2. A. Barone and G. Paterno, *Physics and Applications of the Josephson Effect*. Wiley, New York, 1982.
3. A.A. Burlakov, V.L. Gurtovoi, A.I. Il'in, A.V. Nikulov, and V.A. Tulin, "Superconducting Quantum Interference Device without Josephson Junctions". *JETP Letters*, **99**, pp. 169–173, 2014.
4. W.A. Little and R.D. Parks, Observation of Quantum Periodicity in the Transition Temperature of a Superconducting Cylinder. *Phys. Rev. Lett.* **9**, pp. 9–12, 1962.

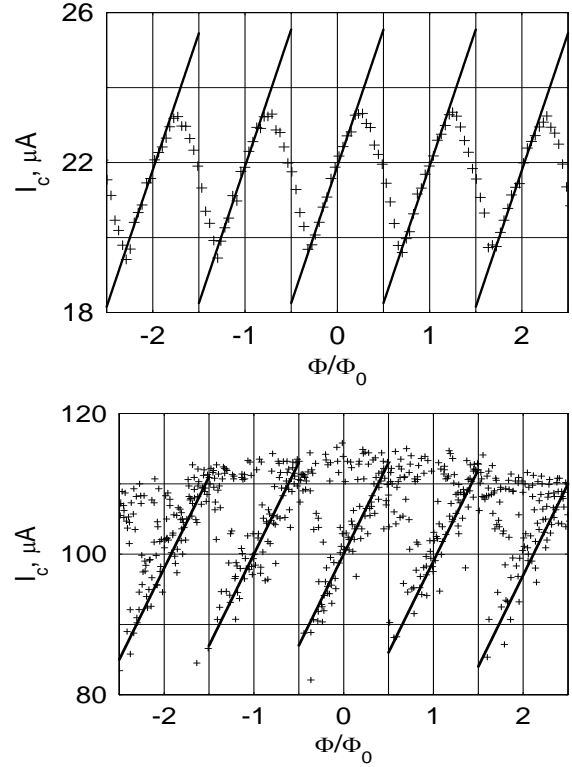


Fig.1. Magnetic dependence of the critical current of aluminium (upwardly) and tantalum (below) rings with asymmetric link-up of current leads. The crosses (+) indicate results of measurements, the lines – theoretical prediction (2). Sizes of the rings: aluminium $r \approx 1 \mu\text{m}$, $l_{long} \approx 1.2\pi r$, $l_{sh} \approx 0.8\pi r$; tantalum $r \approx 0.5 \mu\text{m}$, $l_{long} \approx 1.4\pi r$, $l_{sh} \approx 0.6\pi r$.

The quantum-size Si dots in Si/SiO₂ multilayers via direct wafer bonding

A. Gismatulin¹, G. Kamaev¹, V. Volodin^{1,2}, S. Cherkova¹, A. Antonenko^{1,2}

1. Rzhzanov Institute of Semiconductor Physics SB RAS, 630090 Novosibirsk, Russia.

2. Novosibirsk State University, 630090 Novosibirsk, Russia.

In recent years the attention of researchers was attracted by promising components for nanoelectronics, which called memristor. As many studies show, the memristor characteristics are determined primarily by the architecture of layers and material elements [1]. Memristor switching from a high resistance state (HRS) to a low resistance state (LRS) can be performed by the electric field or by changing of temperature. The metal-insulator-metal structure is most commonly used as the basis of memristor electronic devices. This structure is easily integrated into silicon technology, but such structure is operated at range 0-0.3 V. In this paper we used the structure of Si/SiO₂ with Si nanoclusters. In such structure the conduction channel might be composed of nanoclusters rather than a continuous filament, especially in the HRS.

In the present study, Si/SiO₂ multilayer nanoscale structures, which consist of alternating ultrathin layers of a-Si:H and SiO₂, were obtained on high doped n-type silicon substrates (resistivity of 0.002 Ω·cm) and p-type silicon substrates (resistivity of 0.003 Ω·cm), using a procedure of amorphous silicon (α-Si:H) thin film PECVD and subsequent partial plasma enhanced oxidation in the plasma-chemical reactor with a wide aperture source. Subsequently the plates with deposited layers after the standard processes of surface cleaning and hydrophilization are connected in deionized water and are passed multistage heat treatment. The final stage of direct bonding was held at 1050 °C. As the result of those operations we obtained double-barrier diode structures with silicon nanoclusters built in insulator (Fig. 1). Finally, mesas were formed with size of 5×5 mm².

Photoluminescence (PL), optical FTIR absorption, Raman scattering and cross-sectional high resolution electron microscopy (HREM) were used for the characterizations. The electrical properties of multilayer nanostructures were studied by the measurements of their capacitance-voltage (C-V), conductance-voltage (G-V), and current-voltage (I-V) characteristics. The C-V and G-V characteristics were studied in the frequency range 1 kHz – 1 MHz by using an automated Agilent E4980A multifrequency LCR-Meter.

Switching from the HRS to the LRS was performed by the electric field. The applied electric field has charged electronic states in nanoclusters. To switch back, we must discharge the states in nanoclusters. For this discharge one can use applied electric field of a reverse polarity and thermal heating.

This work is supported by Federal Program for 2014 years, contracts number 2.3 and 3.3.

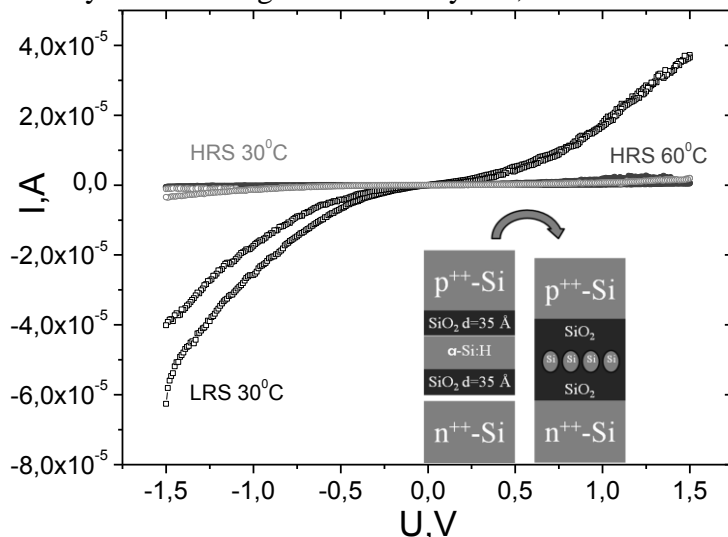


Fig. 1. I-V characteristics for double-barrier diode structures in HRS and the LRS at temperatures: 30 °C, 60 °C.

1. J.J. Yang, D.B. Strukov, and D.R. Stewart. "Memristive devices for computing". Nature Nanotechnology, **8**, pp. 13-24, 2013.

Noise properties of SET transistor made from highly doped SOI

D.E. Presnov^{1,2}, S.V. Amitonov¹, V.I. Rudakov⁴, S.V. Lotkhov³, A.B. Zorin^{2,3}, V.A. Krupenin¹

1. *Laboratory of Cryoelectronics, Moscow State University, 119899 Moscow, Russia,*
vladimir.krupenin@phys.msu.ru

2. *Nuclear Physics Institute, Lomonosov Moscow State University, 119899 Moscow, Russia*

3. *Physikalisch-Technische Bundesanstalt, 38116 Braunschweig, Germany*

4. *Institute of Physics and Technology (Yaroslavl Branch), RAS, 150007 Yaroslavl, Russia*

The single electron tunneling (SET) transistor without conventional tunnel barrier junctions were fabricated from preliminary prepared highly doped silicon on insulator (SOI) film. The doping level of the SOI film was sufficiently high, viz. about 10^{20} cm⁻³. The fabrication method of the SOI-film-based SET structures included As ion implantation, rapid annealing at 925° C, e-beam lithography for the structure patterning, forming a metal mask by the evaporation of Al thin film, reactive-ion etching of SOI film through the formed metal mask. The final trimming of the shape of the structures was realized in the upper silicon layer with the help of repeated processes of isotropic etching in fluorine-containing plasma with intermediate control of electric parameters at temperature $T = 77$ K. Significant suppression of conductivity in the “weak” areas of transistor junctions was also achieved in these processes by means of narrowing of the bridges connecting the transistor island with the source and drain electrodes. The size of resulting island was about 70 nm by 50 nm.

More detailed characterization of our SET transistors was performed in a dilution refrigerator at the bath temperature $T = 15$ mK, i.e. much below the characteristic Coulomb temperature E_C/k_B of the SET transistors. Transport characteristics have been measured at a fixed voltage between the source and drain electrodes and current measurements at different gate voltages. Stability diagram of the transistor, showing (quasi)periodic dependence of Coulomb blockade voltage V_c on the gate voltage V_g , was also measured. The peculiarity of the SOI-based SET transistors with such unusual resistive junctions was a nonlinear dependence of current in the region of small bias voltage (100-200 μ V) clearly observed at the maximum conductance (i.e. in the open state). Interestingly that similar nonlinear behavior of the $I(V)$ -curve was observed earlier in metallic (Al) SET transistors with resistive elements (pieces of high-ohmic Cr film) used instead of tunnel junctions [1].

Spectral density of current fluctuations, having frequency behavior roughly $1/f$, were measured in the frequency range from 0.5-250 Hz at $V \approx V_c$ in different working points of the modulation curve $I(V_g)$. At the point of maximum slope $|\partial I/\partial V_g|$ the measured noise was significantly higher than in the points with a minimum slope $|\partial I/\partial V_g| \approx 0$, i.e. for minimum and maximum currents, indicating the dominant role of charge fluctuations over other sources of noise (including shot noise, fluctuations of the junction conductance, etc.). This behavior is typical for conventional metallic SET transistors with Al/AIO_x tunnel junctions, but different from that observed in Si SET transistors reporter in Ref. [2]. Minimum level of the transistor charge noise (1.6×10^{-4} e/Hz^{1/2} at 10 Hz) was measured at the transport current $I = 0.5$ nA and bias voltage $V = -2$ mV. The data showed a trend of smooth increase of the charge noise while increasing the transport current, which is typical for conventional metallic SET transistors. For example, the increase in transport current up to 3 nA led to the charge noise value 2.5×10^{-4} e/Hz^{1/2} at 10 Hz. Thus, the studied transistors showed substantially better quality than the transistors in Ref. [2]. This may be related to the implantation of the SOI film by heavier ions of As⁺ instead of P⁺, which gave the possibility to use substantially lower accelerating voltage of 6 kV (instead of 50 kV) and further rapid thermal annealing. It is likely that our way of processing SOI film resulted in appreciably smaller amount of defects exhibiting two-level-fluctuator behavior usually leading to enhanced charge fluctuations.

The achieved parameters of our SOI-based transistors, together with the possibility of their integration in silicon technology, allow considering these SET transistors as possible ultrasensitive sensors for scanning probe systems with nanometer spatial resolution.

The work was supported by grant from the Russian Foundation for Basic Research (14-07-00828).

1. V.A. Krupenin, A.B. Zorin, M.N. Savvateev et al. "Single-electron transistor with metallic microstrips instead of tunnel junctions". *J. Appl. Phys.*, **90**, pp. 2411–2415, 2001.
2. V.A. Krupenin, D.E. Presnov, V.S. Vlasenko. "Charge noise in a single-electron transistor based on highly doped silicon-on-insulator". *Rus. Radiotechnika*, **1**, pp. 78–83, 2008.

Unified description of I-V characteristics in field-effect and bipolar transistors based on current density continuity equation solution

G.I. Zebrev

National Research Nuclear University (MEPhI), Moscow, Russia, gizebrev@mephi.ru

Any types of microelectronic devices such as field-effect (FET) or bipolar (BJT) transistors are in fact inhomogeneous structures with output current modulated by external electrodes. Hence, in contrast to homogeneous materials, such as metals, the electric condition should be generally described by the joint solution of the Poisson equation and the current density continuity equation. This approach as applied to field-effect devices has been proposed in [1] and consistently realized for different types field-effect devices including graphene FETs [2], SOI and double-gate transistors [3], and molybdenite MoS₂ monolayer transistor [4]. A unified similar approach for field-effect and bipolar transistors is proposed in this report. Non-uniformity of the structures and space charge effects implies a significant role of non-uniformity of electron (or, hole) density and, hence, of the diffusion component of the total diffusion-drift current. It has been shown in [1] that the diffusion to drift current ratio is imposed in field-effect transistors by the electric charge neutrality condition of the whole structure along the channel. It was shown here that a similar ratio in BJTs arises as a consequence of requirement of smallness of majority carrier in the quasi-neutral transistor's base. This allows describing I-V characteristics in the FETs and BJTs in a unified way based on a solution of current continuity equation in the channels and in the bases.

Current density continuity equation's approach implies (especially in nano-scaled FETs) importance of dependence of effective mobility on driving electric field in the channels. Partially it was realized in early work [5]. Here we intend to present an exact solution of continuity equation in FET taking into account the effects of high-field carrier's saturation velocity in a rigorous manner. Two modes of saturation current in MOSFETs are discussed. Generally, the drain current at a given source-drain voltage is represented as a functional of distribution of electric field along the channel which can be derived with solving of current continuity equation.

1. G.I. Zebrev, R.G. Useinov, "Simple model of current-voltage characteristics of a metal-insulator-semiconductor transistor", *Sov. Phys. Semiconductors*, **24**, pp. 491-493, 1990.
2. G.I. Zebrev, "Graphene Field-Effect Transistors: Diffusion-Drift Theory," Chap. in *Graphene, Theory, Research and Applications*, Intech, 2010; "Small-Signal Capacitance and Current Parameter Modeling in Large-Scale High-Frequency GFETs," *IEEE Trans. Electron. Dev.* **60**, pp. 1799-1806, 2013.
3. G.I. Zebrev et al., "Compact Physical Modeling of Fully Depleted SOI MOSFET," *Proc. SPIE*. 2006. Vol. 6260.
4. G. Sheredeko et al., "Modeling electrostatics of double gated monolayer MoS₂ channel FETs," *MIEL 2014 Proc.*, pp. 107-109.
5. G.I. Zebrev, "Current-voltage characteristics of a metal-oxide-semiconductor transistor calculated allowing for the dependence of mobility on longitudinal electric field," *Sov. Phys. Semiconductors*, **26**, pp. 47-49, 1992.

SOI VLSI Layout Decomposition for Double Patterning Lithography on High-Performance Computer Platforms

V. Verstov¹, L. Zinchenko², V. Makarchuk³

1. Bauman Moscow State Technical University, Moscow, Russia, E-mail: v.verstov@gmail.com

2. Bauman Moscow State Technical University, Moscow, Russia, E-mail: lyudmillaa@mail.ru

3. Bauman Moscow State Technical University, Moscow, Russia, E-mail: vvmakarchuk@gmail.com

Currently, double and multiple patterning technologies are going to be used with extreme ultraviolet lithography (EUV) simultaneously [1]. For the double and multiple patterning technologies VLSI layouts are decomposed into two or more masks. However, high-performance computing platforms are requires for SOI VLSI layout decomposition for double patterning technology because of non-Manhattan layout and huge size of layout data file. Parallel algorithms are required for these computing systems.

Special techniques are requiring handling a non-Manhattan SOI layout including multi-gate transistors with circular structure. We propose a special data structure for the concurrent VLSI layout processing. The VLSI layout represents a set of polygons. Each polygon consists of a set of segments. Each segment is stored as two references to boundary points. Every point is stored in the “events points” array. This data structure allows us to describe non- Manhattan layout.

Our approach is based on the use of a contradiction graph and a modified concurrent breadth-first search algorithm [2]. The proposed approaches were implemented using C++ programming language on Cent OS 5.5 operating system. Additionally, we use the Boost libraries and the OpenMP framework.

In [3] the relative minimal distance between the polygons after the decomposition that is calculated as the ratio of the minimal distance between the polygons of the layer i ($i = 1, 2$) after the decomposition to the minimal distance in the critical layer before the decomposition has been chosen as a fitness function. We discuss our experimental results for test layouts. In average, the minimal distance between the polygons in the layer for all our tests is increased above 35%. It is obvious that the reproducibility of the critical layout layer will be better in a comparison with the initial design. However, this improvement strongly varies for several test cases, from the minimum of 10% for the memory cell to 80% for the adder. In addition, this parameter varies for layers (Layer 1 and Layer 2) that were created after layout decomposition for double patterning. This deficiency has to be overcome to increase yield.

We conclude that the novel layout decomposition algorithm to address design needs for radiation hardened layout design has proposed. It was shown that our approach practically and effectively improves layout quality. It has been implemented using the contradiction graph and our modified concurrent breadth-first search algorithm. Our soft computing approach to manage contradictions in the layouts is novel and has advantage in terms of adaptability. Another aspect of our research is the use of high performance computing platforms for our design iterations. Our experiments using artificial and real-world test cases indicate that minimal distance is increased for all test cases.

Our ongoing research is in the following directions. The irregularity of layouts after decomposition results in lower yield. We discuss our preliminary decomposition optimization results.

This study was partially supported by the Program of the President of the Russian Federation for the Support of Leading Scientific Schools, project LS-2903.2014.9 and Russian Fund for Basic Research, project 13-07-0073-a and 14-07-31074 mol_a.

1. K. Oyama, S. Yamauchi, S. Natori, et al. "Robust complementary technique with multiple-patterning for sub-10 nm node device". Proc. SPIE **9051**, *Advances in Patterning Materials and Processes XXXI*, 90510V, 2014.
2. V.A. Shakhnov, L.A. Zinchenko, V.A. Verstov. "Parallel Algorithm of SOI Layout Decomposition for Double Patterning Lithography on High-Performance Computer Platforms". *Technological Innovation for Collective Awareness Systems*, **423**, pp. 543-550, Springer, 2014.
3. V.A. Shakhnov, L.A. Zinchenko, V.A. Verstov. "Topological Transformation of Submicron VLSIs for Double Lithographical Mask Technology". *Russian Microelectronics*, **42** (6), pp. 427–439, 2013.

Quantum and classical correlations in a system of interacting spins in an external magnetic field

E.B. Fel'dman

Institute of Problems of Chemical Physics, Chernogolovka, Russia, efeldman@icp.ac.ru

An investigation of correlations of different subsystems of many-particle systems is very important in many problems of statistical physics. In the information context, two systems are correlated if each of them contains information about the other. Classical correlations between subsystems do not change after measurements. However, quantum correlations can change as a result of a measurement. One can say that a part of the information was lost when the measurements were performed. According to the current point of view the mutual quantum information describes the total correlation between subsystems of a system [1, 2]. The correlations between two subsystems are absent if and only if the mutual quantum information is zero [3]. The reverse statement is also true [3]. The Bayes equation allows us to rewrite the mutual quantum information through the quantum conditional entropy. Both expressions for the mutual quantum information are equivalent for classical systems but can be different for quantum ones. The difference of the two expressions for the mutual quantum information is called the quantum discord and can be interpreted as the extent of the “quantumness” of the system. The quantum discord characterizes quantum correlations of subsystems of a quantum system. The quantum discord is responsible for the performance of quantum devices and gives them advantages over their classical counterparts [4].

An investigation of the quantum discord is a very difficult problem. It involves both technical difficulties at the calculation of the quantum discord and a subtle physical interpretation of the obtained results. Systems of interacting nuclear and electron spins are very suitable for investigations of quantum correlations. Those model systems have deep connections with the existing experimental technique of magnetic resonance [5] which creates a powerful experimental base for the study of quantum correlations.

We developed [6] analytical and numerical methods for calculations of the quantum discord in two-partite many-qubit systems where one part consists of only one spin and is used in all projective measurements. Our numerical approach is based on the random mutation algorithm [6] which is a modification of the simplified genetic optimization. Our analytical solution is obtained for the quantum discord in a two-partite three-qubit system in the high temperature approximation [5]. It turns out that the maximal value of the quantum conditional entropy depends on the relation between the Larmor frequencies of the subsystems of the system under consideration. As a result, the quantum discord also depends on that relation. We connect quantum correlations with the correlations between interacting spins at different Larmor frequencies. The evolution of the quantum discord (quantum correlations) is investigated both at low and high temperatures. In all cases we compare quantum and classical correlations in the course of the evolution of the spin system.

The work is supported by the Russian Foundation for Basic Research (Grants № 13-03-00017 and № 13-03-12418) and Program №8 of the Presidium of RAS.

1. H. Ollivier, W.H. Zurek. “Quantum discord: a measure of the quantumness of correlations”. *Phys. Rev. Lett.*, **88**, 017901 (4 pp.), 2001.
2. L. Henderson, V. Vedral. “Classical, quantum and total correlations”. *J. Phys. A: Math. Gen.*, **34**, pp. 6899-6905, 2001.
3. S.M. Aldoshin, E.B. Fel'dman, M.A. Yurishchev. “Quantum entanglement and quantum discord in magnetoactive materials”. *Low Temp. Phys.* **40**, pp. 5-21, 2013.
4. A. Datta, A Shaji, C.M. Caves, “Quantum discord and the power of one qubit”. *Phys. Rev. Lett.* **100**, 050502 (4 pp.), 2008.
5. A. Abragam. *The principles of nuclear magnetism*. Clarendon Press, Oxford, 1961.
6. A.Y. Chernyavskiy, S.I. Doronin, and E.B. Fel'dman. "Bipartite quantum discord in a multiqubit spin chain". *Phys. Scr.*, **T160**, 014007 (5 pp), 2014.

Antiferromagnetic anisotropic XXZ chain of spins $S=1/2$ in the presence of an inhomogeneous transverse magnetic field as a basis for the multiqubit quantum register simulation

A.A. Kokin¹, V.A. Kokin²

1. Institute of Physics and Technology of RAS, Moscow, Russia

2. Institute of Radioengineering and Electronics of RAS, Moscow, Russia

Antiferromagnetic anisotropic chain of $N \gg 1$ spins $1/2$ with anisotropy parameter Δ (XXZ model) at low temperature and in the presence of transverse magnetic field $B(x)$ with constant field gradient $\partial B(x)/\partial x = G$ along the chain (x – axis) has been considered.

Hamiltonian of the spin chain was formulated in spin-wave approximation. Assuming that value of field gradient is small and using the method of asymptotic expansion for coefficients of unitary transformation in terms of the field gradient, one obtains the diagonal form of spin Hamiltonian. As a result, the description of virtual spin wave propagation in entire antiferromagnetic spin chain near ground state was obtained. The energy of ground state for chain has received in relation to the value of anisotropy parameter both for gapped ($\Delta > 1$) and for gapless ($\Delta < 1$) cases, in different external fields.

For study of the local properties of spin chains the relatively simple approach based on reduced density matrix for the pair of allocated neighboring spins was used. The matrix elements of reduced density matrix are determined by not only the correlations inside of the spin pair, but they also depend through virtual spin wave states on correlations between the spin pair and the rest part of the entire chain. By using elements the reduced matrix the local energy of ground state, local spin polarization and local toroidal magnetic moment of spin chain were found. The local concurrence was chosen as a measure for local entanglement of quantum states related to spin pair near ground state. Its value was found both for gapped and for gapless cases of the XXZ model. The similar spin chain model only for the gapped case ($\Delta > 1$) has been considered early in paper [1].

Finally, the local concurrence as a parameter of nondiagonal order in quantum phase transition has been investigated.

The one dimension chain of $N \gg 1$ particles with spin $S = 1/2$ being studied is usable as a basis for simulation of different linear multiqubit quantum register, constructed, in particular, on electron and nuclear spins.

1. A.A.Kokin, Proceed. Inst. Phys. Techn. RAS, Vol 24, 2014 (in Russian)

Using radio-frequency electric field to enhance Rydberg atom interaction

D.B. Tretyakov¹, V.M. Entin¹, E.A. Yakshina^{1,2,3}, I.I. Beterov^{1,2}, C. Andreeva^{4,5}, and I.I. Ryabtsev^{1,2,3}

1. *Institute of Semiconductor Physics, Novosibirsk, Russia, E-mail: dtret@isp.nsc.ru.*

2. *Novosibirsk State University, Novosibirsk, Russia*

3. *Russian Quantum Center, Skolkovo, Moscow Region, Russia*

4. *University of Latvia, Riga, Latvia*

5. *Institute of Electronics, Sofia, Bulgaria*

Long-range interactions between highly-excited Rydberg atoms have been proposed for use in a quantum computer based on trapped neutral atoms [1]. To achieve fast two-qubit quantum gates the energy of Rydberg atom interaction should be as large as possible. There are van der Waals or dipole-dipole interactions with different dependences on interatomic distance R (R^{-6} and R^{-3} , correspondingly). Atoms in an identical Rydberg state generally interact via van der Waals interaction, which is much weaker than dipole-dipole interaction at long distances (longer than the Rydberg atom size).

To make identical atoms interact via dipole-dipole interaction, the Rydberg state should be tuned exactly midway between two other Rydberg states of the opposite parity to induce a Förster resonance. It can be tuned using the Stark effect in a dc electric field. The Rydberg states of the opposite parity should be neighboring to initial Rydberg state because dipole moments of transitions between neighboring Rydberg states are larger than between not neighboring ones. However Stark-tuned Förster resonances between neighboring Rydberg states can be obtained for a limited number of Rydberg states. For example, in Rb atoms the Stark-tuning method works for $nP_{3/2}$ states with $n \leq 38$, for $nD_{3/2}$ states with $n \leq 40$, and for $nD_{5/2}$ states with $n \leq 43$ (n is a principal quantum number of the initial Rydberg state).

The dipole-dipole interaction energy depends on a principal quantum number of Rydberg state as n^4 . So for quantum computer one should use Rydberg states as high as possible. In this report we propose to use radio-frequency electric field for inducing "inaccessible" Förster resonances, which cannot be tuned by a dc electric field. It leads to an efficient transition from van der Waals to dipole-dipole interaction. Radio-frequency photons compensate for the energy defect and can provide the tunability of Förster resonances in a wide range of n .

We demonstrate this technique experimentally. The process under study is the Förster resonant energy transfer $\text{Rb}(39P_{3/2}) + \text{Rb}(39P_{3/2}) \rightarrow \text{Rb}(39S_{1/2}) + \text{Rb}(40S_{1/2})$ due to dipole-dipole interaction of a few cold Rb Rydberg atoms in a small laser excitation volume. Experiments were performed with cold ^{85}Rb atoms in a magneto-optical trap. Small Rydberg excitation volume of 30-40 μm size was formed using crossed-beam geometry of exciting laser beams [2]. The energy detuning of this resonance $\Delta = E(39S_{1/2}) + E(40S_{1/2}) - 2E(39P_{3/2})$ was controlled by a weak dc electric field. The dc electric field increases Δ and the resonance could be induced only by the radio-frequency field. Scanning the dc electric field, radio-frequency assisted Förster resonances were obtained for 90, 95, and 100 MHz frequency of the radio-frequency field. Experimental data is compared with numerical simulation results. Radio-frequency assisted Förster resonances are interpreted as intersections of the Floquet sidebands of Rydberg levels appearing in the radio-frequency field.

This work was supported by RFBR (Grant Nos. 13-02-00283 and 14-02-00680), by the Russian Academy of Sciences, by the EU FP7 IRSES Project "COLIMA", and by the Russian Quantum Center.

1. D. Jaksch *et al*, "Fast quantum gates for neutral atoms", *Phys. Rev. Lett.*, **85**, pp.2208-2211, 2000.
2. I.I. Ryabtsev *et al*, "Observation of the Stark-Tuned Förster Resonance between Two Rydberg Atoms", *Phys. Rev. Lett.*, **104**, p.073003, 2010.

Quantum diamond chip under network optical control

A.V. Tsukanov, I.Yu. Kateev, N.A. Orlikovsky, A.A. Orlikovsky

Institute of Physics and Technology, Russian Academy of Science, Moscow, Russia, ikateyev@mail.ru

We propose a structure (Fig. 1) and elements of the diamond chip fabrication technology, which could be used for an experimental study of the spectral and dynamic properties of a quantum register prototype formed by a chain of microresonators (disks and rings) containing NV-centers. Making use of the parameters of NV-systems today exist, we simulate the dissipative population dynamics of two NV-centers located in different parts of the two-qubit register. As follows from our numerical results, high probability of controlled indirect qubit interaction via photon transfer from one center to another can be already achieved at the current diamond photonics technology level. The calculated operating parameters of the resonators and measuring structure (grating) are in good agreement with those that have been used in devices created by leading world science groups. The fabrication technique of lithographic mask is discussed and its roughness is estimated.

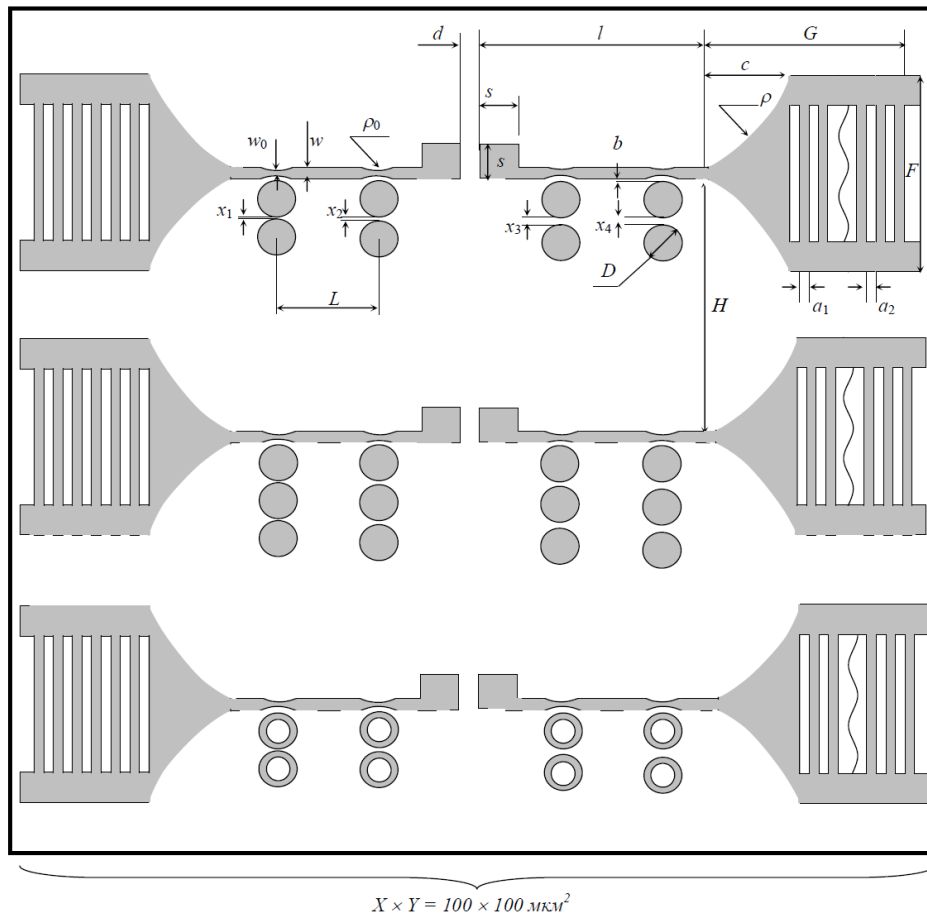


Figure 1. The solid-state diamond quantum chip. Parameters: $x_1 = 80 \text{ nm}$, $x_2 = 100 \text{ nm}$, $x_3 = 120 \text{ nm}$, $x_4 = 150 \text{ nm}$, $D = 5 \text{ }\mu\text{m}$, $L = 3D$, $H = 30 \text{ }\mu\text{m}$, $d = 4 \text{ }\mu\text{m}$, $w = 2 \text{ }\mu\text{m}$, $b = 80 \text{ nm}$, $l = 32 \text{ }\mu\text{m}$, $c = 4 \text{ }\mu\text{m}$, $\rho_0 = 2.58 \text{ }\mu\text{m}$, $G = 12 \text{ }\mu\text{m}$, $F = 20 \text{ }\mu\text{m}$, $s = D$. Microrings: width $r_2 - r_1 = 300 \text{ nm}$, outer radius $r_2 = 2 \text{ }\mu\text{m}$, thickness $h = 500 \text{ nm}$. Substrate thickness (SiO_2) $2 \text{ }\mu\text{m}$. Grating: $a_1 = 125 \text{ nm}$, $a_2 = 138 \text{ nm}$, diamond slab number $N = 20$.

Quantum register in a field-effect transistor channel

M. Rudenko¹, V. Vyurkov^{1,2}, S. Filippov^{1,2}, A. Orlikovsky^{1,2}

1. Institute of Physics and Technology RAS, Moscow, Russia

2. Moscow Institute of Physics and Technology (State University), Moscow, Russia
vyurkov@ftian.ru

Recently, a novel implementation of a solid-state quantum computer based on space states in field-defined double quantum dots (one electron in two adjacent dots) in an ultrathin silicon bar was proposed [1]. To some extent, the structure reminds that of the fin-FET with a number of individual gates. Therefore, the construction follows a natural way of nanoelectronics. Scalability is audible and it opens up a possibility of large-scale quantum computer.

The potential profile confining electrons is created by gates (Fig. 1, upper part). The quantum information can be encoded and processed without charge transfer between dots (every dot contains half of an electron, at that, all electrons are spin-polarized) [2]. Quantum algorithms could be effectuated via manipulation with gate potentials acting only on phase state of qubits. After that the result must be decoded into the basic charge states of qubits (whether an electron inhabits the left dot or the right one). The read-out could be performed via a transmission of current through the channel in a regime of Coulomb blockade. Worth noting during quantum computation the current is switched off and has no influence on a qubit evolution.

To calculate an electron wave function in a double quantum dot the self-consistent solution of 3D Schrödinger and Poisson equations modified for a *single electron* was fulfilled. It allows for the field of image charges in metal gates but excludes the action of the own electron field on itself [3]. The structure corresponds to 10 nm technological node. The simulation of measurement was based on the Landauer-Büttiker formalism for the calculation of current. The transmission probability averaged over the Fermi-Dirac distribution for electrons moving through the channel vs. gate voltage applied to the measured dot was calculated (Fig. 2). It demonstrates the possibility to clearly distinguish between vacant and occupied dots. For example, one should apply 0.01 V for the measured dot and 0.15 V for all others.

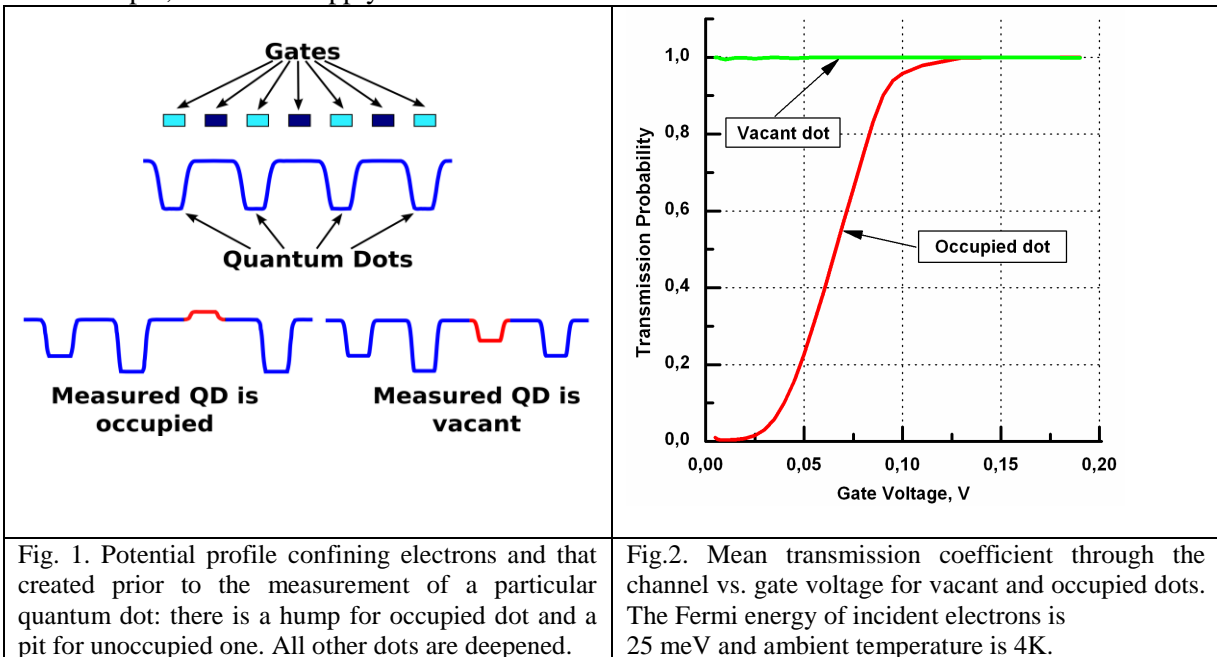


Fig. 1. Potential profile confining electrons and that created prior to the measurement of a particular quantum dot: there is a hump for occupied dot and a pit for unoccupied one. All other dots are deepened.

Fig.2. Mean transmission coefficient through the channel vs. gate voltage for vacant and occupied dots. The Fermi energy of incident electrons is 25 meV and ambient temperature is 4K.

1. S. Filippov, V. Vyurkov, and A. Orlikovsky. "Quantum computing on silicon-on-insulator structure", *Proc. EUROSOI-2011*, Granada, Spain, pp. 101-102, 2011.
2. V. Vyurkov, S. Filippov, and L. Gorelik. "Quantum computing based on space states without charge transfer". *Physics Letters A*, **374**, pp. 3285-3291, 2010.
3. V. Vyurkov, D. Svintsov. "Quantum single electron solitons near metal surface". <http://arxiv.org/abs/1308.3460>, 2013.

Graphene nanoelectronics for high-frequency and low-power applications

A. Orlikovsky, V. Vyurkov, D. Svintsov

Institute of Physics and Technology RAS, Moscow, Russia

Moscow Institute of Physics and Technology (State University) Moscow, Russia

orlikovsky@ftian.ru

Owing to its exceptional properties graphene is regarded as a promising material for nanoelectronics. A huge mobility is obviously beneficial for analog devices. As for digital (logic) circuits, for a long time the application of graphene was ambiguous due to the absence of the bandgap. Even the perfect graphene inserted into a field-effect transistor channel reveals its ambipolar nature and very strong scattering among carriers [1]. This does not allow achieving a sufficient ratio of on-state current to off-state current (ON/OFF) in gate characteristics and current saturation in drain characteristics. The band gap is opened in graphene nanoribbons, bilayers, and chemically modified graphene, however, its value (about 0.2 eV) is much lower than that in usual semiconductors.

Recently a *lateral* tunnel graphene field-effect transistor (FET) was proposed and simulated [2]. Here the source and drain graphene layers are separated by a short gap. This FET combines a high mobility of carriers in graphene for high-frequency performance with a superior ON/OFF ratio in gate characteristics and current saturation in drain characteristics peculiar to common semiconductor FETs. Both the potential barrier inside the gap and carrier densities in source and drain layers are controlled by the top and bottom gates. The gates could be either metallic or made of graphene too (Fig. 1), the latter construction utilizes the benefits of graphene interconnects and opens prospects to all-graphene digital circuits.

The drain characteristic of the proposed FET exhibits a distinct current saturation. This results from saturation of injection current through a thin part of the U-shaped tunnel barrier similar to that in Schottky barrier FETs. The calculated gate characteristics of the proposed transistor demonstrate an exponential tunability of current by gate voltage with subthreshold slope approaching $(60\text{mV/dec})^{-1}$ at room temperature (Fig. 2). Dependence of current on gate voltage in the proposed construction is much stronger than that in *vertical* graphene FETs [3]. The dc voltage applied to the bottom gate can shift the threshold voltage to quite low values. Moreover, the back gate voltage can induce either electron or hole accumulation in the same structure, hence, an analog of CMOS pair looks feasible. Besides, all-graphene circuits could be manufactured on a silicon wafer.

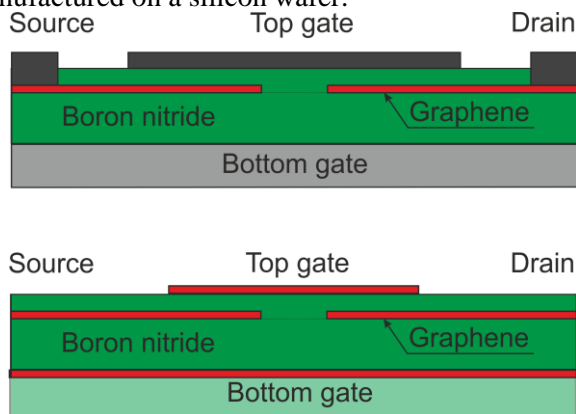


Fig. 1. Proposed structures of graphene tunnel FETs:
FET with metal gates (*top*) all-graphene FET
(*bottom*).

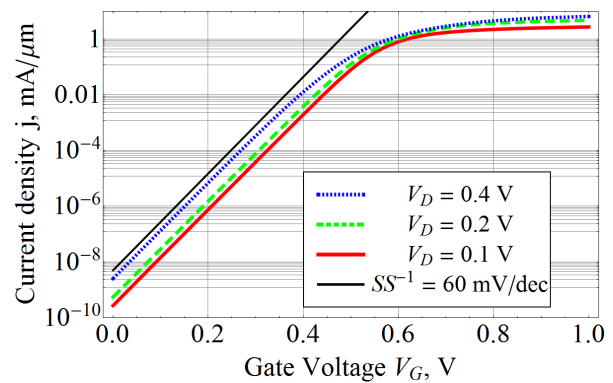


Fig. 2. Calculated gate characteristics of lateral graphene tunnel FET. The dotted line represents the limiting value of the subthreshold slope (SS) at room temperature.

1. D. Svintsov, V. Vyurkov, S. Yurchenko, T. Otsuji, and V. Ryzhii. "Hydrodynamic model for electron-hole plasma in graphene". *J. Appl. Phys.*, **111**, p. 083715, 2012.
2. D. Svintsov, V. Vyurkov, A. Orlikovsky, V. Ryzhii, and T. Otsuji. "All-graphene field-effect transistor based on lateral tunneling". *Journal of Physics D: Applied Physics*, **47**, p. 094002, 2014.
3. R. Britnell et al. "Field-effect tunneling transistor based on vertical graphene heterostructures". *Science*, **335**, pp. 947-950, 2012.

Macroscopic system with large quantum mechanical effect based on the fully depleted SOI transistors in asymmetric mode

V.P. Popov^{1,2}, M.A. Ilnitsky¹, O.V. Naumova¹

1. Institute of Semiconductor Physics, Novosibirsk, Russia, E-mail address popov@isp.nsc.ru

2. Tomsk State University, Tomsk, Russia

The main hopes in promoting silicon planar technology in the nanometer scale region of channel length of CMOS transistors are connected with fully depleted transistors on the structures of silicon-on-insulator (SOI) containing silicon layer and embedded dielectric layer thanks to the complete control of the charge in the channel (and thus drain current) by the voltage at its gate. However, the surface potential on both sides of the silicon layer in such transistors are not independent and are bound by the quantity of the charge induced by both upper usual and lower (from the substrate) gates. There is a "charge coupling" between upper gate and substrate, which manifests as a dependence of electrical characteristics of a silicon layer/dielectric film from the charge on the opposite gate and the voltage on the substrate [1].

The effect of the charge coupling is used in microelectronics in the development and operation of integrated circuits (IC) with variable threshold voltage for CMOS transistors. Change in the potential of the bottom gate as a substrate allows for ion-sensitive nanowire (NW) transistor to operate in subthreshold mode with exponential change in drain current from changes of surface potential induced by bioparticle as a virtual gate in the electrolyte of variable composition [2].

Using analytical and numerical calculations, as well as results of model simulations and experimentally identified values, we compare the threshold voltage V_{th} for lower gate (substrate) in fully depleted SOI n-MOS transistors on a low doped silicon layer with a thickness of 20-60 nm, depending on the value of the bias voltage of the upper polysilicon gate V_{bg} on the same gate dielectric thickness of 200 nm as a buried oxide (BOX). Matching experimental and computational dependencies was obtained for the values of the density of interface states ($>1 \times 10^{12} \text{ cm}^{-2}$) and charges ($>5 \times 10^{11} \text{ cm}^{-2}$) in dielectrics [2]. The results of calculation of threshold voltage V_{th} in comparison with experimental data obtained from the measurements of currents in FD SOI test transistors, as well as their thickness measurements for all layers in the cross sections of electron-microscopic images, showed that although accounting of quantum-size effects for 27 and 37 nm silicon layers slightly reduces the slope of a linear relationship, but significantly (by more than 2.4 and 1.2 V respectively) increases the interval of the linear dependence of threshold voltage especially for interface state density $>3 \times 10^{12} \text{ cm}^{-2}$.

The correct description of the range of voltages with a linear charge coupling effect between two gates can only be achieved by taking into account the quantum corrections even at silicon layer thickness of 60 nm. Such an unusually large thickness value for quantum effect in silicon is explained by electrostatically defined dimension quantization of channel thickness at high transverse electric field due to large difference between the potentials at two gates. Increase in the positive charge on the interface states with the negative bias increases the value of QM effect in 2-4 times due to the effect of quantum capacitance, which affects recharging the traps at the large difference of the potentials on the gates.

It is shown, that for all the studied silicon layer thicknesses maximum value of quantum corrections by electrostatic effect of transverse field dimension exceeds 0.4 V for the V_{th} (or 1-2 orders of magnitude for current flow) and must be taken into account in the development of modern IC on FD SOI transistors with an adjustable threshold voltage, as well as for biochemical sensors on SOI NW transistors.

Thus, new macrosystem based on thick (up to 60 nm) fully depleted SOI transistors with high quantum mechanical (QM) effect was found and investigated theoretically and experimentally. The QM correction of electrostatically enhanced dimensional effect is more pronounced in asymmetric working mode of the transistors with two independent gates.

1. T. Rudenko, A. Nazarov, V. Kilchytska, D. Flandre, V. Popov, M. Ilnitsky, V. Lysenko. Revision of interface coupling in ultra-thin body silicon-on-insulator MOSFETs. *Semiconductor Physics, Quantum Electronics and Optoelectronics*, **16** (3), pp. 299-314, 2013.

2. V.P. Popov, M.A. Ilnitsky, O.V. Naumova, A.N. Nazarov. "Quantum corrections to the threshold voltage for fully depleted SOI transistors with two independent gates". *Semiconductors*, **48** (10), pp. 1348-1353, 2014.

Graphene terahertz electronics and optoelectronics

V. Ryzhii¹, T. Otsuji¹, M. Ryzhii², V. Mitin³, M.S. Shur⁴

1. *Research Institute for Electrical Communication, Tohoku University, Sendai, Japan, v-ryzhii@iec.tohoku.ac.jp*

2. *Department of Computer Sci. and Eng., University of Aizu, Aizu-Wakamatsu, Japan, m-ryzhii@u-aizu.ac.jp*

3. *Department of Electrical Eng., University at Buffalo, Buffalo, USA, vmitin@buffalo.edu*

4. *Department of Electrical, Electron., and System Eng., Rensselaer Polytech. Institute, Troy, USA, shurm@rpi.edu*

The unique properties of graphene layers (GLs), particularly the gapless energy spectrum, relatively strong interband absorption, and pronounced plasmonic effects, provide opportunities to use different GL-based structures in novel active and passive terahertz and optoelectronic devices. The possibility to use for the inter-GL barriers such materials as *h*-BN, WS₂, and similar materials, opens up new prospects to create the devices with enhanced functional abilities.

We discuss the concepts of several terahertz and optoelectronic devices based on single-, double-, and multiple-GL structures:

- (i) Optical modulators, including those involving the resonant excitation of plasma oscillations;
- (ii) Terahertz and infrared lasers using the interband intra- and inter-GL transition;
- (iii) Interband and intraband detectors of terahertz and infrared radiation;
- (iv) Plasmonic resonant terahertz photomixers.

Some of such devices were proposed and realized by different research groups as well as by us and our collaborators. Using the developed models of these devices, we demonstrate the features of their operation and characteristics and the ultimate performance. We show that different terahertz and optoelectronic GL-based devices under consideration can markedly surpass and supplement the devices based on the heterostructures made of the standard semiconductors.

Plasmon-resonant terahertz emitters and detectors and their system applications

S. Boubanga Tombet¹, T. Otsuji¹, V. Popov², and W. Knap³

¹ Research Institute of Electrical Communication, Tohoku University, Japan

² Kotelnikov Institute of Radio Engineering and Electronics (Saratov Branch), RAS, Russia

³ TERALAB and L2C Laboratories, University of Montpellier&CNRS, France

This paper reviews recent advances in the development of plasmon-resonant terahertz (THz) emitters and detectors and their THz system applications. Two-dimensional (2D) plasmon resonance is introduced as the operation principle for broadband emission and detection of THz radiation. Two-dimensional plasmons in submicron transistors have attracted much attention due to their ability to promote emission and detection of electromagnetic radiation in THz range [1, 2]. Coherent plasmonic THz emission can be obtained by the plasma wave instability mechanisms like Dyakonov–Shur Doppler-shift model [1], but it suffers from incoherent broadband emission at 300K originated from thermally excited hot plasmons. On the other hand, hydrodynamic nonlinearities of 2D plasmons in high-electron-mobility transistors (HEMTs) are promising for fast and sensitive rectification/detection of THz radiation [2], which are suffering, however, from poor sensitivity in the case of grating-gate-type broadband antenna structures [3]. In order to cope with these problems, we propose an asymmetric, chirped-dual-grating-gate (AC-DGG) HEMT structure (see Figure 1) [3-8]. Numerical analysis reveals that, in comparison with conventional symmetric DGG structure, the asymmetric DGG exhibits substantially improved (by three to four orders of magnitude) THz detection sensitivity and emissivity [3-5]. We fabricated AC-DGG HEMT emitters and detectors using InAlAs/InGaAs/InP heterostructure materials. Excellent THz emission and detection performances including coherent monochromatic emission at frequencies above 1 THz [5] and the record detection responsivity of 6.4 kV/W at 1 THz [3, 6, 7] and 21.5 kV/W at 0.3 THz [8] were experimentally demonstrated. The fabricated AC-DGG HEMT detectors were used for nondestructive material evaluations (see Figure 1) based on THz imaging [3, 5] successfully reproducing the 2D images of the inside of an IC card, soap bars in a plastic bag, etc. Obtained results encourage to proceed with further industrialization of these plasmonic THz devices for sensing/imaging applications.

We thank D. Fateev, D. Coquillat, F. Teppe, G. Ducournau, Y.M. Meziani, H. Minamide, Y. Wang, H. Ito, Y. Kurita, K. Kobayashi, and Y. Tanimoto for their contribution throughout this work. This work was supported by JST-ANR WITH, JSPS-RFBR JPN-RUS joint program, and RFBR, Russia.

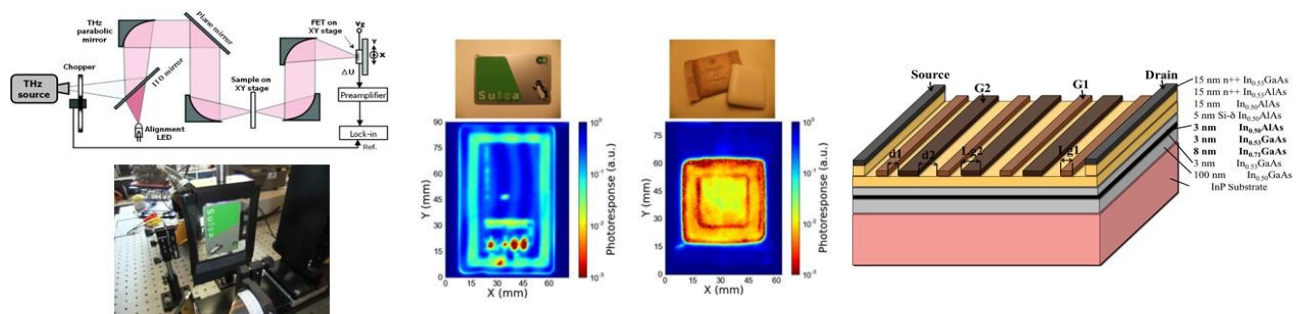


Figure 1. Left: Experimental setup for THz imaging utilizing the AC-DGG HEMT as a THz detector. The THz beam is focused on to the sample and raster-scanned to obtain a 2D image. Middle: Photo images and THz imaging of an IC card, and soap bar measured using the A-DGG HEMT detector [3]. Right: Schematic view for a fabricated AC-DGG HEMT using InP-based heterostructure material systems [6].

1. M. Dyakonov, M. Shur, Phys. Rev. Lett. **71**, p. 2465, 1993.
2. M. Dyakonov, and M. Shur, IEEE Trans. Electron. Dev. **43**, p. 1640, 1996.
3. T. Watanabe, S. Boubanga Tombet, et al. IEEE Sensors J. **13**, p. 89, 2013.
4. V.V. Popov, D.V. Fateev, T. Otsuji, et al., Appl. Phys. Lett. **99**, p. 243504, 2011.
5. T. Otsuji, T. Watanabe, S. Boubanga Tombet, et al., IEEE Trans. Terahertz Sci. Tech. **3**, p. 63, 2013.
6. S. Boubanga-Tombet, Yudai Tanimoto, Akira Satou, et al. Appl. Phys. Lett. **104**, p. 262104, 2014.
7. T. Otsuji, T. Watanabe, S. B. Tombet, et al., J. Opt. Eng. **53**, p. 031206, 2013.
8. Y. Kurita, G. Ducournau, D. Coquillat, A. Satou, et al. Appl. Phys. Lett. **104**, p. 251114, 2014.

Quantum-mechanical and continual models of magnetic dynamics for antiferromagnetic particles in analyzing Mössbauer spectra

I. Mischenko, M. Chuev

Institute of Physics and Technology, Russian Academy of Science, Moscow, Russia, mishchenko@ftian.ru

Since the early beginning of Mössbauer spectroscopy till nowadays it has been successfully used to study the structural, magnetic and thermodynamic properties of magnetic fine particles. Often though for the samples of various magnetic natures the temperature evolution of the spectra has the uniform character and they may be generally described in the framework of many-state relaxation models of magnetic dynamics [1] which as such are applicable only for ferromagnetic (FM) particles. At the same time some experiments show principally different behavior of the Mössbauer absorption curves for antiferromagnetic (AFM) particles, which main feature is the appearance and growth while temperature raising the single peak (or quadrupolar doublet of lines) in the central part of the spectrum together with the maintenance of the resolved magnetic structure. Explanation of such behavior according with the standard dynamic considerations is impossible and requires developing specific models of magnetism for AFM particles.

Recently we proposed a novel approach to the problem, namely, a quantum-mechanical model of thermodynamics for ensemble of ideal AFM nanoparticles in the approximation of slowly relaxing macrospins of magnetic sublattices [2]. This model allowed us, even without involving uncompensated spin, to describe qualitatively the distinction in thermodynamic properties of FM and AFM particles, as well as macroscopic quantum effects observed repeatedly in Mössbauer spectra of AFM fine particles. Moreover, we proved that accounting of uncompensated spin does not change the qualitative pattern of such effects, but lead only to slight quantitative modifications in the shape of absorption spectra for an ensemble of AFM particles [3].

Very recently we developed continual model of magnetic dynamics for an ensemble of compensated AFM nanoparticles in the approximation of two sublattices based on the solution of equation of motion for magnetization vectors of the sublattices under continuous relaxation process [4]. We showed that there exist four normal modes of self-consistent uniform precession of sublattices magnetization vectors around easy axis, two of which are well-known and correspond to the classical theory of AFM resonance in the absence of applied magnetic field, while two others have FM character and have absolutely dropped out from the circle of interest of the researchers. Such form of excitation spectrum actually gives the phenomenological treatment of macroscopic quantum effects observed in the absorption spectra and described in the “quantum” model [2, 3].

The main goal of this contribution is to approve these models as applied to simultaneous analysis of the temperature series of Mössbauer spectra of AFM nanoparticles. First of all we tried the classical description in the simplest approximation of equal magnetic moments of the sublattices and in the slow diffusion limit. However, though it gave principal advantage comparing with FM model, this approach was not quite enough to achieve quantitative compliance with the experimental data in the region of intermediate and high temperatures. Account of the diffusion processes led to formally better agreement with the spectra at high temperatures, but it turned out to be redundant for the rest of the series. Because of it we decided to apply more general quantum-mechanical description and so managed to get a satisfactory agreement with the experiment in the whole temperature range. The further improvement of the found result is possible on the way of involving uncompensated spin distribution or accounting transitions between quantum states of AFM particles.

Authors thanks Russian Foundation for Basic Research for financial support.

1. D.H. Jones and K.K.P. Srivastava. "Many-state relaxation model for the Mössbauer spectra of superparamagnets". *Phys. Rev. B*, **34**, pp. 7542–7548, 1986.
2. M.A. Chuev. "On the thermodynamics of antiferromagnetic nanoparticles by example of Mössbauer spectroscopy". *JETP Letters*, **95** (6), pp. 295–301, 2012.
3. M.A. Chuev. "The role of an uncompensated spin in the formation of a hyperfine structure of the Mössbauer spectra of antiferromagnetic nanoparticles". *Doklady Physics*, **57** (11), pp. 421–426, 2012.
4. M.A. Chuev. "Excitation spectrum and magnetic dynamics of antiferromagnetic nanoparticles in Mössbauer spectroscopy". *JETP Letters*, **99** (5), pp. 278–282, 2014.

Influence of doping on the crystallization kinetics of Ge-Sb-Te thin films for phase-change memory application

A. Sherchenkov¹, S. Kozyukhin², A. Babich¹, Y. Shtern¹, R. Mironov¹

1. National Research University of Electronic Technology (MIET), Moscow, Russia, aa_sherchenkov@rambler.ru.

2. Kurnakov Institute of General and Inorganic Chemistry, Russian Academy of Sciences, Moscow, Russia, sergkoz@igic.ras.ru

Phase-change memory (PCM) devices are actively developed now. This is due to several advantages of such devices in comparison with widespread flash memory. The principle of operation of this memory is based on the reversible phase transition between amorphous and crystalline states. In this case the kinetics of crystallization determines the switching and storage times of memory devices.

Promising materials for PCM application is $\text{Ge}_2\text{Sb}_2\text{Te}_5$. However, the necessity of improving PCM technology requires controlling of the PCM materials, which can be achieved by the doping. So, the aim of this work was to study the crystallization kinetics of $\text{Ge}_2\text{Sb}_2\text{Te}_5$ thin films and influence of doped by Bi and Ti (0, 0.2, 0.5, 1, and 3 wt. %) on this kinetics. Differential scanning calorimetry was used for this purpose.

Thermal evaporation and condensation method was used for thin films fabrication. The composition and structure of the films were determined with using of Rutherford backscattering, X-ray microprobe analysis and X-ray diffraction. It was established that the compositions of the films were close to those of the synthesized materials. According to the X-ray diffraction appearance of $\text{Bi}_2\text{Ge}_2\text{Te}_5$ reflexes indicate on the replacement of Sb by Bi.

Crystallization temperature of $\text{Ge}_2\text{Sb}_2\text{Te}_5$ was determined as 139 °C. Introduction of Bi changed crystallization temperature (T_c) in the range from 138 to 174 °C, while Ti incorporation varied T_c from 130 to 140 °C. The dopants affected also the values of the crystallization peaks.

To determine kinetic parameters (reaction model, effective activation energy and pre-exponential factor) we simultaneously used model-free and model-fitting methods. It was found that crystallization processes for all studied thin films can be described by the second- and third-order reaction models. Conversion dependencies for effective activation energies of crystallization (E_a) and pre-exponential factors were estimated, and existence of compensation effect was observed.

It was established that E_a for $\text{Ge}_2\text{Sb}_2\text{Te}_5$ thin film at the beginning of the phase transition is about 2.0 eV, and continuously decreased with conversion. This decrease may be due to the simultaneous passing of two processes: nucleation and crystallite growth with different activation energies. Wherein the contribution of the first process continuously decreases, while of the second process increases. The same tendency was observed for Bi doped materials. Unexpected rise of E_a was found for $\text{Ge}_2\text{Sb}_2\text{Te}_5 + 0.5$ wt. % Bi thin film (4.0 eV).

Effective activation energies for Ti doped compositions are close to $\text{Ge}_2\text{Sb}_2\text{Te}_5$ thin film except for $\text{Ge}_2\text{Sb}_2\text{Te}_5 + 1$ wt. % Ti. For the last composition nearly double decrease of E_a was observed (1.3 eV). Incorporation of 1 and 3 wt. % Ti is accompanied by the appearance of initial stage with low E_a variation with conversion indicating on the retarding of crystallite grows in these thin films.

Determined kinetic triplets for the crystallization processes in GST225 thin films with different Bi and Ti contents were used to predict the possible transition and storage times of the PCM cells. In most cases (except for $\text{Ge}_2\text{Sb}_2\text{Te}_5$ with 3 wt % Bi and 1 wt. % Ti) doping can improve these parameters. However, calculations showed that the shorter transition time, and longer storage time can be expected for $\text{Ge}_2\text{Sb}_2\text{Te}_5 + 0.5$ wt. % Bi thin films. In this case the probability of spontaneous crystallization at room temperature is very low, while transition time at the programming temperature can be comparable with that for DRAM and SRAM (lower 50 ns).

Thus, in this work the crystallization kinetics of $\text{Ge}_2\text{Sb}_2\text{Te}_5$ thin films, doped with various contents of Bi and Ti was investigated. It was shown that introduction of such dopants influence the thermal properties and processes in the material and their kinetic parameters can be varied in wide range. The possible transition and storage times in the phase-change memory cells on the basis of investigated materials were evaluated. It was shown that $\text{Ge}_2\text{Sb}_2\text{Te}_5 + 0.5$ wt. % Bi thin films has the most promising kinetic characteristics among the investigated materials.

Investigation of transport mechanisms in Bi doped Ge₂Sb₂Te₅ thin films for phase change memory application

P. Lazarenko¹, A. Sherchenkov¹, S. Kozyukhin², M. Shtern¹, S. Timoshenkov¹, D. Gromov¹,
E. Redichev¹

1. National Research University of Electronic Technology (MIET), Zelenograd, Russia, aka.jum@gmail.com

2. Kurnakov Institute of General and Inorganic Chemistry, RAS, Moscow, Russia, sergkoz@igic.ras.ru

Currently, the most popular type of memory for electronic technics is flash memory. But devices based on flash technology have two serious problems: limited cyclability and scaling problems. Thus, creation of the memory devices of next generation is a serious challenge facing the development of electronic technics.

Phase change memory (PCM) is the main candidate for replacement of the flash memory. The work of PCM devices is based on rapid reversible phase transformations between amorphous and crystalline states, which take place in nanovolume of material under low-energy external influences. Materials of the GeTe-Sb₂Te₃ pseudo-binary line, in particular Ge₂Sb₂Te₅ (GST225), are considered to be most promising materials for application in PCM devices. However, performance of PCM devices is needed to be improved.

Authors of the work [2] showed that doping of GST225 with Bi impurity can significantly change thermal, optical and electrophysical characteristics of these chalcogenide glassy semiconductors. But the nature of nonlinear current-voltage (I-V) characteristics, and influence of Bi doping on the electrophysical properties of amorphous Ge₂Sb₂Te₅ thin films is remained open. A clear and correct understanding of the charge carrier transport in Bi doped Ge₂Sb₂Te₅ thin films is of utmost importance for the purposeful optimization of the PCM technology. Thus the aim of this work was investigation of transport mechanisms in Bi doped Ge₂Sb₂Te₅ thin films for PCM application.

The initially doped Ge₂Sb₂Te₅ by different amounts of Bi (0.5, 1, and 3 wt.%) were synthesized by quenching technique [1]. Thin films in amorphous state were prepared by thermal evaporation of these doped materials in vacuum chamber. The thicknesses of the films were determined by atomic force microscopy (NT-MDT SolverPro) to be in the range from 60 to 80 nm. Rutherford backscattering (RBS) method was used to study the compositions of thin films, which were close to those of the synthesized materials.

The set-up on the basis of KEITHLEY 6486 and a voltage control unit NI6008 was used for the investigation of the I-V characteristics of thin films. Planar structures containing Al electrodes with fixed interelectrode distances (7 μm), and deposited upon them GST thin film were fabricated on oxidized c-Si substrates. Current-voltage characteristics of the samples were obtained from room temperature to 70 °C.

The experimental data indicate on the existence of three regions with different I-V dependence of Bi doped GST225 amorphous thin films.

1. Ohmic region at low electric field strength ($E < 10^3$ V/cm). Activation energies of conductivity were calculated for all investigated compositions. Based on the results of spectrophotometry [2] energy band structures were analyzed. Activation energy of conductivity is close to the middle of the mobility gap. Results of thermopower measurements have shown that holes are majority carriers in the investigated thin films.

2. Power dependence in the range of middle electric field strength ($10^3 < E < 10^4$ V/cm). Analysis of experimental data showed that space charge limited current (SCLC) is the most possible explanation for the nonlinear I-V dependence. Position of the trap levels (E_t) controlling transport mechanism, and density of traps (N_t) were estimated with using of Rose and Lampert theories.

3. Exponential dependence at high electric field strength ($E > 10^4$ V/cm). Poole Frenkel effect is possible candidate for explanation. However, further investigations are needed to clarify transport mechanism in this range.

The influence of Bi doping on the charge carrier transport mechanism in GST225 thin films was investigated. It was established that Bi doping can significantly change I-V characteristic, resistivity, mobility gap, Urbach energy, density distribution of localized states, and activation energy of conductivity. Thus, doping of Ge₂Sb₂Te₅ by Bi expands the range of material properties, which is important for the optimization of PCM technology.

1. S. Kozyukhin, A. Sherchenkov, A. Babich, P. Lazarenko, H.P. Nguyen, O. Prikhodko. "Peculiarities of Bi Doping of Ge-Sb-Te Thin Films for PCM Devices". Canadian Journal of Physics, **92**, pp. 684-689, 2014.

Effect of low-voltage field desorption in nanotubes

V. Zhigalov, V. Petukhov, A. Emelyanov, S. Timoshenkov

National Research University of Electronic Technology (MIET), Zelenograd, Russia

E-mail: zhigalov@gmail.com

Stability of field emission current is one of the most important parameter in cold emitters. Gas sorption on the surface changes the emission current. We've learned field emission of carbon single-walled nanotubes and how sorption of different gases affects it.

Two types of nanotube cathodes were investigated: nanotubes grown from gas phase on stainless steel and nanotubes deposited from solution on Si substrate. Anode-cathode distance was 25 μm , threshold voltage about 100 V (field 4 V/ μm). Vacuum 10^{-6} Torr was used during measurements.

After the exposition in atmosphere emission current behavior was changed on both types of cathodes. Typical current curves are shown in Fig. 1. Even short (15 min) exposition on air at atmospheric pressure leads to increase of starting current with following rapid decrease (curve b). If we leave samples in vacuum with voltage off, current continues to decrease from the last value (curve c). Starting values of current with different voltage have good approximation as a line in the Fowler-Nordheim coordinates.

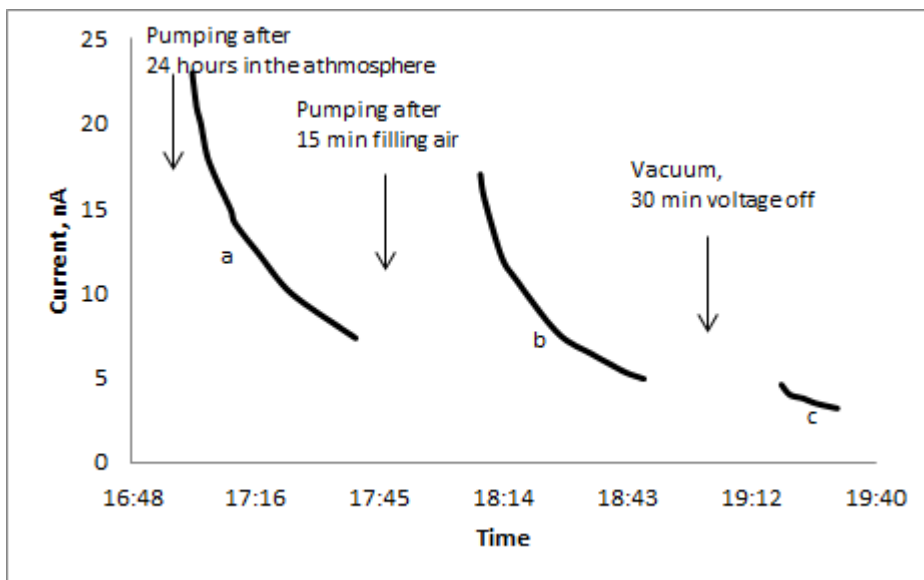


Fig. 1. Exposition on atmosphere affects the dynamics of emission current.

We associate this effect of reversible degradation with some kind of field desorption. The sorbed gases reduce the work function and thus increase emission current. It is known field desorption starts with fields of order 10^8 V/cm [1]. It is 10^4 times greater than field value we used in experiment. If we assume that field enhancement in nanotubes is $10^2 \dots 10^3$ (that is greater than in horizontal nanotubes that we use), this kind of desorption is unusual due to the low field value.

Emission current value after desorption is one-two order lower than initial value measured immediately after exposition. Noise in current is observed, consisting of short (<1 s) peaks of current. Influence of different gases (Ar, N_2 , H_2O vapor, CO_2) to the effect of reversible degradation was also investigated. Speed of current decay and noise value were calculated. Minimal effect of sorption influence was observed for CO_2 , N_2 .

Further investigations will be aimed to reveal the cause of low-voltage field desorption. It is possible that low-voltage desorption is connected to the effect of low-threshold field emission in carbon nanomaterials [2].

1. E.W. Müller. "Field desorption". Physical Review, **102** (3), pp. 618, 1956.

2. A. Yafyasov et al. "Low-threshold field emission from carbon nano-clusters". Ultramicroscopy, **111** (6), pp. 409-414, 2011.

Terahertz radiation detection by GaAs/GaAlAs high electron mobility transistors beyond the hydrodynamic approach

O.A. Klimenko¹, Yu.A. Mityagin¹, N. Dyakonova², W. Knap²

1. P.N. Lebedev Physical Institute of the Russian Academy of Sciences, Moscow, Russia,

E-mail address: oleg.klimenko@mail.ru.

2. Charles Coulomb Laboratory, UMR 5221 CNRS-University Montpellier II, Montpellier, France.

Field effect transistors (FETs) were recently shown to be efficient room temperature terahertz (THz) detectors [1]. With its high operation speed and well developed microcircuit chips fabrication technology, FETs become one of the most favorable devices for fast THz detection that is required for THz imaging and THz wireless telecommunication systems.

The firstly proposed by Dyakonov and Shur [2] mechanism of THz radiation rectification in a FET is based on excitation of 2D nonlinear electron plasma. Both resonant and broadband types of THz detection predicted in [2] were discovered and studied experimentally. And the theory was also developed more in detail. However, the Dyakonov-Shur theory considers only the high electron concentration case, in which one can use a hydrodynamic approach and diffusion transport mechanism dominates in source-drain current, whereas the most sensitive FET operation regime was found to arise at low electron concentration, when ballistic and trap governed current mechanisms become important and the hydrodynamic approach achieves its application limit [3].

In this work we investigate THz broadband detection by GaAs/GaAlAs high electron mobility transistors (HEMTs) in various conditions both fulfilling and exceeding the hydrodynamic approach. The goal was to reveal the key relations and parameters, which define the broadband THz photoresponse (detection signal) in such conditions.

We found that the obtained in the frame of the hydrodynamic approach relation between the broadband THz photoresponse, ΔU , and the channel conductivity, σ , [4]:

$$\Delta U \sim \frac{d \ln \sigma}{d V_g}, \quad (1)$$

where V_g is the gate-to-channel voltage, is still fulfilled even beyond the hydrodynamic approximation.

The experimentally defined subthreshold slope, U^* , was found to be one of the main parameters defining the photoresponse maximal value, ΔU_{\max} , even when the dominating current mechanism changes from the diffusion to the ballistic one:

$$\Delta U_{\max} = \frac{U_a^2}{4U^*}, \quad (2)$$

where U_a is the amplitude of the alternating source-gate voltage induced by the incident THz radiation, which depends on the radiation power and the coupling antenna parameters. Eq. (2) is confirmed also when the dominating current mechanism change causes significant discrepancy between the theoretical and the measured values of the subthreshold slope.

Thus, the developed in the frame of the hydrodynamic approach relations (1) and (2) were found to be valid even beyond the hydrodynamic approximation, so the FET broadband THz photoresponse strictly depends on the channel conductivity and the subthreshold slope at any conditions of the THz radiation detection.

The work was supported by The Ministry of education and science of the Russian Federation (№ MK-4848.2013.2), by the Presidium of the RAS (the program №24), by the Department of physical Sciences of the RAS (programs IV.12 and III.7).

1. W. Knap et al. "Plasma excitations in field effect transistors for terahertz detection and emission". C. R. Physique, **11** (7-8), pp. 433-443, 2010.
2. M.I. Dyakonov and M.S. Shur. "Detection, mixing, and frequency multiplication of terahertz radiation by two-dimensional electronic fluid". IEEE Trans. Electr. Dev., **43**, pp.380-386, 1996.
3. O.A. Klimenko et al. "Temperature enhancement of terahertz responsivity of plasma field effect transistors". J. Appl. Phys., **112**, pp.014506-1-014506-5, 2012.
4. M. Sakowicz et al. "Terahertz responsivity of field effect transistors versus their static channel conductivity and loading effects". J. Appl. Phys., **110**, pp.054512-1-054512-6, 2011.

Tunnel field-effect transistor with electrically induced p-n junction

D. Svintsov, M. Rudenko, V. Vyurkov, A. Orlikovsky

Institute of Physics and Technology, Russian Academy of Science, Moscow, Russia, E-mail svintcov.da@mipt.ru

Tunnel field-effect transistors (TFETs) based on interband tunneling are among most promising candidates for low-power circuits. The low-power switching in TFETs is achieved due to subthreshold slope exceeding the thermionic limit of $(60 \text{ mV/dec})^{-1}$. The common TFET represents a p^+i-n^+ junction with i -region gated by a single gate or by top and bottom gates (Fig. 1A). High doping densities in contacts are required to provide electric field at source junction sufficient for the tunneling to occur. As the length of TFET is scaled down, such doping becomes technologically challenging. Upon increasing the doping density there also emerge tunnel currents through defect states and band-tails [1]. Band tail tunneling contributes to current mostly in deep subthreshold mode (Fig. 1B) and significantly deteriorates the subthreshold slope [2].

In this report, we propose and evaluate a novel TFET with band-to-band tunneling occurring at electrically induced tunnel junction in the undoped region (EJ TFET). In such a TFET the ‘parasitic’ tunnel currents due to defects and band tails are absent, which improves the subthreshold slope. To form the tunnel junction in the undoped region we place an additional gate G_1 (Fig. 1C). Application of negative voltage to it ($\sim -1 \text{ V}$) results in enrichment of channel region with holes and tunnel junction formation (Fig. 1D). The signal voltage is applied to the gate G_2 which operates the band overlap and the tunnel current. Note that gate G_1 is used for electrical doping only and its voltage remains constant causing no additional power consumption.

To evaluate the characteristics of the proposed TFET based on silicon we have used the Kane/Keldysh model of indirect phonon-assisted tunneling allowing for the tails of density of states in the band gap [3]. The band overlap and electric field at the junction were found from numerical solution of Poisson equation.

In Fig. 2 we present the calculated dependencies of TFET current density J (normalized by $j_0 d_{Si}$, where $j_0 = 2.5 \times 10^{11} \text{ A/m}^2$ is the characteristic tunnel current in Kane’s model) on gate voltage V_{G2} . For comparison, we plot the current density of common double-gate (DG) TFET (Fig. 1A) with strongly doped source. The EJ TFET exhibits both higher current and subthreshold slope than its DG counterpart. Higher subthreshold is due to the absence of band tail tunneling while higher current is due to the abrupt drop of potential between gates provided by excess holes under gate G_1 . We also note that the threshold voltage of EJ TFET can be reduced almost to zero by slight ($\sim 10^{18} \text{ cm}^{-3}$) n-doping of the channel. The construction can be also realized on bulk silicon without bottom gate, which, however, reduces the field at the tunnel junction.

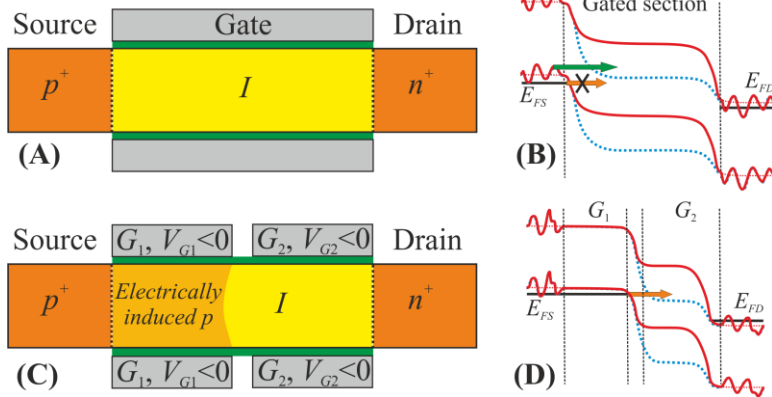


Fig. 1. Schematic device structures of a common DG SOI TFET (A) and proposed EJ TFET (C). Band diagrams of the corresponding devices in the subthreshold mode [(B) and (D)]. Green arrow in (B) indicates band tail tunneling while normal tunneling (orange arrow) is forbidden.

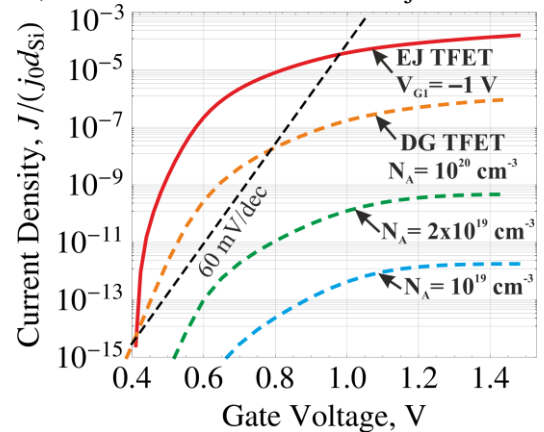


Fig. 2. Calculated gate characteristics of the proposed EJ TFET and DG TFETs at different doping densities. Si layer thickness $d_{Si} = 10 \text{ nm}$, gate oxide thickness $d_{ox} = 2 \text{ nm}$, permittivity $\kappa = 21$

1. B. Bhushan, K. Nayak, and V. Rao. “DC compact model for SOI tunnel field-effect transistors”. IEEE Trans. El. Dev. **59**, pp. 2635-2641, 2012.
2. M.A. Khayer and R.K. Lake. “Effects of band-tails on the subthreshold characteristics of nanowire band-to-band tunneling transistors”. J. Appl. Phys. **110**, p. 074508, 2011.
3. E.O. Kane. “Thomas-Fermi approach to impure semiconductor band structure”. Phys. Rev. **131**, pp. 79-88, 1963.

Memristive switching and neuromorphic functionality of fully-ALD grown HfO_2 -based stacks

Yu. Matveyev, K. Egorov, A. Markeev, and A. Zenkevich

Moscow Institute of Physics and Technology (State University), Moscow, Russia, info@mipt.ru

Despite rapid development of information technologies over the last decades, there are still several areas, such as image recognition, where the biologic brain beats even most powerful computers. The reason is that the biological brain is configured differently and the key is the extremely high ($\sim 10^{15}$ synapses) connectivity between neurons in a network, which offers highly parallel processing power. Recently, it was demonstrated that memristors, which exhibit electrically triggered multilevel resistive switching phenomena, can emulate the functionality of a biological synapse [1]. In addition, the big advantage of the two terminal memristive memory devices is their integrability in 3D cross-bar architecture, which opens an opportunity to devise an artificial neuron network which mimics a biologic neuron network [2].

In this work, we investigate the resistive switching behavior of TiN (20 nm)/ HfO_2 (6 nm)/TiN (20 nm) stacks fully grown by ALD technique, which is the most feasible fabrication process for 3D cross-bar integration. As grown structures require two stage forming process before they exhibit multilevel resistive switching effect (Fig. 1a). The endurance of the switching characteristics in one-pulse switching mode is $> 10^4$ cycles (not shown). By fitting I-V curves (Fig. 1b), we conclude that our structures have the Poole-Frenkel conductivity mechanism. The derived relationship between the effective barrier value and the resistivity of the oxide layer obeys an exponential law (see the inset in Fig 1b), as it is expected in case of hopping conductivity. We therefore claim that positive/negative biasing results in the condensation/dissolution of oxygen vacancies (V_o) from/into the bulk of HfO_2 and the overall concentration of V_o depends on the amplitude of applied bias. The concentration of V_o defines the effective barrier height for electron tunneling which ultimately results in different conductivity across HfO_2 .

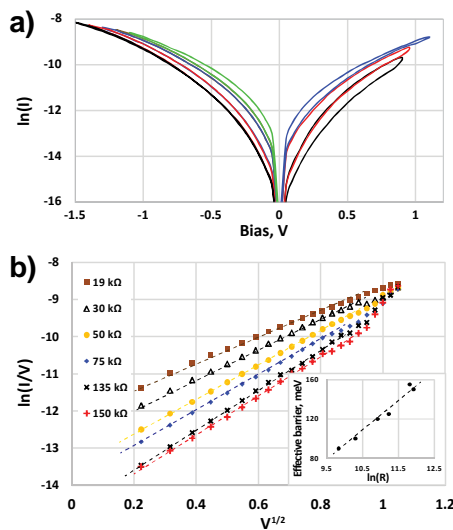


Figure 1. a) DC I-V curves of TiN/ HfO_2 /TiN stacks, illustrating multilevel switching; b) I-V curves plotted $\ln(I/V)$ vs. $V^{1/2}$ coordinates and plot of the effective electron barrier value vs. resistivity of structure (inset).

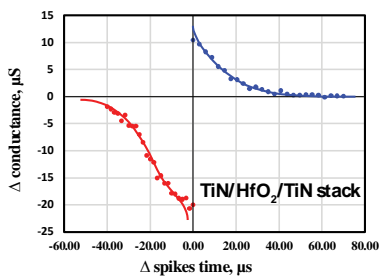


Figure 2. The results of spike-time dependent plasticity test on TiN/ HfO_2 /TiN stacks

In order to check whether the resistance of our TiN/ HfO_2 /TiN devices can be incrementally adjusted (memristive behavior), we applied the sequence of pulses with fixed width and amplitude. The results (not shown) imply that our devices integrate the current, i.e. the resistivity depends on the passed electric charge. The results of “pulse train” tests emulate the “long term plasticity” process in biological synapses [3]. Spike-time dependent plasticity (STDP) is another important property defining the synaptic adaptation rule for competitive Hebbian learning [4]. The results of STDP test performed on ALD grown TiN/ HfO_2 /TiN stacks are presented in Fig. 2. The obtained STDP characteristics are very similar to those of biological synaptic systems, further indicating the neuromorphic functionality of TiN/ HfO_2 /TiN system.

1. S.H. Jo, T. Chang , I. Ebong , B. B. Bhadviya , P. Mazumder, W. Lu, “Nanoscale Memristor Device as Synapse in Neuromorphic Systems”, Nano Lett. **10**, pp. 1297–1301, 2010.
2. D.B. Strukov, “Smart connections”, Nature **476**, p. 403, 2011.
3. S. F. Cooke, T. V. P. Bliss, “Plasticity in the human central nervous system”, Brain **129**, pp. 1659–1673, 2006.
4. W. Gerstner, R. Ritz, H. JL “Why spikes? Hebbian learning and retrieval of time-resolved excitation patterns”, Biol. Cybern. **69**, pp. 503-515, 1993.

Photocurrent Relaxations and Gain in Semiconductor Nanowires

Stepan Petrosyan^{1,2}, Ashkhen Yesayan¹, Suren Nersesyan¹

1. Russian-Armenian (Slavonic) State University, O. Emin str. 123, 0051, Yerevan, Armenia

2. Institute of Radiophysics and Electronics NAS RA, Alikhanyan Brs.1, 0203, Ashtarak, Armenia

E-mail: spetrosyan@rau.am

In this paper we study the transient and steady-state photoconductivity (PC) of semiconductor nanowires (NWR) by putting forward the importance of surface recombination in the photocurrent formation. The phenomenological model based on existence of radius and time dependent surface band bending is able to explain both the dark conductivity and dynamics of PC transients in semiconductor NWs. The dependence of the variation of surface recombination barrier height on the carrier capture by surface states leads to a non-exponential character of PC kinetics.

Analytic equations are derived to calculate current-voltage and lux-ampere characteristics, photoconductivity gain and the photocurrent kinetics under the excitation of light pulses. The analytical results are compared with the experimental data [1-3]. The direct comparison of current voltage characteristics and the qualitative comparison of photocurrent relaxation time calculated with our model for NWR with 160 nm radius exhibit very good agreement with measurements in [1].

The dependences of the photoconductivity gain on intensity of incident light are illustrated in Fig. 1. As it is seen photoconductivity gain is higher for NWs with larger diameters Fig. 1 (a). At small intensities we found very high photoconductive gain (10^8 - 10^9). Such high values of photoconductive gain are reported also in experimental works [2,3]. The sublinear fit ($G_n \sim P^{-k}$) with $k = 0.9$ is shown in Fig. 1 (b). This value of k was used also to fit the data in experimental measurements [3]. This coincidence of photoconductive gain behavior from model and measurements makes evident the accuracy of derived analytical model.

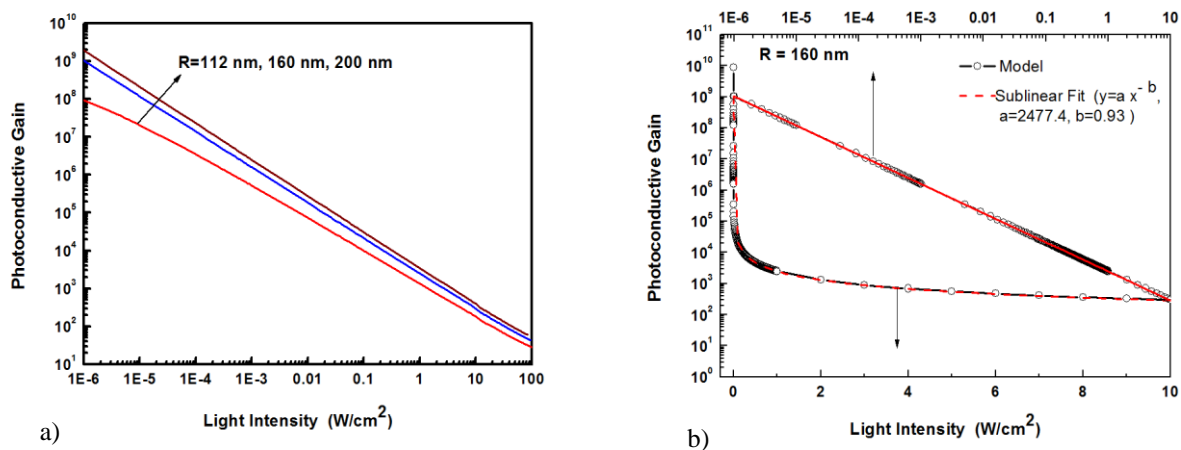


Figure 1. Photoconductive gain as a function of illumination intensity calculated at $V=0.6$ V (a). The photoconductive gain depicted in logscale for different NW diameters (b). The photoconductivity gain calculated for NW with $R=160$ nm and the sublinear fit.

1. N.A. Stanford, et al., "Steady-state and transient photoconductivity in *c*-axis GaN nanowires grown by nitrogen-plasma-assisted molecular beam epitaxy," J. Appl. Phys., **107**, p. 034318, 2010.
2. C. Soci, A. Zhang, B. Xiang, S.A. Dayeh et al., "ZnO Nanowire UV photodetectors with high Internal gain," Nano Letters, **7** (4), pp. 1003-1009, 2007.
3. R.S. Chen, H.Y. Chen, C.Y. Lu, K.H. Chen, et al., "Ultra-high photocurrent gain in *m*-axial GaN nanowires," Appl. Phys. Lett., **91**, p. 223106, 2007.

Oxide Charge Damage Mechanisms in deep sub-micron CMOS-Technologies

Nadya Belova, Derryl D.J. Allman, Tom Meixner, Bruce Greenwood

ON Semiconductor, Phoenix, AZ, USA, E-mail Nadya.Strelkova@onsemi.com , Derryl.Allman@onsemi.com

The integration of Analog and Digital functions into a single design requires a complex technology with multiple isolation wells and good electrical transistor matching characteristics for multiple gate oxides. Various fabrication process modules can induce charging damage which results in transistor functional variance, catastrophic failure of the final device, or degraded reliability.

This paper discusses the various charging mechanisms that may not be understood and accounted for in design rules, models or processes. We will present experimental results observed at different technology nodes fabricated at ON Semiconductor.

Fig. 1 illustrates a high-energy implant charging mechanism, resulting in field-oxide breakdown observed in-line. Figures 2a and 2b present back-end oxide breakdown due to wafer surface charging during the photo lithography process. The charging damage shown in figures 1, 2a, and 2b usually results in low product yield detected immediately at the end-of-line. These defects can also be detected in-line.

More subtle is the gradual oxide degradation which compromises product reliability. Wafer surface charge acquired at photo steps prior to the gate oxide resulted in silicon pit formation (fig. 2c) and subsequent low gate oxide time-to-breakdown. Damage to the gate oxide can be cumulatively introduced by implant, contact, metal, or via etch modules. Figure 3 shows the effect of increasing numbers of poly gate contacts on nMOS threshold voltage.

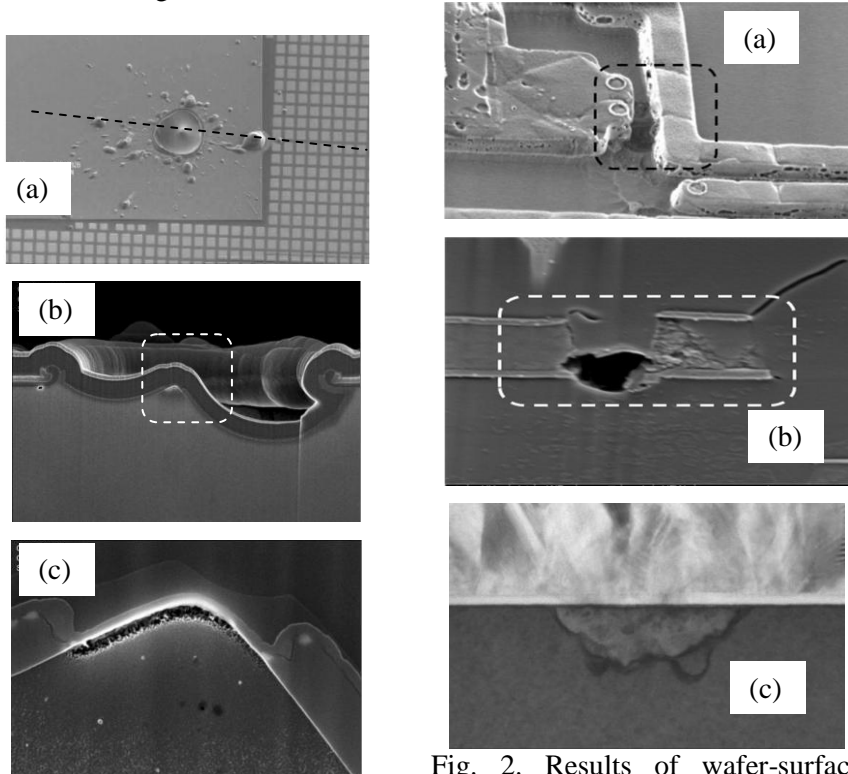


Fig. 1. Field-Oxide breakdown due to Implant charging. Top-down in-line image – (a). The cross-section of defect – (b). Zoomed-in area from the 1b-image shows fully formed Spacer over Poly-Silicon – (c).

Fig. 2. Results of wafer-surface charging due to photo lithography process. Images 2a and 2b show back-end oxide damage: top view – (a) and cross-section – (b). Image 2c shows silicon pitting prior to the gate oxide formation. Silicon pitting resulted in low time-to-breakdown.

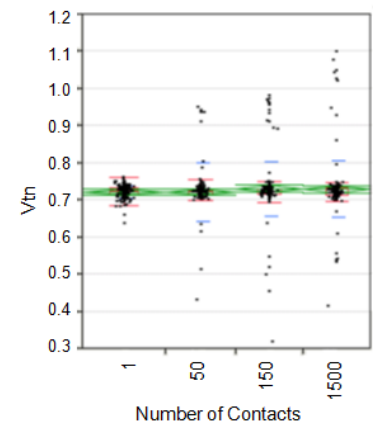


Fig.3. V_{tn} variance versus number of contacts to the poly-gate electrode demonstrates plasma induced charging due to Contact Etch process.

Formation of Si nanocrystals in SiO_x, SiO_x:C:H films and Si/SiO₂ multilayer nano-heterostructures by pulse laser treatments

I.G. Neizvestniy¹, V.A. Volodin^{1,2}, A.A. Gismatulin^{1,2}, G.N. Kamaev^{1,2}, A.H. Antonenko^{1,2},
A.G. Cherkov^{1,2}, V.G. Litovchenko³, I.P. Lisovsky³, I.Yu. Maidanchuk³

1. Rzhanov Institute of Semiconductor Physics, Russian Academy of Sciences, Lavrent'eva ave., 13, 630090, Novosibirsk, Russia, E-mail address: volodin@isp.nsc.ru. 2. Novosibirsk State University, Pirogova street, 2, 630090, Novosibirsk, Russia. 3. V.E. Lashkaryov Institute of Semiconductor Physics NAS of Ukraine, 41 pr. Nauki, 03028, Kyiv, Ukraine.

Interest to dielectric films containing Si nanoclusters is growing due to their perspectives of practical application [1]. The most important application areas are silicon-based optoelectronic devices, non-volatile memory, and tandem solar cells based on lateral Si/SiO₂ quantum well heterostructures. Quantum effects in such hetero-systems become clearly apparent at room temperature. Since in some experiments a single Si nanocrystal originated delta-function-like energy photoluminescence spectra [2], they can be called quantum dots. This work is devoted to development of laser assisted crystallization of SiO_x films and Si/SiO₂ based multi-layer nano-heterostructures. The structural, optical and electrical properties of the obtained Si nanocrystals were studied. The main topic of studying was to explore the influence the stoichiometry, carbon and hydrogen impurities on crystallization of silicon nanoclusters.

Si-rich SiO_x films (0<x<2) were prepared using radio frequency magnetron co-sputtering from two separate Si and SiO₂ (fused quartz) targets onto a Si (001) substrate [3]. The multilayer Si/SiO₂ nano-heterostructures were deposited on Si and glass substrates. First, a-Si:H layer with thickness of several nm was deposited. Afterwards the part of amorphous silicon layer was processed by plasma enhanced oxidation, so that the thickness of the remained a-Si:H layer was diminished. These alternative procedures (depositions and plasma enhanced oxidation) are repeated as many times as the planned periods. Thus, a structure containing from 2 to 6 nano-layers of a-Si:H, inserted between the nano-layers of SiO₂ has been formed. The nanosecond pulse XeCl laser with wavelength of 308 nm and pulse duration of 10 ns was used for laser treatments [4]. A Ti-Sapphire laser with a central wavelength of 800 nm, pulse duration of < 30 fs, pulse energy of up to 0.8 mJ and pulse repetition rate of 1 kHz was also used. Electron microscopy and Raman spectroscopy techniques were used to identify the structure (amorphous or crystalline) of Si in the as-deposited and pulse laser annealed structures. The electrical properties of the structures were also studied.

Raman data show that in some case (depending from technology) as-deposited structures contain hydrogen and carbon. In the case of the multilayer Si/SiO₂ nano-heterostructures the laser fluences needed for its crystallization were found. But, for multilayer a-Si/SiO₂ nanostructures, the threshold for crystallization was very close to threshold of laser ablation [5]. As it was shown from Raman spectroscopy data, using one-step pulse laser treatments one can get only partial crystallization. Probably it is due to high hydrogen concentration in these as-deposited films. The possibility of applying femtosecond laser pulses to crystallize amorphous Si nanoclusters in silicon-rich SiO_x films was demonstrated to yield crystallization of amorphous silicon nanoclusters. Appropriate laser fluences for the crystallization were found for the films with various stoichiometries. The effect of the laser assisted formation of amorphous Si nanoclusters in SiO_x films with relatively low concentration of additional silicon atoms was observed. The approaches can be used for the creation of dielectric films with semiconductor nanoclusters on non-refractory substrates.

The work is supported by RFBR-NAS of Ukraine for 2014-2015 years, contract number 14-07-90403.

1. L. Pavesi and R. Turan. *Silicon Nanocrystals: Fundamentals, Synthesis and Applications*. Willey VCH Verlag, Weinheim, 2010.
2. I. Sychugov, R. Juhasz, J. Valenta, and J. Linnros, *Phys. Rev. Lett.*, **94**, 087405, 2005.
3. T.T. Korchagina, A.K. Gutakovsky, L.I. Fedina, M.A. Neklyudova, V.A. Volodin. *J. Nanoscience and Nanotechnology*, **12**, 8694, 2012.
4. V.A. Volodin, M.D. Efremov, V.A. Gritsenko, S.A. Kochubei. *Appl. Phys. Lett.*, **73**, 1212, 1998.
5. V.A. Volodin, S.A. Arzhannikova, A.A. Gismatulin, G.N. Kamaev, A.Kh. Antonenko, S.G. Cherkova, A.G. Cherkov, S.A. Kochubei, A.A. Popov, S. Robert, H. Rinnert, and M. Vergnat. *Proc. SPIE*, 2013, **8700**, 870008-1.

Investigation of opaque band stability in transmission spectra of 2D photonic crystals with positional disorder by Riccati equation method

M.Yu. Barabanenkov¹, Yu.N. Barabanenkov²

1. Institute of Microelectronics Technology RAS, 142432 Chernogolovka, Moscow Region, Russia; barab@iptm.ru

2. V.A Kotelnikov Institute of Radioengineering and Electronics RAS, Moscow, Russia; barab624@mail.ru

At present there are two alternative approaches to the problem of localization of electromagnetic (EM) waves in randomly inhomogeneous slab of nondissipative medium from the viewpoint of medium density. The self-consistent theory of localization [1] extends the perturbative weak localization treatment of the corrections to classical diffusive behavior of the wave energy. Starting from dilute media in the zero approximation, a numerous corrections are required to describe denser media in which the diffusion coefficient of EM field may goes to zero. An alternative approach from relatively dense random media such as photonic crystals (PCs) with moderate disorder has been proposed by John [2]. PCs feature opaque bands, i.e. frequency ranges for which incident electromagnetic waves are totally reflected because of both microscopic Mie resonant scattering and the Bragg-like multiple scattering [3]. Opaque bands and Anderson localization are closely related. Really, both inhibit waves propagation due to interference in nondissipative media and can only be obtained for strongly scattering media. One of the ways in the framework of this approach of treating localization of EM waves is to study the EM field intensity transmitted through a slab of 2D PCs with disorder as a function of slab thickness at EM field wavelength taken from opaque band in transmission spectrum of perfect 2D PC. It is anticipated that the localization regime is if average transmitted intensity decreases exponentially with PC slab thickness increase. The 2D geometry precludes possible depolarization effect of EM waves which functions as effective absorption [4].

In the currently presented report we investigate by the Riccati equation method a layer-by-layer decay of the incident EM field energy density through 2D photonic crystal and fragility of the opaque band of 2D inverse PCs with positional disorder.

We consider two kinds of 2D PCs. First, a few rows of parallel infinitely extended cylindrical dielectric rods which constitute a square lattice in the perpendicular cross section. Second, a hexagonal packing of cylindrical pores in a non-absorbing matrix (with parameters as in [5]) with positional disorder in a unit supercell of such inverse 2D PCs. The EM wave field energy fluxes transmitted through a slab of both kinds of PCs were evaluated on the basis of Riccati equation with the aid of the Poynting theorem [3]. Calculated transmission spectra show good agreement with experimental results for rigid rods [6] and air pores [5].

Typical transmission spectrum of 2D PC composed of dielectric rods possesses two opaque bands separated by a transparency window [3]. We demonstrate that the lowest Mie resonance defines the spectral position of the localization window where EM field decays exponentially with slab thickness. In the additional opaque band EM field is damped in a sufficiently abrupt manner. Positional disorder has a minor effect on the opaque band of the dielectric rods [6].

Note, complicated shape of an elementary scatterer of inverse PCs practically precludes at least analytical description of resonant scattering process like Mie resonant scattering. Nevertheless, we demonstrate by Riccati equation method (in particular, for Si based inverse PCs tuned to the near IR range of EM waves) that (i) opaque bands of 2D PCs are significantly more stable to the positional disorder than their 3D counterparts like inverse opals; (ii) the opaque band as a whole is more stable to the disordering in the case of TE polarized (electric vector of the incident wave is parallel to the axis of the pores) incident waves; (iii) the opaque band in the spectra of PCs formed by pores with a smaller size is more stable to the positional disordering of pores.

1. P. Wölfle, D.Vollhardt, *Self-Consistent Theory of Anderson Localization*, Electronic Phase Transitions, Elsevier Science, Amsterdam, 1992.
2. S. John, Phys.Rev. Lett., **58**, pp. 2486-2489, 1987.
3. Yu.N. Barabanenkov, M.Yu. Barabanenkov, J. Opt. Soc. Am. A, **23**, pp. 581-585, 2006.
4. E.E. Gorodriichev, A.I. Kuzovlev, D.B. Rogozkin, *Proceedings of SPIE*, **5829**, pp. 74-87, 2005.
5. A. Birner et al, *Materials Science in Semiconductor Processing*, **3**, pp. 487-491, 2000.
6. M. Bayindir, Phys. Rev. B, **64**, pp. 195113-7, 2001.

The optical properties of ZnO nanowire array

Mikhail Yu. Nazarkin, Igor V. Melnikov, Dmitry G. Gromov, Sergey A. Gavrilov, Andrey A. Machnev, Alexey S. Shuliatyev

Department of Electronic Materials, National Research University for Electronic Technology (MIET), proezd 4806, Zelenograd, Moscow 124498, Russian Federation

In this paper, we present optical properties of ZnO nanowire grown as a disordered array on the tip of single-mode optical fiber. Zinc oxide is considered as promising candidate to UV or near-UV lasers and its integration with silica band components can open new possibilities cutting edge technology. In our experiments turned out the reflection spectrum of ZnO nanowire to depart of those that could be expected in the near IR where ZnO absorption is low.

The procedure exploited to create an array of ZnO nanowires on a tip of a single-mode optical fiber is based on a standard technological procedure. In order to provide required level of the surface quality, the magnetosputtering of 30 nm ZnO is executed immediately after the fiber cleaving. This film works as a catalyst for ZnO nanowires to grow and also provides proper adhesion and ordering for the structure to be created in the next step, where low-temperature chemical deposition is used to create an array of ZnO nanowires.

In the next step, the transmission and reflection spectra of the fiber that comprises a bundle of ZnO nanowires grown on its cleaved facets are studied using standard experimental setup. The output of the Er³⁺ broadband source is launched into one piece of SMF-28 followed by a circulator and another length of the SMF-28 that has ZnO nanowires on its facet and is connected to the spectrum analyzer.

The reflection spectra are measured for facet with a seed layer of ZnO on its cleaved surface and with ZnO nanowires that are being grown on this cleaved facet. In both cases, we observed asymmetry in the reflection spectrum which can be associated with forming the Fabry-Perot cavity. Moreover, on spectra from facet with ZnO nanowires one can see a profound asymmetry that does not match the transmission one hence making a temptation to claim an observation of surface polaritons excited along the ZnO nanowires.

Quantum discord in two-qubit systems. General X and CS states

M.A. Yurischev

*Institute of Problems of Chemical Physics of the Russian Academy of Sciences, Chernogolovka, Moscow Region,
142432 Russia, E-mail address: yur@itp.ac.ru*

Quantum discord is a measure of total purely quantum correlations [1]. It plays an important role in quantum information science. Evaluation of quantum discord is a very difficult (NP-complete) problem due to a necessary to solve the optimization problem over all possible measurements on a system. We discuss recent progress in obtaining the practical formulas for calculating the quantum discord for two-qubit models [2, 3].

Firstly, we consider so-called X states. Their density matrices may have nonzero entries only on the main diagonal and anti-diagonal. In papers [2, 3], it has been shown that the quantum discord minimized over all one-dimensional projective measurements (i.e., the von Neumann measurements) can consist for the arbitrary X states maximum of two subdomains where it is expressed in closed analytical forms and a subdomain in which the discord function is given only numerically through a solution of an one-dimensional optimization problem. As a result, we obtain a piecewise-analytic-numerical formula [2, 3]. It is important to emphasize that by this the author found the equations for the *exact* boundaries between all possible three types of subdomains: the boundaries consist of bifurcation points. The 'numerical' (intermediate) subdomain can be absent for the model under question and then the quantum discord has a fully analytical representation [4]. But for some physical systems, that subdomain is present and this is a new result of this year [2].

Secondly, we found a way to calculate the quantum discord for another class of quantum states, namely for the centrosymmetric (CS) density matrices of fourth order. (In n -by- n CS matrix, each i -th row repeats the $(n-i)$ -th one in the inverse order.) Quantum discord is invariant under any local unitary transformations; this is its fundamental property [1]. The author found the local orthogonal universal transformation (double Hadamard transformation) which transforms arbitrary CS matrix of fourth order into X form [2, 3, 5]. After performing this transformation, one should carry out the calculations for the arisen X state.

The approaches developed are illustrated on a number of physical systems. Examples include the weakly anisotropic XXZ dimer in external magnetic field, phase flip channel, dynamics of quantum discord for pairs of spin-carrying particles of a gas in closed nanopore, and many others.

1. K. Modi, A. Brodutch, H. Cable, T. Paterek, and V. Vedral, "The classical-quantum boundary for correlations: Discord and related measures", *Rev. Mod. Phys.*, **84**, pp. 1655-1707, 2012.
2. M.A. Yurischev, "Quantum discord for general X and CS states: A piecewise-analytic-numerical formula", arXiv:1404.5735v1 [quant-ph], pp. 1-32, 2014.
3. M.A. Yurischev, "NMR quantum discord dynamics of spin-carrying molecules of a gas in closed nanopore", *ZhETF* (in press).
4. M. Ali, A.R.P. Rau, and G. Alber, "Quantum discord for two-qubit X states", *Phys. Rev. A*, **81**, 042105, pp. 1-7, 2010; Erratum in: *Phys. Rev. A*, **82**, 069902(E), p. 1, 2010.
5. M.A. Yurishchev, "Quantum discord for two-qubit CS states: Analytical solution", arXiv:1302.5239v3 [quant-ph], pp. 1-8, 2013.

Entanglement resonance

S. Filippov, V. Vyurkov

Institute of Physics and Technology RAS, Moscow, Russia

Moscow Institute of Physics and Technology (State University) Moscow, Russia

sergey.filippov@phystech.edu

Quantum correlations are essential in the physical description of matter structures and some biological processes as well as in the up-to-date quantum information technologies. Quantum entanglement naturally emerges between interacting subsystems [1]. The interaction Hamiltonian is responsible for the entanglement dynamics. Entangling power of unitary transformations was considered in [2]. In present report, we focus on the physics of two-level systems (Fig. 1) and reveal the effect of entanglement resonance: typical interactions result in a rapid entanglement growth if the frequencies of individual qubits coincide. We quantify entanglement by conventional measures (such as linear entropy, negativity, etc.) and find the maximum of corresponding measure during the system evolution. The result is the Lorentzian function of qubit detuning $\delta = \omega_1 - \omega_2$. In fact, if the frequencies differ significantly ($\omega_1 \gg \omega_2$), then the mean-field approach becomes valid and subsystems remain effectively decoupled [1].

Effect of interaction strength is the following: the weaker the interaction between qubits, the narrower is the resonant curve. The effect takes place for various initial states that are supposed to be separable, however, there exist exceptional cases when the resonant entanglement behavior is forbidden, e.g., in the case of doubly excited initial state and the excitation-conserving interaction. Nevertheless, the average over different starting conditions in accordance with the techniques of Ref. [2] still has the prominent resonant form. The influence of decoherence processes can be taken into account by considering and exploiting phenomenological models of longitudinal and transverse relaxation times, however, other types of decoherence can also be considered [3].

The phenomenon of entanglement resonance can be used for creating short- and long-distance correlations among qubits, opening perspectives for entanglement-coupled devices and quantum registers composed of arrays of quantum dots [4].

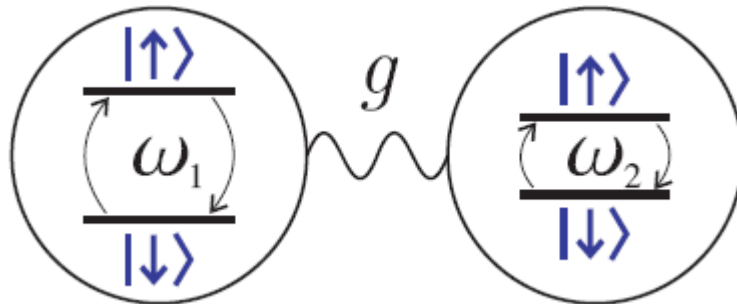


Fig. 1. Schematic view of a two-qubit system under investigation.

1. S. Filippov, V. Vyurkov, "Time evolution of two interacting charge qubits: entanglement and mean field approach", *Quantum Computers and Computing*, **9**, pp. 60-65, 2009.
2. P. Zanardi, C. Zalka, L. Faoro, "Entangling power of quantum evolutions", *Physical Review A*, **62**, p. 030301(R), 2000.
3. S. Filippov, V. Vyurkov, L. Fedichkin, "Effect of image charge on double quantum dot evolution", *Physica E*, **44**, pp. 501-505, 2011.
4. V. Vyurkov, S. Filippov, L. Gorelik, "Quantum computing based on space states without charge transfer", *Physics Letters A*, **374**, pp. 3285–3291, 2010.

Parasitic polarization in Jordan-Wigner fermion system with stationary discord

E.B. Fel'dman and A.I. Zenchuk

Institute of Problems of Chemical Physics, RAS, Chernogolovka, Moscow reg., Russia
e-mail: efeldman@icp.ac.ru, zenchuk@itp.ac.ru

Presently, the quantum discord [1, 2] is known as a reasonable measure of quantum correlations and is considered as an alternative to the already acknowledged entanglement [3, 4]. We investigate the Jordan-Wigner fermion clusters with the stationary distributed pairwise quantum discord [5, 6]. Such clusters appear after the Jordan-Wigner transformation of a spin chain governed by the nearest-neighbor XY-Hamiltonian with the particular initial state having one polarized node [7]. We show that the quantum discord stationarity in such systems is not destroyed by the "parasitic" polarization of at least two types. First type appears because the initial state with a single polarized node is hardly realizable experimentally, so that the low polarization of neighboring nodes must be taken into account. Second, the additional noise-polarization of all nodes is unavoidable. Although the stationarity may not be destroyed by perturbations of the above two types, the parasitic polarizations deform the distribution of the pairwise discord and may destroy the clusters of correlated fermions with equal pairwise discords. Such deformations are studied in this paper.

As an example, we consider the chain of 17 spin-1/2 particles with two cases of initially polarized node: the 6th and the 9th nodes. In the first case we have a following subsystem of fermions with equal pairwise discords (the ideal single node polarization [6]): $Cl = \{1,2,4,5,7,8,10,11,13,14,16,17\}$, while in the second case this cluster is [5] $Cl = \{1,3,5, \dots, 17\}$. All other pairwise discords equal zero and form the discord cluster Z . As was mentioned above, the pairwise discord remains stationary under the parasitic polarization of two neighboring nodes. Therewith the negative effect of parasitic polarization is two-fold. First of all, this polarization destroys the uniform discord distribution in the above clusters. Second, the discords in the cluster Z become nonzero. Consequently, the above clusters Cl are not well separated anymore. We find the threshold value of the parasitic polarization when some discords in Cl become equal to some discords in Z .

The destroying effect of the noise polarization is also studied for the chain of 17 spin-1/2 particles. We show that this effect is similar to the effect of the above two-node parasitic polarization. Low level noise does not significantly deform the discord distribution in the fermion cluster so that the subsystems Cl and Z remain well separated.

Let us emphasize that the studied parasitic polarization deforms the uniform distribution of the pairwise discord in the fermion system, but it does not destroy the discord stationarity. Therefore, the discord stationarity in the Jordan-Wigner fermion system may be taken as a reliable and stable advantage of the considered fermion system in comparison with the original spin system. This encourages us to consider possibility of quantum gate realization on the basis of such systems of virtual particles.

1. L. Henderson and V. Vedral. "Classical, quantum and total correlations" *J. Phys. A: Math. Gen.* **34**, pp. 6899–6905, 2001.
2. H. Ollivier and W.H. Zurek. "Quantum Discord: A Measure of the Quantumness of Correlations". *Phys. Rev. Lett.* **88**, 017901, 4 pp., 2001.
3. S. Hill, W.K. Wootters. "Entanglement of a Pair of Quantum Bits". *Phys. Rev. Lett.* **78**, 5022, 4pp, 1997.
4. A. Peres. "Separability Criterion for Density Matrices". *Phys. Rev. Lett.* **77**, 1413, 3pp., 1996.
5. E.B. Fel'dman and A.I. Zenchuk. "Quantum correlations in different density-matrix representations of spin-1/2 open chain". *Phys. Rev. A*, **86**, 012303, 9 pp., 2012.
6. E.B. Fel'dman and A.I. Zenchuk. "Systems with stationary distribution of quantum correlations: open spin-1/2 chains with XY interaction", *Quant. Inf. Proc.* **13**, pp. 201-225, 2014.
7. E.B. Fel'dman, R. Brüscheiler, and R.R. Ernst, "From regular to erratic quantum dynamics in long spin 1/2 chains with an XY- Hamiltonian". *Chem. Phys. Lett.* **294**, pp. 297-304, 1998.

An analytical calculation of quantum discord in a three-spin system in an external magnetic field

S.I. Doronin, E.B. Fel'dman, E.I. Kuznetsova

Institute of Problems of Chemical Physics, Chernogolovka, Russia, kuznets@icp.ac.ru

We develop an analytical method for the calculation of the quantum discord in a two-partite system consisting of three spins (qubits) at high temperatures. The model can be used for the interpretation of experiments with hetero-nuclear systems [1] and for electron-nuclear ones [2]. The interactions between spins in the two-qubit subsystem are not important for the calculations of the quantum discord. All measurements are performed on the one-qubit subsystem.

Here the main problem is the optimization of the quantum conditional entropy over different sets of measurements. The maximal value of this entropy determines classical correlations in the system. In the initial moment of time the system is in the thermodynamic equilibrium state with the density matrix

$$R(0) = \frac{1}{Z} \exp(b(\omega_A I_z + \omega_B S_z)), \quad (1)$$

where z points in the direction of the magnetic field which is perpendicular to the plane, where the nuclear (electron) spins are; $I_z = I_{z1} + I_{z2}$, I_{zi} ($i = 1, 2$), S_z are the z -projections of the spins of subsystems A and B, ω_A , ω_B are the Larmour frequencies; b is proportional to the inverse temperature of the system and Z is the partition function. In order to create quantum correlations in the system we applied resonance (for spins I and S) 90 –radiofrequency pulses of the magnetic field along the y axis in the rotating reference frame [3]. The evolution of the system is determined by the interactions between the spins of subsystems A and B. The expression for the quantum conditional entropy after measurements on subsystem B can be found analogously to the methods [4,5] for two-qubit systems.

Optimization of the quantum conditional entropy cannot be achieved analytically in a general case for an arbitrary temperature. However, the problem can be solved in the high temperature approximation [3]. We have found the minimal value of the quantum conditional entropy in the course of the evolution of the system at different relations between the Larmour frequencies ω_A and ω_B . Using the optimal values of the quantum conditional entropy it is possible to find the quantum discord which is a measure of quantum correlations. We have found that zz -correlations are responsible for quantum correlations in the system at $\omega_A > \omega_B$. Opposite xx and yy correlations are more important for quantum correlations at $\omega_A < \omega_B$.

There is no analytical approach for the investigation of quantum correlations in the system at low temperatures. However, it is possible to obtain analytical expressions for the quantum discord at low temperatures when the minimal value of the quantum condition entropy is known. In fact, we used a combination of analytical and numerical approaches for the analysis of quantum correlations in the system at low temperatures.

The work is supported by Russian Foundation for Basic Research (Grants № 13-03-00017 and № 13-03-12418) and Program №8 of the Presidium of RAS.

1. A.Y. Chernyavskiy, S.I. Doronin, and E.B. Fel'dman. "Bipartite quantum discord in a multiqubit spin chain". Phys. Scr., **T160**, 014007 (5pp), 2014.
2. K. Sato, S. Nakazawa, R. Rahimi, et.al."Molecular electron-spin quantum computers and quantum information processing: pulse-based electron magnetic resonance spin technology applied to matter spin-qubits". J. Mater. Chem., **19**, pp.3739 – 3754, 2009.
3. M. Goldman. *Spin temperature and nuclear magnetic resonance in solids*. Clarendon, Oxford, 1970.
4. S. Luo "Quantum discord for two-qubit systems". Phys. Rev. A, **77**, 042303 (5pp), 2008.
5. M. Ali, A.R.P. Rau, G. Alber "Quantum discord for two-qubit X states". Phys. Rev. A, **81**, 042105 (7pp), 2010.

Long-distance entanglement with macroscopic Bose-Einstein condensates

Alexey N. Pyrkov¹, Yiming Ji², Tim Byrnes³

1. Institute of Problems of Chemical Physics RAS, 142432, Russia, Chernogolovka, Acad. Semenov av., 1

2. Australian National University, Australia

3. National Institute of Informatics, 2-1-2 Hitotsubashi, Chiyoda-ku, Tokyo 101-8430, Japan

Generation of long-distance entanglement is essential for potential applications of quantum technology such as quantum networks and quantum cryptography. Currently the most promising way of achieving this task is by using photons, due to their long coherence times and fast propagation speeds. In practice, the distance over which quantum information can be transmitted directly is limited due to photon loss and decoherence. In order to overcome this problem in classical telecommunication technology the approach of amplifiers which periodically amplify the signal and copy the classical information before any significant degradation is used. A simple generalization of this approach for quantum information is not possible in accordance to the famous quantum no-cloning theorem. To overcome this difficulty, there have been number of works to investigate the possibility of constructing quantum repeaters to produce long-distance entanglement. The main idea of the approach is that a quantum entangled state over a long distance can be created by entanglement swapping of intermediately located quantum nodes. However, some essential requirements are necessary for quantum repeater: entanglement for elementary links, joint measurements projecting onto entangled states between two elementary links and entanglement purification. Realization of these requirements is still a difficult technological task and what is desirable is a simpler approach which achieves long-distance entanglement with a less demands on the experimental control of the system.

Here, we introduce a new protocol for creating long-distance entanglement between macroscopic qubits. The crux of the idea is to use spin coherent states instead of standard qubits. The spin coherent state could be realized for instance with two-component Bose-Einstein condensate (BEC). In a spin coherent state, the two level systems all occupy the same qubit state and this large duplication gives a natural robustness as a quantum memory [1], since the information is not all contained on a single particle. Furthermore, in this case we can use only local measurement on the number basis for entanglement swapping. Actually, we consider an artificial chain of macroscopic BEC qubits mutually connected by optical fiber in the short fiber limit and investigated entanglement between the ends of the chain depends on length of the chain and measurement results of the qubits in between. We showed that entanglement decays slow with number of sites for the most probable measurement results. We investigated fidelity of the entanglement propagation protocol. Recently we also proposed a protocol for macroscopic BEC teleportation [2] and experimental setup for generation entanglement in the elementary links of BECs [3]. All these give us a basis for quantum networking with macroscopic qubits.

1. T. Byrnes, K. Wen, and Y. Yamamoto, Phys. Rev. A **85**, 040306(R), 2012.
2. A.N. Pyrkov and T. Byrnes, New J. Phys. **16**, 073038, 2014.
3. A.N. Pyrkov and T. Byrnes, New J. Phys. **15**, 093019, 2013.

Quantum discord in the central spin model

V.E. Zobov

L.V. Kirensky Institute of Physics, Russian Academy of Sciences, Siberian Branch, 660036, Krasnoyarsk, Russia, rsa@iph.krasn.ru

Highly mixed state of qubits in the deterministic quantum computation with one qubit (DQC1) [1] is believed to perform a task exponentially faster than any classical algorithm. Even at high temperatures at which there is no quantum entanglement between the control qubit and the mixed ones, but there is a quantum discord [2] – the discrepancy between quantum versions of two classically equivalent expressions for mutual information. What quantum properties are responsible for the DQC1 performance, not yet established [2, 3]. In order to study physics of the quantum discord we now consider the similar system – the central spin model [4, 5], consisting of an electron spin coupled to n nuclear spins and describing by the Hamiltonian: $\hat{H} = \omega_e \hat{S}_z - \sum_j \omega_j \hat{I}_{jz} + \hat{S}_z \sum_j A_{j\alpha} \hat{I}_{j\alpha}$, where ω_e, ω_j are the Larmor frequencies of the electron $S = 1/2$ and nuclear $I = 1/2$ spins, $\hat{I}_{j\alpha}$ is α -component of the spin operator j ($\alpha = x, y, z$), $A_{j\alpha}$ is the hyperfine interaction constant, and we take $\hbar = 1$. As examples we can cite the quantum dots [5], NV-centers in diamond [4], impurities in silicon, etc. After the 90° pulse of microwave magnetic field on the electron spin the free induction decay signal (FID) $g_f(t)$ will be observed in the xy plane. If after a time t the second 180° microwave pulse acts on the electron spin, then at time $2t$ will be observed the spin echo with amplitude $g_e(t)$. At the high-temperature approximation we find

$$g_{(f,e)}(t) = \prod_j (1 - v_j^{(f,e)}(t)), \quad \text{where for FID } v_j^f(t) = 2n_{jx}^2 \sin^2(t\Omega_j/2), \quad \text{and for spin echo } v_j^e(t) = 8n_{jx}^2 n_{jz}^2 \sin^4(t\Omega_j/2); \quad \Omega_j^2 = \omega_j^2 + A_{jx}^2/4, \quad n_{jx} = A_{jx}/(2\Omega_j), \quad n_{jz} = \omega_j/\Omega_j.$$

For the mutual information $I_{(f,e)}$ (the measure of total correlations) and for the quantum discord $D_{(f,e)}$ we find

$$I_{(f,e)} = \frac{\beta^2}{8 \ln 2} [1 - g_{(f,e)}^2(t)], \quad D_{(f,e)} = \frac{\beta^2}{16 \ln 2} [1 - g_{(f,e)}^2(t) - |K_{(f,e)}|],$$

where $K_{(f,e)} = \prod_j (1 - v_j^{(f,e)}(t))^2 - \prod_j [2(1 - v_j^{(f,e)}(t))^2 - 1]$, and $\beta = \omega_e/kT \sim 10^{-3} \ll 1$ is polarization. We investigated the dependences of these quantities on time and on the magnetic field, for both the FID and for the spin-echo signals. We explained the reason for the loss of half of the correlations after the orthogonal projective measurement along any direction. We have shown that it is possible to make measurements without loss if we apply the procedure «unlocking» correlations [6], i.e. repeatedly performing projective measurements onto a complete set of orthogonal states of nuclear spin system and use the results to select the direction of the projective measurement of the electron spin. Our study led to the conclusion that the acceleration of calculating the trace of a unitary in the DQC1 model may result from next well-known property of quantum information. We can in one step (one measurement) to summarize the 2^n results obtained for each term of the quantum superposition, without measuring the intermediate results. While the measurement of intermediate results and their sum corresponds to the classical scheme of computing in which have to perform all 2^n operations sequentially. At the same time the quantum superposition is the necessary but not sufficient condition for non-vanishing quantum discord.

1. E. Knill and R. Laflamme, Phys. Rev. Lett. **81**, 5672, 1998.
2. A. Datta, A. Shaji, and C.M. Caves, Phys. Rev. Lett. **100**, 050502, 2008.
3. B. Dakic, V. Vedral, and C. Brukner, Phys. Rev. Lett. **105**, 190502, 2010.
4. L.T. Hall, J.H. Cole, and L.C.L. Hollenberg, *Analytic solutions to the central spin problem for NV centres in diamond*, arXiv:1309.5921.
5. J. Hackmann and F.B. Anders, Phys. Rev. B **89**, 045317, 2014.
6. S. Wu, U.V. Poulsen, and K. Molmer, Phys. Rev. A **80**, 032319, 2009.

Quantum simulation with multi-pulse sequence

M.M. Kuchеров

*Institute of Space and Information Technology, Siberian Federal University, 660074, Krasnoyarsk, Russia,
MKuchеров@sfu-kras.ru*

Given a general scheme for quantum simulation, $U(t) |s\rangle \Rightarrow \prod_I e^{-iH_I t_I} |p\rangle$, the task is to model the evolution $|s\rangle \xrightarrow{U} |s'\rangle$ using the physical system. $U(t)$ is the desired evolution governing the simulated system, while H_I is the Hamiltonian of the system we use. This evolution stems from a series of steps, whose evolution $e^{-iH_I t_I}$ can be generated by the evolution of a single system P_I using the control operations – radio frequency pulses in the case of NMR. One type of quantum simulation experiments has been established: Multiple pulse (MP) experiments, which were introduced by J.S. Waugh and U. Haeberlen [1] and formalized and extended by B.N. Provotorov and E.B. Fel'dman [2]. We consider the many-body localized (MBL) phase [3] assuming that the evolution is described approximately by the product states $|\downarrow\uparrow\uparrow\downarrow\downarrow\dots\rangle$ with the Hamiltonian

$$H = -\frac{1}{2} \sum_{i(\neq j)} A_{ij} (2I_i^z I_j^z - I_i^+ I_j^-), \quad A_{ij} = -\frac{\gamma^2}{2} \frac{1 - 3\cos^2 \theta_{ij}}{|r_i - r_j|^3}, \quad (1)$$

$$I^+(t) = \sum_i \sum_m x(t)_i P_i^m I_i^+, \quad (2)$$

where $P_i^m = \prod_{j(\neq i)} |m_j^{(j)}\rangle \langle m_j^{(j)}| = \prod_{j(\neq i)} \left(\frac{1}{2} + 2m_j I_j^z\right)$, $m_j = \{-\frac{1}{2}, \frac{1}{2}\}$ [4]. As a result, we found

$$\frac{d}{dt} \dot{x}_i = -i\gamma \langle H_i^z \rangle x_i - \frac{i}{2} \sum_{k(\neq i)} A_{ik} x_k (m_k + m_i), \quad \gamma H_i^z = 2 \sum_{k(\neq i)} A_{ik} I_k^z. \quad (3)$$

The initial state $\mathbf{x}(0)$ is defined by the equilibrium density matrix ρ_0 after rf pulse. Let us consider two spatially separated regions I and II, and a MP sequence WHH-4 applied to the spins of the region I. Starting from an arbitrary eigenstate of H , we initialize the spin of I in a superposition state. It precesses in the magnetic field $h_{\text{eff}}(\text{I})$, which depends on the state of the surrounding spins. WHH-4 allows one to recover the quantum coherence of spin I, by applying a time-reversal ($\pi/2$)-pulses. For the Hamiltonian (1), the precession induced by $h_{\text{eff}}(\text{I})$ over the initial evolution for $3t_1$ is cancelled by the precession accumulated during next evolution for time $3t_1$, independent of the value of $h_{\text{eff}}(\text{I})$. We introduce a modified protocol WHH-4 (m WHH) in the form of the double resonance technique, which is to perturb spins in a remote region II, situated at a distance $d \geq \xi$ (localization length) away from I, halfway through the multi-pulse sequence.

The evolution of many-particle system from the initial state $|p\rangle$ under the multi-pulse sequence m WHH is

$$|\Psi(t_2, t_1)\rangle = e^{-iH_I t_2} R_x^{\pi/2} e^{-iH_I t_1} R_y^{\pi/2} e^{-iH_I t_1} R_{II}^{\pi/2} e^{-iH_I t_1} R_{-y}^{\pi/2} e^{-iH_I t_1} R_x^{\pi/2} e^{-iH_I t_1} R_y^{\pi/2} |p\rangle. \quad (4)$$

Assuming that all interactions except those between spins I and region II are decoupled by this protocol; thus, the decay of the m WHH-4 response directly measures the influence of region II on spin I. In the diffusive phase, both WHH-4 and m WHH-4 responses should decay on a fast timescale set by the spin-spin interaction. In the non-interaction localized phase, both WHH-4 and m WHH-4 responses should saturate at the same nonzero value in the thermodynamic limit, as dephasing is absent. Finally, in the MBL phase, the WHH-4 response should saturate while the m WHH-4 response exhibits slow decay. The first evaluations were done on the model system, and we now plan to proceed to longer spin chains, and study changes in the systems behavior as they get larger. Initial work is geared towards the examination of the ground state, but subsequent work will also look at excitations to study effects of finite temperature.

1. U. Haeberlen and J.S. Waugh. “Coherent Averaging Effects in Magnetic Resonance”. *Phys. Rev.*, **175**, 453-467, 1968.
2. B.N. Provotorov and E.B. Fel'dman. “Thermodynamic effects in multi-pulse NMR spectroscopy in solids”. *Sov. Phys. JETP*, **52**, 1116-1122, 1980.
3. J.H. Bardarson, F. Pollmann, and J.E. Moore. “Unbounded growth of entanglement in models of many-body localization”. *Phys. Rev. Lett.*, **109**, 017202-5, 2012.
4. K.W. Becker, T. Plefka, and G. Sauermaun. “Spin correlation function for free-induction decay in dipolar systems”. *J. Phys. C: Solid State Phys.*, **9**, pp. 4041-4052, 1976.

Exact time-optimal solutions for control of spin $I = 1$ by NMR

V. Shauro

Kirensky Institute of Physics, Krasnoyarsk, Russia, rsa@iph.krasn.ru.

Over the past two decades, various methods for control of quantum systems have advanced substantially in terms of both theory and experimental realization. The relevance of this research due to the high practical importance problems to be solved - from the control of chemical reactions to creation of a quantum computer and quantum communication channels. Unfortunately, analytical approaches for finding the optimal control and estimating the minimum time required to implement the desired quantum transformation with acceptable accuracy are extremely complicated for quantum systems with a large number of states. Currently only few simple models of several qubits represented by spins $\frac{1}{2}$ are known, for which it is possible to find an exact analytical solution of the quantum control problem.

In this work, we solve the problem of time-optimal control for a single nuclear spin $I = 1$ controlled by nuclear magnetic resonance (NMR) techniques. The Hamiltonian of the model has the form

$$H(t) = H_q + u_x(t)I_x + u_y(t)I_y, \quad H_q = q\left(I_z^2 - \frac{1}{3}I(I+1)\right). \quad (1)$$

Here, I_α is the spin projection operator onto the axis α ($\alpha = x, y, z$), H_q is the quadrupole interaction of a nucleus with the axially symmetric crystal field gradient, q is the strength of interaction, and $u_\alpha(t)$ is the projection of the control radio-frequency (RF) field onto the axis α . Spin $I = 1$ is considered as a three-level quantum logic unit - qutrit. In contrast to traditional techniques of control by means weak selective RF pulses exciting individual energy transitions of multilevel system, we assume the strong RF field exciting all transitions simultaneously (non-selective excitation).

Based on the Cartan decomposition [1] it can be shown that the parameters of the control field $u_\alpha(t)$ for the implementation of arbitrary gate U_G on the qutrit can be found from the equation

$$Q_1 \exp(-it_1 H_q) \exp(-i\frac{\pi}{2} I_y) \exp(-it_2 H_q) \exp(i\frac{\pi}{2} I_y) Q_2 = U_G, \quad (2)$$

where $Q = \exp(-i\alpha I_x) \exp(-i\beta I_y) \exp(-i\gamma I_x)$ is a certain non-selective spin rotation (α, β, γ is parameters to be found) implemented by a strong RF field for a negligible time. Solutions of equation (2) for which $t_{1,2} \geq 0$ and $t_1 + t_2$ takes the minimum value are time-optimal. For such solutions, value $T_{\min} = t_1 + t_2$ is the minimum time that the gate can be implemented on system (1) with an arbitrarily small error. We found some particular solutions of equation (2) for the most important gates for qutrit - operators of selective rotation between different states and quantum Fourier transform gate (QFT). We took into account the global phase of gates because it is known that global phase has a significant impact on value T_{\min} [2, 3]. In the case of QFT gate the obtained analytical solution coincide with the numerical estimates obtained earlier [3]. For selective rotation gates, we found unusual dependence of value T_{\min} on the rotation angle for different values of the global phase. This result highlights the importance of considering the global phase in solving the control problem in the context of quantum information processing.

This work was supported by Russian Foundation for Basic Research (project no. 14-07-31086).

1. N. Khaneja, R. Brockett, S.J. Glaser, "Time optimal control in spin systems", *Phys. Rev. A* **63**, 032308, 2001.
2. T. Schulte-Herbrüggen, A. Spörl, N. Khaneja, and S.J. Glaser, "Optimal control-based efficient synthesis of building blocks of quantum algorithms: A perspective from network complexity towards time complexity", *Phys. Rev. A* **72**, 042331, 2005.
3. V.P. Shauro and V.E. Zobov, "Global phase and minimum time of the quantum Fourier transform for qutrits represented by quadrupole nuclei", *Phys. Rev. A* **88**, 042320, 2013.

Preparation Brodband biphotons in the single spatial mode by means of angular dispersion

K. Katamadze^{1,2}, N. Borshchevskaya², A. Paterova², I. Dyakonov², and S. Kulik²

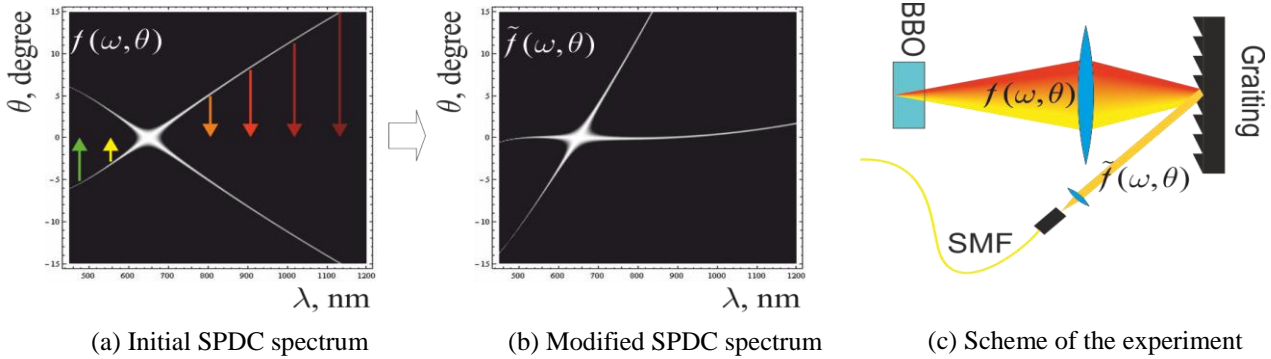
1. Institute of Physics and Technology, Moscow, Russia, k.g.katamadze@gmail.com

2. Lomonosov Moscow State University, Moscow, Russia

Recently, a great deal of attention has been focused on the control of the spectrum of the biphoton field as one of the most popular representatives of the family of non-classical field.

For some applications of quantum information [1, 2] and quantum metrology [3–7], based on the small correlation time and high degree of entanglement, the biphotons with a broad frequency spectrum is required. It is also important to limit their angular spectrum for good coupling with other optical systems (free-space or fiber optical channels, microscopes etc.). Ideally, biphotons should be diffraction-limited and have only one spatial mode.

Usually biphoton field is generated by spontaneous parametric down-conversion (SPDC). Its full frequency-angular spectrum is exactly broad, but it has an X-shape, so different frequencies correspond to different angles (fig. a).



We propose to modify the SPDC frequency-angular spectrum by an angular dispersion element (diffraction grating). So an X-shape converts to a “Plus”-shape and we have a broad frequency spectrum at the single angular mode (fig. b) and can be well coupled to a single-mode optical fiber (fig. c).

The experimental results as well as numerical calculations have been demonstrated.

1. G. Brida, V. Caricato, M.V. Fedorov, M. Genovese, M. Gramegna, and S.P. Kulik. "Characterization of spectral entanglement of spontaneous parametric-down conversion biphotons in femtosecond pulsed regime". *EPL (Europhysics Lett.)*, **87**, 6, p. 64003, 2009.
2. B. Bessire, C. Bernhard, T. Feurer, and A. Stefanov. "Versatile shaper-assisted discretization of energy–time entangled photons". *New J. Phys.*, **16**, 3, p. 033017, 2014.
3. A. Valencia, G. Scarcelli, and Y. Shih. "Distant clock synchronization using entangled photon pairs". *Appl. Phys. Lett.*, **85**, 13, p. 2655, 2004.
4. M. Nasr, B. Saleh, A. Sergienko, and M. Teich. "Demonstration of Dispersion-Canceled Quantum-Optical Coherence Tomography". *Phys. Rev. Lett.*, **91**, 8, pp. 083601–1–4, Aug. 2003.
5. M. D’Angelo, M. Chekhova, and Y. Shih. "Two-Photon Diffraction and Quantum Lithography". *Phys. Rev. Lett.*, **87**, 1, pp. 013602–1 – 013602–4, 2001.
6. J. Squier and M. Muller. "High resolution nonlinear microscopy: A review of sources and methods for achieving optimal imaging". *Rev. Sci. Instrum.*, **72**, 7, p. 2855, 2001.
7. B. Saleh, B. Jost, H.-B. Fei, and M. Teich. "Entangled-Photon Virtual-State Spectroscopy". *Phys. Rev. Lett.*, **80**, 16, pp. 3483–3486, 1998.

Formation of nanovoids arrays in silicon substrate using non-isothermal annealing

V. Rudakov, E. Bogoyavlenskaya, Yu. Denisenko

*Institute of Physics and Technology (Yaroslavl Branch), Russian Academy of Sciences, Yaroslavl, 150007 Russia,
E-mail: valeryrudakov@rambler.ru*

The regular arrays of pores or hollow tubes in Si substrates obtained without the use of photolithographic and electrochemical processes in are now of considerable interest from both technological and scientific points of view. Frequently, pores may be created in a two-stage process including production of gas bubbles in Si substrates by implantation He^+ ions and subsequent annealing. Depending on the process regimes, the porous buried layers are of two kinds: 1) dispersed throughout the thickness of the layer and 2) set of individual pores located in a plane parallel to the surface [1, 2]. In device structures, the pores can perform the effective sinks for mobile Si interstitials and metal ions and compensators of stresses in heterostructures. In porous Si, the effects of direct band optical transitions and discrete electron tunneling are possible. They open up prospects for the creation of three-dimensional arrays of quantum dots for perspective optical and electron devices. Here, the formation of regular structure of hollow tubes oriented deep into the Si substrate may be preferable. The diffusion processes and interface reactions on phase boundaries can modify physical and chemical properties of Si material at these boundaries. It is likely that the regular sets of dislocations and hollow tubes should be coincided. In this case, the entrainment of impurity atoms by the periodic elastic stress fields of the dislocations and sequential “chemical” interactions of these atoms with a dislocation core at small distances occur. The hollow tubes can be formed along axes of screw dislocations or misfit dislocations with screw component. The thermodynamic explanation of this process bases on fact that the core of a screw dislocation plays the role of a strain energy concentrator. If the value of this energy exceeds some critical one, energetically the removal of material along the axis and formation of additional free surface is favorable.

The aim of the present work is further development of defect engineering methods concerned formation of regular arrays of the hollow tubes in Si substrate. The suggested method involves the implantation of O_2^+ and P^+ ions and annealing in non-isothermal reactor under an axial temperature gradient $\text{grad } T$. The process variables in this reactor are: substrate average temperature – $800 \div 1100$ °C, processing time – 5 min, and $\text{grad } T = 50 \div 100$ K/cm. The characteristic property of the annealing is synergistic nature of $\text{grad } T$ action on impurity-defect subsystem of the crystalline substrate (non-uniform thermal field, mechanical stress gradients, non-equilibrium concentrations of intrinsic point defects). Annealed under $\text{grad } T$, the substrates got their further thermal evolution at 1150 °C in standard isothermal furnace. The structure of the *regularly* spaced

hollow tubes was observed on those cleaved substrates whose implanted side had been faced to the cold pedestal during annealing in the reactor ($\text{grad } T < 0$). Corresponding SEM images are presented in Fig. 1. The hollow tube is 300 nm in length and 20 nm in diameter. In Fig. 1a, it is seen a bright contour along the tubes due to charging which occur in a SEM process due to poor conductivity of material. The character of cleavage on the bright-field pattern (Fig. 1b) allows suggesting that amorphous phase on the base of SiO_x is the most probable candidate of being the tube shell material.

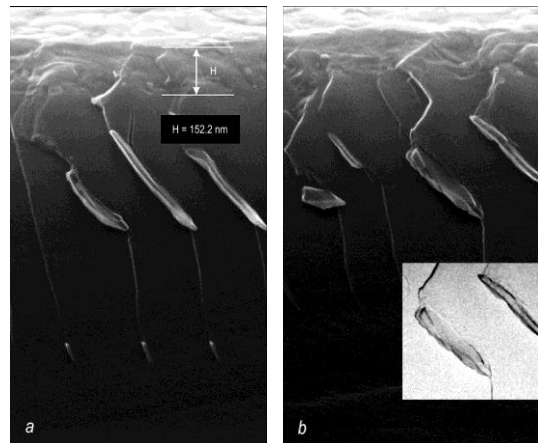


Fig. 1. Panoramic SEM images of the regular arrays of hollow tubes in Si substrates.

1. V. Rainery, M. Saggio, E. Rimini. “Voids in silicon by He implantation: From basic to applications”. *J. Mater. Res.*, **15**, pp. 1449-1476, 2000.
2. N. Hueging, M. Luysberg, H. Trinkause *et al.* “Quantative pressure and strain field analysis of helium precipitates in silicon”. *J. Mater. Sci.*, **41**, pp. 4454-4465, 2006.

Production and electrical properties of W/HfO₂/Si gate structures

V. Rudakov, E. Bogoyavlenskaya, Yu. Denisenko

Institute of Physics and Technology (Yaroslavl Branch), Russian Academy of Sciences, Yaroslavl, 150007 Russia
E-mail: valeryrudakov@rambler.ru

Scaling down of the elements of electronic devices based on MOS transistors requires replacing of a SiO₂ gate layer by ultrathin high-*k* dielectric layers because of the limits of further use of SiO₂. High-*k* dielectric layers are predominantly based on metal oxides with high dielectric constant *k* [1]. The use of such a kind of insulator makes it possible to essentially increase the physical thickness *d* of a dielectric in comparison with the thickness of initial tunnel-transparent SiO₂ layer (about 1 nm). Herewith, the specific capacitance of the MOS structure may stay the same or even rise. Simultaneously, the problem of leakage currents caused by direct tunneling is solved [2]. Today, HfO₂ and dielectric compounds on its base with the values of *k* = 15 ÷ 30 are among the most promising high-*k* materials [3]. However, the presence of these high-*k* insulators in gate stack structures poses a number of problems connected with the relationships between the material properties of HfO₂ and Si substrate such as they are. This work is dedicated to the fabrication and investigation of the ultrathin multilayer W/HfO₂/Si(100) structures, especially from the point of view of formation and transferring of new phases at the interfaces and investigation how these processes influence the electrical parameters under the RTA (Rapid Thermal Annealing) conditions. All the structures were fabricated by rf magnetron sputtering using *p*-type (boron doped) (100) Si wafers with resistivity of 12 Ω · cm and three plasma compositions (Ar, N₂, Ar-N₂). The W(150 nm)/HfO₂(5 nm)/Si(100) structures only obtained in Ar plasma were subjected to three types of annealings: 1) at 500 °C in vacuum for 30 min (the chamber of magnetron sputtering), 2) at 950 °C for 12 s (RTA-1), and 3) at 980 °C for 5 s (RTA-2). RTAs were carried out in Ar atmosphere. In N₂ atmosphere or in Ar-N₂ mixture, the

W(150 nm)/HfO₂(5 nm)/X/Si(100) structures were formed, where X is a barrier nitride layer. These structures were then subjected to RTA-2. Contact pads were formed by photolithography and dry etching. Depth profiling of the oxide phases appeared at the interfaces of the structure layers was accomplished by secondary ion mass spectrometry (SIMS). Both *C-V* and *I-V* characteristics were obtained using a Keithley 4200-SCS instrument, where the *C-V* characteristics were measured according to the ultrathin insulator technique [4]. By SIMS, it was found that the annealing of the W/HfO₂/Si(100) structures at 950 °C causes the formation of a WO_x phase at the W/HfO₂ interface and a HfSi_xO_y phase at the HfO₂/Si(100) interface. As a result, the entire oxide layer becomes 30 % thicker than the initial HfO₂ film. Here, according to the *C-V* investigations, the specific capacitance in accumulation *C*_{max} and *k* decrease (*k*: from 27 to 23). When the annealing temperature grows to 980 °C, a Hf_xSi_yW_zO oxide phase appears and parameters *C*_{max} and *k* decrease further. All the *C-V* curves (Fig. 1) demonstrate complete modulation of the capacitance throughout the scan interval. Referring to the *I-V* investigations (inset in Fig. 1), the considerable reduction in the leakage currents occurs in the structures included nitride barrier layer, i.e. in the W/HfO₂/X/Si(100) structures.

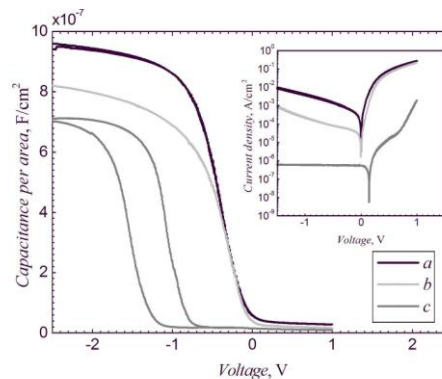


Fig. 1. *C-V* and *I-V* characteristics taken after RTA-2 (980 °C, 5 s, Ar) and plasma-chemical etching of W for the (a) W(150 nm)/HfO₂(5 nm)/Si(100) structure, (b) W(150 nm)/HfO₂(5 nm)/X/Si(100) structure with the Si substrate pretreated with the nitrogen plasma, and (c) W(150 nm)/HfO₂(5 nm)/X/Si(100) structure with a SiN barrier layer.

1. *Synthesis, Properties, and Applications of high-permittivity dielectrics in silicon devices*. Ed. by A.L. Aseev and V.A. Gritsenko, SO RAN, Novosibirsk, 2011 (in Russian).
2. J. Robertson. "High dielectric constant oxides". *Eur. Phys. J. Appl. Phys.*, **28**, pp. 265-291, 2004.
3. S.-W. Jeong, K.S. Kim, M.T. You *et al.* "HfSi_xO_y-HfO₂ gate insulator for thin film transistors". *J. Korean Phys. Soc.*, **47**, pp. S401-S403, 2005.
4. K.J. Yang and C. Hu. "MOS capacitance measurements for high-leakage thin dielectrics". *IEEE Trans. Electron Devices*, **46**, pp. 1500-1501, 1999.

Optically transparent fluoro-containing polyimides films with low dielectric permeability

V. Kravtsova¹, M. Umersakova¹, R. Iskakov², O. Prikhodko³, N. Korobova⁴

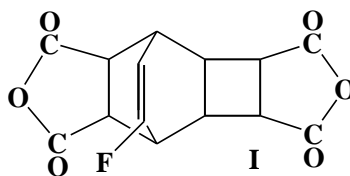
1. A.B. Bekturov Institute of Chemical Science, Almaty, Republic of Kazakhstan, vadamkr@mail.ru

2. Kazakh-British Technical University, Almaty, Republic of Kazakhstan, r.iskakov@mail.ru

3. al-Farabi Kazakh National University, Almaty, Republic of Kazakhstan, prikhodko_o@mail.ru

4. National Research University of Electronic Technology (MIET), Zelenograd, Russia, korobova3@mail.ru

In the last few years there are various and broad investigations for polymeric materials with the lowest dielectric permeability and high mechanical performances for microelectronics, or as interlayered dielectrics, as well as manufacture of chemically resistant materials, etc. [1, 2]. One of those polymers is polyimide of aromatic structure. Further investigation in this area brings our attention to also polyimides with alicyclic structure where fluorine atoms could be in both dianhydride and diamine fragments of the polymeric chain. For example polyimide synthesized on the basis of various diamines and fluorine-containing dianhydride with the heteroatom at the endoethylene link as shown in diagram:



Polyimides were synthesized by reaction of polycondensation between the mentioned monomers in aprotic solvents of the amide type in the presence of catalysts of either acidic or basic natures. Polymers with higher molecular weight could be achieved by using esters of phosphoric acids. Main properties of the synthesized polyimide have been investigated. It was found that depending on the initial diamine the final polymers vary their dielectric permeability values (ϵ). Values of dielectric permeability were within 1.91–2.84 at electric field frequency 1 kHz and relative humidity about zero. If relative humidity was about 50% then ϵ values increased up to 2.01–3.03. But in general, this characteristic for alicyclic polyimides was lower compared with aromatic polyimides (2.9–3.4) [3].

Optical properties of polyimides based on fluorine-containing dianhydride and 4,4'-oxydianiline, and non-substituted form of dianhydride, and their composition with soluble emerald type of polyaniline have been studied in visible and UV ranges of spectra. Polymer films were prepared according to the procedure described in [3]. In this paper we show that, transparency range of the polyimides and their compositions with the electroconductive polyaniline were within 120–240 nm depending on the film thickness and nature of the initial solvent. The data shown high transparency of polyimides based on tricyclodecenic structures in the main chain within the above-mentioned wave range. Durability for mechanical breakage of polyimide films achieved 160–170 MPa, and elongation was 32–38 %. Analyses of thermal stability for fluoro-containing polyimides showed their destruction temperature on 15–20 °C higher in compare with non-halogenic analogues. Polymer films with thickness from 5–7 to 160–180 microns can be prepared.

1. C. Pan, T. Ali, Y. Ling, and C. Chiang. *Low dielectric constant organic polymers for interlayer dielectrics*. Amer. Chem. Soc. - Polym. Prepr., **37** (1), pp. 152–153, 1996.

2. M. Keshtov, E. Said-Galiev, V. Kochurov, and A. Khokhlov. *New polyimide-polyoxometalate nanocomposite materials with nanoporous structure and ultra-low dielectric constant, formed in supercritical carbon dioxide*. AIP Conf. Proc., **277**, p. 1459, 2012.

3. B. Zhubanov, V. Kravtsova, R. Iskakov R. et al. *Polymeric Composites based on Alicyclic Polyimide and Polyaniline*. Russian Journal of Applied Chemistry, **81** (12), pp. 2151–2154, 2008.

Formation of gold and silver cluster arrays using vacuum-thermal evaporation on a non-heated substrate

D.G. Gromov¹, A.I. Savitskiy¹, L.M. Pavlova¹, N.I. Borgardt¹, Y.S. Grishina¹, A.Y. Trifonov²

1. National Research University of Electronic Technology (MIET), Zelenograd, Russia, savitskiy-andrey@mail.ru

2. Lukin Research Institute of Physical Problems, Zelenograd, Russia,

The interest to nanoparticles arrays has been associated with their wide range of application. Metal nanoparticles are used for surface-enhanced Raman scattering, sensing, plasmonic and photonics [1-3]. In relation to the micro- and nanoelectronics arrays of nanoparticles can be used in memory cell which is kind of next generation non-volatile memory that has attracted increasing attention in recent years as a possible replacement for flash memory [4-6].

In the present work we investigated silver and gold cluster array formation on non-heated thin film substrate of amorphous carbon by means vacuum-thermal evaporation of small quantity of material. In basic experiments two series of samples with a different thickness (1-20 nm) were prepared from weight portion 0.6-11 mg, the distance between evaporator and deposition surface was 20 cm. The samples were annealed in vacuum (the residual pressure 1×10^{-5} Torr) at 350 °C for 30 min. The study of the resulting samples was performed using a transmission electron microscope Tecnai G2 20 S Twin of the company FEI, equipped prefix EDAX for X-ray energy dispersive microanalysis. The investigation of the samples of both series by TEM showed the significant dependence of the particle size and the density of their location on the surface on the quantity of condensing Ag and Au or on the virtual film thickness. The interesting results obtained in the work formed the basis of the model which expands understanding condensation processes, nucleation and growth of the crystalline phase from the gas phase.

1. N.G. Khlebtsov, "T-matrix method in plasmonics: An overview", *J. Quantitative Spectroscopy and Radiative Transfer*, **123**, pp. 184-217, 2013.
2. N.C. Lindquist, P. Nagpal, K.M. McPeak, D.J. Norris, S.-H. Oh, "Engineering metallic nanostructures for plasmonics and nanophotonics", *Reports on Progress in Physics*, **75**(3), 036501, 2012.
3. J.Z. Zhang, C. Noguez, "Plasmonic optical properties and applications of metal nanostructures", *Plasmonics*, **3**, pp. 127-150, 2008.
4. C.-P. Hsiung, H.-W. Liao, J.-Y. Gan, T.-B. Wu, J.-C. Hwang, F. Chen, M.-J. Tsai, "Formation and instability of silver nanofilament in Ag-based programmable metallization cells", *ACS Nano*, **4**(9), pp. 5414-5420, 2010.
5. J.H. Jun, K. Cho, J. Yun, S. Kim, "Switching memory cells constructed on plastic substrates with silver selenide nanoparticles", *J. Materials Science*, **46**(21), pp. 6767-6771, 2011.
6. N.J. Lee, B.H. An, A.Y. Koo, H.M. Ji, J.W. Cho, Y.J. Choi, Y.K. Kim, C.J. Kang, "Resistive switching behavior in a Ni-Ag₂Se-Ni nanowire", *Applied Physics A*, **102**(4), pp. 897-900, 2011.

Electrical properties of ALD HfO₂ (EOT 0.47 nm)

A. Molchanova^{1,2}, A. Rogozhin¹

1. Institute of Physics and Technology of RAS (IPT RAS), Moscow, Russia, rogozhin@ftian.ru.

2. Moscow Institute of Physics and Technology (State University), Moscow, Russia.

Since 2007 the microelectronic industry has started to use high-k dielectrics with metal gates (HKMG) in high performance MOSFETs [1]. It is well known that SiO₂-based interfacial layer appears at the HfO₂/Si interface [2]. In this work properties of HfO₂ formed by plasma-enhanced atomic layer deposition (PEALD) and interfacial layer are investigated.

HfO₂ was deposited on HF-last Si (100) wafers (B-doped, 1.1·10¹⁵ cm⁻³) by PEALD, followed by tungsten deposition by DC magnetron sputtering. Contact areas were defined using standard photolithographic process, followed by wet etching in 5% hydrogen peroxide (H₂O₂). The postmetallization annealing (PMA) was performed at 425 °C for 30 min.

Structure of the dielectric stacks was investigated by spectroscopic ellipsometry before W deposition. The thickness of interfacial layer was estimated to be 1-1.5 nm. Capacitance-voltage (CV) and current-voltage (IV) characteristics were measured before and after PMA. Dielectric constants were estimated under two-layer model (high-k and interfacial layers; C is the capacitance, $\epsilon_0 = 8.85 \cdot 10^{-14}$ F/cm, S is the area, d , k are the thickness and the dielectric constant of the layer):

$$C^{-1} = (\epsilon_0 S)^{-1} \frac{d_{IL}}{k_{IL}} + \frac{(\epsilon_0 S)^{-1}}{k_{high-k}} d_{high-k} \quad (1).$$

For high-k layer dielectric constant values before and after PMA were equal to 21.5 and 11, respectively (fig. 1). Under the assumption of SiO₂ interfacial layer its thickness was estimated to be 1.8 nm in the unannealed samples. On the other hand it seems that dielectric layer in annealed samples is quite homogeneous with $k = 11$. It appears that silicon and oxygen diffusion during annealing led to hafnium silicate formation. The lowest equivalent oxide thickness (EOT) was obtained after PMA and equals to 0.47 nm. The leakage current for this sample at 1 V gate voltage was about 10 A/cm².

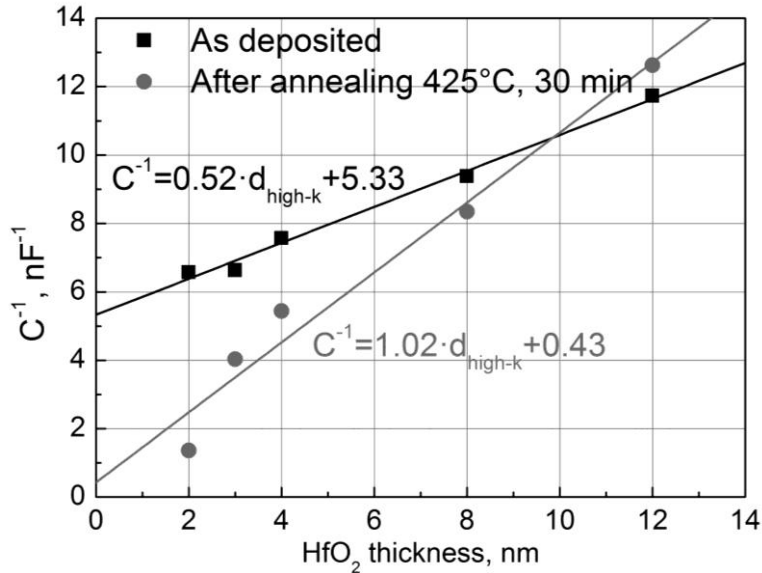


Fig. 1. Reverse capacitance vs. high-k layer thickness.

Densities of interface and volume charges in annealed structures were estimated from flatband voltage $V_{FB}(d_{high-k})$ dependence. It seems that charge density in the volume of high-k is extremely high (1.61·10¹⁸ cm⁻³). It can lead to high threshold voltage and low mobility due to remote coulomb scattering. Density of interface charge is equal to 1.03·10¹² cm⁻². The value is rather moderate and might be lowered by additional annealings. This work was supported by RFBR, research project №14-07-00844 A.

1. K. Mistry et al., IEDM Tech. Digest, p. 247, 2007.

2. T. Ando, Materials, 5, p. 478, 2012.

Electrochemical formation of Ag-Sn layers on copper plates

V.M. Roschin, M.S. Mikhailova, I.N. Petukhov, V.R. Kukhtyaeva, M.S. Vagin
National Research University of Electronic Technology (MIET), Zelenograd, Moscow, Russia,
E-mail: shunya2000@mail.ru

Lead-free solders are widely used for assembling micromodules and printed circuit boards (PCB) due to the environmentally friendly and promising technology.

At present, there are several basic types of lead-free solders, but the most interesting ones from the point of view of reliability and higher operating performance, which are necessary for the technology of surface mounting of microelectronic components, are alloys on the basis of tin and silver with copper, bismuth, and antimony additives. The ratio of the components in such solders is the subject of constant debate, and it can vary depending on the technological requirements and the equipment being used [1].

The aim of this work was to develop the process of electrochemical formation of Ag-Sn layers of the required composition on the copper surface.

In the series of experiments on the test sample represented by the copperplate (cathode), the layers of silver and tin were deposited in series by electroplating. For electrochemical formation of the silver layer, there was chosen the electrolyte on the basis of silver nitrate (40 g) and potassium iodide (400 g) dissolved in 1 L of deionized water. For the deposition of tin, there was used stannous sulphate (100 g), dissolved in 1 L of 2N sulfuric acid [2]. These electrolytes are stable enough on long storage, and the deposition from them is little sensitive to the process temperature, and it is characterized by good reproducibility. As a result of the experimental analysis of the electrolytes there was chosen the optimal value of the cathode current density (for Ag 0,53 A/dm², for Sn 0,27 A/dm²) which allows us to obtain homogeneous fine-crystalline coating. At increasing of the cathode current density there was observed the increase of crystallites sizes in the coating being deposited, and as a result, the increase in the surface roughness and bad adhesion.

The results of the experiments on the layered structure formation on the basis of the system Ag-Sn on the copperplate are presented in the Table 1.

Table 1 Parameters and results of the experiments

Number of the sample	Deposition of Ag		Deposition of Sn		Tin content, mass percent, %
	Deposition time, min	Mass of the deposited material, g	Deposition time, min	Mass of the deposited material, g	
1	10	0,0070	20	0,0033	32
2	18	0,0130	20	0,0033	20
3	2,5	0,0014	34	0,0073	84
4	10	0,0074	40	0,0073	50

As a result of the conducted experiments there was developed the technology of electrochemical deposition of Ag-Sn layers on the copperplates with good reproducibility of the required composition. With the help of this technology it is possible to form layerwise solder structures with the required composition and alternation of layers depending on the necessary melting temperature of the solder, wettability of the soldered areas, and also the improvement in electrical and mechanical parameters of soldered contacts of the components being mounted.

1. A. Ivasik, Y.A. Koval'. "Lead-free soldering in details". Radiocomponents J., **3** (3), pp. 14-16, 2005 (in Russian).
2. V.R. Kukhtyaeva, I.N. Petukhov, K.S. Sen'chenko, A.S. Savvateeva. "Investigation of processes of local formation of lead-free solder contacts for mounting integrated circuit chips". Infrastructure of the objects of environmental and technical geosystems. Collection of scientific papers. pp. 60-74. Moscow: MIET, 2013 (in Russian).

Heat release efficiency improving in multilayered aluminum-copper nitride composite thermite materials

D.G. Gromov¹, E.A. Lebedev¹, A.S. Shuliatyev¹, Yu.I. Shilyaeva¹, Y.P. Shaman², D.I. Smirnov³, A.A. Dudin⁴, and E.P. Kirilenko⁵

1. National Research University of Electronic Technology (MIET), Zelenograd, Moscow, Russia,

E-mail: dr.beefheart@gmail.com

2. Science Manufacturing complex "Technological Center", Zelenograd, Moscow, Russia

3. Lebedev Physical Institute of Russian Academy of Science, Moscow, Russia

4. Institute of Nanotechnology of Microelectronics of Russian Academy of Science, Moscow, Russia

5. Science-Technological center "Nano- and Microsystems technics", Moscow, Russia

Over the recent years thermite materials have attracted increasing attentions due to their exceptional combustion characteristics and have already found various applications: development of the new generation of energetic materials, dramatically improve of conventional soldering technologies like "Flip chip" for interconnecting semiconductor devices, such as IC chips and microelectromechanical systems, by using such materials as local heat sources [1-3]. Research and development of a method of start temperature manipulation and increasing efficiency of chemical reactions in such thermite systems is still being the main technology task for scientists and researchers.

In this work the thermite material type based on multilayer aluminum-copper nitride structure is presented. Thermodynamic calculation and analysis of combustion effects in such composite are performed. Experimental DCS studies of multilayer thermite composite were held and possibility of start temperature manipulation and chemical reaction efficiency increasing were shown.

Thermite multilayer Al/CuN foils of different total and bilayer thickness (from micro to nanosize) were fabricated by magnetron sputtering from Al and Cu (in nitrogen atmosphere) targets onto silicon substrates that rotated in front of the targets. Thermal effects measurements were performed by differential scanning calorimetry in temperature range from 50 to 1000 °C. Heating velocity changes from 5 to 50 degrees per minute. Structural and elemental analysis performed by X-ray diffraction (XRD) and X-ray energy-dispersive spectroscopy (XEDS) measurements.

It was shown that the main DSC-peak temperature increased and reaction propagation velocity decreased with bilayer thickness, and the peak form and position also depends on nitrogen pressure during the magnetron sputtering. The structure and element analysis were performed by XRD and XEDS. Obtained experimental results allowed to correct the proposed mathematical model.

1. M.R. Weismiller, J.Y. Malchi, J.G. Lee, R.A. Yetter, T.J. Foley, "Effects of fuel and oxidizer particle dimensions on the propagation of aluminum containing thermites", Proceedings of The Combustion Institute, **33**, pp. 1989-1996, 2011.
2. M. Petrantoni, C. Rossi, V. Conedera, D. Bourrier, P. Alphonsw, C. Tenailleau, "Synthesis process of nanowired Al/CuO thermite", Journal of Physics and Chemistry of Solids, **71**, pp. 80-83, 2010.
3. M. Petrantoni, C. Rossi, L. Salvagnac, V. Conedera, A. Esteve, C. Tenailleau, P. Alphonse, Y.J. Chabal, "Multilayered Al/CuO thermite formation by reactive magnetron sputtering: Nano versus micro", J. Applied Physics, **108**, 084323, 2010.

TaN_x and Ta/graded Ta(N)/TaN multilayer diffusion barriers

V. Kalnov¹, I. Khorin^{1,2}, N. Orlikovsky¹, A. Rogozhin¹

1. Institute of Physics and Technology of RAS, Moscow, Russia, rogozhin@ftian.ru.

2. Moscow State Technical University of Radioengineering, Electronics and Automation (MSTU MIREA), Moscow, Russia.

Ta-based materials are the widespread choice as the diffusion barriers in copper metallization. Bi-layer Ta/TaN_x system is great for copper diffusion barriers and adhesion promoter. In the composite barrier, the TaN_x film is used as an adhesion layer between the Ta and dielectric films. Furthermore the amorphous TaN_x film is better than the polycrystalline Ta film to prevent copper diffusion into the dielectric layer. The Ta layer contributes to the adhesion ability between the TaN_x and copper metals. In addition, it has been investigated that the Ta film has better wettability than that of the TaN_x film for copper nucleation [1]. On top of a TaN_x underlayer, Ta grows in the low resistivity body-center cubic phase (α -Ta, $\rho = 15\text{--}60 \mu\Omega \times \text{cm}$), whereas directly on the dielectric the high resistivity tetragonal β -Ta phase ($\rho = 150\text{--}210 \mu\Omega \times \text{cm}$) would grow [2]. The presence of oxygen containing impurities is an important factor for the growth and nucleation of β -Ta during sputter deposition [3]. The phase transformation from β - to α -Ta occurs at a temperature between 300 °C and 400 °C, however, oxygen impurities within the Ta layer or the presence of oxygen can result in a significantly higher transition temperature.

The TaN_x microstructures of thin films as well as electrical properties depend greatly on the deposition parameters. Hence, in the reactive sputtering process chosen in this work, the N₂-to-Ar gas ratio was a major factor influencing the electrical resistivity of TaN thin films. Variations in stoichiometry are common in TaN_x films due to their defect structure. Consequently, the properties of the films strongly depend on the deposition conditions [4].

TaN_x thin films were deposited onto Si(100) substrates in N₂/Ar ambient by DC reactive magnetron sputtering. Dependences of film deposition rate and resistivity of layers TaN_x on the nitrogen maintenance in a mix of gases for a range $p(\text{N}_2)/(p(\text{N}_2)+p(\text{Ar}))$ from 2.5 to 25 % are received. The curve of deposition rate has a maximum at value $p(\text{N}_2)/(p(\text{N}_2)+p(\text{Ar}))=5\text{--}10$ %. Furthermore, the increasing of N₂ partial pressure will cause "target poisoning" and lead to the sputtering mode change from metal to nitride. So the deposition rate declines. An increase of the electrical resistivity from 157 to 451 $\mu\Omega \times \text{cm}$ is observed when the partial N₂ pressure increases from 2.5-25%. EDX has found the nitrogen content in films correlates with pressure of nitrogen in the chamber during film deposition.

Structures Cu (50 nm)/Ta (30 nm)/Ta (N) (5 nm)/Ta_xN_x (15 nm) were reactively sputtered on substrates SiO₂ (200 nm)/Si (100). For the deposition of tantalum nitride the N₂/Ar flow ratio has been fixed on 15 %. A graded Ta(N) layers were deposited by gradually decreasing of N₂ flux to zero. Resistivity of structures decreases with reduction of the power of Ta target, and with enlarging of the power of Cu target. The minimum value of structure resistivity ($4.1 \times 10^{-2} \Omega/\square$) was received at Ta and Cu power values of 100 and 450 W, respectively. Annealing at temperatures 300 and 400 °C leads to decrease of structure resistivity. However, after annealing at 500 and 600 °C the sheet resistance of the samples increases abruptly. This indicates that Cu diffuses into TaN_x film and the diffusion barrier is failed. The minimum value of resistivity ($3.2 \times 10^{-2} \Omega/\square$) was received for structure in which both layers, Ta and Cu, were formed at power of 100 W with subsequent annealing at temperature 300 °C. Nanopics 2100 AFM was used to measure the root-mean-square (RMS) of surface before and after annealing. The evolution of a structure surface after annealing was investigated by SEM. It was detected a crystallites growth on the structure surface after 500 °C annealing. The crystallites density depends on conditions of a barrier layer deposition. This data well correlates with sheet resistance measurements.

1. T. Hara, K. Sakata, A. Kawaguchi, and S. Kamijima. "Control of Agglomeration on Copper Seed Layer Employed in the Copper Interconnection". *J. Electrochem. Solid-State Lett.*, **4** (11), pp. C81-C84, 2001.
2. Y.-S. Wang, W.-H. Lee, Y.-L. Wang, C.-C. Hung, and S.-C. Chang "The electrical property of plasma-treated Ta/TaN_x diffusion barrier". *J. Phys. Chem. Solids*, **69**, pp. 601–604, 2008.
3. A. Schauer and W. Peters "The influence of film thickness on the formation of β -Ta and b.c.c.-Ta". *Thin Solid Films*, **27** (1), pp. 95–99, 1975.
4. N. Frety, F. Bernard, J. Nazon, J. Sarradin, and J.C. Tedenac "Copper Diffusion Into Silicon Substrates Through TaN and Ta/TaN Multilayer Barriers". *J. Phase Equilib. Diffus.*, **27** (6), pp. 590-597, 2006.

Surface treatment of polyimide film for metal magnetron deposition in vacuum

V. Petrov, D. Vertyanov, S. Timoshenkov

National Research University of Electronic Technology (MIET), Moscow, Zelenograd, Russia,

E-mail: petrovvasiliy.s@yandex.r, evolutionden@mail.ru, spt@miee.ru

Miniature electronic devices made on flexible substrates are widely used in electronic industry, especially in aerospace instrumentation. Using polyimide base for board formation provides light weight, bend ability, radiation resistance, and cost reduction. Microcircuit in frameless design has been increasingly used to reduce device weight and size. Technology of weldless and solderless mounting [1] is one of the developing directions.

Solderless assembly process differs from the standard that production takes place in the reverse order. First crystals set then structural layers are formed. No need for large areas for components or for brazing surface are such mounting advantages. It makes possible to simplify the wiring of the array components. Moreover, there is no need for drilling the holes with a high ratio of length to height throughout the assembly. When the solder is not used for connection manufacture [2] there is a possibility of reducing the number of layers required for the design and also no problem about the short-circuit, breakage, voids, hillocks or residues of tin.

Our goal was to obtain a defect-free flexible base with stable electrical characteristics for further metallization by magnetron method. Surface of domestic polyimide film for various types of treatment has been studied. Several types of domestic production polyimide films such companies as ESTROKOM and ELIFOM with thicknesses of 12, 20 and 25 microns were selected as materials for study. Studying the surface by a Scanning Electron Microscope (SEM) was showed that the film supplied from the manufacturer with a surface defects, however it is necessary an additional treatment for the subsequent formation of the polyimide layer for metallization process. As the main method of producing a polyimide film is watering, so clearly traced furrows and grooves, as well as sharp peaks and deep troughs, traces of air bubbles have been shown by microscope. Various kinds of surface treatment at different temperatures from 23 °C to 60 °C have been performed.

It was found out that the solution temperature influences the process speed, but the quality of the resulting surface has no effect. Impact on the film surface may be small and superficial, so we try using more active micro-etching solution. Only a partial smoothing of the maximum irregularities height from 250 nm to 150 nm was after treatment in a weak activating solution - dimethylformamide. Sulphate potassium bichromate was used as a strong etching solution. Smoothing irregularities were observed, but because of the high solution activity surface layer was destroyed and the defect structure was preserved. The resulting structures were not suitable for the magnetron sputtering of metals.

We applied lacquer PO-1-40 on the surface similar to the polyimide structure for alignment defects on polyimide films. To achieve a high degree of planarization, lacquering was carried out by spin coating. At the optimum ratio of the rotation speed 2000 rpm and time 30 sec, we were getting a uniform layer of lacquer. It is smoothed after curing all the irregularities on the surface of the polyimide film. Due to a related structure, lacquer has high adhesion and close to the coefficient of polyimide thermal expansion, as well as low moisture absorption of 0.4%. It should be noted that the polyimide film becomes less flexible and ductile that it does not affect the adhesive properties

1. D.V. Vertyanov, V.S. Petrov, P.N. Konstantinov. "Comparative analysis of two technologies frameless mounting crystals on a flexible substrate multichip module". Microelectronics and computer science – 2013, **20th** National Interuniversity Scientific and Technical Conference of Students and Graduate Students, p. 83, 2013.
2. J. Fjelstad. *Flexible Circuit Technology*. Fourth Edition. Publishing Inc, 2011, pp. 458-457.

FMR evidence of High- T_c ferromagnetism in $Mn_{52}Si_{48}$ thin film

S. Kapelnitsky^{1,2}, A. Drovosekov³, N. Kreines³, V. Rylkov², V. Tugushev², S. Zhou⁴

1. Institute of Physics and Technology RAS, Moscow, Russia, kapelnitski@gmail.com

2. NRC “Kurchatov Institute”, Moscow, Russia, vrylkov@mail.ru

3. P.L.Kapitza Institute for Physical Problems RAS, Moscow, Russia, drovosekov@kapitza.ras.ru

4. Helmholtz-Zentrum Dresden-Rossendorf, Institute of Ion Beam Physics and Materials Research, Dresden, Germany, s.zhou@hzdr.de

Recently, above-room Curie temperature $T_c \approx 330$ K which exceeds by an order of magnitude the value ($T_c \approx 30$ K) for the bulk MnSi material, was observed in the nearly-stoichiometric $Mn_{1-x}Si_x$ ($x \approx 0.5$) thin films [1, 2] using static magnetic field, magneto-transport and magneto-optic measurements. Below, ferromagnetic resonance (FMR) method in the frequency range from 7.65 to 54.34 GHz is used to study 70 nm thick $Mn_{52}Si_{48}$ films prepared by pulse laser plasma deposition (PLD) on Al_2O_3 (0001) substrate at 340 °C.

The FMR resonance line has the nearly Lorenz form, the resonance field is isotropic when the external field lies in the film plane. In order to explain the orientation dependence of FMR vs. angle between the external field and the direction normal to the film plane, both the 2nd and 4th order effective magnetic anisotropy fields should be taken into account:

$$E = -\mathbf{H}\mathbf{M} + (1/2)(4\pi + K_2)M_z^2 - (1/4)K_4M_z^4/M_S^2, \quad (1a)$$

$$\mathbf{H}_{\text{eff}} = \mathbf{H} - (4\pi + K_2)M_z\mathbf{z} + K_4M_z^3/M_S^2\mathbf{z}, \quad (1b)$$

where \mathbf{M} is the magnetisation vector, M_S is the saturation magnetisation value, K_2 and K_4 are dimensionless anisotropy parameters. Resonance frequency is given by the Kittel formula.

The best fit of experimental data for the ‘in plane’ and ‘normal to plane’ orientations of the external field is achieved for the *second order easy plane* and *fourth order easy axis* anisotropy fields. The values of parameters are $K_2 = 8.3$ and $K_4 = 6.1$ at $T = 4.2$ K (magnetization $M_S = 440$ Gs was taken from the static measurements data). The matching of the ‘in plane’ and ‘normal to plane’ magnetization curves, gives respectively $K_2 = 5.4$ and $K_4 = 5.5$ assuming the (1b) expression for the net anisotropy field. That is in good agreement with K_2, K_4 obtained from the FMR data.

The temperature dependence of anisotropy fields in the temperature range 4.2-350 K was calculated from magnetization and FMR data. Magnetic anisotropy fields $H_{a2} = K_2M_S$, $H_{a4} = K_4M_S$ value decreases from $H_{a2} = 3.7$ kOe, $H_{a4} = 2.7$ kOe, at 4.2 K to zero values at Curie temperature.

High- T_c ferromagnetic order $Mn_{52}Si_{48}$ thin films, prepared by PLD method, discusses within the spin-fluctuation (paramagnon) model [3] for weak itinerant ferromagnets with embedded defect-induced local moments.

The angular dependence of magnetic anisotropy in Eqs. (1a, b) might be attributed to the magneto-elastic deformation effects and complex texture of the film induced by the film-substrate interface. Both phenomena lead to the random in-plane orientation of deformed nanometer size $Mn_{52}Si_{48}$ crystallites with the texture axis normal to the interface. Eqs. (1a,b) may be obtained in frame of the model [2] in the fourth-order approximation over the spin-orbit interaction between itinerant electrons and defect-induced local moments, taking into account the perturbation of crystal potential of the film by the deformation and texture effects near the film-substrate interface.

The work is partially supported by RFBR (grants 13-07-12087, 13-07-00477).

1. V.V. Rylkov, S.N. Nikolaev, K.Yu. Chernoglazov et al. “High-temperature ferromagnetism in $Si_{1-x}Mn_x$ ($x \approx 0.5$) nonstoichiometric alloy”, JETP Lett., **96**, pp. 272–280, 2012.
2. V.V. Rylkov, E.A. Gan’shina, O.A. Novodvorskiy et al. “Defect-induced high-temperature ferromagnetism in $Si_{1-x}Mn_x$ ($x \approx 0.52-0.55$) alloys”, Eur. Phys.Lett, **103**, pp. 57014-57020, 2013.
3. V.N. Men’shov, V.V. Tugushev, S. Caprara, “High-temperature ferromagnetism in Si:Mn alloys”, Phys. Rev. B **83**, pp. 035201-035213, 2011.

Study of growth kinetics of amorphous carbon nanopillars formed by PECVD

D. Gromov¹, V. Borgardt¹, Y. Grishina¹, A. Doncova², E. Kirilenko², and S. Dubkov¹

1. National Research University of Electronic Technology (MIET), Moscow, Russia (sv.dubkov@gmail.com)

2. Science-Technological Center "Nano- and Microsystems Technics", Russia, Moscow

Recently, the growth of carbon nanostructures has attracted much attention because these flakes (CNFs), pillars (CNP) and wires have many potential applications in electronic devices and as field emitter materials for use in flat panel displays due to their low turn-on voltage [1]. Their high surface area also makes CNPs/CNFs attractive for electrochemical applications, such as fuel cell electrodes and supercapacitors [2]. In recent years, much effort has been made to elucidate the mechanism of SWNT [3] growth. Although significant progress has been made in the production and kinetics of the growth of CNTs by CVD, but understanding mechanism of the growth another form of carbon structures is still incomplete.

In this work carbon nanostructures formed by PECVD with glow-discharge plasma on direct current. The synthesis of carbon nanostructures held in a temperature range 100-350 °C without using a metal catalyst. The CO gas was used as a source of carbon. In the first stages, we selected three silicon substrates and carbon nanostructures formed at different temperatures: flakes – 350 °C, pillars – 250 °C, carbon film – 100 °C. After measuring the height of the deflection of the samples were counted mechanical stresses of carbon nanostructures. The results are shown in Table 1.

Table 1 - Results of the measurements of the mechanical stresses in carbon nanostructures

Sample	Carbon nanostructure	Inflection, [mkm]	e, Value of deformation in the structure	σ , Tension in the film, [MPa]
1	Film	9,4	15×10^{-4}	227
2	Pillars	2,3	3×10^{-4}	57
3	Flakes	3,9	6×10^{-4}	96

As can be seen from Table 1, significant tensions have carbon nanopillars. Mechanical stress carbon nanopillars can be compared with the mechanical stresses of pyrolytic carbon [4]. Model of growth of carbon nanopillars was proposed. It is assumed that the pillars are formed under high mechanical stresses arising in the course of their growth. The growth kinetics of carbon nanopillars: (1) formation of a thin carbon layer; (2) rupture of a thin carbon layer and the formation of carbon clusters; (3) vertical growth of the carbon fibers in combing nanopillars.

1. G. Gu. T. Ito. "Field emission characteristics of thin-metal-coated nano-sheet carbon films". *App. Sur. Sci.*, **257**, pp. 2455-2460, 2011.
2. Y. Kato, T. Obara, I. Yamanaka, S. Mori, A. Dipu, J. Ryu, Y. Ujisawa, M. Suzuki. "Performance analysis of active carbon recycling energy system". *Progress in nuclear energy*, **53**, pp.1017-1021, 2011.
3. G. Eres, C. Rouleau, M. Yoon, A. Puretzky, J. Jackson, D. Geohegan. "Model for self-assembly of carbon nanotubes from acetylene based on real-time studies of vertically aligned growth kinetics". *J. Phys. Chem. C.*, **113**, pp.15484-15491, 2009.
4. H. Choon, L. Jai-Young, S. Oh. "Mechanical properties of isotropic pyrolytic carbon deposited in a tumbling bed". *Carbon*, **23**, pp 487-492, 1985.

The increase in the conductivity of the layers of composite nanomaterials with carbon nanotubes

A.Y. Gerasimenko¹, L.P. Ichkitidze^{*1}, S.V. Selishchev¹, E.V. Blagov², A.A. Pavlov²,
E.P. Kitsuk³, Yu.P. Shaman³

1. National Research University of Electronic Technology (MIET), Zelenograd, 124498 Moscow, Russia

*e-mail: leo852@inbox.ru

2. Institute of Nanotechnology of Microelectronics of the RAS, 119991 Moscow

3. Scientific-Manufacturing Complex "Technological Centre", MIET, Zelenograd, 124498 Moscow

The electrical conductivity of the layers of composite nanomaterials consisting of carboxymethyl cellulose (CMC, matrix) and different type of carbon nanotubes (CNTs, filler) studied. The aqueous dispersion consisted of 4 wt.% CMC and 0.05÷2.5 wt.% CNT, which was applied by screen printing on flexible (polyimide (PI), cotton cloth (CC), pigskin, office paper (OP) with a density of ~ 80 g/m²) and solid substrate (Si plastics with a sublayer SiO₂ (Si/SiO₂), a coverslip glass (CS)). Layers had thickness 0.5÷10 μm. Single-walled CNTs (SWCNTs) had diameters of ~ 1 nm, length > 0.5 μm, and multiwall CNTs (MWCNTs) with diameter 10÷20 nm and length > 10 μm. The samples were of rectangular shape with dimensions 3÷5 mm 15÷30 mm. Current-voltage characteristics were measured four-probe method.

It has been established that the laser radiation is significantly increased conductivity layers. Immediately after application, when the layers were still in the "liquid state", half of the layers covering the opaque plate, and the other was exposed to continuous irradiation by laser radiation (LI, wavelength of 970 nm, power density of 0.05÷0.5 W/cm², the diameter of laser beam ~ 30 mm, continuous mode). It has been established that the laser radiation is significantly increased conductivity σ of layers. In particular, in layers of SWNT growth σ reached up to 300%, and in layers of MWCNTs - up to 30% relative to the layers that are not subject LI.

Additional multiplication σ implemented due to thermal processing layers. Annealing at 200±10 °C (PI, Si/SiO₂, CS) resulted an increase the σ in 3÷4 times for all samples on the initial layers, not subjected to LI or heat treatment.

After multiple bends layers on flexible substrates the substantial changes of their σ have not been detected. For example, when bending by 180° with a bending radius of 1 mm and a cycle of 1000 times of samples on substrates of CC and OP the conductivity varies by not more than ± 20% relative to baseline values. After many twists layers of substrates does not flake its, does not crack and retains its previous appearance.

Physical mechanisms of the effect of LI and thermal processing on σ are complex and varied. For example, perhaps under the influence of LI the ties of SWNTs aqueous dispersion (CMC+CNT) are destroyed, and the nanotubes are more straightened and more uniformly distributed in the composite nanomaterials. Heat treatment, apparently promotes transparency electric contact between CNT layers or between the CNTs and the matrix. Undoubtedly, the proposed mechanisms contribute to the growth Heat treatment, apparently promotes transparency electric contact between CNT layers or between the CNTs and the matrix. Undoubtedly, the proposed mechanisms contribute to the growth σ .

Thus, under the action of laser radiation and heat treatment was able to increase the conductivity of the layers of the composite nanomaterial more than an order of magnitude. The following order of the values were: σ ~ 10 kS/m in layers with SWCNTs and ~ 1 kS/m in layers with MWCNTs.

Investigated layers are relevant in a flexible and classical microelectronics, for example, a compound of nanoscale elements in medical applications such as conducting electrodes.

This work was supported by Russian Ministry of Education (Contracts No.14.430.11.0006 and No.14.575.21.0044).

Study of hydrogen states in a-Si:H films, dehydrogenization treatments and influence of hydrogen on nanosecond pulse laser crystallization of a-Si:H

V.A. Volodin^{1,2}, M.S. Galkov^{1,2}, N.A. Safronova^{1,3}, G.N. Kamaev^{1,2}, A.H. Antonenko^{1,2},
S.A. Kochubey¹

1. Rzhanov Institute of Semiconductor Physics, Russian Academy of Sciences, Lavrent'eva ave., 13, 630090, Novosibirsk, Russia, E-mail address: volodin@isp.nsc.ru. 2. Novosibirsk State University, Pirogova street, 2, 630090, Novosibirsk, Russia. 3. Novosibirsk State Technical University, 20 Prospekt K. Marksa, 630073, Novosibirsk, Russia.

Structures based on hydrogenated amorphous silicon (a-Si:H) on various substrates (including not refractory ones) are widely applied in giant microelectronics devices, such as flat panel displays based on active matrix thin-film transistors and solar cells [1]. The a-Si:H films produced by plasma enhanced chemical vapor deposition (PECVD) methods, contain up to 40% atoms of hydrogen. The influence of hydrogen on the optical and electrical properties of the films and their degradation is important. Therefore, the development of express and non-destructive methods for control of the hydrogen concentration in thin films continues to be an actual task to date. Previously, from a comparative analysis of IR spectroscopy and Raman scattering spectroscopy, the ratios of the integral intensities of Raman peaks on the Si-H and Si-H₂ bonds to the intensity of Raman scattering at the Si-Si bonds were experimentally determined [2]. Knowing these ratios, it is possible to measure the hydrogen concentration, moreover, separately in Si-H and Si-H₂ states [2]. Proposed quantitative method for determining of the hydrogen concentration from analysis of the Raman spectra is an express, non-destructive method and can be used for "in situ" monitoring of the hydrogen. In previous work [2] it was also found that the intensity of Raman scattering by vibrations Si-H bonds is approximately 2.6 times higher than the intensity of Raman scattering by vibrations Si-H₂ bonds at the same concentration of hydrogen. The aim of this work was to determine the polarization dependence of Raman scattering by stretching vibrations of silicon-hydrogen bonds and find the form of the corresponding Raman tensors.

In this study we have investigated the films obtained using the PECVD methods at temperatures from 100 to 380 °C. Raman spectra were recorded at room temperature in backscattering geometry, the line of Ar laser with a wavelength of 514.5 nm was used for excitation of Raman scattering. The position of Raman peaks can determine the state of hydrogen in the films as the stretching vibrations of Si-H bonds (~ 2000 cm⁻¹) and Si-H_n bonds (~ 2100 cm⁻¹) [3]. IR-spectroscopy, spectroscopy of transmission and reflectance of light, and spectral ellipsometry were also used for studying.

From analysis of Raman intensities in different polarizations the Raman tensors for Si-H and Si-H₂ bonds were determined. The regimes for dehydrogenization of thick (up to 1 micron) a-Si:H films were found.

The nanosecond pulse XeCl laser with wavelength of 308 nm and pulse duration of 10 ns was used for pulse crystallization of as-deposited and dehydrogenated films. As it was studied earlier, for a-Si:H films with high hydrogen concentration, the threshold for crystallization is very close to threshold of laser ablation [4]. As result of presented studying, it was obtained, that for pulse laser crystallization of a-Si:H films without damages and hydrogen blistering, the optimal concentration of hydrogen should be not higher than 10-15%. The developed approaches can be used for crystallization of a-Si:H films and based on these films nanostructures deposited on non-refractory substrates.

The work is supported by RAS, contract number 24-29.

1. G.J.H.M. Wilfried and Van Sark, Thin Films and Nanostructures, **30**, p. 1, 2002.
2. V.A. Volodin, D.I. Koshelev, Journal of Raman Spectroscopy, **44**, p. 1760, 2013.
3. M.H. Brodsky, M. Cardona, J.J. Cuomo, Phys. Rev., **B16**, p. 3556, 1977.
4. V.A. Volodin, S.A. Arzhannikova, A.A. Gismatulin, G.N. Kamaev, A.Kh. Antonenko, S.G. Cherkova, A.G. Cherkov, S.A. Kochubei, A.A. Popov, S. Robert, H. Rinnert, and M. Vergnat. Proc. SPIE, 2013, **8700**, 870008-1.

Mechanism of formation of nanoscale silicon phase in oxide matrix by light beams treatments

V.G. Litovchenko¹, I.P. Lisovsky¹, I.Yu.Maidanchuk¹, S.A. Zlobin¹,
I.G. Neizvestniy², V.A. Volodin^{2,3}, G.N. Kamaev²

1. V.E. Lashkaryov Institute of Semiconductor Physics, Kyiv, Ukraine, E-mail address: lvg@isp.kiev.ua.

2. Institute of Semiconductor Physics, Russian Academy of Sciences, Novosibirsk, Russia.

3. Novosibirsk State University, Novosibirsk, Russia.

Silicon nanosized inclusions formation as a result of phase separation in silicon suboxides (SiO_x) due to furnace thermal treatments is a wide spread technology. However, this procedure is sufficiently long-term and does not allow to infer the mechanism of silicon phase separation. Thus, carrying out short-form radial processes such as photon annealing (RTA) seems to be rather challenging.

Films of nonstoichiometric silicon oxide ($\text{SiO}_{1.3}$) were exposed to powerful pulsed illumination of halogen lamps which led to sample heating within the temperature range of 300–1000 °C (“Impuls-3” installation) in the nitrogen environment. Infrared (IR) and photoluminescence (PL) spectra were measured; film structure was investigated using high-resolution electron microscopy. IR band connected with absorption on Si–O bonds (peak position in the range of 1000 – 1100 cm^{-1}) depends on the oxide composition and enabled us to determine oxygen and silicon atoms ratio before and after annealing. That gives the possibility to evaluate the amount of silicon which is separated in the form of nano-inclusions and their specific volume in the oxide matrix. The presence of PL band within the red and near IR regions indicates nanosilicon formation; its position makes it possible to estimate the structure of silicon inclusions (amorphous or crystalline). Silicon nano-crystals were visualized by electron microscopy and their parameters (size and concentration) were determined.

It was shown that under temperatures higher than 900 °C phase separation process in the oxide films is terminated during about 1 s of radial anneal. Under smaller temperatures the slower kinetics of silicon concentration growth was observed with achievement of saturation. The latter occurred at 40, 10 и 4 s for the temperatures of 600, 650 and 700 °C, respectively. Under low temperatures formation of amorphous silicon inclusions surrounded with nonstoichiometric silicon oxide took place. Under the temperatures close to 1000°C silicon nano-crystals embedded in SiO_2 matrix were observed. This fact was proved by electron microscopy data, the size of nano-crystals being of 3 ± 0.5 nm.

The kinetic curves of thermostimulated silicon phase separation make it possible to estimate the parameters of the process of atoms diffusion which determines the formation of silicon nanoparticles. It was found that the diffusion coefficients calculated (10^{-8} – 10^{-10} cm^2s^{-1} within the temperature range of 1000–300 °C, respectively) exceed up to ten orders of magnitude those which is typical for silicon atoms in SiO_2 films (10^{-15} – 10^{-20} cm^2s^{-1} within the temperature range of 1200–1000 °C, respectively). Hence, wide spread hypothesis that silicon atoms diffusion defines the thermostimulated silicon phase separation contradicts our results.

On the other hand, silicon nanoparticles may be formed in the result of oxygen atoms diffusion from weakly oxidized complexes $\text{SiO}_y\text{Si}_{4-y}$ ($1 \leq y \leq 3$) to heavily oxidized ones. In particular, silicon-rich molecular complexes (mainly SiOSi_3) loose oxygen atoms due to SiO_x films annealing and turn into SiSi_4 tetrahedra. Released oxygen atoms diffuse to oxygen-rich molecular complexes (like SiO_3Si) and turn them into SiO_4 tetrahedra. As a result of such scenario the inclusions of silicon are created surrounded with silicon dioxide area. Analysis of the band shape of the IR-absorption spectra indicates that transformation of oxygen structural arrangement in oxide films under heat treatments occurs exactly this way. Moreover, for silicon oxide films typical magnitudes of the diffusion coefficient of oxygen atoms (10^{-11} – 10^{-14} cm^2s^{-1} within the temperature range of 1000–400 °C, respectively) exceed significantly those of silicon atoms and agree with our results well enough. These facts prove the hypothesis that exactly mobile oxygen atoms migration underlies the mechanism of thermostimulated phase separation in SiO_x films.

The work is supported by RFBR-NAS of Ukraine for 2014-2015 years, contract number 14-07-90403, and by State Program on Sensor products for 2008-2017 years (projects 1.1.4; 1.1.6).

New generation photoelectric converter structure optimization using nano-structured materials

A. Dronov, I. Gavrilin, A. Zheleznyakova

National Research University of Electronic Technology (MIET), Moscow, Russia, E-mail: noiz@mail.ru

Over the past 15 years there has been active development of new ideas for creating solar cells based on nanostructured materials. Due to the large interphase area in nanostructured materials light absorption and charge separation occurs several times more effective than in non-nanostructured materials. In particular, dye-sensitized solar cells based (DSSC) are promising and potentially low-cost alternative to traditional solar cells based on semiconducting p-n-junctions [1]. The efficiency of such converters under laboratory conditions was more than 11% [2]. However, a significant disadvantage of such solar cells is the presence of liquid between the electrodes, which significantly reduces the operating temperature range of such devices, which in turn reduces the application range and the period of its operation, and also requires additional requirements to the substrate and the photoelectrode. In order to avoid further problems of instability, a new concept of solid-state solar cell called ETA-cell (extremely thin absorber) in which the dye is replaced by solid inorganic semiconductor absorber was suggested. The conversion efficiency about 2-5% was achieved in such solar cells which demonstrate the ETA concept validity [3]. In work [4] the optimal thickness of the adsorber layer obtained by SILAR (Successive Ionic Layer Adsorption and Reaction) deposition method for ETA-cell, which is from 25 to 35 nm was found. ETA-cell concept further development resulted to using porous anodic titanium oxide (PAOT) with a high effective surface as a photoelectrode [5]. In this work, influence of anodizing process parameters on PAOT geometric parameters was studied to optimize and increase ETA-cell efficiency. During the calculations optimal geometrical parameters were obtained. Parameters such as anodizing voltage, electrolyte composition and temperature, as well as the anodic oxidation process time were selected for this investigation. To investigate the CVC during the measurements the samples were illuminated with the light source with the power density of 100 mW/cm². The results are shown in table 1.

Table 1. Results of the measurements of the test-structure characteristics of solar cells.

Type of TiO ₂ photoelectrode	U_{oc} , mV	J_{sc} , mA/cm ²	Efficiency, %	FF, %
Not nanostructured	543	3,23	0,92	23,0
Optimized morphology	660	11,61	2,81	39,0

Using the optimized TiO₂ photoelectrode layer with 2 μm porous layer thickness and pore diameter more than 80 nm the ETA-cell efficiency has been increased by 3 times comparing to non-nanostructured TiO₂ photoelectrode.

Further improving of ETA-cell effectiveness is possible by using various chalcogenide semiconductor compounds in adsorber layer and top transparent electrode material optimization.

1. B. O'Regan and M. Grätzel. "A low-cost, high-efficiency solar cell based on dye-sensitized colloidal TiO₂ films". *Nature*, **353**, pp. 737–740, 1991.
2. M. Grätzel. "Conversion of sunlight to electric power by nanocrystalline dye-sensitized solar cells". *J. Photochem. Photobiol. A.*, **164**, pp. 3–14, 2004.
3. C. Lévy-Clément, R. Tena-Zaera, M.A. Ryan, A. Katty, and G. Hodes. "CdSe-Sensitized p-CuSCN/Nanowire n-ZnO Heterojunctions". *Adv. Mater.*, **17**, pp. 1512–1515, 2005.
4. I. Oja, A. Belaidi, L. Dloczik, M.-Ch. Lux-Steiner, Th. Dittrich. "Photoelectrical properties of In(OH)_xSy/PbS(O) structures deposited by SILAR on TiO₂". *Semiconductor Science and Technology*, **21** (4), pp. 520-526, 2006.
5. A. Belov, I. Gavrilin, S. Gavrilov, A. Dronov, A. Shulyatyev. "Application of highly-ordered TiO₂ nanotube arrays in photovoltaic converters with ultra-thin absorbing layer on a flexible carrier" (in Russian) *News of Higher educational institutions. Electronics*, **2** (88), pp. 38-42, 2011.

Research of band structure features of hexagonal planar photonic crystals

A. Friman

P.N. Lebedev Physical Institute 53 Leninskij Prospekt, Moscow, 119991, Russia. friman_a@sci.lebedev.ru

Planar photonic crystals attract significant interest at last decades due to their perspectives at optoelectronics. Under study photonic structures have the same lattice symmetries as graphene and possess the same energy bands features.

Band structures and transmission spectra of hexagonal planar crystals were calculated using the plane wave expansion (PWE) [1] and the Finite Difference Time Domain (FDTD) [2] methods. Two types of hexagonal planar photonic crystals were simulated: air filled holes at a GaAs wafer and GaAs rods in air (Fig. 1a, b).

Energy bands touch was observed at K point of Brillouin zone of planar photonic crystal constructed of GaAs rods in air that similar to Dirac points at graphene [3]. Energy surfaces near corner of Brillouin zone (K point) shown at Fig. 2a. Band gap appearance at K point found out with increasing off-diagonal components of ϵ -tensor (Fig. 2b).

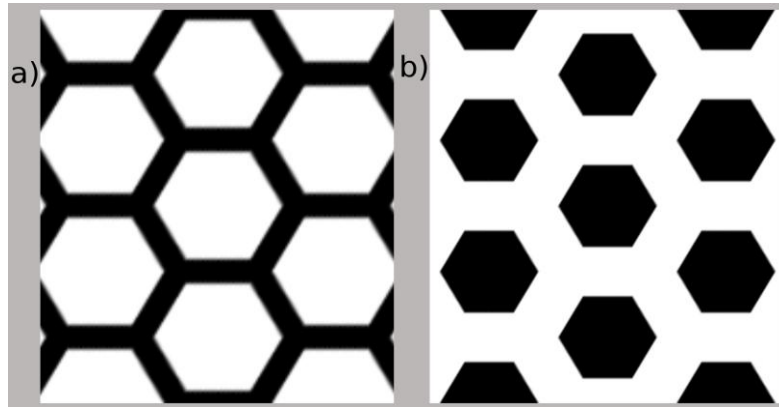


Fig. 1: Photonic crystal structures: a) air holes at GaAs wafer; b) GaAs rods at air.

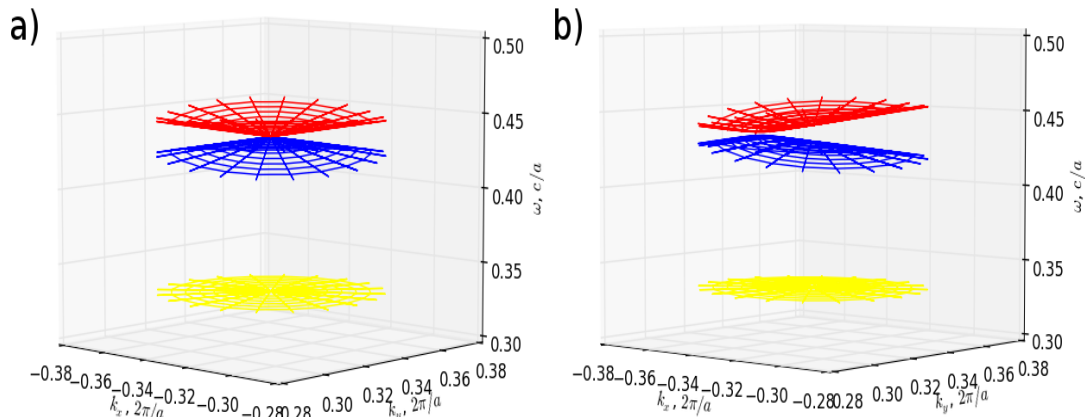


Fig. 2: Energy surfaces near corner of Brillouin zone: a) GaAs rods at air; b) Modified material with off-diagonal components of ϵ -tensor rods at air.

1. K.M. Ho, C.T. Chan, and C.M. Soukoulis, "Existence of a photonic gap in periodic dielectric structures," *Phys. Rev. Lett.*, **65**, pp. 3152-3155, 1990.
2. A. Taflov, "Application of the finite difference time-domain method to sinusoidal steady state electromagnetic penetration problems", *IEEE Trans. Electromagn. Compat.*, **22**, pp.191-202, 1980.
3. G.W. Semenoff. "Condensed-Matter Simulation of a Three-Dimensional Anomaly", *Phys. Rev. Lett.*, **53**, pp. 2449-2452, 1984.

Different methods of forming multicomponent metal sulfide by SILAR-techniques

S. Gavrilov, A. Zheleznyakova, A. Dronov, A. Presnukhina, E. Popova

National Research University of Electronic Technology (MIET), Moscow, Russia, E-mail address: Stushka@bk.ru

Using multicomponent sulfides as functional layers of solar cells with extra-thin absorber (ETA-cell) is one of the most promising directions for solar energy development. Multicomponent semiconductor based on zinc, copper and tin sulfides will significantly reduce the cost of new generation solar cells. The main advantages of this material are the high value of the absorption coefficient and the band gap. These parameters can be defined by controlling the compound stoichiometry and changing elements ratio included in the material. The principal components of the compound are widespread and non-toxic. The absorption coefficient of $\text{Cu}_2\text{ZnSnS}_4$ (CZTS) is 10^4cm^{-1} . It is equivalent to 90% of the absorption of light incident on a 100 nm^2 surface area. CZTS has p-type conductivity [1].

The most promising multicomponent sulfides formation method which can reduce the cost of energy converters is chemical deposition. In particular, special interest is paid to successive ionic layer deposition and reaction (SILAR) technique.

Complex semiconductor compounds formation by SILAR-technique can be carried out in two ways. In the first case it is sufficient to mix the respective ion source solutions in the desired proportions. $\text{Cu}_2\text{ZnSnS}_4$ deposition was carried out from aqueous solutions of CuCl_2 , SnCl_2 , $\text{Zn}(\text{NO}_3)_2$, and Na_2S (Fig. 1a). The various metal ions concentration in the ion source solution corresponds to the stoichiometric composition of the desired material. One monolayer of material is formed by one cycle of deposition. In the second case solutions-precursors were prepared separately for each element: CuCl_2 , SnCl_2 , and $\text{Zn}(\text{NO}_3)_2$ (Fig. 1b). Deposition of each sulfide CuS , SnS , and ZnS held alternately. One cycle in this case comprises four subcycles. As a result, one layer of CZTS contains CuS , SnS , and ZnS layers. The sequence and quantity of sulfide monolayers is determined by semiconductor compound stoichiometric composition. The formed structures were annealed in air for 30 minutes at 150 C .

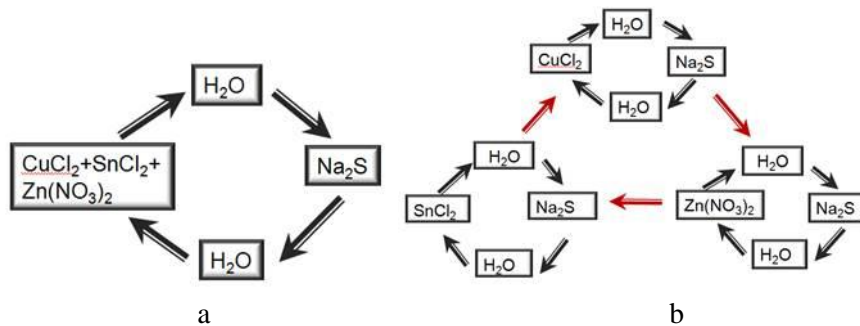


Fig. 1. The approximate scheme of the formation of compound semiconductor by the first (a) and the second (b) ways.

Obtained films were investigated by EDS analysis and optical spectroscopy using the porous anodic alumina as a matrix for deposition.

It was established that the precursor-solutions have a significant influence on the formed films composition. This influence is largely manifested during the multicomponent compounds formation by the first way of SILAR-technique. Films obtained by the second method leads to cleaner films which are closer to the stoichiometric composition of desired material. However, even usage of the second method it should be very accurate ion source solutions choosing.

1. J.J. Scragg, P.J. Dale, L.M. Peter, G. Zoppi, I. Forbes. *New routes to sustainable photovoltaics: evolution of $\text{Cu}_2\text{ZnSnS}_4$ as an alternative absorber material*, Phys. Stat. Sol. (b) **245** (9), pp. 1772–1778 (2008).
2. S.A. Gavrilov, A.V. Zheleznyakova, E.N. Redichev, and N.I. Popenko. *The influence of solution-precursors on optical properties of In_2S_3 films deposited by successive ionic layer deposition and reaction*, Semiconductors, **44** (13), pp. 1649–1653, 2010.

Correlative Compositional Analysis of Fiber-Optic Nanoparticles

E. Norman¹, H. Francois-Saint-Cyr², I. Martin², W. Blanc³, P. LeCoustumer⁴, C. Hombourger¹,
D. Neuville⁵, D.J. Larson², T.J. Prosa², and C. Guillermier⁶

1. CAMECA SAS, 29, quai des Gresillons, 92230 Gennevilliers Cedex, France

2. CAMECA Instruments Inc., 5500 Nobel Drive, Suite 100, Madison, WI, 53711, USA

3. Université Nice Sophia Antipolis, CNRS, LPMC, UMR7336, 06100 Nice, France

4. Université Bordeaux 3, Géo-ressources et Environnement, EA4592, 33607 Pessac, France

5. Institut de Physique du Globe de Paris, 1 rue Jussieu, 75005 Paris, France

6. National Resource for Imaging Mass Spectroscopy, Cambridge, MA 02139, USA

Development of new active optical fiber devices requires materials with augmented intrinsic properties, using luminescent ion-doped silica as a host glass. Nanoparticles (NPs) in optical fibers can provide this augmentation as they can combine the sturdiness and low cost of silica with particular spectroscopic behavior that would not appear in a pure silica local environment. Ideally, NPs would fully encapsulate luminescent ions to produce engineered spectroscopic properties. This technology would be of great interest for a large domain of applications: high power fiber lasers, random lasers, light sources with new wavelengths and telecommunications.

As silicate systems have a large phase immiscibility domain when they contain divalent metal oxides (such as Mg), one can take advantage of thermal treatments inherent to the MCVD process to obtain NPs through phase separation. NPs are formed *in situ* during material deposition and subsequent processing. Although glass-ceramics were discovered in 1950's, there is a great demand on experimental data to understand the early stages of nucleation [1]. Modern glass ceramics are generally obtained through many trial-and-error processing steps, involving variations in composition as well as thermal treatments. Although classical nucleation theory was the first model proposed to explain those phenomena, growth rate mismatches could encompass several orders of magnitude. According to this capillary assumption-based model, nuclei properties are the same as those of the bulk (same structure and composition). Recent articles disprove assumption of structure, pointing toward NPs structural changes [2] and transition from amorphous nuclei to crystalline NPs [3]. Compositional changes for small particle sizes (~1-10 nm) have been measured in alloys with Anomalous Small Angle X-Ray Scattering (ASAXS) [4] and in steels with Atom Probe Tomography (APT) [5]. Recent developments in APT has allowed the extension of such studies to glass-ceramics [6], and in the current work, we report experimental data disproving the second capillary assumption at the early stage of nucleation-growth process.

Composition of NPs was investigated using APT, NanoSIMS, and Transmission Electron Microscope. In these studies APT was able to identify the features and quantify their internal concentration of Mg, P, and Er for particles in the 1 – 10 nm size range. These results will be discussed in detail. The mechanisms for particle nucleation and growth in optical fibers are very important as increased understanding of these processes is expected to lead to improvements in the performance of these materials.

1. N. Karpukhina *et al.*, Chemical Society Review (2014), DOI 10.1039/C3CS60305A.

2. S.Y. Chung *et al.*, Nature Physics, **5**, p. 68, 2009.

3. P. Tan *et al.*, Nature Physics, **10**, p. 73, 2014.

4. D. Tatchev *et al.*, Journal of Applied Crystallography, **38**, p. 787, 2005.

5. M.D. Mulholland, D.N. Siedman, Acta Materialia, **59**, p. 1881, 2011.

6. D.J. Larson *et al.*, "Local Electrode Atom Probe Tomography" (Springer, New York 2014).

Thermodynamic analysis and physical properties of $(\text{TlInSe}_2)_{1-x}(\text{TlGaTe}_2)_x$ solid solutions

M. Asadov¹, S. Mustafaeva², A. Mammadov¹

1. Institute of Catalysis and Inorganic Chemistry named after M.F. Nagiyev, Azerbaijan National Academy of Sciences, pr. H. Javid 113, Baku, AZ1143 Azerbaijan. E-mail: mirasadov@gmail.com

2. Institute of Physics, Azerbaijan National Academy of Sciences, pr. H. Javid 131, Baku, AZ1143 Azerbaijan. E-mail: solmust@gmail.com

TlInSe_2 and TlGaTe_2 single crystals are typical representatives of chain-layered semiconductors and attract a lot of attention due to their interesting physical properties. These properties include strong anisotropy of the electric parameters related to special features in the crystalline structure. TlInSe_2 single crystal has a wide range of physical characteristics of practical importance, such as high photo- and X-ray-sensitivity. The purpose of this work: thermodynamic analysis, the study of physical properties of $(\text{TlInSe}_2)_{1-x}(\text{TlGaTe}_2)_x$ ($x = 0-1$) solid solution crystals.

Unlimited solid solutions are formed in binary and ternary systems, in the presence of the proximity of the crystal lattices of the initial components, ionic radii and electronegativity of anions. We carried out thermodynamic study of the TlInSe_2 - TlGaTe_2 system based on the data of physicochemical analysis.

Equation of temperature and concentration dependence of Gibbs free energy ΔG_T^0 of formation of solid solutions of non-molecular compounds for ternary and quaternary systems was used as a model.

Concentration dependence ΔG_T^0 of solid solutions is characterized by a negative deviation from the additive dependence. This agrees with the physico-chemical analysis and testifies the unlimited solubility in the solid state in TlInSe_2 - TlGaTe_2 system.

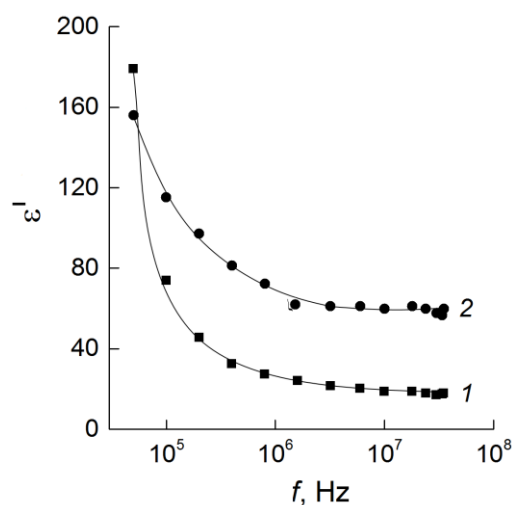


Figure. Frequency dispersion of real part of complex dielectric permittivity of TlInSe_2 single crystal (curve 1) and $(\text{TlInSe}_2)_{0.5}(\text{TlGaTe}_2)_{0.5}$ solid solution (curve 2), $T = 300$ K.

Figure shows the frequency dependence of ϵ' for $(\text{TlInSe}_2)_{0.5}(\text{TlGaTe}_2)_{0.5}$ (curve 2) and TlInSe_2 (curve 1) for comparison. At frequencies $f \geq 10^5$ Hz ϵ' values of solid solution are of 1.5-3.3 times higher than that of TlInSe_2 . ϵ' value of TlInSe_2 decreased by one order, and $(\text{TlInSe}_2)_{0.5}(\text{TlGaTe}_2)_{0.5}$ to 2.6 times with increasing frequency from 50 kHz to 35 MHz. In other words, dielectric permittivity dispersion of $(\text{TlInSe}_2)_{0.5}(\text{TlGaTe}_2)_{0.5}$ solid solution decreased significantly in comparison with TlInSe_2 . The results

demonstrate that the dielectric dispersion in the studied crystals TlInSe_2 and $(\text{TlInSe}_2)_{0.5}(\text{TlGaTe}_2)_{0.5}$ has a relaxation nature.

Based on thermodynamic analysis and concentration dependence of physical properties, it was found that there is anion-cation substitution in TlInSe_2 - TlGaTe_2 system. Frequency dispersion of real and imaginary components of complex dielectric permittivity, loss tangent and ac-conductivity of crystals of solid solutions are studied in the 50 kHz-35 MHz frequency range. Continuous series of $(\text{TlInSe}_2)_{1-x}(\text{TlGaTe}_2)_x$ solid solutions is forming throughout entire concentration range. We determined dielectric characteristics of samples, their frequency dispersion and nature of dielectric losses.

1. S.N. Mustafaeva, M.M. Asadov, A.I. Dzhabbarov. "Dielectric Properties and Charge Transfer in $(\text{TlInSe}_2)_{0.1}(\text{TlGaTe}_2)_{0.9}$ for the DC and AC Current". Physics of the Solid State, **56** (6), pp. 1096-1110, 2014.

Phase equilibria and dielectric materials of $\text{Li}_2\text{O}-\text{B}_2\text{O}_3-\text{Yb}_2\text{O}_3$ system

M. Asadov and N. Akhmedova

Institute of Catalysis and Inorganic Chemistry named after M.F. Nagiyev, Azerbaijan National Academy of Sciences, pr. H. Javid 113, Baku, AZ1143 Azerbaijan E-mail: mirasadov@gmail.com

For the directed synthesis of new materials and the search for prospective compounds the reliable information on the phase relations in the binary, ternary and multicomponent systems is required. Multicomponent oxide materials play an important role in finding and creating new functional inorganic materials. Materials based on complex oxides of rare earth metals have a variety of physical and physico-chemical properties. These materials can be used as optical materials, oxygen sensors, ionic conductors, catalysts, etc. [1].

Phase-diagram data (compounds and crystallization conditions of individual phases) are of practical importance in the search for new multicomponent phases including and glassy phases.

Selection of $\text{Li}_2\text{O}-\text{B}_2\text{O}_3-\text{Yb}_2\text{O}_3$ system caused by, on the one hand, its poor scrutiny, on the other hand - in the presence of its constituent binary systems of crystalline oxides and glasses with special optical and electrical properties. Borates, for example, have nonlinear optical properties, high refractive index, dielectric constant and low dielectric loss.

According to phase diagram of the polythermal section $\text{Li}_2\text{O}\cdot 2\text{B}_2\text{O}_3-\text{Yb}_2\text{O}_3\cdot \text{B}_2\text{O}_3$, solid solutions based on $\text{Li}_2\text{O}\cdot 2\text{B}_2\text{O}_3$ (α) and YbBO_3 (γ) crystallize simultaneously at $800\text{ }^\circ\text{C}$ (7.5 mol% $\text{Yb}_2\text{O}_3\cdot \text{B}_2\text{O}_3$). The polymorphic transformations of $\text{Yb}_2\text{O}_3\cdot \text{B}_2\text{O}_3$ compound, progressing through eutectoid reaction at $460\text{ }^\circ\text{C}$ and metatectic reaction at $925\text{ }^\circ\text{C}$, are detected on thermograms. According to physico-chemical analysis, the polythermal section of $\text{Li}_2\text{O}\cdot 2\text{B}_2\text{O}_3-\text{Yb}_2\text{O}_3\cdot \text{B}_2\text{O}_3$ is quasi-binary and allows to partially triangulate the $\text{Li}_2\text{O}-\text{B}_2\text{O}_3-\text{Yb}_2\text{O}_3$ system. In the $\text{Li}_2\text{O}\cdot 2\text{B}_2\text{O}_3-\text{Yb}_2\text{O}_3\cdot \text{B}_2\text{O}_3$ system one of the components, YbBO_3 has a polymorphism. YbBO_3 has two polymorphs at temperatures of $577\text{ }^\circ\text{C}$ and $1041\text{ }^\circ\text{C}$. Polymorphism of YbBO_3 compound is also evident in alloys of polythermal section of $\text{Li}_2\text{O}\cdot 2\text{B}_2\text{O}_3-\text{Yb}_2\text{O}_3\cdot \text{B}_2\text{O}_3$. Polymorphic transformation temperature is lowered by the addition of $\text{Li}_2\text{O}\cdot 2\text{B}_2\text{O}_3$ component to the YbBO_3 .

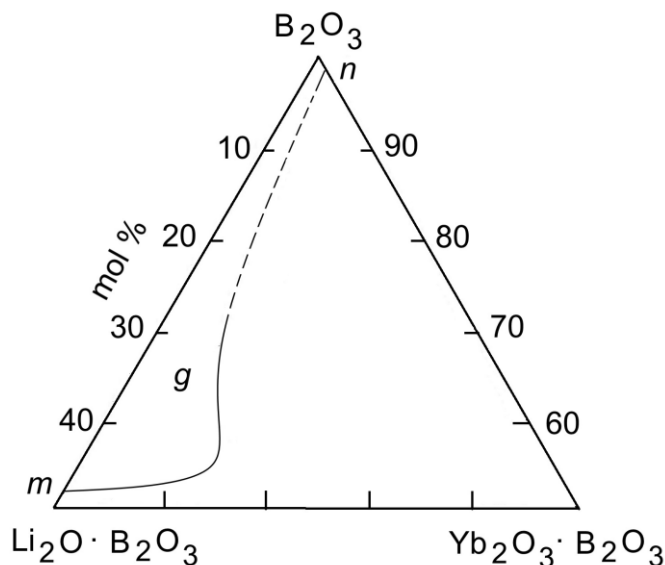


Figure shows the section of the $\text{Li}_2\text{O}\cdot 2\text{B}_2\text{O}_3-\text{B}_2\text{O}_3-\text{Yb}_2\text{O}_3\cdot \text{B}_2\text{O}_3$ phase diagram obtained from the DTA, XRD, and microstructural data for $\text{Li}_2\text{O}\cdot 2\text{B}_2\text{O}_3-\text{Yb}_2\text{O}_3\cdot \text{B}_2\text{O}_3$ and other alloys including in $\text{Li}_2\text{O}\cdot 3\text{B}_2\text{O}_3-\text{Yb}_2\text{O}_3\cdot \text{B}_2\text{O}_3$.

It was established that the glassy phase exists in a broad region in $\text{Li}_2\text{O}\cdot 2\text{B}_2\text{O}_3-\text{B}_2\text{O}_3-\text{Yb}_2\text{O}_3\cdot \text{B}_2\text{O}_3$ system. Two points (m and n) on the concentration triangle $\text{Li}_2\text{O}\cdot 2\text{B}_2\text{O}_3-\text{B}_2\text{O}_3-\text{Yb}_2\text{O}_3\cdot \text{B}_2\text{O}_3$ connects the border region of glass (g). Vitrification of samples based on boron oxide B_2O_3 observed even at low cooling rates of the melt. Glasses from the g area are obtained in the quenching regime. We refined borders of $m-n$ vitrification in $\text{Li}_2\text{O}\cdot 2\text{B}_2\text{O}_3-\text{B}_2\text{O}_3-\text{Yb}_2\text{O}_3\cdot \text{B}_2\text{O}_3$ system. The obtained data can be useful for the preparation of new dielectric and semiconductor materials.

1. M.M. Asadov and N.A. Ahmedova. "Fusion Diagrams in the $\text{BiBO}_3-\text{YbBO}_3$ and $\text{Bi}_4\text{B}_2\text{O}_9-\text{YbBO}_3$ Systems". *Int. J. Thermophys.* DOI 10.1007/s10765-014-1673-6.

Local electronic properties of thin NiNb oxidized films

A.S. Trifonov^{1,2}, S.V. Ketov³, A. Shluger^{3,4}, D.V. Louzguine-Luzgin³

1. Faculty of Physics, Lomonosov Moscow State University, 119991 Moscow, Russia, ovtchenkov@mail.ru.

2. Skobeltsyn Institute of Nuclear Physics, Lomonosov Moscow State University, 1(2), Leninskie Gory, Moscow 119991, Russia.

3. WPI-AIMR, Tohoku University, Sendai 980-8577, Japan.

4. Department of Physics and Astronomy, University College London, London WC1E 6BT, United Kingdom

We investigated the local electronic properties of oxidized NiNb amorphous films using contact mode of atomic force microscopy. Two types of samples were measured: natural oxide with thickness ~ 4 nm (type 1) and artificially oxidized film with thickness ~ 15 nm (type 2). All samples showed non-linear asymmetric local current-voltage characteristics at tip loading up to 500 nN. The samples of type 1 have electron conductivity whereas samples of type 2 demonstrated hole-type conductivity.

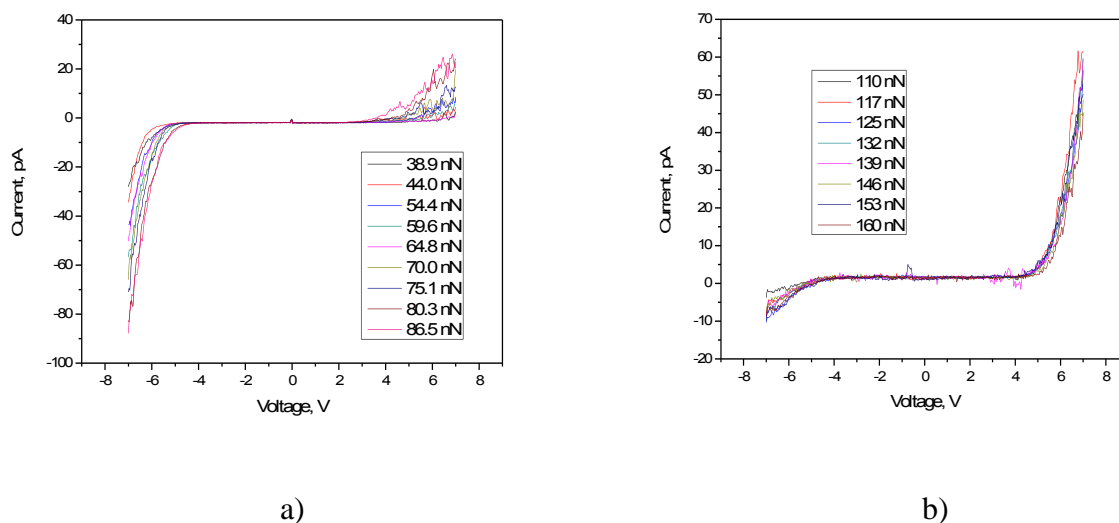


Fig. 1. Local current-voltage characteristics for 4 nm oxide layer thickness sample (a) and 15 nm oxide layer thickness sample (b).

Phase separation and electronic properties in $(\text{K}_{0.7}\text{Na}_{0.3})_x\text{Fe}_{2-y}\text{Se}_2$ single crystal

A.S. Trifonov^{1,2}, Y.A. Ovchenkov¹, D.E. Presnov^{1,2}, A.I. Boltalin³, M. Liu³, I.V. Morozov³,
A.N. Vasiliev^{1,4,5}

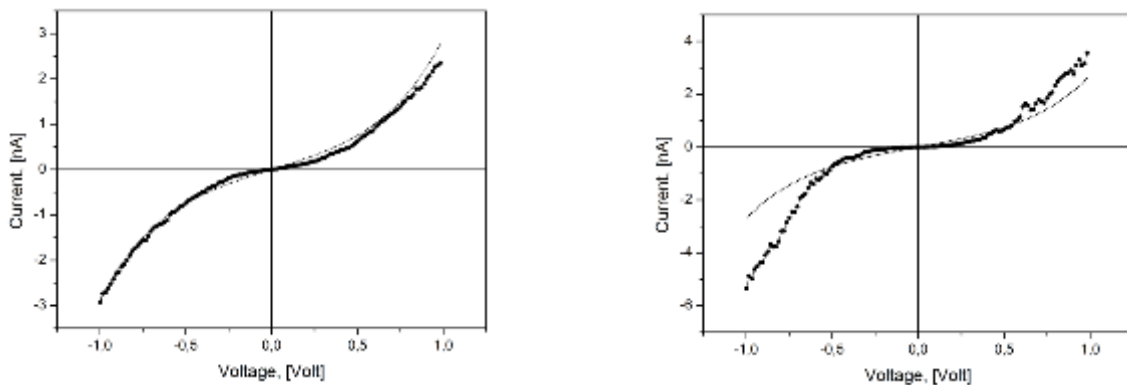
1. Faculty of Physics, Lomonosov Moscow State University, 119991 Moscow, Russia, ovchenkov@mail.ru.

2. Skobeltsyn Institute of Nuclear Physics, Lomonosov Moscow State University, 1(2), Leninskie Gory, GSP-1,

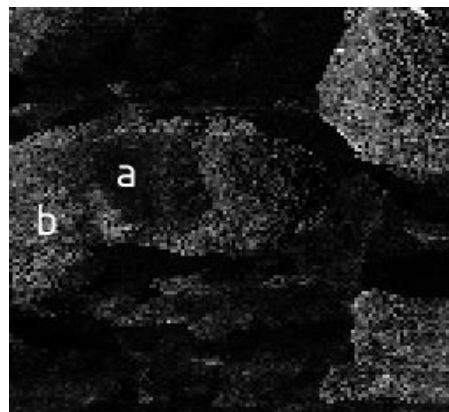
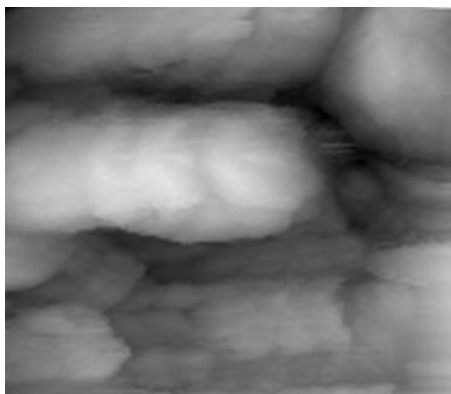
Moscow 119991, Russia. 3. Faculty of Chemistry, Lomonosov Moscow State University, 119991 Moscow, Russia.

4. Theoretical Physics and Applied Mathematics Department, Institute of Physics and Technology, Ural Federal University, Ekaterinburg 620002, Russia. 5. National University of Science and Technology (MISIS), Moscow 119049, Russia.

We investigated the microstructure of the iron selenide superconductor $(\text{K}_{1-z}\text{Na}_z)_x\text{Fe}_{2-y}\text{Se}_2$ with composition $(\text{Na}_{0.32(2)}\text{K}_{0.68(2)})_{0.95(4)}\text{Fe}_{1.75(2)}\text{Se}_2$, $T_c = 32$ K and a near 100% Meissner screening volume fraction. The $(\text{K}_{0.7}\text{Na}_{0.3})_x\text{Fe}_{2-y}\text{Se}_2$ single crystals were grown by self-flux method, as described in detail elsewhere [1]. Topography and electron transport properties were studied using electron microscopy and ultra-high vacuum scanning tunneling microscopy techniques. Room temperature STM measurements reliably identify spatial variations of the local electronic properties of this material. The studied crystals consist of continuous regions with significantly different shapes of current-voltage curves reflecting different electronic transport properties of these regions. Fitting of the local current-voltage curves with the Simmons model [2] for metal-dielectric-metal structure confirmed a phase separation in the sample to metal and semiconducting phases. The observed regions have dimensions in the range of several tenths of a micrometer and indicate a phase separation in the sample.



Experimental (solid) and fitted (dash) local current-voltage characteristics for different phases.



STM topography (left) and the error of simulations with the Simmons formula (right). **a** and **b** marks indicate the positions where CVC (**a** – left, **b** - right) were recorded.

1. M.V. Roslova, S.A. Kuzmichev, T.E. Kuzmicheva, Y.A. Ovchenkov, M. Liu, I.V. Morozov, A.I. Boltalin, A.V. Shevelkov, A.N. Vasiliev. Cryst. Eng. Comm., **16**, pp. 6919–6928, 2014.

2. J.G. Simmons. J. Appl. Phys. **35**, 2472 (1964); J. Appl. Phys, **34**, 1793, (1963).

Strain induced properties of the strong spin-orbit semimetal SrIrO₃ thin films

Yu.V. Kislinskii^{1,4}, K.I. Constantinian¹, G.A. Ovsyannikov^{1,2}, Yu. Khaydukov³,
A.M. Petrzhek¹, A.V. Shadrin¹, A.E. Sheyerman¹

1. Kotel'nikov Institute of Radioengineering and Electronics RAS, 125009 Moscow, Russia, yulii@hitech.cplire.ru
2. Chalmers University of Technology, SE-41 296 Gothenburg, Sweden, gena@hitech.cplire.ru
3. Max-Planck Institute for Solid State Research, 70 569 Stuttgart, Germany, yury.khaydukov@frm2.tum.de
4. Shubnikov Institute of Crystallography, 119333 Moscow, Russia yulii@hitech.cplire.ru

Semimetal SrIrO₃ is a member of the Ruddlesden–Popper structure with infinite lattice. Conductivity of the SrIrO₃ decreases with temperature (like semiconductor behavior) but resistivity at room temperature $\rho(300) \sim 1 \text{ m}\Omega\cdot\text{cm}$ is too low for semiconductors [1]. Type of carriers in the SrIrO₃ was studied by thermopower measurement and hole-type conductivity was observed [2]. We study transport mechanisms in SrIrO₃ thin films by resistance measurements versus temperature. XRD crystal structure of the films and Hall effect were used for sample characterization as well.

The SrIrO₃ films with thicknesses 20÷300 nm were deposited by laser ablation on NdGaO₃ and SrTiO₃ substrates in oxygen atmosphere. Deposition temperatures were of 760÷790 °C that provide an epitaxial grown of the films. Electrical measurements were made by four point method through Pt contacts. For Hall measurement micro bridges were patterned and magnetic fields up to 10³ Oe were applied.

Films on NdGaO₃ substrates have low resistivity $\rho(300) \sim 0.5\div 2 \text{ m}\Omega\cdot\text{cm}$. Conductivity increases with temperature increase in range 4.2÷300 K. For SrIrO₃ films deposited on SrTiO₃ substrates conductivity shows metallic behavior: resistivity decrease with temperature becomes lower. However, a minor deviation took place: at low temperatures resistivity slightly grows with temperature decrease. Applicability of model of disordered metal [3] and model of weak localization [4] for the conductivity versus temperature dependencies will be discussed. Parameters of thin films of 20 nm in thickness that have variable range hopping conductivity will be compared along with the Hall effect data.

This work was supported partially by the RAS, RFBR projects 14-07-00258, 14-07-93105, Scientific School grant NSH-4871.2014.2.

1. F.X. Wu, J. Zhou, L.Y. Zhang, et al. “Metal-insulator transition in SrIrO₃ with strong spin-orbit interaction”. *Journal of Physics: Cond. Matt.* **25**, 125604, 2013.
2. N. Keawprak, R. Tu, T. Goto. “Thermoelectric properties of Sr-Ir-O compounds prepared by spark plasma sintering”. *Journal of Alloys and Compounds* **491**, 441, 2010.
3. J. Yoshida, T. Nagano, T. Hashimoto. “Current transport and electronic states in *a,b* – axis-oriented YBa₂Cu₃O₇/PrBa₂Cu₃O₇/YBa₂Cu₃O₇ sandwich-type junctions”. *Phys. Rev. B* **53**, 8623, 1996.
4. R. Scherwitzl, S. Gariglio, M. Gabay, et al. “Metal-insulator transition in ultrathin LaNiO₃ films”. *Phys. Rev. Lett.* **106**, 246403, 2011.

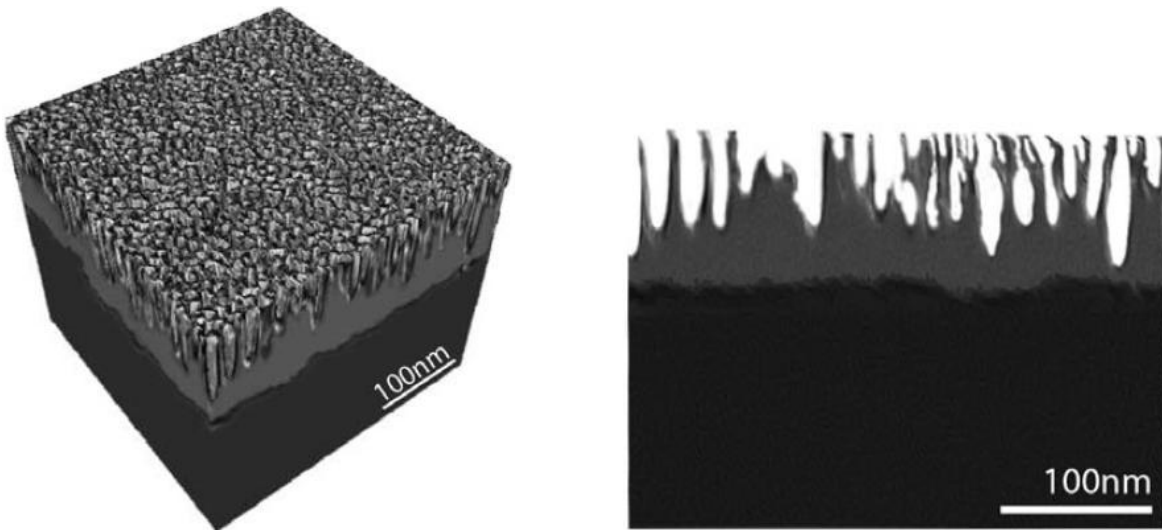
Modeling approach to aluminum anodization process

A.N. Belov, S.A. Gavrilov, V.I. Shevyakov, and M.I. Vorobiev

National Research University of Electronic Technology (MIET), Moscow, Russia, E-mail: belov@dsd.miee.ru

Over past few decades, a notable part of researchers in material sciences has been widely studying valve metals porous oxide films. Those films have found their appliance in wide range of industries quite fast. Qualitative leap in porous oxide formation technology and theory was brought by nanotechnologies development. Low temperature formation, high process repeatability and pore parameters variation (from tenth to hundreds of nanometers) allow for rich number of applications in functional electronics. Generic understanding of alumina formation mechanisms and its structure is still been developed, and numerical simulation plays significant role in assisting those studies. Therefore, development of numerical simulation models to support theoretical findings is the essential task in porous oxide formation phenomena studies.

Known models present in the field of porous oxide formation studies describe metal-oxide and oxide-electrolyte interfaces evolution in time with height-fields [1, 2]. This kind of interface representation imposes quite strict constrains onto described surface morphology and its development during numerical simulations. Such constrains disallow interface overhangs or pore formation non-orthogonal to main film plane, blocking better pattern prediction and characterization. We propose approach for modeling thin aluminum film anodization in three dimensions using variation of coupled map lattice on volumetric grid, which is capable of capturing porous and nonporous aluminum oxide growth and electrochemical polishing modes. Model derivation is based on Parkhutik and Shershulsky understandings. Numerical simulation results for various initial conditions are shown and compared to experimental data. The figure below shows simulation results of alumina anodization in 0.5M sulfuric acid solution with applied voltage equal to 25V and simulation time 40 seconds. Discussed model allows for simulating three modes of aluminum electrochemical oxidation:



electropolishing, formation of nonporous or porous films. It gives a possibility to qualitatively visualize and study approximate pores birth and interface patterns development of metal-oxide and oxide-electrolyte interfaces, pattern formation during electropolishing and nonporous oxide growth. Model allows reproducing important geometrical characteristics of real alumina samples. Nevertheless, discussed model should be treated as quite simplified one: it is necessary to account for mechanical strain influence on activation energies of aluminum oxidation and dissolution reactions; for space charge presence in oxide layer and migration of ions inside oxide layer. Lack of the mentioned effects is main drawbacks of the proposed model.

1. S.K. Thamida and H.-C. Chang. "Nanoscale Pore Formation Dynamics During Aluminum Anodization", *Chaos*, **12**, pp. 240-245, 2002.
2. L.G. Stanton and A.A. Golovin. "Effect of ion migration on the self-assembly of porous nanostructures in anodic oxides", *Phys. Rev B.*, **79**, pp. 035414, 2006.

Nanostructured chalcogenide materials for memory switching devices

O. Pyatilova, R. Rozanov, S. Gavrilov, A. Zheleznyakova, A. Belov, V. Shevyakov,
A.V. Shcherbakova

National Research University of Electronic Technology (MIET), Moscow, Zelenograd, e-mail: Silova87@gmail.com

The memory resistor, or memristor based on the solid-state electrolyte (SSE) have roused interest in recent years [1]. The resistive switching memory cells efficiency, such as reliability, durability, speed of action, increasing of the specific useful characteristics, and reducing the energy costs, etc., depends on the solid-state electrolyte conductivity. The perspective materials for memristor development are metal chalcogenides (Ag-Se, Ag-S, Ag-Ge-Se, Cu-S [2]) and oxides WO_3 , TiO_2 [3]. The main property of the chalcogenide is high value of conductivity σ_i at $T = 293$ K. Thus, this material exhibits the memristor-like behavior. Metal sulfides, formed by different methods, such as electrochemical deposition, high-temperature sulphidation, chemical vapour deposition etc., are used as active layers for memory devices.

In the present work we synthesized Cu_2S , Bi_2S_3 films as thin as 30 and 20 nm, respectively, by ionic layer adsorption method during 15 deposition cycles. We investigated the morphology and electrical properties of the formed material. The thickness was measured by atomic force microscopy (AFM). As can be seen from the measured I - V characteristics (Fig.1), this materials exhibit the memristor-like behavior at the high electric field $E \sim 10^5$ V/cm.

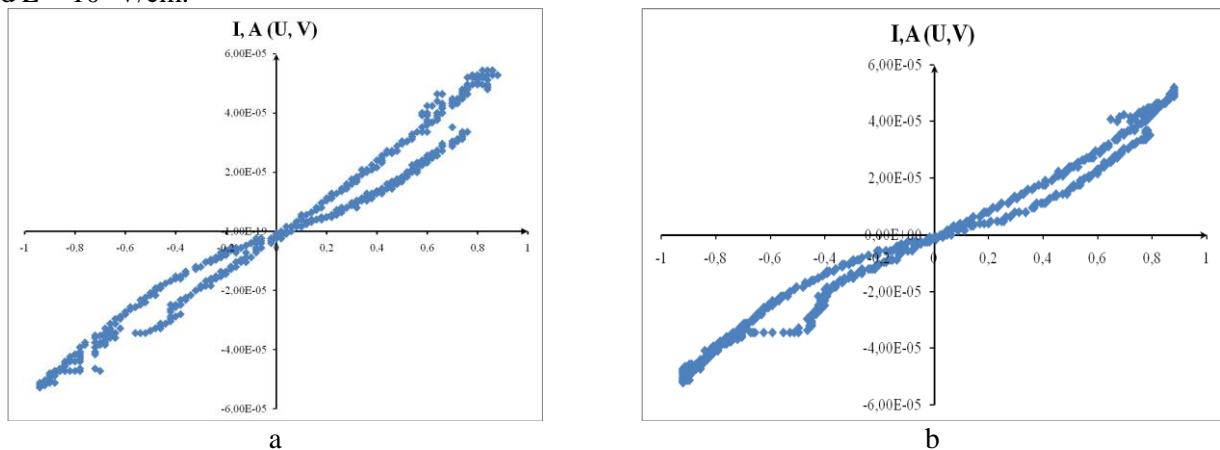


Fig. 1. I - V curves of the Cu_2S film with a thickness of 30 nm (a) and Bi_2S_3 film with a thickness of 20 nm (b)

Cu_2S and Bi_2S_3 thin films show semiconductor behavior at low bias voltages, whereas they exhibit reproducible bipolar resistance switching at higher bias voltages. The transition between both types of behavior is observed by hysteresis in the I - V curves, indicating decomposition of the Cu_2S and Bi_2S_3 and formation of a conductive path between the electrodes [4], due to ionic transport (Cu^+ and S^{2-}). The ionic conductivity (σ_{Cu^+} , $\sigma_{\text{S}^{2-}}$) was calculated for the investigated films by equation (1):

$$\sigma_i = d/(RS), \quad (1)$$

where R is a resistance defined by the linear I - V curve, S is a contact area between Au probe and film ($650 \mu\text{m}^2$), d is a film thickness.

It should be noted that the ionic conductivity (σ_{Cu^+} , $\sigma_{\text{S}^{2-}}$) is consistent with the tubular data for solid state electrolytes (10^{-3} - $10^{-2} \Omega^{-1}\text{cm}^{-1}$). Thus, Cu_2S , Bi_2S_3 films, formed by ionic layer adsorption method, can be used as active layers for resistive switching memory cells.

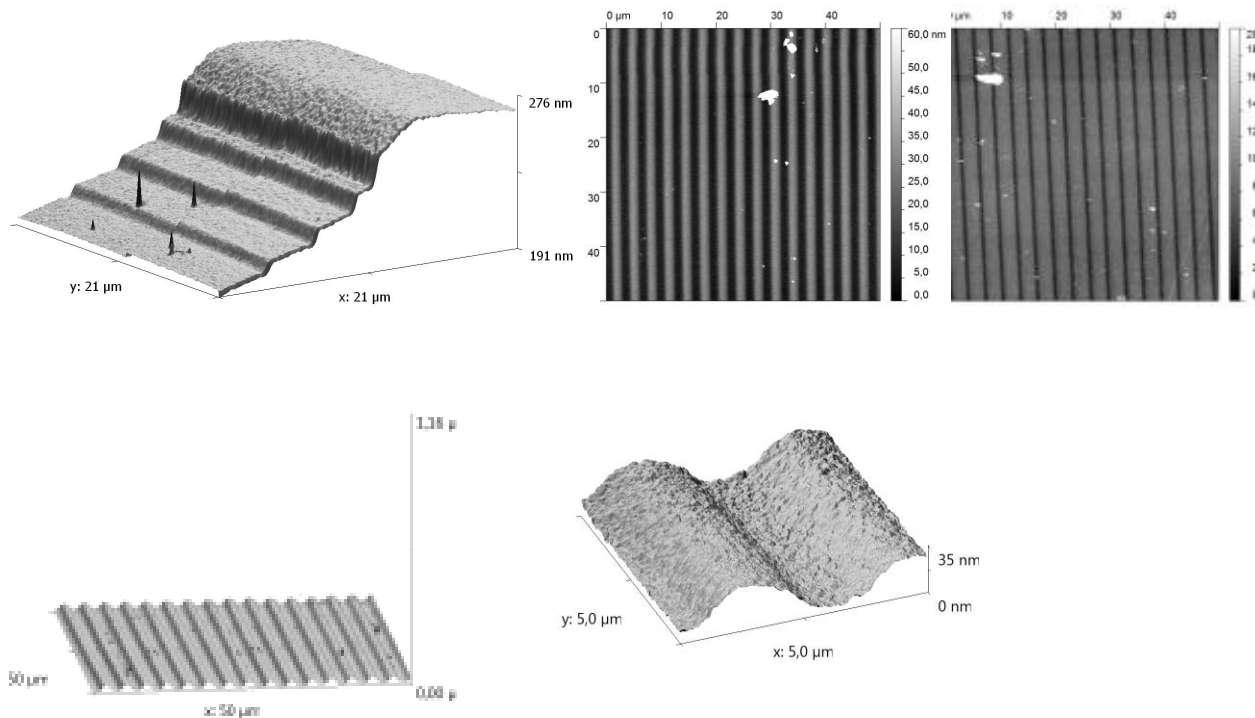
1. T. Hasegawa, K. Terabe, T. Tsuruoka, and M. Aono "Atomic Switch: Atom/Ion Movement Controlled Devices for Beyond Von-Neumann Computers". *Adv. Mat.*, **24**, pp. 252–267, 2012.
2. Sakamoto et al. "Nanometer-scale switches using copper sulfide". *Appl. Phys. Lett.*, **82**, pp.3032, 2003.
3. Ch. Liang, K. Terabe, T. Hasegawa, M. Aono "Resistance Switching in Anodic Oxidized Amorphous TiO_2 Films". *Appl Phys. Express*, **1**, p.064002, 2008.
4. M. Morales-Masis, H.-D. Wiemhofer, and J. M. van Ruitenbeek "Towards a quantitative description of solid electrolyte conductance switches". *Nanoscale*, **2**, pp. 2275–2280, 2010.

Some peculiarities of the new dry method of mask (relief) formation by direct electron-beam etching of resist

M.A. Bruk¹, E.N. Zhikharev², D.R. Streltsov¹, V.A. Kalnov², A.V. Spirin¹, A. Rogozhin²
 1. Karpov Institute of Physical Chemistry, Moscow, Russia. E-mail: marbruk@yandex.ru
 2. Institute of Physics and Technology of the Russian Academy of Sciences, Moscow, Russia.

The authors have proposed [1], the new "dry" method of the image formation in some positive resists by their direct etching during electron beam exposure (Dry Electron Beam Etching of Resist - method DEBER). The method is based on the emergence in polymer resist at the temperatures close to the glass transition temperature (or higher temperature) of the electron-stimulated chain depolymerization reaction, with release of volatile products (monomer) which are removed from the vacuum chamber during the exposure. The method is applicable to resists capable at the above mentioned conditions to the effective depolymerization up to monomer (PMMA-polymethyl methacrylate and other polymethacrylates, poly- α -methyl styrene, polymethylisopropenylketone et al.). DEBER method allows 10-300 times greater sensitivity PMMA resist in electron-lithographic process. The method also allows to create the spatial 3D-shape structures with a very high vertical resolution (about 3nm) and low surface roughness (by the order of 1 nm), which is substantially better than in the traditional "wet" method. Disadvantages of the DEBER method include low lateral resolution (about 100-150nm) and low images contrast (0.7-1.5). When solving problems for which the requirements for these parameters are not too high, the method apparently can be of considerable practical interest. This paper presents some new results concerning mechanism, characteristics and capabilities of the method DEBER. In particular, it is shown that the DEBER method is very convenient for fabrication the relief spherical (or aspheric) and sinusoidal micro- and nanostructures. The examples are given of obtaining spatial 3D-structures with good accuracy by Z-axis. It is shown that for image formation both high energy beams (tens keV energy) and low-energy beams (0.1-1 keV) can be successfully used. The data presented, according to the authors, indicate significant potential for the applied matters of the method DEBER, in particular for the fabrication of optoelectronics elements (diffraction gratings, micro lenses, optical waveguides, anti-reflective coatings, etc.).

1. M.A. Bruk, E.N. Zhikharev, D.R. Streltsov, V.A. Kalnov, A.V. Spirin. The new dry method of mask (relief) formation by direct electron-beam etching of resist. *Microelectronic Engineering*, **112**, December 2013, P. 1-4.



Inductively coupled plasma parameters and etching mechanisms in ternary mixtures of CF₄, C₄F₈, O₂ and Ar

A. Efremov¹, Junmyung Lee², and K.-H. Kwon³

1. Ivanovo State University of Chemistry & Technology, Ivanovo, Russia, amefremov@yandex.ru.

2. Korea University, Sejong, South Korea, lee_jm@korea.ac.kr

3. Korea University, Sejong, South Korea, kwonkh@korea.ac.kr

Fluorocarbon (FC) gases such as CF₄ and C₄F₈ are widely used in the microelectronic industry for the dry patterning of silicon and silicon-based dielectrics (SiO₂, Si₃N₄). In most of the existing processes, these gases are combined with Ar or O₂ in a form of binary gas mixtures with the aim of accelerating the physical etching pathway, increasing the F atoms' yield and suppressing polymerization. Recently, many dry etching processes require optimization in order to satisfy the requirements concerning of device dimensions and performance. The ternary gas systems provide more pathways in the changes of gas-mixing ratios for obtaining the optimal process conditions. For example, one can keep the fraction of FC gas constant, but change the ratio between O₂ and Ar. Since the composition of the feed gas is different compared with the conventional FC/Ar or FC/O₂ mixtures, some principal differences in plasma parameters and densities of plasma active species can take place.

The goal of this work was the study of CF₄/C₄F₈/Ar, CF₄/O₂/Ar and C₄F₈/O₂/Ar inductively coupled plasmas with an aim of understanding how the gas mixing ratio influences on the plasma parameters and densities of active species. The focus was on the parameters directly connected with the dry etching mechanisms, such as the ion energy flux, F atom density, and the CF_x ($x = 1-3$) radical density.

The experiments were carried out in a planar inductively-coupled 13.56 MHz plasma reactor. The process conditions were: total gas flow rate (q) of 40 sccm, gas pressure (p) of 4–10 mTorr, input ICP power (W) of 800–900 W and bias power (W_{dc}) of 150–200 W. The feed gas mixture compositions were set by adjusting the partial gas flow rate of the components within $p = \text{const}$. Langmuir probe diagnostics provided the data on electron temperature (T_e), ion current density (J_+) and total positive ion density (n_+). The relative changes in densities of some neutral species were controlled by optical emission spectroscopy via I/I_{Ar} ratios. In order to determine the absolute densities and fluxes of plasma active species, the simplified global (zero-dimensional) plasma model operating with volume-averaged plasma parameters and a Maxwellian approximation for the electron energy distribution function was applied. The model directly involved the experimental data on T_e and n_+ as input parameters.

For the CF₄/C₄F₈/Ar gas system, we kept the constant 50% fraction of Ar, but varied the ratio between CF₄ and C₄F₈ within the remaining 50%. Therefore, the variation of C₄F₈ content in a feed gas in the range of 0–50% corresponded to the transition between CF₄/Ar and C₄F₈/Ar gas systems. It was found that such change in feed gas composition results in monotonically increasing ion energy flux, but in monotonically decreasing F atom flux, neutral/charged ratio, and the F/CF_x ratio. The last fact makes the C₄F₈-based plasma a much stronger polymerizing system compared with CF₄-based plasma under the same operating conditions.

For the CF₄/O₂/Ar and C₄F₈/O₂/Ar gas systems, we kept the constant 50% fraction of the FC gas, but varied the ratio between O₂ and Ar within the remaining 50%. Therefore, the variation of O₂ content in a feed gas in the range of 0–50% corresponded to the transition between FC/Ar and FC/O₂ gas systems. It was found that such change in feed gas composition in both gas systems results in a similar change in the ion energy flux with an expected negative impact on the efficiency of the physical etching pathway. In the in CF₄-based gas mixture, an increase in the O₂ fraction in a feed gas leads to monotonically increasing F atom density due to an effective realization of atom-molecular processes involving O and O(¹D) with the resulting electron-impact dissociation of fluorine-containing reaction products. The non-monotonic change of fluorine atom density, as has been reported in several works for the binary CF₄/O₂ system, was not found. In the C₄F₈-based plasma, the F atom density decreases monotonically toward more oxygenated gas mixtures. Here, the mechanisms discussed do not work because of the fast decay of O₂ in the reaction with CF and C species that pre-determines the much lower densities of O and O(¹D).

The model-based analysis of etching kinetics for both Si and SiO₂ in all three investigated gas systems showed the possibility of the non-monotonic effects of gas mixing ratios on the etching rates due to the changes in reaction probability through the balance of surface sites occupied by reaction products and/or polymer species. These were clearly confirmed by experiments.

Monte Carlo Simulation of Boron Doping Profile of Fin and Trench Structures by Plasma Immersion Ion Implantation

I. Shahsenov¹, A. Miakonkikh², and K. Rudenko²

1. *Moscow Institute of Physics and Technology (State University), Moscow, Russia*

2. *Institute of Physics and Technology (FTIAN), Moscow, Russia, miakonkikh@ftian.ru.*

ITRS roadmap for the devices in the sub-32nm technology imply move to FinFET-based structures which have shown prospective due to their scalability by maintaining high drive current at scaled voltages and smaller gate dimensions, and in particular by their beneficial short channel effects and leakage control. As in planar transistor, the performance of FinFET depends on the serial resistance of the source/drain regions [1]. Due to the 3D-geometry of FINFETs and the need to obtain identical lateral dopant profiles on the top and the sidewall of the FINs, the classical doping strategies might not be applicable and alternative doping strategies such as plasma immersion doping may represent an interesting alternative. Although shown to be conformal for macroscopic features, the latter is less obvious on nanoscale objects with dimensions smaller than the plasma sheath thickness.

Another way to improve conformality of doping is to use plasma at higher pressure to make ion to have a number of collisions moving through plasma sheath which change direction of ion movement and energy of ions.

In the present work we calculate dopant concentration distribution in the structured (fin or trench) sample accounting for geometric shadowing effects (ions at curtain angle of incidence couldn't achieve shadowed part of trench wall and bottom). Effects of deposition and resputtering of dopant containing films were not taken into account, as well as ions reflected from walls of trench. We also ignore inelastic collisions in sheath.

First we calculate energy and angle distribution function of ions moving through the sheath. Second we calculate contribution of ions with given energy and angle to the dopant distribution in the sample. For later task we use truncated normal distribution which is applicable for the case $R_p < 3\Delta R_p$, where R_p is projected range, and ΔR_p is standard deviation in direction of projectile. To obtain the distribution function of the angles and energy we use statistical data collected by TRIM code, which simulates the process of interaction of implanted ions with the plasma sheath.

Sheath thickness was estimated using experimental values of electron temperature and plasma density in the ICP reactor [2].

Doping profile of trenches 100 nm x 100 nm and fins 100 nm x 100 nm will be presented for various pressures and applied voltage.

1. Vandervorst et al.: Probing doping conformality in fin shaped FET structures. *J. Vac. Sci. Technol. B*, **26** (1), 2008.

2. Ya. Sukhanov, A.Ershov, K. Rudenko et. al. On the Parameters of Inductively Coupled and Microwave BF_3 Plasmas Used for Plasma Immersion Ion Implantation, *Plasma Process. Polym.*, **2**, pp. 472–479, 2005.

Melting behaviour of electrochemically grown Ag-Sn structures in the temperature range 25-500 °C

Yu.I. Shilyaeva, M.S. Mikhailova, N.V. Rakhmanova, A.I. Merkulova
National Research University of Electronic Technology (MIET), Zelenograd, Moscow, Russia,
E-mail: shyliava@gmail.com

Development of promising materials for use as lead-free solders for mounting the crystals and components on precision printed circuit boards is being conducted for quite a long time. In this regard, special attention is paid to low-melting metals and alloys, however the search continues for the optimal binary and ternary systems. The aim of current study was to investigate the effect of composition on thermodynamic properties of electrochemically grown Ag-Sn structures in the temperature range 25-500 °C.

The test structures Ag-Sn with different Sn content were prepared by sequential electrochemical deposition of silver and tin on the pre-treated copper foil from the corresponding electrolyte solutions. Electrodeposition was carried out at the room temperature in a two-electrode cell, the anode material was identical to the metal being deposited.

The test portions of the obtained samples of 10-15 mg were investigated by means of differential scanning calorimeter, DSC 204 F1 Phoenix (sensitivity: 3.2 $\mu\text{V/mW}$). The heating of the samples was conducted in the aluminum crucibles at the rate of 10 °C/min in the argon atmosphere in the temperature range 25-500 °C. Empty aluminum crucible was used as a reference. The sample fragment was cut in the shape of the disk and was placed on the bottom of the crucible, and then pressed with the lid with the upturned convex side down, in order to provide good contact of the material with the bottom of the crucible. The lid of the crucible was punched before sealing. In the identical conditions there were obtained DSC curves for the samples with different Sn content. In the DSC curves (Fig. 1), there was observed complex endothermic peak during heating at the temperatures corresponding to the melting of Ag-Sn near eutectic compositions.

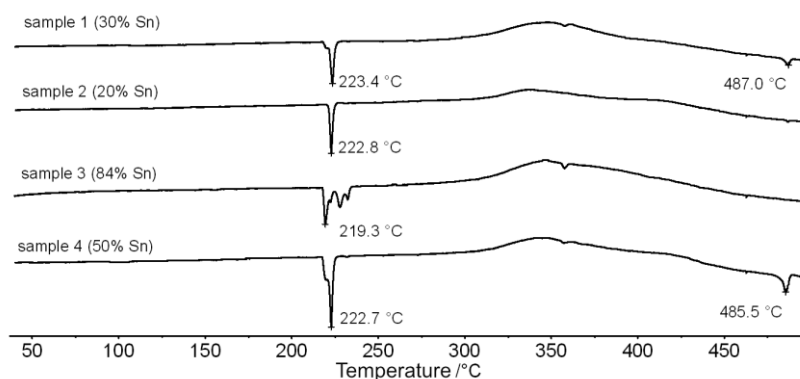


Fig. 1. DSC-traces of Ag-Sn system with different Sn content.

Heat absorption in the high temperature region is observed at a temperature corresponding to the melting of Ag-Sn peritectic composition in accordance with the phase diagram [1]. As it follows from the data in Fig. 1, this effect is the most clearly defined in the case of samples 1 and 4. It was noted that the intensity of this effect depends on the content of tin in the sample. For all samples heated over the melting point of the peritectic composition, there was noted the lack of eutectic crystallization peak during cooling. The eutectic melting peak was also not observed upon subsequent reheating. The observed melting behavior is extremely interesting from the practical viewpoint: after the treatment at an appropriate temperature, the structures will have better mechanical properties during the operation of electronic components at elevated temperatures. These data will allow to develop processes of manufacturing of Ag-Sn systems with prescribed thermodynamic characteristics and to determine the temperature ranges of stability of Ag-Sn structures for use as a contact metallization.

1. N.P. Lyakishev, editor. *Phase Diagrams of Binary Metallic Systems: reference book in 3 vol.* (in Russian). Mashinostroenie, Moscow, 1996.

Experimental and computational thickness determination of ultra-thin surface films using backscattered electrons spectra in SEM

S. Kupreenko¹, N. Orlikovsky², E. Rau¹, A. Tagachenkov³, A. Tatarintsev²

1. Moscow State University, Moscow, Russia. 2. Institute of Physics and Technology RAS, Moscow, Russia.

3. Institute of Nanotechnology and Microelectronics RAS, Moscow, Russia. E-mail: rau@phys.msu.ru

Multilayer structures, including thin films deposited on bulk substrates, are very important system for modern nanotechnology applications. As a consequence, the development of quantitative and nondestructive determination of local film thickness is to demand.

In this report the energy distribution of backscattered electrons (BSE) of different film-substrate combination film thickness are calculated and measured in scanning electron microscopy (SEM). It is shown that the value of each spectra I_{sf} for given energy E_p can be represented by the sum of a constant background signal I_{s0} due to the substrate and a contribution I_f proportional to the thickness d of the layered film:

$$I_{sf}^m = I_{s0} + (I_{f0} - I_{s0}) \left(I_f^m / I_{f0}^m \right), \quad I_{f0}^m = \left[1 - \exp\left(-A(2.1d/R)^p / (1 - 2.1d/R)\right) \right]$$

In these expressions I_{sf}^m is the amplitude of the energy spectra $N(E)$ of the film-substrate structure (see Fig. 1), I_{s0} and I_{f0} the signal value of the bulk substrates with atomic numbers Z_s and Z_f correspondingly, at the same electron energy $E_p = E_{sf}^m$, factor I_f^m / I_{f0}^m present the signal variation of BSE spectra in dependence of film thickness d relative to the massive target. The material parameters A , p and R we find from next expressions: $A = R / x_c = 2.22 \exp[0.0022(Z+1)]$ [1], where η_0 is the BSE coefficient, R is the range of primary electrons penetration depth [2], x_c is the most probably energy distribution depth.

The experimental and calculated results are shown as example in Fig. 2 for Au-film on Si-substrate and for Al-film on Au-substrate. Both results are in a good agreement. The thickness resolution is 2-3% and the practical resolution is in order of 0.2-0.3 nm.

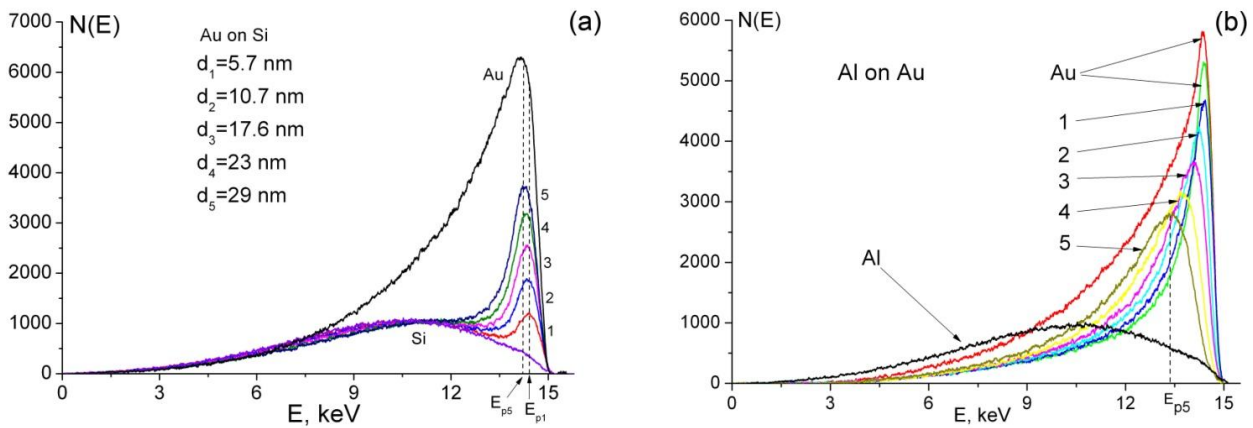


Fig. 1. Backscattered electron spectra of Au film with different thickness d on bulk Si at primary electron energy $E_0=15$ keV (a) and Al-films on Au-substrate (b).

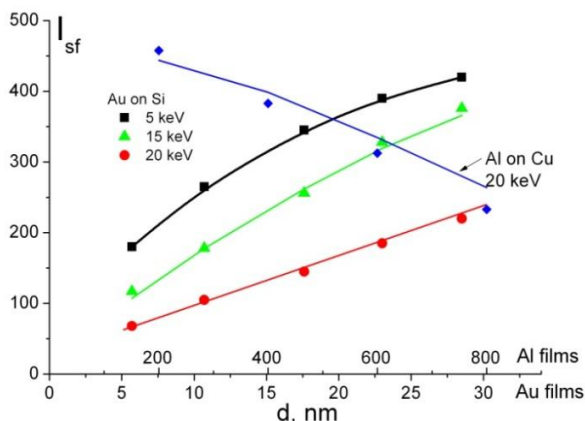


Fig. 2. Experimental and calculated value of peaks I_{sf}^m in dependence of different film thickness on substrates.

Reference:

1. E.I. Rau, S.A. Ditsman, S.V. Zaitsev et. al. Bull. RAS: Physics. 2013. V. 77. P. 969.
2. K. Kanaya, S. Okayama. J. Phys. D: Appl. Phys. 1972. V. 5. P. 43.

X-ray reflectometry measurements of Si-surface modified layers produced by high dose He⁺ plasma immersion implantation

A. Lomov, A. Miakonkikh

Institute of Physics and Technology (FTIAN), Moscow, Russia, miakonkikh@ftian.ru.

Modification of surface layers of silicon by energetic ions from plasma and beam source is applied for surface amorphisation and introducing defects, nanovoids and bubbles in subsurface layers. Amorphisation is needed for preventing light implants like boron from channeling during ion doping [1]. The diffusion of boron and phosphorus is strongly depends on phase state of silicon and number density of point defects [2]. Bubbles and nanovoids produced by implantation could play positive role in doping profile engineering during afterimplantation anneal [3]. Nanoporous silicon also was used in photoemitters and photovoltaic cells [4]. The stated above means that it is critical to develop a technique for nondestructive measurements of amorphous and porous layers thickness.

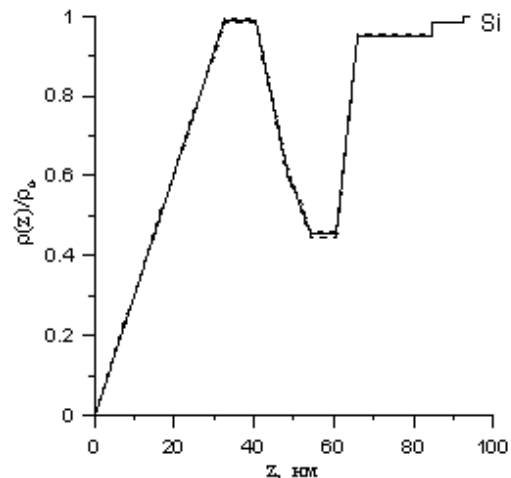
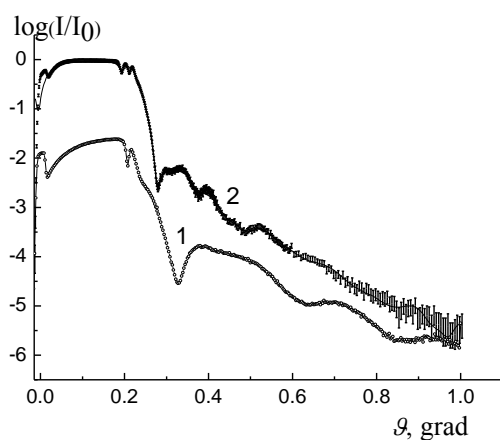


Fig. 1. Measured curves of X-ray reflectivity for He⁺ implanted samples ($D = 5 \times 10^{17} \text{ cm}^{-2}$): 1) $E = 2 \text{ keV}$, 2) $E = 5 \text{ keV}$

Fig. 2. Simulated profile of electron density of implanted sample $D = 5 \times 10^{17} \text{ cm}^{-2}$, $E = 5 \text{ keV}$

The native oxide free silicon (100) wafers was implanted by helium on a plasma immersion ion implanter of FTIAN construction in energy interval 2-5 keV with surface doses 6×10^{15} - $5 \times 10^{17} \text{ cm}^{-2}$. X-ray reflectivity curves (Fig. 1) were measured in $\omega/2\theta$ scheme. Electron density profile of samples were calculated taking into account experiment geometry, measurement errors, diffuse scattering from density inhomogeneities. Analysis shows that electron density changes linearly on the surface-vacuum interface and top layer remains density value close to silicon. From the doses of $1.2 \times 10^{16} \text{ cm}^{-2}$ formation of sublayer with lower density starts. Thickness of porous layers increases with implantation dose. Pore size about 5 nm was determined from reflectivity curves. Comparison with TEM measurements is given. Obtained results shows that x-ray reflectivity measurements could be successfully applied to measurements of thin buried porous silicon layers.

The reported study was partially supported by RFBR, research projects No 12-07-00745-a and 14-07-31293.

- [1] S.B. Felch, Z. Fang, B.W. Woo, R.B. Liebert, S.R. Walther, and D. Hacker. Plasma doping for the fabrication of ultra-shallow junctions *Surf. Coat. Technol.* **156**, 229, 2002.
- [2] S. Mirabella, D. De Salvador, E. Napolitani, E. Bruno, and F. Priolo, Mechanisms of boron diffusion in silicon and germanium, *J. Appl. Phys.* **113**, 031101, 2013.
- [3] E. Bruno, S. Mirabella, F. Priolo, E. Napolitani, C. Bongiorno, and V. Raineri, He induced nanovoids for point-defect engineering in B-implanted crystalline Si, *J. Appl. Phys.* **101**, 023515, 2007;
- [4] A.V. Myakonkikh, A.E. Rogozhin, K.V. Rudenko, V.F. Lukichev. Photovoltaic effect in a structure based on amorphous and nanoporous silicon formed by plasma immersion ion implantation, *Russian Microelectronics*, **42**, pp. 246-252, 2013.

Modification of cantilevers for atomic force microscopy using the method of exposure defocused ion beam

Yu.A. Chaplygin¹, V.I. Shevyakov¹, S.Y. Krasnoborodko²

1. National Research University of Electronic Technology (MIET), Moscow, Russia, E-mail: Shev@dsd.miee.ru

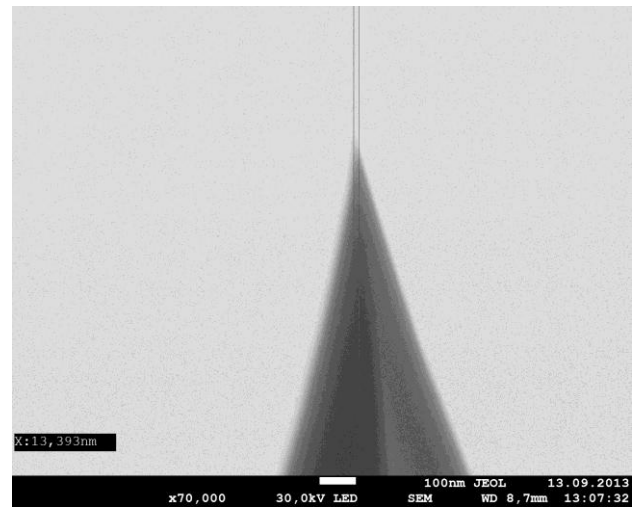
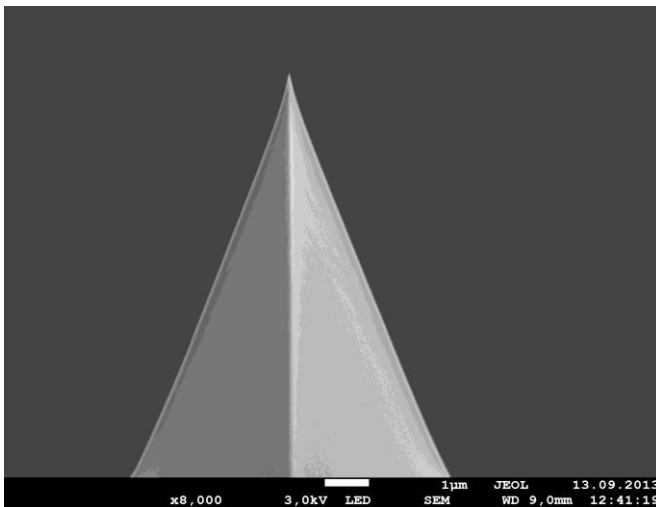
2. NT-MDT Co, Zelenograd, Moscow, Russia, E-mail: serg@ntmdt.ru

Atomic force microscopy (AFM) is widely used method for the determination of the geometric parameters of objects with nanometer spatial resolution. One of the serious problems in the AFM is the interpreting the results, because AFM image obtained not always coincides the characteristic for the measured objects. This is exhibited in a significant distortion of the AFM images in case of scanning surfaces with uneven relief or with objects that is smaller than the radius of the cantilever tip. Therefore, development of the cantilevers with ultra sharp tips is the essential task.

Group methods of manufacturing silicon cantilevers using microelectronics technology allow you to create probes with a radius of tips of 10 nm and above. Sharpening of the silicon tips cantilevers using focused ion beam is effective method, but it is not suitable for group processing that reduces the value of this method.

This work is focused on investigation of the tips sharpening process using a defocused ion beam. The group of cantilevers was placed on silicon substrate. Experiments were carried out in a specialized technological device containing Kaufman source designed to implement the method of ion-beam etching with an ion beam diameter of 200 nm. The design of the substrate holder enables to orient the substrate at an angle to the ion beam, depending on the mode of etching and to rotate substrate holder in the area of the beam.

The theoretical calculation of the dependence of the cantilevers etching profile from the ion beam incidence angle and the experimental results of etching cantilevers at different angles of incidence of the ion beam Ar^+ (0 to 90 degrees) are presented. The figure shows SEM image of the cantilever tip after ion etching at different magnifications.



The best result is realized when the symmetry axis of the tip is oriented at an angle of 75° to the direction of the ion beam movement. The reducing in the size of the tip radius in 2.5 times was determined. The comparative analysis of the efficiency of standard and sharpened cantilevers was performed for the silicon [1] and nano profiled aluminum test structures [2].

1. V. Bykov, A. Gologanov, V. Shevyakov. "Test structure for SPM tip shape deconvolution". Appl. Phys. A, **66**, pp. 499-502, 1998.

2. A. Belov, S. Gavrilov, A. Tikhomirov, Yu. Chaplygin, V. Shevyakov. "Test structures to determine tip sharpness". Nanotechnology in Russia. **5**, pp. 377-381, 2010.

Non-uniformly doped SOI based FETransistor with Nanowire channel

D. Presnov^{1,2}, A Miakonkikh³, I. Bozhjev², V. Rudakov⁴, A. Trifonov^{1,2}, V. Krupenin²

1. Skobeltsyn Institute of Nuclear Physics, Lomonosov Moscow State University, 119991 Moscow, Russia,

2. Laboratory of Cryoelectronics, Moscow State University, 119991 Moscow, Russia, denis.presnov@phys.msu.ru

3. Institute of Physics and Technology RAS, 117218, Moscow, Russia.

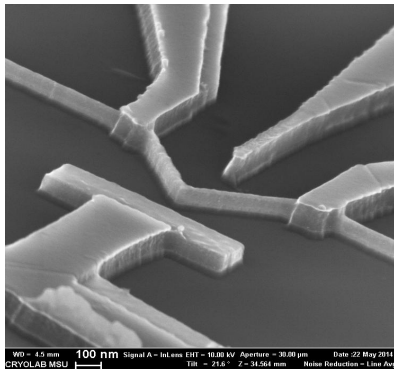
4. Institute of Physics and Technology (Yaroslavl Branch), RAS, Yaroslavl 150007, Russia.

Last decades the ultra-sensitive electric field/charge sensors for application in various fields of physics, chemistry, biology and medicine are in the grate interest of researches. Silicon nanowire field effect transistor (NW FET) is one of the best and promising tools on this field. Due to its high sensitivity [1], mechanical stability and CMOS compatible fabrication methods [2] the NW FETs based on silicon-on-insulator (SOI) are the good base elements for future practical devices and systems.

To have a high level of sensitivity the dopant concentration in the nanowire should be low ($10^{15} - 10^{16} \text{ cm}^{-3}$), but, at the same time, the source and drain regions should have a good electrical and mechanical contact to the output leads. The NW FETs with Schottky barriers show the good characteristics [2], but the low-ohmic interface is still in our mind to develop the high-sensitive and low-noise FETs.

Experiments with non-uniformly Arsenic doped SOI [3] demonstrated the possibility of establishing ohmic contacts to nanowire channel using highly-doped layer. In this work we present the fabrication method for NW FET using single e-beam lithography process. The method is based on the self-aligned bi-metallic mask, which at the same time plays the role of the contact leads to the nanowire.

The Soitec[®] «Unibond» SOI wafers with 110/200 nm device/oxide layers with original dopant (boron) concentration $\sim 10^{15} \text{ cm}^{-3}$ were successfully implanted with additional low-energy boron ions. The Plasma Immersion Ion Implantation (PIII) from BF_3 plasma technique [4] was used with ion energy 1 keV and doses $1 \times 10^{13} \text{ cm}^{-2}$. After rapid thermal annealing (RTA) at $T = 950 \text{ }^\circ\text{C}$ during 4 sec the concentration of boron was about 10^{20} cm^{-3} at the top 10 nm layer of SOI film with 11 kOhm/ \square layer resistance.



The single lithography process over 200 nm PMMA one-layer resist was followed by the process of deposition of Cr and Al films, using angle-evaporation technique [5]. Deposition process formed the masks for nanowire (Al) and outer electrodes (Cr+Al). The design of the mask was developed so that the 10 nm Cr film, 1st evaporated at the 45°, cover only the electrodes region, while the narrow lines stays free of metal due to shadow effect of the resist walls. The 2nd, normal, evaporation of the 15 nm Al film forms the mask for the nanowire at these lines. After the 1st anisotropic etching in SF_6 plasma the Al was removed and the 2nd etching step reduces the thickness only of the nanowire, keeping the high doped Si top layer under the Cr mask on the electrodes (fig. 1).

Finally, by the help of developed process we have got the structures, where nanowire was formed from low-doped bottom silicon layer and, at the same time, the outer electrodes have the good ohmic contact to the drain and source leads. The transport characteristics of the non-uniformly doped transistors showed a weak asymmetry in current-voltage curves and the good signal-to-noise ratio at room temperatures. Due to the wide working range one can found the most optimal working point depending on the incoming signal. The work is supported by grants from the Russian Foundation for Basic Research (14-07-00828, 12-07-00236-a).

1. J. Salfi, I.G. Savelyev, M. Blumin, S.V. Nair, and H.E. Ruda. "Direct observation of single-charge detection capability of nanowire field-effect transistors", *Nature Nanotech*, **5**, pp. 737-741, 2010.
2. D.E. Presnov, S.V. Amitonov, P.A. Krutitskii, V.V. Kolybasova, I.A. Devyatov, V.A. Krupenin, and I.I. Soloviev. "A highly ph-sensitive nanowire field-effect transistor based on silicon on insulator". *Beilstein Journal of Nanotechnology*, **4**, pp. 330–335, 2013.
3. S.V. Amitonov, D.E. Presnov, V.I. Rudakov, and V.A. Krupenin. "Field-Effect Transistor with Nanowire Channel Based on Heterogeneously Doped SOI". *Russian Microelectronics*, **42** (3), pp.160–164, 2013.
4. K. Rudenko, S. Averkin, V. Lukichev, A. Orlikovsky, et al. "Ultra Shallow $p^+ - n$ Junctions in Si Produced by Plasma Immersion Ion Implantation". *Proceedings of SPIE*, **6260**, pp.626003-1 – 626003-9, 2005.
5. S.J. Koester, G. Bazán, G.H. Bernstein, and W. Porod. "Fabrication of ultrasmall tunnel junctions by electronbeam lithography". *Rev. Sci. Instrum.* **63**, pp. 1918-1921, 1992.

Noise characteristics of silicon FET with nanowire channel

D.E. Presnov^{1,2}, I.V. Sapkov¹, I.V. Bojiev¹, A.V. Rjevskiy¹, V.A. Krupenin¹

1. Laboratory of Cryoelectronics, Lomonosov Moscow State University, 119899 Moscow, Russia,

vladimir.krupenin@phys.msu.ru

2. Skobeltsyn Institute of Nuclear Physics, Lomonosov Moscow State University, 119899 Moscow, Russia

The new approach bring us the ultrahigh-sensitive field/charge sensors with nanometer scale spatial resolution based on the modified field-effect transistors (FET) with silicon nanowire channel. They are a little less sensitive as compared with the best single-electron transistors, but have a great advantage because they can operate over a wide temperature range [1].

The experimental structures with with nanowire-channel were fabricated from the commercially provided Soitec ® «Unibond» Silicon-On-Insulator (SOI) wafers by standard methods of micro- and nanoelectronics (e-beam and optical lithography, metal deposition, wet and reactive-ion etching of different materials) [2, 3]. Transport and noise characteristics of the transistors were studied.

The drain-to-source current characteristics were measured in a wide range (50×100 points array) of transport and gate voltages. From the experimental data the response of the transistor to gate voltage changes (dI/dV_g) were calculated and estimated the transistor charge sensitivity. At the same time the low-frequency (0-500 Hz) spectra of the current fluctuations were taken in the same range of gate and drain-to-source voltages. Obtained data allowed us to define the optimal transistor`s operating region with a maximum signal to noise ratio and to evaluate the ultimate charge/field sensitivity of the sensor.

Evaluations of the charge sensitivity of the transistor at room temperature have shown that these values are in the range of 0.16-0.3 e/Hz^{1/2} for transistors with different channel's width (100-400 nm) and length (1.5-5 mkm).

Further research and development will allow us to create real sensor devices based on field-effect transistors with a nanowire channel for use in various fields of science, technology and medicine.

The work is supported by grant from the Russian Foundation for Basic Research (14-07-00828).

1. J. Salfi, I.G. Savelyev, M. Blumin, S.V. Nair, and H.E. Ruda. "Direct observation of single-charge-detection capability of nanowire field-effect transistors". *Nature Nanotechnology*, **5** (10), pp. 737-741, 2010.
2. D.E. Presnov, S.V. Amitonov, and V.A. Krupenin. "Silicon nanowire field effect transistor made of silicon-on-insulator". *Russian Microelectronics*, **41** (5), pp. 310-313, 2012.
3. D.E. Presnov, S.V. Amitonov, P.A. Krutitskii, V.V. Kolybasova, I.A. Devyatov, V.A. Krupenin, and I. I. Soloviev. "A highly pH-sensitive nanowire field-effect transistor based on silicon on insulator". *Beilstein Journal of Nanotechnology*, **4** (1), pp. 330-335, 2013.

Self-organization phenomena during electrochemical formation of nanoclusters in silicon

N. Arzhanova¹, M. Prokaznikov¹, A. Prokaznikov²

1. Yaroslavl Demidov State University, Yaroslavl, Russia, E-mail address: natarzhanova@mail.ru

2. Institute of Physics and Technology (Yaroslavl Branch), Yaroslavl, Russia, E-mail address: prokaznikov@mail.ru

Porous space formation in solids attracts attention of many scientific groups around the world due to wide spectrum of possibilities for practical application. In spite of a large number of works in this field of scientific activity there are some problems that still remain to be unsolved; among them one could distinguish three extremely important classes. First, it is a specific of chemical reactions that results in porous space formation with low dimension. Second, – dynamics of electrolyte/solid system and its analytical description. Third – the problem of fractal properties in formed porous space. In this work two last aspects were considered and arguments were presented that confirm assumptions putting forward. In this work the role of processes was investigated, that occur on the border between different media, in dynamics formation of electrochemical reactions of silicon with fluoride contained electrolytes during pores formation reactions in silicon matrix during nanostructuring of surface and the bulk. It was shown that regularities of exchange of charges between different media through the surface can explain observed anodization regimes: stable, oscillating and chaotic ones. Suggested approach makes it possible to explain the regime of anodization which is connected with synchronized variation of pores contours walls as well as with global oscillating processes in the system silicon/electrolyte what allow to construct three dimensional electronic systems. An analytical description of processes on the border and an analysis of solutions for presented equations showed the presence of Andronov-Hopf bifurcation in the system (see Fig. 1).

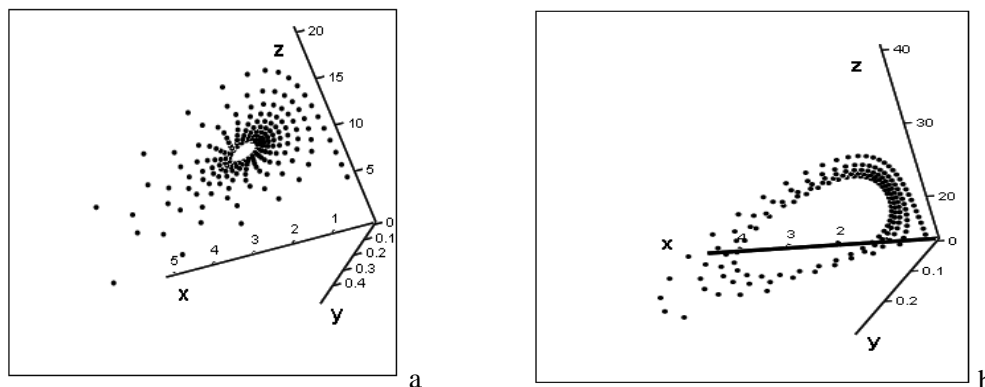


Figure 1. Solutions: focus (a) and limiting circle (b)

The processes that occur on the border of two media are closely connected with the phenomena in the bulk of a crystal and put together the united process. Basing on an analysis of the results of experiments and computer simulations it was demonstrated that technological regimes of pores formation in silicon/electrolyte system are controlled by delivery of holes to the border of two media. The dimensional computer model was developed. It describes pores clusters formation in silicon as well as it takes into account different aspects of behavior of anodization process including electric potential variation in the system by changing of border configuration of the crystal with an electrolyte. Computer model was realized in the form of program package which makes it possible to carry out the investigations of dynamics formation in a three dimensional porous cluster. The peculiarity of regime was investigated which is connected with holes transport and is described by equations that are scale invariant with respect to affine transformations of spatial and temporal variations. Scale invariance of the system is closely connected with specific character of distribution of charge along a border which in turn is connected with a local curvature of the formed surface. Porous clusters formed under such regimes have fractal self-similarity properties.

A systematic modeling study of chemical mechanical polishing for copper interconnects

T.M. Makhviladze, M.E. Sarychev

Institute of Physics and Technology, Russian Academy of Sciences, Moscow, Russia, tarielmakh@mail.ru

A systematic modeling study of chemical mechanical polishing for copper interconnects in terms of key physical and chemical mechanisms, CMP process parameters, planarization quality characteristics and process optimization was performed. The consideration is based on our previous theoretical and modeling results [1-3] taking into account the recent modifications and improvements following from the last experimental developments.

The main processes included in the model are as follows:

- formation of the passivating layer having some initial thickness on the copper surface;
- diffusion of Cu^+ ions and tunneling of copper conductivity electrons from the copper surface through the passivating layer to its outer surface contacting with the slurry;
- chemical reactions of the Cu^+ ions and electrons propagating the passivating layer with the slurry components; the reactions result in further growth of the passivating layer and formation of soluble compounds of copper which can be then removed by the slurry flow.

The modified full and closed set of equations of the process kinetics is derived and analyzed. Its solutions are obtained for the steady-state regime as to the chemical reactions in two limiting cases when Cu^+ ion diffusion through the passivating layer predominates over their electromigration or vice versa. The estimates of the CMP rate and limiting values of passivating layer thickness for these two modes are carried out and give reasonable results which correlate with experimental data on silicon nano- and microelectronics structures. In particular, the model makes it possible to understand the existence of an ultimate thickness of passivating layers observed in recent experiments and to evaluate a characteristic time required to reach it. These results allowed us to refine significantly previous conclusions and dependences obtained in papers [1, 2].

According to the our new detailed analysis, as the most important outcome of the experimental data on CMP, the conclusion could be done that a passivating layer being formed during the chemical interaction of the slurry with the metal surface has to be the controlling factor for the whole CMP process used in the modern silicon technology.

Special attention is given to the effects of copper dishing and SiO_2 thinning on planarization quality. The influences of slurry chemistry and thickness of the copper layer on dishing are modeling and analyzed in detail. The dishing effects for variable polishing times and different patterns are studied in dependence on these two factors, namely, thickness of Cu layer and the slurry composition.

The modeling results for chemical mechanical planarization of damascene structures are also presented. The model takes into account the most important process parameters such as slurry and pad properties. Dishing for the damascene structures is found to be strongly dependent on the line width. It seems to us that this dependence is modeled adequately and reliably for the first time. These results can be useful for the modeling and optimization of the planarization and polishing for a variety of materials and different process conditions.

1. T.M. Makhviladze and M.E. Sarychev. "A new model for the copper CMP kinetics". Proc. SPIE., **7025**, pp. 7025 1-8, 2008.
2. T.M. Makhviladze and M.E. Sarychev. "Modeling of surface processing for copper metallization". Proc. of the Phys.-Techn. Inst., *Quantum computers, micro- and nanoelectronics: physics, technology, diagnostics and modeling*, ed.by V.F. Lukichev, vol.19, pp. 139-155, Nauka, Moscow, 2008 (in Russian).
3. T.M. Makhviladze and M.E. Sarychev. "Advanced model of the copper CMP process for silicon nanotransistor technology". Proc. of the X Int. Conf. "Silicon-2014", p. 74, A.P. Vinogradov Institute of Geochemistry SB RAS, Irkutsk, Russia, 2014.

Modeling Griffith crack propagation at interfaces between materials containing point defects

R.V. Goldstein¹, T.M. Makhviladze², M.E. Sarychev²

1. Institute for Problems in Mechanics, Russian Academy of Sciences, Moscow, Russia, goldst@ipmnet.ru

2. Institute of Physics and Technology, Russian Academy of Sciences, Moscow, Russia, sarych@yandex.ru

The problem of strength reliability of many layer structures used in the up-to-date micro- and nanoelectronic circuits is still extremely actual up to now [1]. That is why the modeling the processes of crack propagation at interfaces of joined materials is of specific significance. Therefore development of models making it possible to formulate an adequate criterion of realization of different regimes of the kinetics of crack growth becomes a necessary step in this activity.

Formulation of a correct criterion of crack growth in solids is an actual fundamental problem up to now. The well known Griffith criterion for cracks growing in absolutely elastic homogeneous solids has the form [2] $E_c = W_a$, where for a homogeneous solid $W_a = 2\gamma$ (γ is the surface tension coefficient of the material) is the separation work required to form the crack surfaces (per unit area), E_c is the elastic strains energy being consumed for formation of a crack unit area. The Griffith criterion reflects the equilibrium thermodynamics conditions for crack growth. It connects the minimal value of mechanical stress at excess of which the material becomes unstable relatively the further crack formation. Thus the Griffith criterion gives the condition of crack formation but does not indicate a kinetic regime of its propagation.

In [3] the approach on the base of the nonequilibrium thermodynamics was used in order to obtain a more general criterion for crack growth in a homogeneous material with the quasistatic kinetics taken into account. This approach allowed involving the crack propagation rate in the criterion.

In the present work using the nonequilibrium thermodynamics approach we obtained a criterion of quasistatic growth of Griffith cracks along an interface of joined materials. It is assumed that the rate of crack propagation is sufficiently small. As a result the solid system under consideration gains negligibly small kinetic energy, and it has a same temperature in the whole volume. Under these assumptions one can write the first and second laws of thermodynamics at every instant of time, the second law being wrote in the form of the system entropy growth with time.

We considered both the case of pure joined materials and the case of materials containing such point defects as vacancies or atomic impurities. Like the case of crack formation in a homogeneous material the criterions obtained involve the rate of crack propagation. That is why they include both the case of crack growth and the case of its healing. If the joined materials contain point defects then the nonequilibrium consideration with the specific properties of the crack subsurface layers taken into account allows obtaining the corresponding criterion which has the same form as one in the absence of the defects but the quantities involved in it depend now on the defect concentrations.

For the case of vacancies as point defects using our previous results on defect concentration dependence of the interfacial separation work [4] we analyzed in detail the criterion obtained. In particular, if the vacancies are only in one of the joined materials the equation determining the vacancy concentration, at which the regime of crack growth can change into the regime of crack healing, was derived. The solution of this equation was found at some reasonable simplifications, and the conditions on the system parameters, at which the solution exists, were obtained. The estimations of the crack length and vacancy concentrations, at which the transition between the mentioned regimes can take place, were carried out.

1. T.M. Makhviladze and M.E. Sarychev. "Electromigration theory and its applications to integrated circuit metallization". Proc. SPIE., **7521**, p.752117, 2010.

2. V.D. Biggs. "Fracture", in *Physical metallurgy*. ed. by R.W. Cahn, **3**, Ch. XX, North-Holland Publ. Comp., Amsterdam, 1968.

3. J.R. Rice. "Thermodynamics of the quasi-static growth of Griffith cracks". J. Mech. Phys. Solids, **26**, pp. 61-78, 1978.

4. R.V. Goldstein, T.M. Makhviladze, and M.E. Sarychev. "Modeling the kinetics of lattice defect adsorption into the interface of joint materials". J. Surface, **5**, pp.712-717, 2011.

"Extrinsic" compact model of the MOSFET with the correct account of nonzero differential conductance in the saturation regime

V. Turin¹, S. Matyukhin¹, G. Zebrev², S. Makarov³, C.-H. Kim⁴, B. Iñiguez⁵, M. Shur⁶

1. State University ESPC, Orel, Russia, voturin@ostu.ru

2. National Research Nuclear University (MEPhI), Moscow, Russia, gizebrev@mephi.ru

3. LLC "Integrated Solutions", Moscow, Russia, makarov@is-eda.ru

4. LPICM, Ecole Polytechnique, CNRS, 91128 Palaiseau, France, chang-hyun.kim@polytechnique.edu

5. Rovira i Virgili University, Tarragona 43007, Spain, benjamin.iniguez@urv.cat

6. Rensselaer Polytechnic Institute, Troy, New York 12180, USA, shurm@rpi.edu

Compact models of semiconductor devices are relatively simple mathematical models that can adequately describe their characteristics. These models usually are realized in the form of C or Verilog-A code and are implemented into electrical circuit simulators, which are important part of the modern EDA software. As devices are miniaturized and novel materials are used, the compact modeling becomes more challenging. In previous papers [1, 2], we have shown that neither entry-level MOSFET compact models, like MOSFET Level 1, nor BSIM3/4 models, that are industry standard, do not reproduce a monotonic decrease of the differential conductance with increasing drain-to-source bias from a high value in linear regime up to nonzero or even negative value in saturation regime. To overcome this drawback, we have suggested in [1, 2] a simple and versatile approach for a correct account of the differential conductance in the saturation regime that provides a monotonic decrease of the differential conductance from its maximum value to minimum value. We have presented all the equations for an "intrinsic" MOSFET compact model (that does not include the source and drain resistances). The developed approach is quite versatile and can be used in compact models for various types of semiconductor devices. However, parasitic source and drain resistances become one of the performance-limiting factors for the development of modern nanoscale MOSFETs, short channel TFTs and organic FETs [35]. Even in the conventional vertical MOSFET using double diffusion, the drain resistance strongly affect the output characteristics. Hence, analytical models accounting for the source and drain resistances can be useful for theoretical studies and for more precise compact model parameters extraction. They could also improve the convergence and speed of compact modeling. In presented work, we generalize the previously obtained "intrinsic" equations to develop an analytical "extrinsic" compact model of the MOSFET that accounts for the source and drain resistances. All the equations are presented in the conventional and normalized forms. We have also incorporated the "extrinsic" MOSFET compact model into the EDA software Symica as a Verilog-A module.

1. V.O. Turin, A.V. Sedov, G.I. Zebrev, B. Iñiguez, and M.S. Shur. "Intrinsic compact MOSFET model with correct account of positive differential conductance after saturation". Proc. SPIE, **7521**, 75211H, 2009.
2. V. Turin, G. Zebrev, S. Makarov, B. Iñiguez, and M. Shur. "The correct account of nonzero differential conductance in the saturation regime in the MOSFET compact model". Int. J. Numer. Model. El., **1969**, 2014.
3. E. Chen, A. Wang, H. Chen, W. Hsieh, T.-H. Yu, T. Shen, J. Wu, C.H. Diaz. "Modeling Source/Drain Contact Resistance in Nanoscale MOSFETs". Proc. of SISPAD, pp. 344 - 347, 2012.
4. M.S. Shur, V.O. Turin, D. Veksler, T. Ytterdal, B. Iñiguez, and W. Jackson, "Compact Iterative Field Effect Transistor Model", in Proceedings of Workshop on Compact Modeling, NSTI-Nanotech 2006, **3**, pp.648-651, 2006.
5. C.-H. Kim, Y. Bonnassieux, G. Horowitz. "Compact DC Modeling of Organic Field-Effect Transistors: Review and Perspectives". IEEE Transactions on Electron Devices, **61** (2), pp. 278-287, 2014.

Mesoscopic Electromechanical Transducer Simulation: Transfer-Matrix Approach

I. Lysenko, L. Molchanova, N. Pristupchik
Southern Federal University, Taganrog, Russia, nkpristupchik@sfnu.ru

The paper describes the simulation method for tunneling transducers of nanoelectromechanical systems. The tunneling transducer is a system of two identical plane electrodes, which can be moved relatively to each other, changing spatial gap between the electrodes. Bias voltage applied to the electrodes. The output signal of the transducer is tunneling current density [1].

To describe quantum transport in the two-electrode micromachined tunneling transducer one can use one-dimensional, steady-state, linear Schrödinger equation:

$$-\frac{\hbar^2}{2m_0} \frac{\partial^2 \psi(x)}{\partial x^2} + U(x, \varphi_{wf}, d, \Delta U) \psi(x) = \varepsilon \psi(x), \quad (1)$$

where $\psi(x)$, m_0 and ε are the electron wavefunction, mass and energy, respectively, \hbar is Planck's constant and $U(x)$ is the potential energy function depending on parameters: φ_{wf} – electrode work function, d – distance between the electrodes, ΔU – bias voltage applied to the electrodes.

The main idea of the transfer matrix approach is in the fact that quantum tunneling through nanostructures can be treated as scattering process. To describe interaction of the tunneling particle with the system is sufficient to define transfer-matrix for each allowed state ε and compute transmission coefficient [2]:

$$S_{\alpha\beta}^{\varepsilon} = D_0^{-1} \prod_{i=1}^N [D_i P_i D_i^{-1}] P_{N+1}; \quad (2)$$

$$T(\varepsilon) = 1 - (|S_{21}|/|S_{11}|)^2, \quad (3)$$

where D_i and P_i are discontinuity and propagation matrices, respectively; $S_{\alpha\beta}^{\varepsilon}$ is a transfer matrix computed for energy ε and $T(\varepsilon)$ is corresponding transmission coefficient.

Tunneling current density can be calculated by the formula [3]:

$$J(\Delta U, d) = \frac{-qm^*k_0T_0}{2\pi^2\hbar^3} \times \int_0^{\infty} T(\varepsilon) \times \ln \left[\frac{1 + \exp(-E/k_0T_0)}{1 + \exp(-(E + q\Delta U)/k_0T_0)} \right] d\varepsilon, \quad (4)$$

where k_0 is Boltzmann constant, T_0 is absolute temperature, q is electron charge. Performing the integration for different bias voltages ΔU and distances d , one can get a family of current-voltage characteristics.

It is possible to state that conductive polymer is some kind of multi-electrode mesoscopic electromechanical transducer. From this point of view one can generalize method described above to perform first-principle simulation of the metal-polymer composites similar to quantum tunneling composite described in [4].

This study was supported by the Ministry of Education and Science of Russia (project no. 213.01–11/2014–12).

1. B.G. Konoplev, N.K. Pristupchik, and E.A. Ryndin, “A simulation method for displacement transducers based on the tunneling effect”, *Vestnik Yujnogo nauchnogo centra RAS*, **8**, № 4, pp. 20–26, 2012.
2. J.A. Monsoriu, F.R. Villatoro, M.J. Marin, J.F. Urchueguia, and P.F. Cordoba, “A transfer matrix method for the analysis of fractal quantum potentials”, *European Journal of Physics*, **26**, pp. 603–610, 2005.
3. R. Tsu and L. Esaki, “Tunneling in a finite superlattice”, *Applied Physics Letters*, **22**, pp. 562–564, 1973.
4. D. Bloor, K. Donnelly, P.J. Hands, P. Laughlin, and D. Lussey, “Metal-polymer composite with unusual properties”, *Journal of Physics D: Applied Physics*, **38**, pp. 2851–2860, 2005.

Configuration transition and electron density redistribution in molecular switches based on trans-polyacetylene

M.N. Zhuravlev¹, A.A. Gorbatsevich^{1,2}, T.S. Kataeva¹

1. National Research University of Electronic Technology (MIET), Moscow, Russia, aagor137@mail.ru

2. P.N. Lebedev Physical Institute of the Russian Academy of Sciences, Moscow, Russia

Tremendous progress of modern information technologies is closely related to the element downsizing. In a broader context, the design of new switching and memory components as tiny as a single molecule present a formidable challenge on the road toward miniaturization in future nanotechnology. Organic polymers with conjugated bonds are among the most promising research objects. They have various stable configurations and conformations with different energy and can be converted from one state to another by an external excitation such as light, electricity, etc. [1]. One is able to control the HOMO-LUMO gap value and other electronic properties in a wide range.

The simplest structure of a molecular switch is Y-branch formed by combination of three polyacetylene molecules. For such molecule in the tight binding approximation, it has been shown, that an unusual type of electronic states localized near the point of change in topology [2]. Their energies depend on the configuration of valence bonds in the branching point. In the presence of a double bond, bound states exist in pairs inside the energy gap near conduction-band minimum and valence band maximum, i.e., for both electrons and holes similar to polaronic states. In the case of single bonds, there is a single state located in the middle of the forbidden band. Branching point connected via single bonds with their nearest neighbors is similar to a soliton in a linear polyacetylene molecule.

Ab initio simulations support this picture though electronic energy spectrum strongly depends upon the size and structure of molecular cluster. The calculations were performed by density functional theory technique using hybrid exchange-correlation functional B3LYP and fully optimized geometry. There exist three possible scenarios of Y-branch construction from polyacetylene linear molecules. In the first case, the one trans-polyacetylene molecule attaches to other instead hydrogen atom without changing the types of chemical bonds between atoms. Carbon atom at the connection point is in the sp^2 hybridized state and is coupled by double π -bond with one of the branches. Nonplanar and nonsymmetry configuration of the molecule corresponds to state with the lowest energy. Atoms in the connected polyacetylene chains are out of the plane, which contains the branch point and its nearest neighbors.

Strong topological defect in the branch point leads to qualitative restructuring of the HOMO and LUMO orbitals and changes the bandgap in compare with the linear molecule. The wave function of HOMO-orbital becomes localized near the branch point. Localization radius ranges from 22 to 35 lattice periods for different branches. It should be noted, that the amplitude of the wave function depends on the relative orientation of the branches. It is lower in the chain attached to the linear molecule by forming splitter.

The second type of Y-branch occurs when three polyacetylene chains are connected in one point via single bonds. In this case, the topological bound state is similar to a soliton in a linear molecule and is located near the middle of the forbidden band. Electron-electron interaction shifts slightly this level down relative to the midgap.

Y-branch of the second type can proceed to the molecular configuration of the third type, caused by the change of carbon atom hybridization from sp^2 to sp^3 . In this situation, the delocalized HOMO and LUMO π -orbitals rupture and the wave functions of these states turn into zero at the branch point. However, the chains cannot be considered isolated from each other because there is interchain interaction explicitly accounted in the DFT technique. Note that, unlike the intrachain interactions, interchain interaction occurs π -orbitals, angled less than 90° . I.e. the interchain bond is intermediate between π and σ -character relationships. Excluding the interaction between the branches π -orbitals are triply degenerate states corresponding to an isolated chain of polyacetylene. Interchain interaction leads to a partial removal of the degeneracy.

1. *Molecular Switches. Second Edition.* Edited by B.L. Feringa and W.R. Browne. WILEY-VCH Verlag & Co. KGaA, Weinheim, Germany, 2011.

2. A.A. Gorbatsevich, M.N. Zhuravlev. "Topological Bound States". JETP Letters, **90**, pp. 582-586, 2009.

Image formation in a layer of tungsten with resolution of 32 nm by electron beam lithography

O. Borzenkova¹, O. Gushin², S. Zaytsev¹

1. *Moscow Institute of Physics and Technology (State University), Moscow, Russia, email: oksana.borzenkova@gmail.com.*

2. *Research Institute of Molecular Electronics, Zelenograd, Russia.*

This paper describes the results of research to form Line-Space structure in tungsten layer using two different electron resists. One of them is positive resist from JSR Corporation EP555JE, another was negative resist EN038 from Tokyo Okha.

It should be noted that the presence of tungsten layer on the silicon surface can significantly affect the dimensions of the output of secondary electrons when the sample is irradiated by an electron beam, which may require changes in the technological parameters of the lithographic process as compared to those used in lithography using single-crystal silicon substrates. Also the change of substrate material may influence the quality of the adhesion of the resist layer to the substrate and as a consequence, the mechanical stability of the structures produced.

To optimize lithography process of line-space structures, a series of experiments designed to study the effect of the modernization of the lithographic pattern on the results of lithography. The structures bellow was made be this technology.

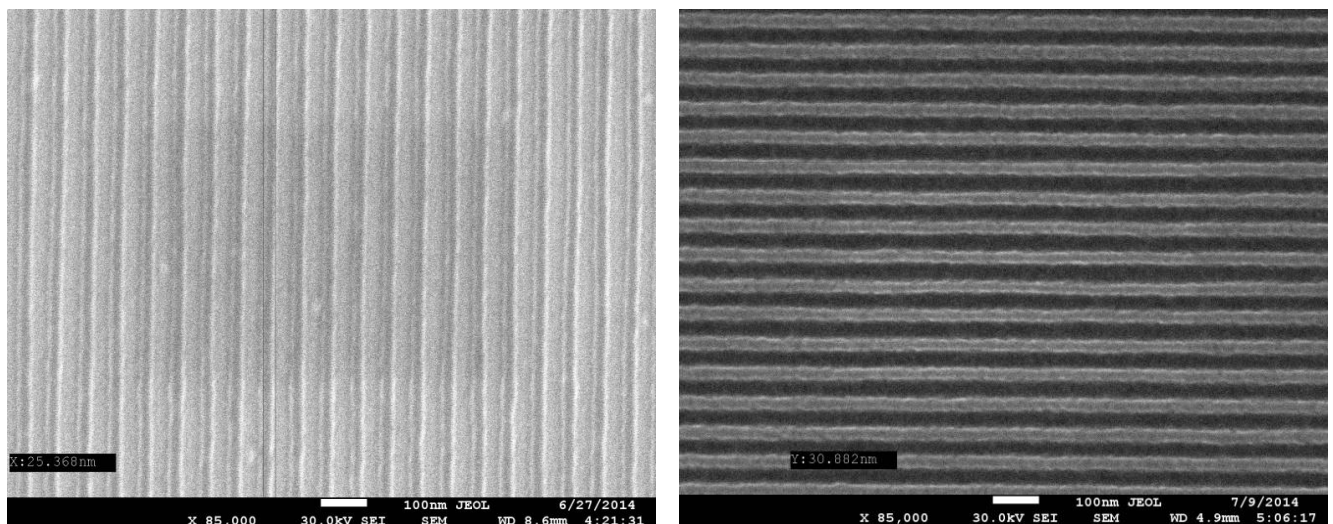


Fig.1. SEM-image LS (line-space) structure with CD = 32 nm using EP555JE (left) and EN038 (right) resists.

Small-scale vacuum system for deposition of multilayer metal films - “MVU TM – Magna 3M”

V. Odinokov, G. Pavlov, V. Panin, V. Raschinsky, A. Shpakov, A. Shubnikov
JSC “Research Institute of Precision Machine Manufacturing” (JSC NIITM)

When designing various semiconductor devices based on thin film technologies for producing high quality multilayer coatings all layers must be deposited on the substrate in one process (vacuum) cycle [1]. Deposition of thin films of various metals on substrates by magnetron sputtering in discharge plasma in one vacuum cycle provides productivity increase and sufficiently high adhesion strength between the substrate and the adhesive layer, and between separate layers of the coating.

This article deals with basic information about the design and technological capabilities of the new small scale vacuum installation “MVU TM – Magna 3M” designed to: - processing training; - scientific research; - development of technological process; - low-volume production.

Fig. 1 shows a main view (a) of “MVU TM – Magna 3M” installation and its schematic configuration (b).

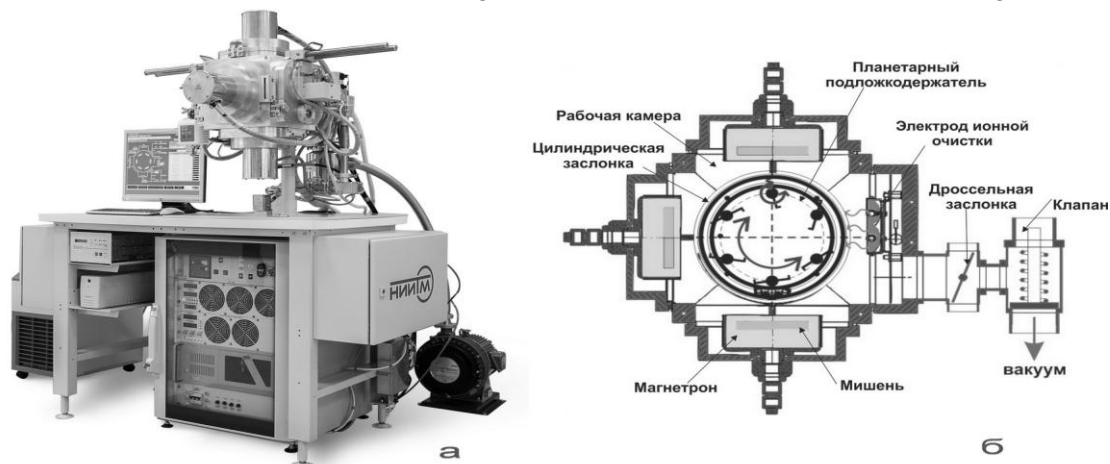


Fig. 1. Main view (a) and schematic configuration (b) of “MVU TM – Magna 3M”.

It consists of the process module mounted on the frame, control and power-supply rack located under the frame, gas cabinet and hydropneumatic panel attached to the frame, on the right and left sides of the control and power-supply rack respectively. Process module consists of the vacuum chamber in the form of a cube with 274 mm edges size. Magnetrons are located at the bottom, front and top flanges of chamber. Unit of substrate holders is located at the right side of the flange and the shutter (screen) unit at the left side of the flange. To download the substrates, as well as for convenient operation of the installation, unit of the substrate holder and shutter unit move along the guide. Working chamber and technological components are cooled with cold water. Flow of process gases into the chamber and gas puffing at the end of the spraying process occurs respectively via the electromagnetic valves. Six pyroceramics plates with dimensions of 48×60 mm² are fastened in special holders that are attached to the rotary drive via geared transmission. During the process they make planetary movements around its axis and about the axis of rotary drive. Oil-free vacuum system provides a residual pressure in the chamber at least 5×10^{-4} Pa. Halogen lamps are used for heating. Ion-plasma cleaning of plates is carried out at an argon pressure of 2 Pa before deposition. After pretreatment the three magnetrons are turned on and target cleaning are carried out. The operating pressure of argon is 0.1-1.0 Pa and sputtering power of each target is in a range of 1.5-3 kW. Multilayer coatings with alternating layers of chromium or vanadium and copper or aluminum are obtained in one technological cycle by magnetron sputtering onto pyroceramics plates with dimensions of 60×48 mm and thickness of 0.25 – 2 mm. Moreover, experiments on deposition of single coatings of these metals were held. Control of the deposition process was carried out with respect to processing time

Odinokov V.V., Panfilov Y.P. Type classification of vacuum nanotechnological equipment by specified productivity. // Nanoengineering. 2011. №11. PP. 7 – 18.

Arc plasma jet treatment of the silicon surface at gate oxidation and contact formation

G. Pavlov

JSC "Research Institute of Precision Machine Manufacturing" (JSC NIITM), Zelenograd, Russia

Earlier [1], we described pre-gate oxidation cleaning of silicon wafer using the new single-step dry method of arc plasma jet [2] treatment (APJT). We showed that Si wafer cleaning surface improves some properties of MOS structures in comparison to wet chemical cleaning.

Cleaning of the silicon surface before film deposition is a key procedure in the synthesis of silicide (CoSi_2) and, hence, in the production of the metal-semiconductor contact. This study deals with a new method of surface cleaning using arc plasma jet treatment (APJT) at atmospheric pressure. The results show that cleaning of the Si surface using APJT (Ar/CClF_3) improves the Schottky barrier contact parameters in comparison with conventional wet HF final cleaning and additional cleaning using in situ Ar-ion-beam sputter etching. Moreover, substantially longer time of wafer exposure to air between final cleaning and metal deposition is acceptable. Auger electron spectroscopy shows that APJT removes oxygen from the Si surface.

Ex situ etching of native silicon oxide in buffered HF water solution is the most often used final procedure before metal deposition. The main disadvantage of this cleaning is the high rate of Si reoxidation during exposure to air; therefore, the time between the final cleaning and metal deposition should be minimized. Moreover, HF does not remove carbon and hydrocarbons which may significantly deteriorate contact performance. Combinations of *ex situ* wet and in situ dry Si cleaning with vapor/gas/plasma processes have found general use. However, plasma etching, ion-beam sputtering (IBS), and other *in situ* dry-cleaning processes deteriorate the contact parameters by radiation damage because of ion bombardment and contaminants of non-volatile compounds remaining after etching (usually, C-F polymers or hydrogen).

It should be noted (Table 1) that the oxide was not removed completely after wet cleaning, and the series resistance of the structures was therefore relatively high. These contacts had low breakdown voltages, high ideality factors, and a large scatter of the potential barriers.

Table 1. CoSi_2 Schottky contact parameter of after various clean mode

Clean mode of Si	Contact barrier, eV	Ideality factor	Breakdown voltage, V	R, Ω
Without clean	0.53	7.0	76	1710
HF, 20 min exp.	0.56	3.6	47	1330
HF	0.57	1.38	37	1030
HF + IBS	0.58	1.22	75	870
APJT	0.65	1.13	86	790

We may therefore conclude that the final cleaning of silicon surface using APJT at atmospheric pressure is available and has a number of advantages over the conventional techniques.

1. G.Ya. Pavlov. MRS Spring Meeting Proc., **386**, p. 293, 1995.
2. G. Pavlov et al. U.S. Patent 5,474,642 December 12, 1995.

Formation of fast neutral particle beams and their using for selective etching

V. Kudrya, Yu. Maishev, S. Shevchuk

Institute of Physics and Technology, Moscow, Russia, E-mail address: kvp.ftian.ru

Two fast neutral particle beam (FNPB) sources with annular and racetrack shaped output slits based on the ion source family "Radical" with a cold cathode, crossed electrical and magnetic fields, and closed electron drift [1] have been constructed and successfully tested. These sources can generate the neutral beams consisting of atoms, radicals, and molecules depending on the working gas and the discharge mode. Some theoretical aspects related to operation of such sources were considered in our papers [2-5]. In this report new experimental and theoretical results related both characteristics of the FNPB sources and etching rates and selectivities obtained using these sources are described.

An analysis of ion beam neutralization efficiency in a gas phase was made based on a simple mean free pass length approximation with three types of collisions between fast particles and thermal particles: ion-neutral charge-exchange collision, ion-neutral elastic collision, and neutral-neutral elastic collision. Analytical expressions for the output beam neutrality coefficient K_{neutr} and ion beam neutralization efficiency K_{eff} and their maximum values were obtained. In the case of the working gas Ar in the ion energy range of 4-400 eV the following estimation were calculated: $K_{\text{neutr max}} \leq 0.57$, $K_{\text{eff max}} \leq 0.30$. It indicates that only the gas-phase mechanism of ion neutralization can not provide high-performance transformation of ion beams into neutral beams.



Then, the FNPB source construction including the ion source "Radical", a channel of neutralization, and an electrostatic deflection system is described. The output beams of the FNPB sources "Neutral-100K" (annular output slit) and "Neutral-110L" (racetrack shaped output slit; see the photography) were analyzed using etching experiments, an ion current probe, and a flow-through calorimeter designed in our laboratory. The working gases used were Ar, O₂, and C₆H₁₂. Using the several methods of measurements provides us with both the averaged neutral particle energy E_{av} and the total neutral particle flux S .

Etching rates and selectivities were measured for the working gases Ar, CF₄, C₃F₈, and SF₆ and the Si substrates, thermal SiO₂, and thin films W, NbN, TiC, and TiN deposited by (reactive) ion-beam sputtering. It should be noted that the highest selectivities (relatively SiO₂) were achieved with C₃F₈: ~16 (W), ~16 (TiC), ~11 (TiN), ~11 (Si), and ~10 (NbN).

At last, decreasing the CV-characteristics shift of a Si/SiO₂ (25 nm) interface due to using neutral beams instead of ion beams was obtained. The built-in charge decreasing estimation gives $\Delta Q = 4.4 \times 10^{12} \text{ e/cm}^2$. It is in a good agreement with the published results.

1. Y. Maishev, J. Ritter, Y. Terentiev, L. Velikov. "Cold-cathode ion source with propagation of ions in the electron drift plane". Patent USA No. 6,130,507, Date of Patent: October 10, 2000.
2. A.V. Degtyarev, V.P. Kudrya, Yu.P. Maishev. "Mathematical Simulation of an Inclined Neutralization Channel for a Plasma Source of Neutral Beams". Russian Microelectronics, **38**, pp. 171-179, 2009.
3. A.V. Degtyarev, V.P. Kudrya, Yu.P. Maishev. "Simulation results for three neutralization channel designs of a fast neutrals beam source". Proc. SPIE, **7521**, 75211G, pp. 1-9, 2009.
4. A.V. Degtyarev, V.P. Kudrya, Yu.P. Maishev. "Mathematical Simulation of the Influence of a Focusing Channel Surface on the Angle Characteristics of a Bundle of Rapid Neutral Particles". Russian Microelectronics, **39**, pp. 405-410, 2010.
5. V.P. Kudrya, Yu.P. Maishev. "Calculation of the flow capacity of a gas channel in the sources of beams of fast neutral particles by means of the Monte-Carlo method". Russian Microelectronics, **42**, pp. 184-188, 2013.

Carbon and fluorine co-implantation for boron diffusion suppression in extremely ultra shallow junctions

A. Miakonkikh¹, A. Rogozhin¹, V. Rudakov², K. Rudenko¹, and V.F. Lukichev¹

1. Institute of Physics and Technology, Moscow, Russia, miakonkikh@ftian.ru

2. Institute of Physics and Technology (Yaroslavl Branch), Yaroslavl, Russia

One of the crucial technologies in manufacturing sub-22nm CMOS devices is formation of 2-8 nm S/D highly doped regions with sharp profile of doping impurity and high level of activation. Interaction of doping atoms with defected Si-lattice during activation of impurity by RTA or flash annealing extremely influences on the final results of process. Well-known fact of boron impurity transient enhanced diffusion (TED) and formation of boron interstitial clustering (BIC) [1] counteracts to receive expected results. Annealing should be short enough to prevent concentration profile from widening due to diffusion, but insufficient annealing lead to non-completed recrystallisation of defected layer, and cannot remove deep EOR defects [2]. The advance of co-implantation into pre-amorphised Si-layers simultaneously or sequentially in mode of plasma immersion ion implantation (PIII), is that implantation does not require adding new steps into process flow. Additional positive effect is the elimination deactivation channels for boron and enhanced stability of obtained junctions [3]. Our study of co-implantation for extremely ultra shallow junction is aimed to suppression of main diffusion mechanisms for boron in presence of carbon or fluorine.

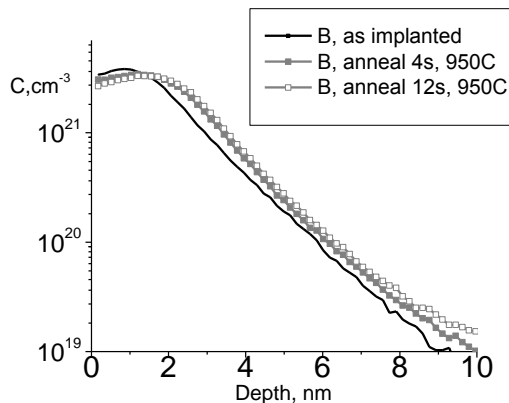


Fig. 1. SIMS profile of boron at BF₃ plasma doped samples, as implanted and after RTA.

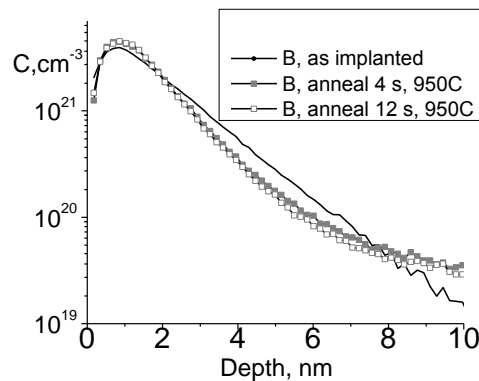


Fig. 2. SIMS profile of boron at BF₃ and CF₄ plasma doped samples, as implanted and after RTA.

Experiment was carried out in same chamber of experimental PIII tool. First, the pre-amorphisation of Si was done by PIII of He⁺ ions. Then boron doping with co-implanted F was made from BF₃ plasma ($D_B = 2.7 \times 10^{14} \text{ cm}^{-2}$; applied voltage of 1 kV). Finally, the carbon impurity was introduced by implantation carbon ions from CF₄ plasma. Ion energy (1 keV) and dose ($D_C = 3 \times 10^{14} \text{ cm}^{-2}$) of the later step was chosen to provide highest concentration of carbon in upper 10 nm layer. RTA were performed in two steps (400 C for 1 min, and 950 C for 4-12 sec), and multistep (4 sequential heating-cooling steps) routines.

Boron, fluorine and carbon concentration profiles were measured by SIMS. It was shown that in boron and fluorine implanted samples widening doping profile with annealing is observed (see Fig. 1), while in carbon co-implanted samples steady narrowing of profile can be seen during rapid annealing (see Fig. 2). Narrowing occurs in the region of highest carbon concentration, and could be as high as 1 nm.

Dependence of this effect on the carbon concentration was studied, as well as positive role of multistep annealing for pure boron implanted samples.

The reported study was partially supported by RFBR, research projects No 12-07-00745-a and 14-07-31293.

1. S. H. Yeong et al, Journal of The Electrochemical Society, **155** (2), pp. H69-H75, 2008.
2. S.B. Felch, A. Mayur, V. Parihar, F. Nouri, K.S. Jones, D.E. Zeenberg, and B.E. Jones, Mater. Res. Soc. Symp. Proc., **912**, 0912-C04-03, 2006.
3. N.E.B. Cowern, B. Colombeau, J. Benson, A.J. Smith, W. Lerch, S. Paul, T. Graf, F. Cristiano, X. Hebras, and D. Bolze, Appl. Phys. Lett., **86**, 101905, 2005.
4. S. Mirabella et al J. Appl. Phys., **113**, 031101, 2013.

Simulation of devices based on carbon nanotubes and graphene

I.I. Abramov, V.A. Labunov, N.V. Kolomejtseva, I.A. Romanova

Belarusian State University of Informatics and Radioelectronics, Minsk, Belarus, E-mail: nanodev@bsuir.edu.by

Some electrical, optical, thermal and mechanical properties of carbon nanomaterials will determine their various applications. In the paper results of simulation of different devices based on carbon nanotubes (CNT) and graphene are described.

Development of radio receiver based on CNT (nanoradio) is the perspective direction of the CNT application. The review of achievements and the analysis of development problems of nanoradio based on CNT are presented in [1].

This problem is characterized by very high degree of complexity. Nanoradio of the type I (based on only single CNT) is nanoelectromechanical system and one should be simulated at the level of quantum mechanical models. The analysis shows that it is simply impossible at a modern level of computer facilities. Therefore two perspective approaches to nanoradio simulation, namely [1]: 1) multilevel approach; 2) approach on the basis of model hierarchy were emphasized. Both approaches were realized.

Multilevel approach was realized in cooperation with colleagues from BNTU. It was used for simulation of nanoradio on a single CNT (type I). In particular, various constructions of nanoradio on single CNT and the CNT bundles of different geometry were investigated at different applied voltage. Quantity of electrodes, distances between CNT and their diameter were taken into account. The operability of the investigated devices in the radio-frequency range [2, 3] was shown.

Unfortunately, a rather rigorous technique of multilevel simulation [2, 3] requires high-capability computers. As a result, the corresponding models are of limited usefulness and this approach is applicable only for nanoradio of the type I.

In this regard the second approach, based on hierarchy of various models, was also realized. In particular, the technique of express simulation of nanoradio based on CNT of the type I and of the type II is developed. Developed models can be used for calculation of nanoradio characteristics such as: 1) resonant frequency of CNT; 2) oscillation amplitude of CNT; 3) CNT IV-characteristics depending on different factors. Results of device simulation based on single-wall and multi-wall CNT are given in the paper.

Graphene-based nanostructures have recently attracted a great deal of attention for their unique fundamental properties and various potential applications [4]. IV-characteristics of nanoscale resonant tunneling structure based on graphene in SiC substrate were calculated. As well as it was investigated the influence of different parameters on the electrical characteristic of graphene-based nanostructures and diodes. All results were obtained with the use of NANODEV system on PC [5, 6].

1. I.I. Abramov, V.A. Labunov. "Problems and perspectives of development of nanoradio based on carbon nanotubes". 21st Int. Crimean Conf. "Microwave & Telecommunication Technology" (CriMiCo'2011), Sevastopol, **1**, pp. 28-30, 2011.
2. I.I. Abramov, V.V. Barkaline, E.A. Belogurov, V.A. Labunov, A.S. Chashynski. "Simulation of resonant excitation of electromechanical vibrations in carbon nanotube radio receiver". 21st Int. Crimean Conf. "Microwave & Telecommunication Technology" (CriMiCo'2011), Sevastopol, **2**, pp. 803-805, 2011.
3. V. Barkaline, I. Abramov, E. Belogurov, A. Chashynski, V. Labunov, A. Pletezhov, Y. Shukevich. "Simulation of carbon nanotubes and resonant excitation of their mechanical vibrations by electromagnetic field for nanoradio applications". *Nonlinear Phenomena in Complex Systems*, **15**, No. 1, pp. 23-42, 2012.
4. I.I. Abramov, N.V. Kolomejtseva, V.A. Labunov, I.A. Romanova, A.S. Basaev "Simulation of hybrid integrated structures based on carbon nanotubes". *J. of nano- and microsystem technique*, **5**, pp. 11-15, 2014.
5. I.I. Abramov, I.A. Goncharenko, S.A. Ignatenko, A.V. Korolev, E.G. Novik, A.I. Rogachev. "NANODEV: A nanoelectronic-device simulation software system". *Russian Microelectronics*, **32**, No. 2, pp. 97-104, 2003.
6. I.I. Abramov, A.L. Baranoff, I.A. Goncharenko, N.V. Kolomejtseva, Y.L. Bely, I.Y. Shcherbakova. "A nanoelectronic device simulation software system NANODEV: New opportunities". *Proc. of SPIE.*, **7521**, edited by Kamil A. Valiev, Alexander A. Orlikovsky, pp. 75211E1-1-11, 2010.

Numerical modeling of functionally integrated injection lasers-modulators

B. Konoplev, E. Ryndin, M. Denisenko

Institute of Nanotechnology, Electronics and Electronic Equipment Engineering of Southern Federal University, Taganrog, Russia, ryndinator@gmail.com

A simulation of injection lasers processes dynamics is performed by using the kinetic equations conventionally [1]. Constructing methods and structures of functionally integrated injection lasers-modulators are presented in [2 – 5]. Numerical simulation of these lasers-modulators requires consideration of the unevenness of spatial distribution of electrons, holes and photons concentrations, speed of radiative recombination (spontaneous and stimulated) in active area and in the lasers-modulators peripheral areas. To solve this problem in [6] proposed a model developed on the basis of the semiconductor fundamental system of equations and the laser kinetic equations.

In this work the proposed model was modified, developed software and the results of numerical simulation of transients in functionally integrated injection lasers-modulators were performed. In the modified model the rate of radiative recombination R determined in accordance with the terms:

$$R = \sqrt{np - n_i^2} \left(\frac{1}{\tau_s} + \alpha \cdot n_{ph} \right),$$

where n , p , n_{ph} – the concentrations of electrons, holes, and photons, respectively; n_i – intrinsic concentration; α – the optical gain coefficient; τ_s – the spontaneous recombination lifetime of the carriers.

To analyze the applicability limits of the proposed model the comparative analysis of numerical modeling results of transient processes in the conventional injection lasers with double heterostructures obtained by using the proposed model on the one side and kinetic equations on another. The simulation was performed for lasers, characterized by the optical gain coefficient $2,8 \cdot 10^{-6} \text{ cm}^3/\text{s}$, active region width from 20 to 100 nm, the life time of a photon in the laser resonator from 0,1 to 1,1 ps, the share of spontaneous radiation in laser mode 10^{-4} , spontaneous radiative recombination time 4 ns.

According to the results of the comparative analysis, in the considered range of laser active region width changing and the photon life time there is a significant irregularity of spatial distributions of the charge carriers and photons concentrations, and the speed of radiative recombination processes, which indicates the expediency of using the proposed model even for the conventional injection lasers modeling and makes quantitative difference in the characteristics of transient processes, obtained on the basis of the proposed model and kinetic equations solution. This difference increases with the lasers active region width and the photon life time increasing.

This study was supported by the Russian Foundation for Basic Research (projects 13-07-00274, 14-07-31234), and by the Ministry of Education and Science of Russian Federation (project 8.797.2014K).

1. Jianjun Gao, “Optoelectronic integrated circuit design and device modeling”, Beijing: Higher Education Press, 310 p., 2011.
2. B.G. Konoplev, E.A. Ryndin, and M.A. Denisenko, “Integrated Injection Laser with Amplitude Modulation in Terahertz Band”, Abstracts of International Conference “Micro- and nanoelectronics - 2009”. Moskow – Zvenigorod, Russia, p. O1-28, 2009.
3. B.G. Konoplev, E.A. Ryndin, and M.A. Denisenko, Patent RU 2400000 C1, 2010.
4. E.A. Ryndin, M.A. Denisenko, “A Functionally Integrated Injection Laser–Modulator with the Radiation Frequency Modulation”, Russian Microelectronics, **42** (6), pp. 360–362, 2013.
5. B.G. Konoplev, E.A. Ryndin, and M.A. Denisenko, “Injection Laser with a Functionally Integrated Frequency Modulator Based on Spatially Shifted Quantum Wells”, Technical Physics Letters, **39** (11), pp. 986–989, 2013.
6. B.G. Konoplev, E.A. Ryndin, and M.A. Denisenko, “A dynamic simulation model for functionally integrated injection laser-modulator”, Abstracts of International conference “Micro and nanoelectronics – 2012”. Moskow – Zvenigorod, Russia, p. O1-18, 2012.

Carrier dynamics and stimulated radiative terahertz transitions between Landau levels in cascade GaAs/AlGaAs quantum well structures

M.P. Telenkov^{1,2}, A.A. Kutsevol², Yu.A. Mityagin^{1,3}, V.V. Agafonov¹

1. P.N. Lebedev Physical Institutes, Moscow, Russia, maxim_telenkov@mail.ru

2. National University of Science and Technology (MISiS), Moscow, Russia, maxim_telenkov@mail.ru

3. National Research Nuclear University (MEPhI), Moscow, Russia, yumityagin@mail.ru

A new mechanism of stimulated terahertz emission due to inter-Landau level transitions in cascade quantum well structures in strong magnetic field under a condition of sequential resonant tunneling was proposed and theoretically confirmed [1-3]. The carrier distribution over Landau levels was studied in resonant tunneling GaAs/AlGaAs quantum well structures under tunneling pumping of the upper subband. The numerical calculations of the Landau level populations for various values of pumping intensity (tunneling time), magnetic field and the structure doping were carried out. The population inversion between zeroth Landau level of the upper subband and the first Landau level of the lowest subband was shown to exist in wide range of the magnetic field strength. So the stimulated emission of terahertz radiation can be achieved on the transitions between these LLs, and the emission frequency, determined by the relation

$$\hbar\omega = \Delta E_{12} - \hbar\omega_c \quad (1)$$

(ΔE_{12} is a subband spacing, ω_c is a cyclotron frequency), can continuously be tuned by the magnetic field strength variation.

An effective method of lifting the selection rule forbidding the transition of interest was found. It was proposed to tilt the magnetic field with respect to the layers along with an asymmetric design of the structure period. Significant values of the transition matrix element were achieved if two coupled quantum wells of different widths were used as a period of the resonant tunneling structure. The main reason of the effect was the different localization of the subband wavefunctions - the 1st subband one is localized mainly within wide quantum well, while that of the 2nd subband is shifted to the narrow well.

The electron kinetics studies were carried out in periodic quantum well structures with such asymmetric double quantum well period in a tilted magnetic field. The motivation was the expectation that this dislocation of wave functions can lead to a considerable decrease of the upper laser level scattering rate and consequently to the increase of its population. The inter-Landau level scattering rates as well as Landau level populations were calculated as functions of the well parameters, strength and direction of the magnetic field. A significant increase of the upper level lifetime (about order of magnitude) was demonstrated as well as its population, resulting in a considerable improvement of the optical gain.

This work was supported by the RFBR (project 12-02-00564) and NUST «MISiS» (grant no. 3400022).

1. M.P. Telenkov, Yu.A. Mityagin, and P.F. Kartsev. "Intersubband population inversion and stimulated transition between the Landau level in resonant tunneling multiple quantum-well structures". JETP Letters, **92**(6), pp. 401-404, 2010.

2. M.P. Telenkov, Yu.A. Mityagin, and P.F. Kartsev. "Intersubband terahertz transitions in Landau level system of cascade GaAs/AlGaAs quantum well structures in strong tilted magnetic field". Nanoscale Research Letters, **7**, pp. 491-495, 2012.

3. M.P. Telenkov, Yu.A. Mityagin, and P.F. Kartsev. "Carrier kinetics and population inversion in Landau level system in cascade GaAs/AlGaAs quantum well ". Optical and Quantum Electronics **46** (6), pp. 759-767, 2014.

Application of the iterative approach to Eigenmode Expansion method for the solution of Maxwell's equations

Igor Semenikhin¹ and Mauro Zanicoli²

1. Institute of Physics and Technology RAS, 117218 Moscow, Russia, isemenihin@gmail.com

2. ARCES-DEIS University of Bologna and IUNET, 47521 Cesena (FC), Italy, mauro.zanicoli@unibo.it

Over the past decades an increasing interest has been devoted to the rigorous solution of Maxwell's equations in order to study the optical properties of optoelectronic devices including image sensors, nanostructured solar cells, photonic crystals and diffraction gratings [1, 2]. Many methods to solve the Maxwell's equations have been developed to date [2, 3]. From the computational point of view the solution of Maxwell's equations leads to the need of processing a system of linear (or in some cases nonlinear) equations or an eigenvalue problem or both of these. These problems may be solved either by direct or iterative approach. The choice between these two approaches depends on many factors, the main of which is the computational algorithm on which they are based.

In the last years the direct methods to solve systems of equations and eigenvalue problems have been widely used. Recently, due to a rapid increase in complexity of the simulated devices and the continuously rising demand of accuracy that leads to the need of solving very large systems of linear equations, iterative methods have gained interest. To date a number of algorithms have been developed to solve Maxwell's equations within iterative approach [4-9]. Its implementation can significantly reduce the computational time. For example, iterative implementation of Generalized Source Method, differential and finite-element methods can reduce the number of arithmetic operations from cubic to linear dependence on the number of Fourier modes used in calculations [4-6].

In case of Eigenmode Expansion or "modal" methods, which are typically adopted in order to model light propagation in fiber optics and in silicon photonics devices, iterative approaches are also exploited to speed up calculations, for instance to solve eigenvalue problems using Arnoldi method [7-9]. However, the computational complexity of such solutions as well as of the available modal algorithms are of order of the third power of the number of eigenmodes used, which is the same of the direct approach. In this work we propose an iterative technique that allows to reduce the computational complexity of modal methods from the third power to the second power of the number of eigenmodes.

1. K. Yasumoto, *Electromagnetic Theory and Applications for Photonic Crystals*, CRC Press, 2005.
2. E. Popov, Editor, *Gratings: Theory and Numeric Applications, Second Revisited Edition*, AMU, PUP, Marseille, 2014.
3. G. Bao, L. Cowsar, and W. Masters, *Mathematical Modeling in Optical Science*, SIAM, 2001.
4. A. Shcherbakov, A. Tishchenko, "New fast and memory-sparing method for rigorous electromagnetic analysis of 2D periodic dielectric structures," *Journal of Quantitative Spectroscopy and Radiative Transfer*, **113**(2), pp. 158–171, 2012.
5. Y.-C. Chang, G. Li, H. Chu, and J. Opsal, "Efficient finite-element, Green's function approach for critical-dimension metrology of three-dimensional gratings on multilayer films," *J. Opt. Soc. Am. A* **23**, pp. 638-645, 2006.
6. I. Semenikhin, M. Zanicoli, C. Fiegna, V. Vyurkov, E. Sangiorgi, "Computationally efficient method for optical simulation of solar cells and their applications," *Proc. SPIE 8700, International*, p. 870012-1 (12 pages), 2012.
7. J.G. Wangüemert-Pérez, R. Godoy-Rubio, A. Ortega-Moñux, and I. Molina-Fernández, "Removal of the Gibbs phenomenon and its application to fast-Fourier-transform-based mode solvers," *J. Opt. Soc. Am. A* **24**, pp. 3772-3780, 2007.
8. B. Portier, F. Pardo, P. Bouchon, R. Häidar, and J.-L. Pelouard, "Fast modal method for crossed grating computation, combining finite formulation of Maxwell equations with polynomial approximated constitutive relations," *J. Opt. Soc. Am. A* **30**, pp. 573-581, 2013.
9. I. Semenikhin and M. Zanicoli, "Computationally efficient finite-difference modal method for the solution of Maxwell's equations," *J. Opt. Soc. Am. A* **30**, pp. 2531-2538, 2013.

Approaches to a dies decoupling during failure analysis of the 3D package integrated circuits

G. Molodtsova, R. Milovanov, D. Zubov, E. Kelm

Institute of Nanotechnology of Microelectronics, Russian Academy of Science, Russia, 119991 Moscow, Leninsky Prospekt, 32A, Milovanov_r@inbox.ru

During failure analysis of integrated circuits (IC), it is often necessary to have opportunity to inspect surface of die. But modern IC processing technology often provides integration of a number of overlapping dies in one package (3D package type). In this case upper die complicate access to low die. Thus finding techniques which provide opportunity to inspect surface of each die is actual.

One way which specifies consecutive removing of each die with grinding machine ASAP-1 is presented in [5]. Serious disadvantages of such approach are risk of lower die damage and complete destruction of upper die. Thus, in present work we consider approaches to a die decoupling with etching die attach film (paste) by fuming nitric acid during a long time and several cyclic change of the IC's (die's set) temperature. Our experimental research shows ability of use both approaches to a die decoupling.

Die's set, which was exposed to fuming nitric acid during several hours, decoupled to four separate chips with clean non-damage surface (fig. 1). But we should be note that aluminum bonding pads were removed. Thus such an approach limits further IC failure analysis only with deprocessing.

Approach to dies decoupling with cyclic change of the IC's temperature means consecutive heat and cooling of die's set. Fourfold repeat of heat/cooling cycle leads to pairwise decouple of die's set. Additional 3 cycles leads to complete dies decoupling. Thereby approach which based on cyclic change of the IC's temperature provide to safe bonding pads and give opportunity to use a majority of failure analysis techniques.

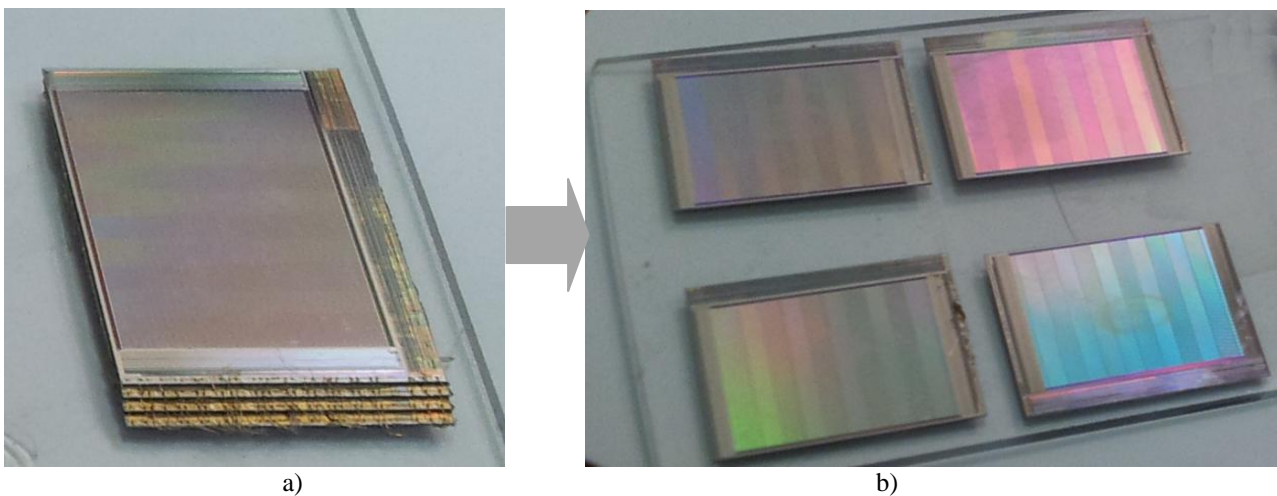


Fig. 1. View of die's set before (a) and after (b) decoupling.

1. Yuan Xie, Yibo Chen, Guangyu Sun, Jin Ouyang, *Three-dimensional Integrated Circuits: Design, EDA, and Architecture*. Springer, 2010.
2. Philip Garrou, Christopher Bower, Peter Ramm, *Handbook of 3D Integration: Volumes 1. Technology and Applications of 3D Integrated Circuits*. Wiley-VCH Verlag GmbH & Co, 2012.
3. Beck F. *Integrated circuit failure analysis*. John Wiley & Sons. 1998.
4. Ross R.J. *Microelectronics failure analysis. Desk reference. Sixth Edition*. ASM International. 2011.
5. <http://www.ultratecusa.com>
6. Toh CH, Mehta Gaurav, Tan Hua Hong, Ong Wilson PL, *Die Attach Adhesives for 3D Same-Sized Dies Stacked Packages*. Electronic Components and Technology Conference, 2008.

Electrochemical recovery of damaged bonding area during failure analysis of the modern integrated circuits

D. Zubov, E. Kelm, R. Milovanov, G. Molodtsova

Institute of Nanotechnology of Microelectronics, Russian Academy of Science, Russia, 119991 Moscow, Leninsky Prospekt, 32A, Milovanov_r@inbox.ru

During failure analysis (FA) of modern integrated circuits (IC) we may wish to do some investigation, which consist of simultaneous inspection die's surface and signal injection to IC's pad. It's easy to do when IC die isn't encapsulated (the procedure looks like "wafer test" [3]). But when IC die encapsulated, we need to expose its surface completely (decapsulate it). For IC's with plastic package (most common type of IC package) removing of package usually doing with warm fuming nitric acid [4] and after it die's surface investigates with different types of microscopy (optical, electron, IR, etc.) [5].

Some FA procedures require signal injection to IC's bonding area (pads). Such injection may be done with contact probes. But difficulty of long time probe holding on pad, make recover dies bonding more preferentially.

Such approach implementation may be obstruct by damaged pad (fig. 1a), which re-bonding is ruled out. So recovery of damaged bonding area is necessary for further FA. In present work we consider different types of bonding area damages and approaches to their electrochemical recovery using silver and copper.

Experimental researches were done with aqueous solutions of silver nitrate and copper sulfate. We researched different solutions concentration and current magnitude influence on density and uniformity of forming pad layer (recovering pad). During electrochemical pad recovery with silver nitrate we obtained fine-dispersed silver around pad or macrocrystalline dendrite structures. Pad recovery with copper sulfate permit to deposit thin copper layer on damaged area (fig. 1b). Further thermocompression bonding allowed to re-bond recovered pad.

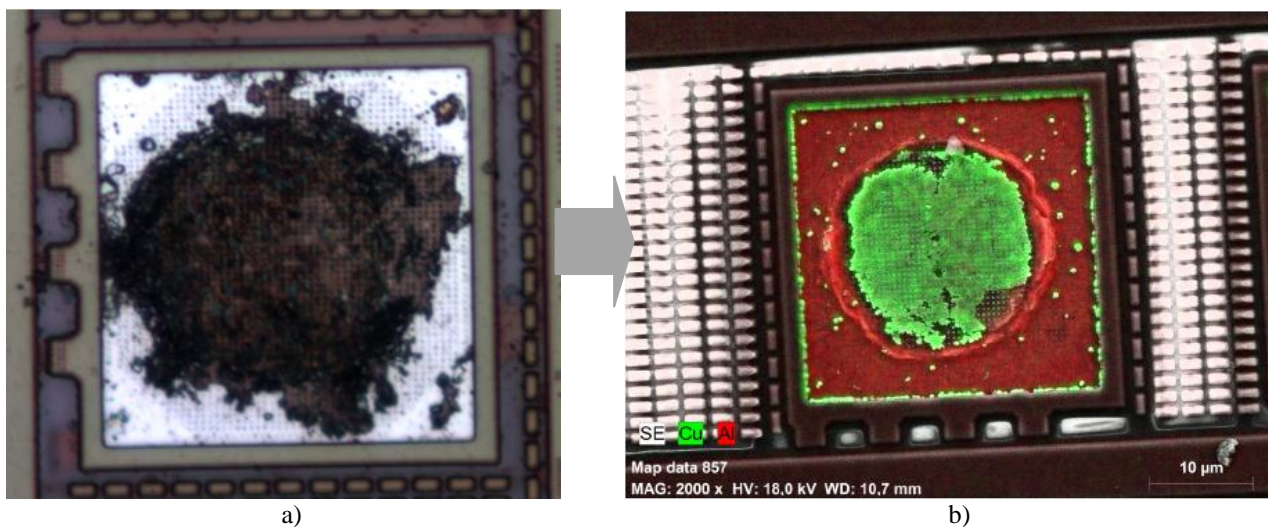


Fig. 1. View of die's damaged bonding pad before (a) and after (b) recovery.

1. Gary S. May, Costas J. Spanos, *Fundamentals of semiconductor manufacturing and process control*. John Wiley & Sons, 2006.
2. Peter Van Zant, *Microchip Fabrication: A Practical Guide to Semiconductor Processing, Fifth Edition*. McGraw-Hill, 2004.
3. Scotten W. Jones, *Introduction to integrated circuit technology, Fifth Edition*. IC Knowledge LLC, 2012.
4. Beck F. *Integrated circuit failure analysis*. John Wiley & Sons. 1998.
5. Ross R.J., *Microelectronics failure analysis. Desk reference. Sixth Edition*. ASM International. 2011.

Non-destructive electromigration testing method development for metallization of integrated circuits based on the rate of resistance change

S.O. Safonov

National Research University of Electronic Technology (MIET), Moscow, Russia, safonov.sergey1987@gmail.com

This work focuses on the analysis of resistance-time relationship, obtained during the accelerated EM testings in order to elaborate non-destructive testing methods. This method was based on the accelerated testing methods of conductors at the constant temperature. The task of the work was – to analyze assemblage of curves of time-resistance relationship (fig.1) and try to correlate the intermediate values of the test time and the metallization line failure moment.

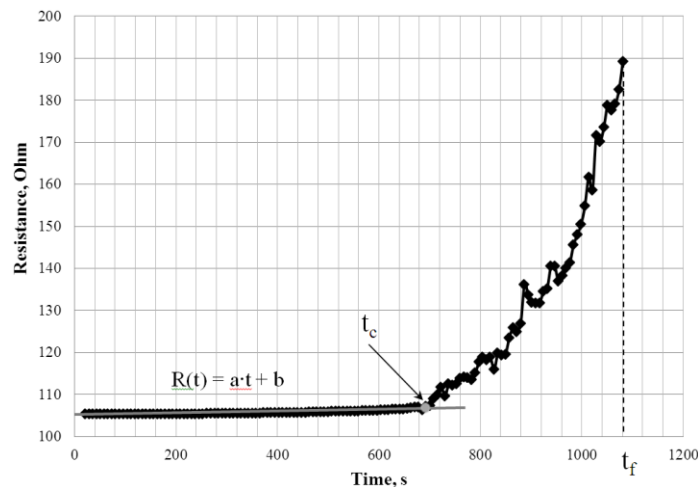


Fig. 1. The time-resistance relationship in main region of electromigration testing (t_c is the inflection point, t_f is the time-to-failure).

The research revealed several specific sections and correlated the line section parameters with time to failure. This correlation can be formulated by

$$a = A \times t^B$$

where $a \approx \Delta R / \Delta t$ is a line's slope in the section line, A, B are constants, t is the time-to-failure.

Besides, the diagram shows an inflection point, which is the start time of the structural changes accumulation in the metal conductor (t_c in Fig. 1). Further data analysis obtained during the experiment showed that the value of time t_c and t_f are linearly related.

Accordingly, the conclusion that can be drawn from the above is that the correlation between parameters of the studied time-resistance relationship in linear section and the moment of the conductor failure, the inflection point existence make it possible not to bring the conductor until failure during the EM testing.

1. Lee T.C., Tibel D., Sullivan T.D., Forhan Sh. "Comparison of isothermal, constant current and SWEAT wafer level EM testing methods". 39th IEEE Ann. Int. Rel. Phys. Symp., 2001, Cat. No. 01CH37167, pp. 172-183.
2. Doan J.C., Bravman J.C., Flinn P.A., Marieb T.N. "The relationship between resistance changes and void volume changes in passivated aluminum interconnects". 37th IEEE Ann. Int. Rel. Phys. Symp., 1999, Cat. No. 99CH36296, p. 209.
3. Giroux F., Gounelle C., Mortid P., Ghibaudo G. "Wafer-level electromigration tests on NIST and SWEAT structures". IEEE Int. Conf. on Micro. Test St., **8**, pp. 229-232, 1995.

Atomic mechanisms of misfit dislocation nucleation in heteroepitaxial system Ge/Si(001)

O.S. Trushin¹, S.-C. Ying², E. Granato³, T. Ala-Nissila⁴

1. Institute of Physics and Technology (Yaroslavl Branch) of RAS, Yaroslavl, Russia, otrushin@gmail.com.

2. Department of Physics, Brown University, Providence, USA.

3. Laboratorio Associado de Sensores e Materiais, Instituto Nacional de Pesquisas Espaciais, Sao Jose dos Campos, SP, Brasil.

4. Department of Engineering Physics, Aalto University, Espoo, Finland.

Heteroepitaxial systems play an important role in modern microelectronic technology. Due to the lattice mismatch between the film and the substrate, considerable elastic strain energy is accumulated in epitaxy. For sufficiently thick films, defects will form leading to the relaxation of strain energy and to the loss of coherent epitaxy. Controlling the film-substrate interface quality and preventing defect formation is an important problem of modern technology. Experimental methods at present do not allow either a detailed study of the defect core at the atomic level or the time evolution of the system during defect nucleation process. Therefore, theoretical modeling plays an important role in the studies of defect formation mechanisms [1].

In this work we studied atomistic mechanisms of misfit dislocation nucleation in Ge/Si(100) heteroepitaxial system. We explored this system in three dimensions using molecular statics methods with Stillinger-Weber semi-empirical interatomic potential [2]. We used combination of Repulsive Bias Potential activation procedure and Nudged Elastic Band method for generating Minimum Energy Paths for transitions from the coherent epitaxial (defect free) state to the state containing an isolated defect (misfit dislocation). In this way we were able to shed more light on microscopic mechanisms of strain relaxation with misfit dislocation nucleation and estimate activation barrier for such transition [3]. We studied relaxation processes in models of different sizes containing up to 80000 atoms. Our simulations showed that at the first stage 60° dislocation is nucleated through half loop formation in $(1\bar{1}1)$ plane. At the next stage the second 60° dislocation is formed in mirror reflection $(\bar{1}11)$ plane. Finally 90° dislocation is created by reaction of those two 60° dislocations according to the following reaction: $\frac{a}{2}[011](1\bar{1}1) + \frac{a}{2}[\bar{1}0\bar{1}](\bar{1}11) = \frac{a}{2}[\bar{1}10](001)$, here a – is lattice constant. Typical results of the simulations are shown in fig.1. Here final state of the system containing 90° dislocation is shown in fig.1a and corresponding energy profile along Minimal Energy Path is shown in fig.1b.

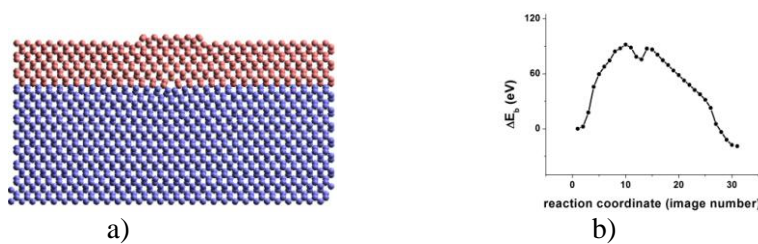


Fig.1 a) Sideview on the model with misfit dislocation at the interface, b) Energy profile along Minimal Energy Path for transition from defect free state to the state containing single 90° dislocation.

In conclusion we studied misfit dislocation nucleation process in Ge/Si(100) heteroepitaxial system using molecular statics. Our results show presence of high energy barrier for thermal activation of that process. This work has been supported by Russian Foundation for Basic Research under the grant № 14-07-00139A.

1. R. Hull, "Misfit strain and accommodation in SiGe heterostructures", in a book *Germanium Silicon: Physics and Materials* (ed. by R. Hull and J. Bean), Academic Press, San Diego, 1999.
2. F. Stillinger, T. Weber "Computer simulations of local order in condensed phases of silicon", *Phys. Rev. B*, **31**, pp. 5262-5271, 1985.
2. O.S. Trushin "Modeling of elastic strain relaxation processes in heteroepitaxial systems", *Russian Microelectronics*, **37**, pp. 1-11, 2008.

Modeling of processes of phase formation in binary metal systems under ion bombardment

S. Krivelevich

Institute of Physics and Technology (Yaroslavl Branch), RAS, Yaroslavl, Russia, s.krivelevich@mail.ru

It was shown [1] that exposure of the surface of binary metallic systems of inert gas ions, allows to create films of various compositions. When this occurs there is formation of intermetallic compounds at temperatures lower than in the absence of ion bombardment. During irradiation, for example, the system Ni-Al intermetallic compound layer in the surface region is formed at temperatures close to 300 °C, while, in the absence of irradiation of intermetallic compound formation is observed only when 400 °C. The composition of the resulting layer and its thickness during irradiation are practically independent of the ion current density, and determined by the temperature of the substrate and the dose of ion bombardment. It is important to note that the thickness of the formed layers can be several times greater than the average projected range of ions. Film thickness in the initial samples also can be several times greater than the projected range of the ions. Obtained experimental results permit to assume that formation of an intermetallic compounds is defined by the synthesis reaction rate and diffusion mass transfer of components through the layer formed in the near surface region. The reaction rate can be determined by the number of phonons generated by incident ions scattered and/or in transition regions with reacting components and should be proportional to the ion current density and to the dose of bombarding ions. It is necessary to account that the same reactions are exothermic. Therefore, phonon scattering at the initial Ni/Al interface leads to the formation of thin layer one or several intermetallic compounds. This is due to the fact that the rate of exothermic reactions of intermetallic compounds is directly proportional to the flow of phonons generated incident ions, and provides additional opportunities to manage the development of intermetallic coatings based on aluminum.

It was found [2] that the process of phase formation in the binary system outside the area of range of the primary ions can be described by a vector order parameter, which is a linear combination of the concentrations of all the chemical elements in the system in all available states. However, when describing the construction of real systems have difficulty order parameter associated with a large number of independent variables in the appropriate equations. For example, in the description of Ni-Al total number of independent variables is equal to sixteen, even if one neglects the presence of structural defects. Analysis of experimental data shows that the process of phase formation in these systems is a sequence of phase formation with a gradual increase in the content of one of the components and, consequently, a decrease in the content of the second component. Given this fact, can significantly reduce the number of independent variables at each stage of the phase formation process. Thus, in this paper we propose a theoretical approach to effectively describe the processes of phase formation in binary metal systems under ion bombardment.

1 V.I. Bachurin, S.A. Krivelevich, "Influence of Argon Ion Bombardment on the Formation of Intermetallic Compounds in the Nickel-Aluminum System", *J. Surface Investigation*, **3**, pp. 313-316, 2009.

2 S.A. Krivelevich, "O vybore parametrov poryadka pri opisani dálnodeyistvuyushogo vliyaniya ionnoyi implantacii". *Vestnik Nizhegorodskogo Universiteta. Ser. Fizika tverdogo tela*, Issue 1 (6), pp. 144-151, 2003 (in Russian).

The impact of quantum noises on Grover's search algorithm and Quantum Fourier Transform

Yu.I. Bogdanov^{1,2,3}, B.I. Bantysh^{1,2}, V.F. Lukichev¹, A.A. Orlikovsky¹, I.A. Semenihi¹,
A.S. Holevo⁴, A.Yu. Chernyavskiy^{1,5}

1. Institute of Physics and Technology, Russian Academy of Sciences, Moscow, Russia.

2. National Research University of Electronic Technology (MIET), Moscow, Russia.

3. National Research Nuclear University (MEPhI), Moscow, Russia.

4. Steklov Mathematical Institute, Russian Academy of Sciences, Moscow, Russia.

5. Faculty of Computational Mathematics and Cybernetics, Lomonosov Moscow State University, Moscow, Russia.

Two approaches of studying Grover's algorithm and quantum Fourier transform are considered: one based on statistical modeling using Monte Carlo method and the other based on the theory of quantum operations. It was shown that these approaches are consistent with each other.

Approximate analytic equations describing the fidelity of quantum algorithms versus the number of qubits and noise level are obtained.

The expediency of using supercomputer technologies for creation of computer-aided design (CAD) of quantum computer hardware is demonstrated.

This work was supported in part by Russian Foundation of Basic Research (projects, 13-07-00711, 14-01-00557), and by the Program of the Russian Academy of Sciences in fundamental research.

A study of amplitude and phase relaxation impact on the quality of quantum information technologies

Yu.I. Bogdanov^{1,2,3}, B.I. Bantysh^{1,2}, V.F. Lukichev¹, A.A. Orlikovsky¹, A.Yu. Chernyavskiy^{1,4}

1. Institute of Physics and Technology, Russian Academy of Sciences, Moscow, Russia.

2. National Research University of Electronic Technology (MIET), Moscow, Russia.

3. National Research Nuclear University (MEPhI), Moscow, Russia.

4. Faculty of Computational Mathematics and Cybernetics, Lomonosov Moscow State University, Moscow, Russia.

The influence of amplitude and phase relaxation on evolution of quantum states within the formalism of quantum operations is considered. The model of polarizing qubits with noises determined by the spectral degree of freedom appearing during light propagation inside anisotropic mediums with dispersion is studied. An approximate analytic model for calculation of phase plate impact on polarizing state with dispersion influence is suggested.

The amplitude and phase relaxation impact on quantum correlations that characterize entanglement of a system of qubits is considered. Quantum correlations are described in terms of negativity, the distance to PPT-state and the measure based on the minimization of entropy of measurements.

This work was supported in part by Russian Foundation of Basic Research (projects, 13-07-00711, 14-01-00557), and by the Program of the Russian Academy of Sciences in fundamental research.

The study of classical dynamical systems using quantum theory

Yu.I. Bogdanov^{1,2,3}, N.A. Bogdanova²

1. Institute of Physics and Technology, Russian Academy of Sciences, 117218, Moscow, Russia

2. National Research University of Electronic Technology (MIET), 124498, Moscow, Russia

3. National Research Nuclear University (MEPhI), 115409 Moscow, Russia

We have developed a method for complementing an arbitrary classical dynamical system to a quantum system using the Lorentz system as an example. The Schrödinger equation for the corresponding quantum statistical ensemble is described in terms of the Hamilton-Jacobi formalism and second quantization methods. We consider both the original dynamical system in the coordinate space and the conjugate dynamical system corresponding to the momentum space. Such simultaneous consideration of mutually complementary coordinate and momentum frameworks provides a deeper understanding of the nature of chaotic behavior in dynamical systems.

We have shown that the new formalism provides a significant simplification of the Lyapunov exponent calculations.

This work was supported in part by Russian Foundation of Basic Research (project 13-07-00711), and by the Program of the Russian Academy of Sciences in fundamental research.

Mutually Unbiased Bases and SIC-POVM as special cases in the family of solutions to the Fekete packing problem in complex space

Yu. I. Bogdanov^{1,2,3}, L.V. Belinsky^{1,2}

1. Institute of Physics and Technology, Russian Academy of Sciences, 117218, Moscow, Russia

2. National Research University of Electronic Technology (MIET), 124498, Moscow, Russia

3. National Research Nuclear University (MEPhI), 115409, Moscow, Russia

Tight frames have many applications in quantum informatics, communications, coding theory, and other fields. We examine a family of frames consisting of numerical solutions to the Fekete packing problem in complex space. This family appears to contain full sets of Mutually Unbiased Bases in prime power dimensions as well as Symmetrical Informationally Complete Positive Operator Valued Measures (SIC-POVM) in all dimensions. Other frames of interest in this family are transitional frames in which the number of vectors lies between that of full sets of Mutually Unbiased Bases and Symmetrical Informationally Complete POVMs. These results demonstrate another connection between mutually unbiased bases and SIC-POVMs and may be of interest in the study of their existence in various dimensions.

This work was supported in part by Russian Foundation of Basic Research (project 13-07-00711), and by the Program of the Russian Academy of Sciences in fundamental research.

Root approach for estimation of statistical distributions and quantum states

Yu.I. Bogdanov^{1,2,3}, N.A. Bogdanova²,
F.Yu. Ignatiev³, D.Yu. Kulko³, M.A. Podtserkovsky³

1. Institute of Physics and Technology, Russian Academy of Sciences, 117218, Moscow, Russia

2. National Research University of Electronic Technology (MIET), 124498, Moscow, Russia

3. National Research Nuclear University (MEPhI), 115409 Moscow, Russia

Based on the root approach to reconstruction of statistical distributions and quantum states, we study a family of statistical distributions in which the probability density is the product of a Gaussian distribution and an even-degree polynomial. A method for estimating parameters of the distributions using the root approach in the Chebyshev-Hermite basis is presented. The method is based on the original algorithm for estimating the complex psi-function developed within the framework of this paper. This approach is generalized to a wider set of statistical distributions, including the exponential, the binomial and the Poisson distributions. In such cases the Chebyshev-Hermite polynomials are replaced by Laguerre, Kravchuk and Charlier polynomials, respectively.

The results of present paper are of interest for the development of tomography of quantum states and processes.

This work was supported in part by Russian Foundation of Basic Research (project 13-07-00711), and by the Program of the Russian Academy of Sciences in fundamental research.

Qubit modification of JCH model for two molecules

Yu.I.Ozhigov^{1,2}, N.A.Skovoroda³

1. *Lomonosov Moscow State University, Moscow, Russia, E-mail address: ozhigov@cs.msu.su.*

2. *Institute of Physics and Technology RAS, Moscow, Russia.*

3. *Lomonosov Moscow State University, Moscow, Russia, E-mail address: chalkex@gmail.com*

We model the interaction of two bipartite molecules through the exchange of photons. This includes the exchange of photons between molecules in course of association – dissociation, pumping of the system with photons of high energy and relaxation – flying off photons with lower energy. We use Lindblad operators to reflect the interaction with the environment: photon exchange and spatial movement of the parts of molecules in dissociated state. The language of qubits we use for the possible application of our model to quantum processors on the interaction of several atoms with separate photons.

We use the qubit modification of Jaynes-Cummings-Hubbard (JCHq) model, limited by two photons of three possible frequencies: the photon of pumping and two photons with lower energy, and its polariton modification, in which every passage of photons between molecules is connected with the absorption or emission of photons by atoms. The model requires at least 12 qubits: 6 to each molecule. Interaction with the environment via photons we represent by Kossovsky-Lindblad equation on the density matrix of electrons and photons.

Hamiltonian elements and coefficients of Lindblad operators are assumed to be randomly distributed with the normal law. This allows us to take into account the influence of vibrational and rotational degrees of freedom for the associated form of molecules, and reflect roughly their interaction with electronic states, that in principle can be valuable, for example, for Rydberg electrons. It is assumed that in the dissociated state the both parts of molecules move chaotically and do not keep the coherence. We establish numerically

a) the dependence of the relaxation time on the transition probability of a photon between associated molecules and the amplitude of interaction between molecules and photons, when no photon pumping from outside takes place,

b) the evolution of population of the electronics eigen states and the evolution of the degree of coherence and the degree of agreement of density matrices in both versions of the model, when photon pumping from outside takes place.

We have also built and analyzed the computational model of this process in Mathematica-9. In particular, we describe the essence of the artifact of incomplete relaxation in the qubit model with the fuzzy semantics, when the description of photons depends on their number ([1]).

Computational models of the qubit type are significant for the quantum computers of chemical type, which are designed to the simulation of the behavior of many atom systems on quantum level. In such models we presuppose that all secret codes (like Grover solution of the equation $f(x) = 1$) are given in advance, for example, as an oracles. In such models of a quantum computer the limitation on the total number n of qubits is strict; for supercomputers $n = 30$ is now the upper bound of capabilities.

1. Yu.I. Ozhigov, N.A. Skovoroda. "Simulation of electronic state relaxation for two level atoms in qubit representation". Vestnik MSU, ser. Computational mathematics and cybernetics, accepted for publication, 2014.

Why energy of magnetic dipole moment in magnetic field is not taken into account in the theory of flux qubit?

V.L. Gurtovoi and A.V. Nikulov

Institute of Microelectronics Technology, Russian Academy of Sciences, 142432 Chernogolovka, Moscow Region, Russia. E-mail: nikulov@iptm.ru

A creation of quantum computer is one of the most actual problems of last years [1]. Its main element is quantum bit (qubit), a quantum system in superposition of two permitted states. The typical example of such system is spin of electron. Measurement of projection of an electron magnetic dipole moment on any direction give two values $+\mu_B$ and $-\mu_B$, equal the Bohr magneton $\mu_B = -e\hbar/2m$. Now numerous publications are devoted to theoretical [2] and experimental [3] investigations of persistent-current qubit [4] or flux qubit [5]. The qubit effective Hamiltonian is represented by the Pauli spin matrices σ_z, σ_x [5, 6], that is

$$H_q = \varepsilon\sigma_z - \Delta\sigma_x \quad (1)$$

as well as the spin 1/2 Hamiltonian. The energy difference $2\varepsilon = 2\mu_B B_z$ between two states in (1) is determined by the energy of magnetic dipole moment μ_B in magnetic field B_z for spin [7]. The magnetic dipole moment of flux qubit has opposite direction in the two states of (1), as well as in the case of spin 1/2, and equals approximately $|M_z| = |I_p S| \approx 10^5 \mu_B$ for typical values of the persistent current of a flux qubit $I_p \approx 1 \mu\text{A}$ and its area $S \approx 1 \mu\text{m}^2$ [5]. But the energy $E_M = M_z B_z = I_p S B_z \approx I_p \Phi$ of magnetic moment M_z in magnetic field B_z is not taken into account in the theory of flux qubit [4-7].

Why could the theory disregard this energy? This question critical for the validity of the flux qubit theory will be considered in this work. Prof. Anthony Leggett has noted [8] that the Hamiltonian

$$\hat{H} = \frac{1}{2m} \sum_a [-i\hbar\nabla_a - qA]^2 \quad (2)$$

used for the description of quantum effects in superconductors [9] includes only the kinetic energy and that perhaps our naive tendency to identify the Hamiltonian with the energy is (as in some cases involving time-dependent forces) misleading. Indeed, the energy of magnetic dipole moment in magnetic field is absent in (2) as well as in the classical Hamiltonian. Therefore one can obtain only the kinetic energy of the persistent current flowing along superconducting loop (equal $E_k = I_p(\Phi - 0.5\Phi_0)$ in the case of flux qubit [5, 6]) using the Hamiltonian (2). On the other hand we know that the energy $E_M = M_z B_z$ should exist. The essence and reason of this contradiction will be discussed.

A.V. Nikulov thanks for helpful discussion of the problem of the energy of magnetic dipole moment in magnetic field Prof. Anthony Leggett (University of Illinois, USA), Prof. Jorge Hirsch (University of California, USA) and Prof. Jorge Berger (Ort Braude College, Israel).

1. M.A. Nielsen and I.L. Chuang, *Quantum Computation and Quantum Information*. Cambridge University Press, 2000.
2. Shang-Yu Huang and Hsi-Sheng Goan, "Optimal control for fast and high-fidelity quantum gates in coupled superconducting flux qubits", *Phys. Rev. A* **90**, 012318, 2014.
3. K.G. Fedorov, A.V. Shcherbakova, M.J. Wolf, D. Beckmann, and A.V. Ustinov, "Fluxon Readout of a Superconducting Qubit", *Phys. Rev. Lett.* **112**, 160502, 2014.
4. J.E. Mooij, T.P. Orlando, L. Levitov, Lin Tian, Caspar H. van der Wal, Seth Lloyd, "Josephson Persistent-Current Qubit", *Science* **285**, pp. 1036-1039, 1999.
5. I. Chiorescu, Y. Nakamura, C.J.P.M. Harmans, J.E. Mooij, "Coherent Quantum Dynamics of a Superconducting Flux Qubit", *Science* **299**, pp. 1869-1871, 2003.
6. M.-Ch. Yeh and A.J. Leggett, "The escape physics of single shot measurement of flux qubit with dcSQUID", arXiv: 1401.4186, 2014.
7. Yu. Qiu, W. Xiong, L. Tian, and J.Q. You, Coupling spin ensembles via superconducting flux qubits. *Phys. Rev. A* **89**, 042321, 2014.
8. A.J. Leggett, private correspondence, 2014.
9. N. Byers and C.N. Yang, Theoretical Considerations Concerning Quantized Magnetic Flux in Superconducting Cylinder. *Phys. Rev. Lett.* **7**, pp. 46-49, 1961.

Biology inspired path towards a quantum computer

V. Ogryzko¹, Yu. Ozhigov²

1. INSERM, Institute Gustave Roussy, Paris XI, Villejuif, France, E-mail address: vogryzko@gmail.com

2. Lomonosov Moscow State University, Moscow, Russia, E-mail address: ozhigov@cs.msu.su

We present arguments in favor of fundamentally quantum nature of Life, and consider the biological way to a quantum computer, as a viable alternative to the Feynman's quantum computer of microelectronic type. The main purpose of a quantum computer - search for unknown solutions of some generalized equation of the form $F(x) = 1$, which in the classical paradigm of computing is sought by brute force. Any biological system (cell, an organism, a population) solves the problems of this type, and at any level of organization: from nucleotide residues to proteins to large populations. We propose that, without contradicting the quantum theory and observations, one can treat live bacterial cell as being in a close to ground-state quantum system of a finite number of qubits. The question of the role of 'quantum effects' in biology is understandably very difficult, because it is extremely challenging to apply the experimental technique that accurately captures these effects to a living system. We argue that the best approach to the study of Life at the quantum level should be based on adiabatic quantum computer with inbuilt decoherence. Such a computer could be provided within a certain generalization of the Jaynes-Cummings-Hubbard model, including decoherence. We also tried to accurately formulate the conditions necessary for the application of the methods of quantum theory to living organisms.

1. Bordonaro M, Ogryzko V. Quantum Biology at the Cellular Level-elements of the research program. (*Biosystems*. 2013 112(1):11-30)
2. Ogryzko V. Quantum information processing at the cellular level. Euclidean approach. <http://arxiv.org/abs/0906.4279>
3. Y. Ozhigov, Quantum selfish gene (biological evolution in terms of quantum mechanics), <http://arxiv.org/abs/1402.4713>

Quantum computation and the problem of free will in quantum mechanics

V.V. Aristov and A.V. Nikulov

Institute of Microelectronics Technology, Russian Academy of Sciences, 142432 Chernogolovka, Moscow District, Russia. E-mail: nikulov@iptm.ru

The idea of quantum computation is based on the most paradoxical principle of quantum mechanics – EPR correlation. The exponential increase of the computational resources with the number of quantum bits has attracted numerous admirers of this idea. The admirers disregard the subjective essence of the EPR correlation. A. Einstein, B. Podolsky and N. Rosen [1] considered the EPR correlation to be unreal because of its contradiction with local realism. E. Schrodinger has defined the EPR correlation as ‘entanglement of our knowledge’: “Maximal knowledge of a total system does not necessarily include total knowledge of all its parts, not even when these are fully separated from each other and at the moment are not influencing each other at all” [2]. According to this fair definition, the enormous computational resources of quantum computer exist in the mind of the observer rather than in reality. The admirers of quantum computation misinterpret violation of the Bell’s inequalities as an empirical corroboration of the orthodox quantum mechanics and reality of the EPR correlation. They ignore the Bell’s opinion that violation of his inequalities could mean that “Apparently separate parts of the world would be deeply and conspiratorially entangled, and our apparent free will would be entangled with them” [3].

The opposite views about the Bell’s inequalities was accentuated as far back as 1985: “In the question of whether there is some fundamental problem with quantum mechanics signaled by tests of Bell’s inequality, physicists can be divided into a majority who are ‘indifferent’ and a minority who are ‘bothered’” [4]. Those who are ‘indifferent’ believe that the EPR correlation testifies to new opportunities of quantum mechanics whereas those who are ‘bothered’ understand that this subjective principle testifies against quantum mechanics. The ‘bothered’ scientists discuss now the question “Whose knowledge could be represented with the density matrix?” [5] and the problem of free will in quantum mechanics [6-12]. In his talk [9] at the General meeting of Russian Academy of Sciences Nobel Prize Winner 1999 and Recipients of Lomonosov Gold Medal 2010 Gerard ‘t Hooft expresses a doubt that the mathematician Conway has free will, in order to save his belief in quantum mechanics. This doubt of the established physicist in free will of the thinking subject is doubtful. It will be accentuated in this work that the controversy about free will in quantum mechanics of itself calls in question the reality of quantum computation.

1. A. Einstein, B. Podolsky, and N. Rosen “Can Quantum - Mechanical Description of Physical Reality Be Considered Complete?” *Phys. Rev.* **47**, pp. 777-780, 1935.
2. E. Schrodinger, “Die gegenwartige Situation in der Quantenmechanik,” *Naturwissenschaften* **23**, 807-812; 823-828; 844-849, 1935. Translation published in *Quantum Theory and Measurement*. edited by J.A. Wheeler and W. H. Zurek, Princeton University Press, Princeton. pp. 152-167, 1983.
3. J.S. Bell, “Bertlmann’s socks and the nature of reality”. *Journal de Physique*, **42**, pp. 41-61, 1981.
4. N.D. Mermin, “Is the moon there when nobody looks? Reality and the quantum theory”. *Physics Today*, **38**, pp. 38-47, 1985.
5. N.D. Mermin, “Whose Knowledge?” in *Quantum (Un)speakables - From Bell to Quantum information*, eds. Reinhold Bertlmann and Anton Zeilinger, Springer, pp. 271- 280, 2002; arXiv: quant-ph/0107151
6. J. Conway and S. Kochen, “The Free Will Theorem”. *Found. Phys.* **36**, pp. 1441-1473, 2006.
7. A. Bassi, G.C. Ghirardi, “The Conway-Kochen Argument and Relativistic GRW Models”. *Found. Phys.* **37**, pp. 169-182, 2007.
8. R. Tumulka, Comment on The Free Will Theorem. *Found. Phys.* **37**, pp. 186 - 297, 2007.
9. Gerard ‘t Hooft, “The Free-Will Postulate in Quantum Mechanics”. *Herald of Russian Academy of Science* **81**, pp.907-911 (2011); arXiv: quant-ph/0701097 (2007).
10. J.E. Pope, A. Kay, “Limited measurement dependence in multiple runs of a Bell test”. *Phys. Rev. A* **88**, 032110, 2013.
11. E. Cator, K. Landsman, “Constraints on determinism: Bell versus Conway-Kochen”. arXiv: 1402.1972, 2014.
12. R. Hermens, Conway-Kochen and the Finite Precision Loophole. arXiv: 1404.2114, 2014

Quantum key distribution over 300 km

R. Ozhegov^{1,2}, M. Elezov¹, Y. Kurochkin³, V. Kurochkin⁴, A. Divochiy², V. Kovalyuk^{1,2},
Y. Vachtomin², K. Smirnov^{1,2,5}, and G. Goltsman^{1,2,5}

1. Moscow State Pedagogical University, 1 Malaya Pirogovskaya st., Moscow, 119435, Russia

2. CJSC "Superconducting Nanotechnology", 5/22 Rossolimo st., Moscow, 119435, Russia

3. Russian Quantum Center, Skolkovo, Moscow Reg., 143025, Russia

4. Institute of Semiconductor Physics, 13 Pr. Lavrentyeva, Novosibirsk, 630090, Russia

5. Moscow Institute of Electronics and Mathematics, National Research University Higher School of Economics, Moscow, 109028, Russia

We discuss the possibility of polarization state reconstruction and measurement over 302 km by Superconducting Single-Photon Detectors (SSPDs). Because of the excellent characteristics and the possibility to be effectively coupled to single-mode optical fiber many applications of the SSPD [1, 2] have already been reported. The most impressive one is the quantum key distribution (QKD) over 250 km distance [3]. This demonstration shows further possibilities for the improvement of the characteristics of quantum-cryptographic systems such as increasing the bit rate and the quantum channel length, and decreasing the quantum bit error rate (QBER). This improvement is possible because SSPDs have the best characteristics in comparison with other single-photon detectors.

For this demonstration we used the two-channel system for registering single photons in the visible and near IR ranges. The system is cryogen-free refrigerator and included a compact low-power cold head SRDK-101D and an optimized cryostat. Optical coupling was realized by aligning a single-mode fiber 9 μm diameter with the sensitive areas of the detectors each with an area of $7 \times 7 \mu\text{m}^2$. After the final adjustment, the optical unit was mechanically fixed on the cold finger of the closed-cycle cryostat. The system had a level of dark counts of less than 1 cps, with a quantum efficiency of 12 % (for 1.55 μm wavelength) at 2 K for channel 1 and channel 2.

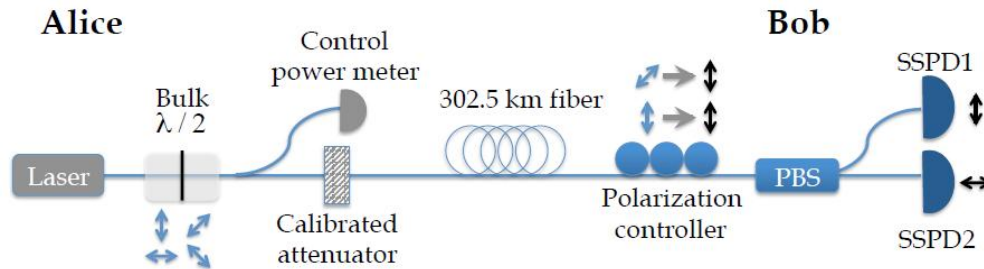


Fig. 1. Experimental setup. Alice prepares a quantum state by the bulk $\lambda/2$ plate, attenuates it to the single photon level and sends to Bob via a quantum channel. Bob reconstructs polarization and sets the corresponding BB84 basis and measures the state with SSPD

Photon number	QBER
0.2	4.1%
0.5	3.4%
1.0	1.7%

Pulse rate, $\mu=1$	Bit rate
20 MHz	15,7
80 MHz	61,7
120 MHz	103,3

Table 1. QBER means photon number per pulse (μ) (left) and bit rate versus pulse repetition rate (right).

We have demonstrated the possibility of polarization state reconstruction and measurement over 302.5 km with superconducting single-photon detectors. On the tables shown the relative error QBER (quantum bit error rate) versus mean photon number per pulse (μ) and bit rate (BR) to the frequency of the laser pulse repetition. It gives strong support to the SSPD employing for fiber-optical quantum key distribution systems with the best characteristics as of today such as secure bit rate, quantum bit error rate and the length of a quantum channel.

1. Goltsman G.N. et al. Picosecond superconducting single-photon optical detector, Appl. Phys. Lett. **79**, 705, 2001.
2. Korneev A., et al. Recent Nanowire Superconducting Single-Photon Detector Optimization for Practical Applications, IEEE Transactions on Applied Superconductivity, **23**, Issue 3, 2013.
3. Stucki D. et al. High rate, long-distance quantum key distribution over 250km of ultralow loss fibres, New Journal of Physics, **11**, 075003, 2009.

High-temperature single-electron transistor based on a gold nanoparticle

S.A. Dagesyan¹, A.S. Stepanov², E.S. Soldatov¹, G. Zharik¹

1. Faculty of Physics, Lomonosov Moscow State University, Moscow, Russia, dagesyan@physics.msu.ru

2. Scobeltsyn Institute of Nuclear Physics, Lomonosov Moscow State University, Moscow, Russia.

Continuing progress in miniaturization of basic components in electronic circuits allows to search for new physical phenomena as a basis for a future nanoelectronics. One of such effects taking place on a nanometer scale is a correlated tunneling of electrons. The simplest device that allows to observe an effect is a single-electron transistor [1]. It consists of two electrodes with a central conducting island between them separated from each other by tunnel junctions and a third electrode capacitively coupled with an island. The effect can be destroyed by thermal or quantum fluctuations. So the transistor can operate only if the following condition is performed:

$$\frac{e^2}{2C} \gg kT \quad (1)$$

C is the total capacitance of SET, T is the operating temperature. It's clear that room temperature applications of the device require an extremely low capacitance value (10^{-19} - 10^{-18} F). It means that the island must be less than 3 nm in diameter.

In this work we report about formation of single-electron transistors based on single gold nanoparticles functionalized by octanethiol (2-4 nm, commercially available). Electrodes of the devices were formed using a standard electron-beam lithography combined with an electromigration technique [2]. The electromigration effect was used to form nanometer scale gaps in 60-70 nm wide and 14 nm thick nanowires. Nanoparticles were placed into gaps using a self-assembling from the toluene solution. A concentration of the solution was chosen empirically by diluting the initial solution for maximize probability to find a single nanoparticle in the gap. The presence of a nanoparticle in the gap was established by electrical measurements in a liquid nitrogen temperature. We found out that scanning electron microscope imaging of the gaps dramatically changes their electrical characteristics, so images of the resulting structures were obtained only when all other investigations were completed.

The obtained systems were characterized by measuring a bias current (I) as a function of both drain (V_d) and gate voltage (V_g). Using this data 2D stability diagrams ($I(V_d, V_g)$) were constructed for wide range of operating temperatures. Coulomb diamonds can be seen on diagrams clearly demonstrate a single-electron character of an electron transport. The maximal obtained value of a Coulomb blockade that corresponds to the charging energy of the nanoparticle is almost 300 mV. It is more than values available in literature for the similar system [3]. This result was achieved by using the smaller nanoparticles. It allows to investigate a single-electron systems potential for very practically important high-temperature applications.

This work was supported by "Russian fond of basic research" (grants № 12-07-00816-a, № 14-07-31328)

1. K.K. Likharev, "Single electron devices and their applications", Proc. of IEEE, vol. 87, No. 4, 1999.
2. A.S. Stepanov et al., "Formation of molecular transistor electrodes by electromigration", Proc. SPIE, 752112, 2009.
3. N. Okoboyashi et al., "Uniform charging energy of single-electron transistors by using size-controlled Au nanoparticles", Appl. Phys. Lett., 100, 033101, 2012.

Arsenic Dopant Single-Atom Single-Electron Transistor

D.E. Presnov¹, V.V. Shorokhov², S.V. Amitonov², V.A. Krupenin², S.A. Dagesyan²

1. Skobeltsyn Institute of Nuclear Physics, Lomonosov Moscow State University, 1(2), Leninskie Gory, GSP-1, Moscow 119991, Russia, vladimir.krupenin@phys.msu.ru.

2. Faculty of Physics, Lomonosov Moscow State University, Leninskie Gory, Moscow 119991, Russia.

Last five years there is a great interest in creating true several nanometers and angstrom scale electronic elements, which are the main components of the future mass production technology for ultrahigh-density electronic devices with atomic functional structure. This interest encourages worldwide development of corresponding theoretical and fabrication methods [1–4]. Two inevitable effects with the same characteristic energy scale (0.1-1 eV) determine properties of such a small devices: Coulomb effects and spatial quantization.

The most simple single-atom functional electronic device is a single-atom single-electron transistor (SASET), in which a somehow selected atom or a chain of such atoms are placed between the source, drain, and control electrodes. In this device the selected single atoms play the role of active charge centers with discrete energy spectrum. In this work we present our latest achievements - a realization of a single-electron transistor with an island formed by a single arsenic dopant in silicon. This approach is based on the so-called «silicon-on-insulator» technology.

The As SASET transistor developed in our group consist of: silicon solid bridge connecting lead electrodes with a localized impurity atom in it; Source and drain lead electrodes which are widened prolongation of the bridge with a high dopant concentration providing a high conductance; control or gate electrode or electrodes, which are located close to the bridge.

Electronic transport properties of the fabricated transistor were studied by measuring its current stability diagram (CSD). CSD digital processing clearly indicates the presence of correlated tunneling of electrons and the discreteness of the energy spectrum of the effective charge center.

The key feature of measured CSD is a strong influence of charge traps. This influence is due to SOI technology which is based on dopants. That is why the SASET selected charge center – single arsenic dopant is surrounded by great amount of charge traps which are other arsenic dopants.

1. D. Moraru, M. Ligowski, K. Yokoi, T. Mizuno, and M. Tabe. Single-Electron Transfer by Inter-Dopant Coupling Tuning in Doped Nanowire Silicon-on-Insulator Field-Effect Transistors. *Appl. Phys. Express* **2**, 071201, 2009.
2. D. Moraru *et al.* Atom devices based on single dopants in silicon nanostructures. *Nanoscale Res. Lett.* **6**, 479, 2011.
3. B. Roche *et al.* Detection of a Large Valley-Orbit Splitting in Silicon with Two-Donor Spectroscopy. *Phys. Rev. Lett.* **108**, 206812, 2012.
4. M. Tabe *et al.* Single-Electron Transport through Single Dopants in a Dopant-Rich Environment. *Phys. Rev. Lett.* **105**, 016803, 2010.

Single-electron transistor with suspended electrodes based on single gold nanoparticle

I.V. Sapkov, E.S. Soldatov

Faculty of Physics, Lomonosov Moscow State University, Russian Federation, esold@phys.msu.ru

Till this moment the miniaturization of element base of electronics is in good agreement with well-known Moore's Law [1]. But farther miniaturization assumes work with feature's sizes as small as units of nanometers and with all their quantum specificity. It's still looks like a problem even for improved classical approaches and we still can expect that with molecular electronics one could reach these sizes to produce new storage devices of ultrahigh capacity, various sensors, including chemical and biosensors.

One of the basic devices of molecular electronics is molecular single-electron transistor *i.e.* molecule that placed between two electrodes, where the gate electrode electrostatically modifies the potential of the molecular orbitals. It works on the basis of single-electron tunneling.

The problem of creation of such device can be split into two parts. The first one is to create leading electrodes with a gap between them, which allow investigations to be made with nanometer sized objects. The second problem is placing and binding of single molecule between such electrodes.

Earlier we already described the method of creation of suspended nanogaps between metallic thin film electrodes [2, 3]. On the first step we produced suspended blank-electrodes with gap's width about 30 nm with standard nanolithography and etching techniques. After that with additional evaporation of gold metal we formed the gate of nanotransistor and shrink it's nanogap to prescribed sizes simultaneously. In the case of undesired bridging of electrodes by additional gold film we used method of electromigration to restore it. The size of restored nanogaps was also about few nanometers. It is significant that our approach works not only for shrinking down of the gap but also for reconstruction of one. To the best of author's knowledge there are no methods suggested before with such property..

In this report we investigate placing and binding of single molecule between such electrodes and measure their characteristics in various conditions. We used two types of functionalized gold nanoparticles produced by Sigma-Aldrich with declared range of sizes: 2-4 nm and 4-6 nm. We provide series of experiments to find optimal concentration of particles and parameters of their incorporation into the gap. With these parameters over 25% of experiments shows single nanoparticle in the gap after inspection of it by scanning electron microscope. I-V characteristics were also measured. Few of them clearly showed single-electron regime at liquid nitrogen temperature, and few - even at room temperature.

Obtained results disclose applicability of suggested and realized method of creation single-electron transistor with suspended nanogap. It demonstrates single-electron transport through single gold nanoparticle and potentially can be used to produce various extremely sensitive sensors, including chemical and biosensors.

The work is supported by grant from the Russian Foundation for Basic Research (12-07-00816a).

1. G.E. Moore. "Cramming more components onto integrated circuits", *Electronics Magazine*, **4**, 1965.
2. I.V. Sapkov, E.S. Soldatov. "Narrowing of nanogap for purpose of molecular single-electronics", *Proc. SPIE 8700*, International Conference Micro- and Nano-Electronics 2012, 87000O, 2013.
3. I.V. Sapkov; E.S. Soldatov; V.G. Elensky. "Method of creation of monomolecular transistor with overhanging electrodes ", *Proc. SPIE 7025*, Micro- and Nanoelectronics 2007, 70250P, 2008.

A Simplified Analytical Model of Merged MOS

V. Rakitin¹, A. Rakitin²

1. F. V. Lukin Research Institute of Physical Problems, Moscow, Russia, vlarak@rambler.ru

2. Lomonosov Moscow State University, Moscow, Russia, alexander.v.rakitin@gmail.com

Multigate MOSFET have been attracting increasing amounts of attention with the development of semiconductor nanometer technology [1]. The merged MOS transistor (MMOS) is one such device. The MMOS combines an NMOS and a PMOS within one structure and thus acts as an inverting amplifier. It is efficient at minimal topological size (10 nm or less) and at supply voltages below 0.5 V down to 0.1 V, as is shown by previous studies [2].

In this paper, we propose a simplified mathematical model of the MMOS that allows us to make the calculation of its parameters significantly easier, and use it to obtain the IV curve and the transfer characteristic of the device.

For an undoped channel of the MMOS, Fig. 1, the potential ψ , when normalized by the thermal capacity ($\phi_T = kT/q$), satisfies the Poisson equation which takes the form

$$\nabla^2 \psi = \frac{1}{2} \exp(\psi - v_n) - \frac{1}{2} \exp(v_p - \psi) = \exp \mathcal{G} \cdot \sinh(\psi - v), \quad (1)$$

where the dimensions are expressed in the Debye length ($L_D = \sqrt{\epsilon_{si} \phi_T / (2qn_i)}$), v_n and v_p indicate

normalized quasi-Fermi levels for electrons and holes, respectively, v and \mathcal{G} are their half-sum and half-difference. The quasi-Fermi levels are assumed to be constant in the y cross section, and satisfy the boundary conditions shown in Fig. 1. The two-dimensional partial differential equation (1) and the equation for the current carriers can be reduced to a system of transcendental equations, assuming that the currents flow along the x axis and the carriers do not recombine. Integrating the electron and hole current densities on the cross section, followed by integrating the total current along the channel results in the dependence of current densities on external (boundary) conditions, i.e. the current-voltage characteristic of the MMOS transistor.

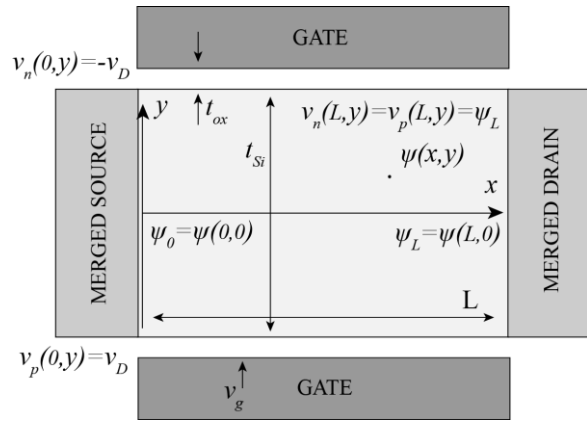


Fig. 1. Structure of the CMOS channel and boundary conditions for

In the most simple cases when $v \approx 0$ and ψ_0 is near zero, it is possible to obtain an exact solution for current densities. That solution also fits the case of much smaller

channel thickness compared to the Debye length.

$$i_n = qn_i \mu_n \frac{\phi_T}{L_D} \exp(v_g) \frac{\exp(-\psi_L) - \exp(v_D)}{\text{Ei}(-A \sinh(L/L_D + \alpha)) - \text{Ei}(-A \sinh(\alpha))}, \quad (2)$$

$$i_p = qn_i \mu_p \frac{\phi_T}{L_D} \exp(v_g) \frac{\exp(v_D) - \exp(\psi_L)}{\text{Ei}^*(A \sinh(L/L_D + \alpha)) - \text{Ei}^*(A \sinh(\alpha))}. \quad (3)$$

The MMOS transfer characteristic $\psi_L(v_g)$ follows from the connection between currents and external potentials in statements (2) and (3). The transfer characteristic can be found from the following implicit equation if the channel is sufficiently long, leading to A being negligibly small.

$$v_g = \frac{1}{2} \frac{\mu_p}{\mu_n} \ln \frac{\exp(v_D) - \exp(\psi_L)}{\exp(v_D) - \exp(-\psi_L)} \quad (4)$$

The total current through the MMOS is equal to the sum of currents of electrons (2) and holes (3).

1. J. Song et al. "A Review on Compact Modeling of Multiple-Gate MOSFETs". IEEE Tran. CS, **56**, pp. 1858-1869, 2009.

2. V. Rakitin "Modeling Low-Voltage Merged MOS Devices", Abstracts ICMNE 2012, p. P1-10, 2012.

Nanowire Field Effect Transistor for Biosensor Applications

D. Presnov^{1,2}, G. Presnova³, M. Rubtsova³, I. Bozhjev², V. Krupenin²

1. Skobeltsyn Institute of Nuclear Physics, Lomonosov Moscow State University, 119991 Moscow, Russia,

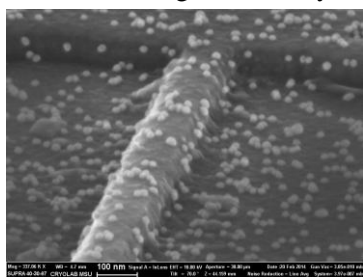
2. Laboratory of Cryoelectronics, Lomonosov Moscow State University, 119991 Moscow, Russia,
denis.presnov@phys.msu.ru

3. Faculty of Chemistry, Lomonosov Moscow State University, 119991 Moscow, Russia.

During the past decades experimental studies of semiconductor nanowire field-effect transistors (NW FET) or FET with nanowire channel have been in a great interest of researchers. Due to high surface-to-volume ratio of the NW, transistor can serve as the basis for ultra small bio- and chemical sensors with femtomole sensitivity to the certain type of objects [1, 2].

In this work, we present Si NW FET fabricated [3, 4] by traditional methods from silicon-on-insulator (SOI) with a high pH sensitivity; and the methods of antibodies high density immobilization on silicon nanowire surface. The main aim of our research is to combine these two approaches, and, thus in the next future step, to use NW FET as ultrasensitive sensor for detection the antibodies on its surface.

For the structure fabrication we used the Soitec[®] Unibond SOI wafers with a thickness of top silicon layer – 110 nm and 200 nm of buried oxide. A high-resolution electron microscope Supra 40 (Carl Zeiss) with ELPHY-Quantum lithographic attachment (Raith) used to define the nanowire in the positive PMMA resist, and the combination of photo and electron lithography also used in the next steps for the Ti contact pads and SiO₂ isolation layers fabrication [3]. Schottky barriers are formed between silicon contact pads and Ti electrodes. Fabricated transistors were electrically studied in air and in buffer solutions with different pH values. The pH sensitivity of our Si NW FET was reached its maximum value of 59 mV per unit pH. The maximum charge sensitivity of Si NW FET estimated theoretically can reach the value of $5 \times 10^{-3} \text{ e/Hz}^{1/2}$ [4].



Another approach is the application of our nanowire as the biosensor for determination of prostate-specific antigen (PSA) [5]. We investigated the process of sandwich antigen-antibody complex formatting on a surface of silicon. Monoclonal antibodies specific to PSA were covalently immobilized on silicon, then they interacted with the antigen followed by interaction with a conjugate of second polyclonal antibodies covalently attached to gold nanoparticles (Fig.1.). Different methods for covalent immobilization of proteins on the surface of modified silicon were studied.

The nanoparticles included in the immune complexes on the surface were identified by the same Supra 40 scanning electron microscopy (SEM). Determination of the number of immune complexes was performed by counting the number of gold nanoparticles in the working areas of the microchip [6]. Antibodies nonspecific to PSA were used as control. The method developed is characterized by high specificity, as well as a high ratio of the analytical signal/background ratio. The good correlation of the immune complexes density between model silicon system and the nanowire itself was achieved. The developed system we suggest to use for the future investigations with direct immobilization of the antibodies on the nanowire FET.

The work is supported by grants from the Russian Foundation for Basic Research (14-07-00828,13-04-01137a).

1. Y. Cui, Q. Wei, H. Park, C.M. Lieber, “Nanowire nanosensors for highly sensitive and selective detection of biological and chemical species”, *Science* **293**, no. 5533, pp. 1289-1292, 2001.
2. J. Hahn & C.M. Lieber, “Direct ultrasensitive electrical detection of DNA and DNA sequence variations using nanowire nanosensors”, *Nano Lett.* **4**, pp. 51-54, 2004.
3. D.E. Presnov, S.V. Amitonov, V.A. Krupenin, “Silicon nanowire field effect transistor made of silicon-on-insulator”, *Russian Microelectronics*, **41** (5), pp. 310–313, 2012.
4. D.E. Presnov, S.V. Amitonov, P.A. Krutitskii, V.V. Kolybasova, I.A. Devyatov, V.A. Krupenin, and I.I. Soloviev. "A highly ph-sensitive nanowire field-effect transistor based on silicon on insulator". *Beilstein journal of nanotechnology*, **4**, pp. 330–335, 2013.
5. B. Zhang, B. Liu, et.al, “Competitive-type displacement reaction for direct potentiometric detection of low-abundance protein”, *Biosensors and Bioelectronics* **53**, pp. 465–471, 2014.
6. M. Rubtsova, G. Presnova, M. Ulyashova, Y. Pobolelova, E. Filatova, D. Presnov, and A. Egorov, “Identification of genes of bacterial enzymes beta-lactamases on silicon microchips using gold nanoparticles as a label” *FEBS Journal*, **280**, Suppl. 1, p. 284, 2013.

I-V Features of MIS Memristors in Conductive State

A.E. Berdnikov, A.A. Popov, A.A. Mironenko, V.D. Chernomordick, V.N. Gusev
Institute of Physics & Technology (Yaroslavl Branch), Russian Academy of Sciences, Yaroslavl, 150007, Russia;
e-mail: imiraslab4@yandex.ru

The effect of conductive switching was investigated in metal – insulator – semiconductor structures (MIS). Such devices are called as memristors. Insulator was produced by low frequency plasma enhanced chemical vapor deposited silicon rich oxide or multilayer structure. Appearance or disappearance of conductive filament with nanosize diameter under supplied voltage explained conductive switch effect [1, 2].

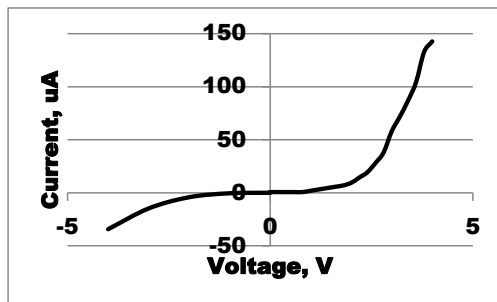


Fig.1. I-V plot of MIS memristor with p-type silicone.

I-V plot of MIS memristors in conductive state is not linear, see fig.1. Model based on spreading resistance in semiconductor was offered for an explanation of I-V plots. Spreading resistance depended from diameter of contact to semi-infinite low conductive material, in our case crystalline silicon. In semi-spherical approach spreading resistance defined by equation (1). This approach is possible if thickness of silicon substrate and size of back metal contact to semiconductor are much larger filament's diameter.

$$R = \rho / (2\pi d) \quad (1)$$

where ρ is silicon resistivity, d is the diameter of the contact. Filaments diameters were calculated using total resistance of memristor. Diameters values were from 1 to 3 micrometers for difference samples. This value is significantly greater than experimental estimation [1]. It means that we must take effective diameter, which defined of area size with additional carrier density.

Conductive filament in silicon suboxide probably formed from silicon. It means that we can consider the semiconductor structure in the plane band approximation. We supposed that the current in the filament is provided by electrons moving.

Four cases were considered: semiconductor p- or n- type vs. two type of applied voltage polarity. In case of positive voltage applied to silicon electrons injected from filament. In area near filament additional density of carrier (electrons) appears and effective contact diameter increased. In case of negative voltage applied to n-type silicon electrons collected from semiconductors area. Difference between these cases is not principle. Spreading resistance decreased then current increase.

In case of negative voltage applied to p-type silicon carriers in semiconductor generated under electric field near filament. It means that current in memristor under applied voltage less than energy of electron-hole generation is negligible. Then applied voltage become greater dissociation energy current appears and area of additional carrier density formed. After that effective contact diameter increased and spreading resistance decreased.

As a result of spreading resistance influence shape of IV plots of MIS memristors with p-type semiconductor are non-linear and asymmetric. At low applied voltage rectifier effect is observed. This effect may be used in memory device design.

1. A.E. Berdnikov, V.N. Gusev, A.A. Mironenko, A.A. Popov, A.V. Perminov, A.C. Rudy, V.D. Chernomordick. "Conductivity Switching Effect in MIS Structures with Silicon-Based Insulators, Fabricated by Low-Frequency Plasma-Enhanced Chemical Vapor Deposition Methods". *Semiconductors*, **47**, p. 641, 2013.
2. Mehonic A., Cueff S., Wojdak M., Hudziak S., Jambois O., Labbe C., Garrido B., Rizk R., Kenyon A. "Resistive switching in silicon suboxide films". *Journal of Applied Physics* **111**, 074507, 2012.

Quality control at different stages of MTJ fabrication

O.S. Trushin, V.V. Naumov, A.A. Mironenko, N.M. Timina, O.M. Koroleva
Institute of Physics and Technology (Yaroslavl Branch), RAS, Yaroslavl, Russia, otrushin@gmail.com

Magnetic Tunneling Junction (MTJ) is an important element of modern MRAM cell. It is believed that MRAM might be the next generation of computer memory. Therefore optimization of the technology for MTJ fabrication is of very important task. Achievement of high functional characteristics of MTJ requires intensive quality control at different stages of the technological route. In this work we discuss different aspects of quality control during this route. For this purpose we studied experimentally technology of typical MTJ fabrication.

Two kinds of spin-tunnel structures: 1) symmetrical - $\text{CoFe}(10\text{HM})/\text{Al}_2\text{O}_3(2\text{HM})/\text{CoFe}(30\text{HM})/\text{SiO}_2(200\text{HM})/\text{Si}$ and 2) nonsymmetrical - $\text{Ta}(3\text{HM})/\text{FeMn}(15\text{HM})/\text{CoFe}(5\text{HM})/\text{Al}_2\text{O}_3(3\text{HM})/\text{CoFe}(5\text{HM})/\text{Ta}(5\text{HM})/\text{SiO}_2(200\text{HM})/\text{Si}$ were deposited using RF magnetron sputtering at TETRA SCR-650. Quality of multilayer structure has been studied using TEM. Cross-section of as deposited thin film structure is shown in fig.1a. In this image numbers denote the following layers: 1 - the first magnetic layer, 2 - tunnel barrier, 3 - the second magnetic layer. In this picture we see inhomogeneous interface between layers 1 and 2 due to possible oxygen diffusion. Control of magnetic properties of those structures was done using Kerr-effect magnetometry. Hysteresis loop of as deposited structure is characterized by presence of typical steps, showing separate switching of two magnetic layers.

On the next stage multilayer structure has been subjected to photo-lithography processing to get MTJ patterning following well documented technology [2]. In this way MTJ junctions with different lateral dimensions (5×15 , 7×21 , 10×30 μm) were fabricated. Typical voltage-current characteristics of MTJ junctions of variable sizes are shown in fig.1b. Results of experimental measurements were compared with the theoretical model [2] and from the approximation two parameters of the structure were estimated: $E_b = 2$ eV (height of energy barrier) and $d = 3.8$ nm (thickness of the barrier). This value of barrier thickness agrees well with the results of TEM analysis (4-5 nm) [3].

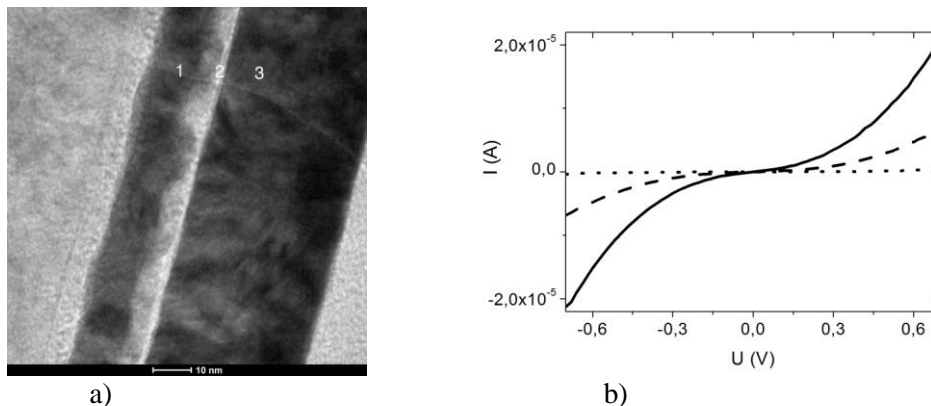


Fig.1 a) TEM image of the cross-section of nonsymmetrical MTJ, b) Voltage-Current characteristics of symmetrical tunnel junctions with different sizes (10×30 μm – solid line, 7×21 μm – dashed, 5×15 μm - dotted).

In conclusion, we have studied typical MTJ fabrication process and developed methodology for quality control at different stages of technological route. These results might be useful for optimization of MRAM technology.

This work has been supported by the program for fundamental research at the division of nanotechnology and informatics of RAS.

1. W.J. Gallagher, S.S.P. Parkin, et.al. "Microstructured magnetic tunnel junctions" J. Appl. Phys., **81**, pp. 3741-3746, 1997.
2. J.G. Simmons "Generalized formula for the electric tunnel effect between similar electrodes separated by thin insulating film", J. Appl. Phys., **34**, pp. 1793-1803, 1963.
3. O.S. Trushin, et al. "Problems of experimental implementation of MRAM cell" Proceedings of the XVIII International symposium on Nanophysics and Nanoelectronics, 10-14 March, N. Novgorod, Russia, 2014.

Switching of magnetic nanoring by a circular field

O. Trushin¹, N. Barabanova²

1. Institute of Physics and Technology (Yaroslavl Branch), RAS, Yaroslavl, Russia, otrushin@gmail.com

2. Faculty of Physics, Yaroslavl Demidov State University, Yaroslavl, Russia, natalybarabanova@gmail.com

Magnetic rings have long history of applications in industry for information storage. Shape of a ring provides optimal conditions for flux closure and presence of two stable states with circular magnetization (clockwise and counterclockwise). This kind of memory utilizing magnetic coils for reading and writing lost competition with semiconductor devices long time ago due to problems with miniaturization of existing technology.

Recently new interest to magnetic rings as memory cells has appeared due to progress in microelectronic technology. In 1999 new design of a memory cell based on magnetic nanoring has been proposed and the patent being issued [1]. The information is stored in such cell as a state of magnetization of the ring. Magnetization switching is performed using circular magnetic field generated by direct wire aligned along axis of a ring perpendicular to its plane (fig.1). The reading of the information is performed by comparison of the response on a pulse of a current in the given ring and in a reference element.

In this work we study the process of magnetization reversal in nanosize ring using micromagnetic simulation with home-made program MICROMAG [2].

Single layer permalloy rings of variable sizes have been modeled. For all rings the difference of external and internal radii was equal to 100 nm. Thus, each ring was characterized by the size of internal radius, which varied in a range 100 - 500 nm.

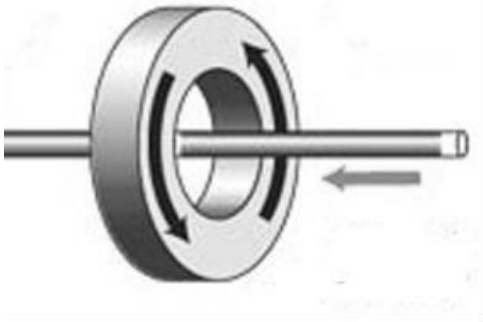


Fig. 1. Scheme of a magnetic ring memory cell with a direct wire generating a circular field.

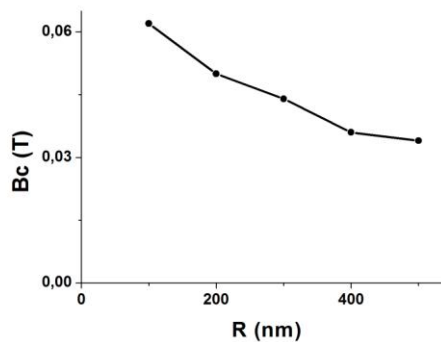


Fig. 2. Dependence of the coercivity field (B_c) on the internal radius of a ring.

Our simulation showed that coercivity field for such a ring is in the range of 0.05 T and gradually reduced with increasing of its radius (fig.2). Such magnitude of magnetic field can be generated by a direct current with magnitude of around 1 mA. It has also been found that breaking the ring can further reduce its coercivity. Thus our simulation supports possibility of experimental realization of this concept of memory cell.

1. V.M. Dubovik, et al. "Method of toroid write and read, memory cell and memory device for realizing the same", USA patent US6266289 B1, 2001.

2. O.S. Trushin, N.I. Barabanova "Micromagnetic software package MICROMAG and its application to study elements of spintronics", Russian Microelectronics, **42**, pp. 176-183, 2013.

Coherent control of magnetic cluster dynamics by short electromagnetic pulses

A.V. Kuznetsov¹, N.V. Klenov^{1,2}, I.I. Soloviev^{1,2}, O.V. Tikhonova¹

1. Lomonosov Moscow State University, Moscow, Russia, E-mail address: nvklenov@gmail.com

2. Lukin Scientific Research Institute of Physical Problems, Zelenograd, Moscow, 124460 Russia

Growing performance of modern electronics, coupled with the increasing degree of integration of electronic circuits opens the way for intensive investigations of challenging mechanisms for implementing fast and compact (in the limit - operating on the atomic time and spatial scales) magnetic memory elements. Ultimate performance of memory elements determined by the speed with which we can control the magnetic moment of domains, magnetic clusters, magnetic nanoparticles, and in the future - individual atoms. Typical results for magnetization reversal times using conventional for nanoelectronics magnetic fields / spin-polarized currents are of about a few nanoseconds [1-2].

Circularly polarized electromagnetic pulse of duration of a few tens of femtoseconds can switch magnetic domain on much smaller time scales [3]. The developed description of these intriguing experimental results is based on the classical theory of the inverse Faraday effect and the macroscopic models of the magnetic momentum dynamics (the Landau-Lifshitz-Gilbert equation) [1]:

$$\frac{d\mathbf{M}}{dt} = -\frac{\gamma}{\beta} [\mathbf{M}\mathbf{H}] - \frac{\alpha\gamma}{M_s\beta} [\mathbf{M}[\mathbf{M}\mathbf{H}]], \beta = 1 + \alpha^2 \quad (1)$$

Here we present our approaches to the consistent fully quantum description of the process of magnetization reversal in collective of atoms by means of ultrashort electromagnetic pulses. In the simplest model of an atomic (two-level) system with a magnetic moment we analyzed from the first principles the speed of magnetization reversal and the physical mechanisms of the observed effects.

In addition, consideration of the observed effect in the framework of the macroscopic theory of the magnetic moment was fulfilled, that allowed to compare the quantum and classical solutions and to identify the presence and role of quantum opto-magnetic effects on the femtosecond time scale. The coordinate system for magnetic momentum dynamics investigation and the example of our results for reversal time in the frame of ‘macroscopic approximation’ are presented in Fig. 1.

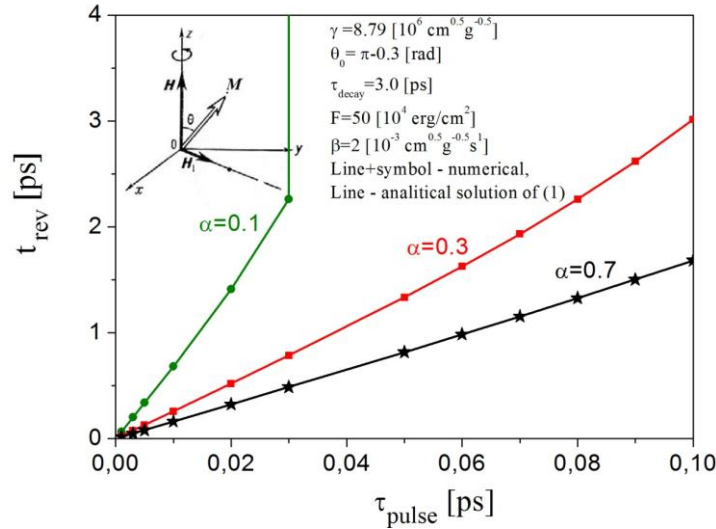


Fig. 1. The coordinate system for magnetic momentum dynamics investigation (inset) and magnetic moment reversal time vs laser pulse duration in the frame of macro-spin approximation.

1. A.L. Pankratov, S.N. Vdovichev, I.M. Nefedov. "Effect of noise on the high-speed reversal of single-domain uniaxial magnetic nanoparticles". *Physical Review*, **78**, p. 052401, 2008.
2. D.C. Ralph, M.D. Stiles. "Spin transfer torques". *Journal of Magnetism and Magnetic Materials*, **320**, pp. 1190-1216, 2008.
3. J.-Y. Bigot, M. Vomir, E. Beaupaire. "Coherent ultrafast magnetism induced by femtosecond laser pulses". *Nature Physics*, **5**, pp. 515-520, 2009.

Unusual critical current in a long quasi-one-dimensional superconducting wire with a narrowing

V.I. Kuznetsov

Institute of Microelectronics Technology and High Purity Materials, Russian Academy of Sciences,
Chernogolovka, Moscow Region, Russia, E-mail address: kvi@iptm.ru

Critical current in quasi-one-dimensional superconducting wires with cross-section dimensions less than the double superconducting coherence length $2\zeta(T)$ and devices with a weak link was extensively studied [1]. Surprisingly, the critical current of a long superconducting quasi-one-dimensional wire of the total length several times exceeding the double charge imbalance length $2\lambda_Q(T)$ [1] and the cross-section constriction of a length less than $2\lambda_Q(T)$ has not been virtually studied. We measured magnetic-field-dependent critical current in a long quasi-one-dimensional superconducting wire with the cross-section constriction at temperatures T slightly below the critical temperature T_c . The magnetic field H was directed normal to the substrate surface. Selected experimental data are given in Figs. 1 and 2 for the wire (inset of Fig. 1). The 30 nm thick wire was prepared by thermal aluminum deposition onto a silicon substrate by the lift-off electron beam lithography. The wire of the total length 70 μm and the basic width 0.4 μm has a narrowing slightly longer than 1 μm and 0.23 μm wide in the wire center. The widths and thickness were less than $2\zeta(T)$. The direct current through I_1 and I_2 probes passed through the whole wire. Two critical superconducting currents versus H , one – a switching current $I_s(H)$ at which voltage arises between the V_1 and V_2 probes in the wire narrow central part, and the other – a retrapping current $I_r(H)$ at which the voltage disappears, were determined from current-voltage curves measured at various fields (Fig. 2). In addition, the temperature dependences of the switching current $I_s(T)$ and retrapping current $I_r(T)$ were measured in zero field (Fig. 1).

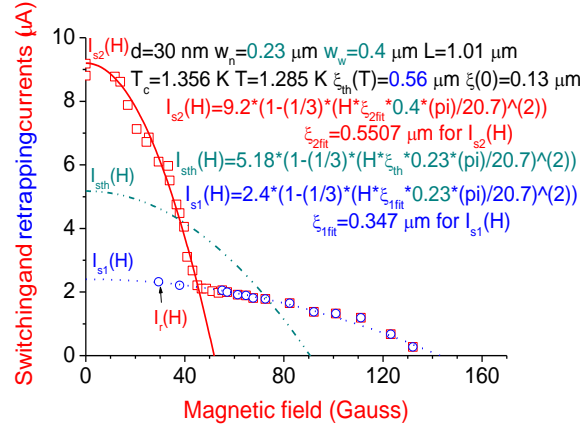
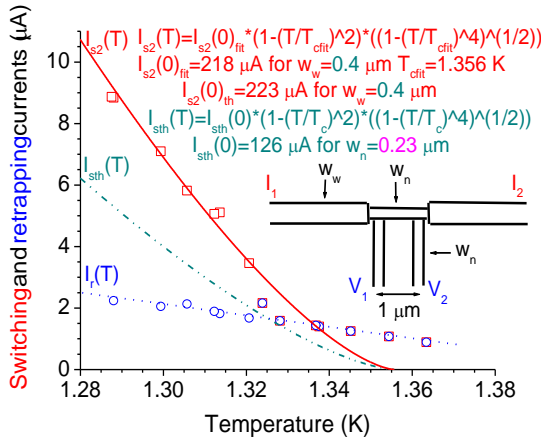


Fig. 1. Measured switching current vs. T (squares) is approximated by the $I_{s2}(T)$ function (solid line). Measured retrapping current vs. T (circles) is fitted by the $I_r(T)$ function (dotted line). Theoretical switching current $I_{sth}(T)$ for the wire $w_n = 0.23 \mu\text{m}$ wide is presented by a dash-dot-dotted line. All the curves are given at $H = 0$. The inset is a sketch of the structure.

Fig. 2. Measured switching current vs. H (squares) is approximated by the $I_{s2}(H)$ function (solid line) in low fields and by the $I_{s1}(H)$ function (dotted line) in high fields. Measured retrapping current (circles) is approximated by the $I_{s1}(H)$ function in high fields. Theoretical current $I_{sth}(H)$ for the wire $w_n = 0.23 \mu\text{m}$ wide is presented by a dash-dot-dotted line.

It is seen from Figs.1 and 2 the theoretical curves of the switching current $I_{sth}(T)$ and $I_{sth}(H)$ which do not include the effect of the wire wide parts differ strongly from the experimental data. The measured switching current $I_{s2}(T)$ in $H = 0$ exceeds the depairing current $I_{sth}(T)$ almost by two times. In low fields, the switching current $I_{s2}(H)$ is fairly well described by the suppression of the superconducting order parameter in the wire wide parts. In high fields, the switching current $I_{s1}(H)$ mainly depends on the suppression of the order parameter in the wire narrow part. The switching and retrapping currents coincide only at high T and H . The results show that the critical current is not a local quantity determined by narrowing but it depends on the strong long-range coupling of electron transport in the wire narrow and wide parts.

1. K. Likharev. "Superconducting weak links". Rev. Mod. Phys., **51**, pp. 101-159, 1979; A. Barone and G. Paterno. *Physics and Application of the Josephson Effect*. John Wiley and Sons, New York, 1982.

Geometry precise correction of receiving parabolic antenna by means of Josephson elements phased array

A. Karuzskii, A. Perestoronin, A. Tskhovrebov, L. Zherikhina
P.N. Lebedev Physical Institute RAS, Moscow, Russia, tshovrebov@yandex.ru

Inaccuracy of the size of a parabolic mirror at the production stage, temperature instability of geometrical and physical parameters arising directly during exploiting – all leads to a significant reduction in the effective area of the reflecting surface [1]. These parasitic effects make very urgent to develop methods for fast correction of nonparabolicity in reflector, collectively known as "adaptive optics." Of course, the non-mechanical adjustment methods of the reflector's geometrical imperfections are of the particular interest and here, low-noise micro-cryo-components with non-linear electrical characteristics can be very useful as a base. Apparently, the most versatile non-linear cryoelement with a speed of operation limited by width of the superconducting gap $f < \frac{\Delta}{2\pi\hbar}$ ($f < 0.5$ THz for classical and $f < 5$ THz for high-temperature superconductors) is a contact with a Josephson properties.

As microwave receivers Josephson junctions are typically used in one of two alternative modes: as a detector [16] which registers radiation by reduction of the height of the first Shapiro step [2], or as a detector-mixer which uses strong nonlinearity ($\frac{\partial^2 V}{\partial I^2} / \frac{\partial V}{\partial I} = (10^4 \div 10^5) V / W$) of the current-voltage characteristics that occurs in the range of superconducting gap voltage $V \approx \frac{\Delta}{2e}$ and in the condition of artificial suppression of the Josephson current amplitude under a small magnetic field [3, 4]. The first type detectors have sensitivity at $NEP \approx (10^{-12} \div 10^{-14}) W/\sqrt{Hz}$, while the structures with suppression of the Josephson current, commonly referred to as SIS-mixers, in detection mode reach the level of $NEP \approx 10^{-16} W/\sqrt{Hz}$.

Suppose that an orbital radio telescope works at a wavelength lying in the range $1 \text{ mm} \leq \lambda \leq 1 \text{ cm}$ (corresponding to frequencies $30 \text{ GHz} \leq f \leq 300 \text{ GHz}$). Consider the possibility of using 2D matrix of SIS mixers placed on a flat square $3 \times 3 \lambda^2$ as a radiation detector. It is supposed to place a sufficiently close-packed array of mixers in the focal plane of a parabolic mirror (the size of "Josephson pixel" together with wires would be approximately $3 \times 3 \div 30 \times 30 \text{ mcm}^2$). Those rays that will not fall into focus due to mirror's geometric imperfections, i.e. touch the plane of the array at a distance from the focal point more than $\lambda/2$, will be captured by "peripheral" SIS mixers. Correction of geometric imperfections should be brought to "redirection" with further taking into account with corresponding phase shift of electrical signals coming from the peripheral mixers into channels, which corresponds to "focus" pixels arranged in the center circle with a radius of $\lambda/2$, where the rays should have to get in the absence of distortions. Under superheterodyne conversion the Josephson SIS mixer, of course, keeps the ratio between the phase of the received RF signal and heterodyn phase oscillations. This permits us to perform summing of signals from the "peripheral" mixers taking into account phase shifts not directly at microwave frequencies, but at significantly lower intermediate ($f_{np} = |f_{cfr} - f_{ret}|, f_{np} \ll f_{cfr}$) frequencies (assuming that all SIS mixers are served by one local oscillator).

The work was performed under the auspices of the grant RFBR № 13-08-01190 "Development and modeling method of high-precision positioning Space Telescope in orbit".

1. N.S. Kardashev, V.V. Hartov, V.V. Abramov, et.al. *Astronomical Journal*, **90** (3), pp.179-222, 2013.
2. S. Shapiro, A.R. Janus, S. Holly. *Rev. Mod. Phys.*, **36**, pp.223-225, 1964.
3. A.I. Golovashkin, V.G. Elenskij, K.K. Likharev *Josephson Effect and its Applications*. Moscow: Nauka, 1983 (in Russian).
4. A. Barone, G. Paterno. *Physics and Applications of the Josephson Effect*. John Willey and Sons, New York, 1981.

Photoresponse beyond the red border of the internal photoeffect

M. Dresvyannikov, A. Karuzskii, A. Perestoronin, A. Tskhovrebov, L. Zherikhina
P.N. Lebedev Physical Institute RAS, Moscow, Russia; E-mail: tshovrebov@yandex.ru

In cloudless weather, Rayleigh scattering [1], which is proportional to $1/\lambda^4$, is significant mostly in shortwave range of visible spectrum. That is why the color of the clear sky is blue, and the sun takes on a reddish hue during a sunrise or sunset. At the same time the whiteness of clouds and milky sky point out the intensive Rayleigh scattering throughout visible spectrum, which makes harder to track aircraft in the atmosphere and near ($D < 1000000$ km) space [2]. Thus with the transition from the near-infrared range $\lambda \approx 1 \mu\text{m}$ to the far infrared one $\lambda \approx 10 \mu\text{m}$ via attenuation of the Rayleigh scattering, cloudiness can be reduced by 4 orders about $(1 \mu\text{m})^4 / (10 \mu\text{m})^4 = 10^4$. The choice of 10- μm range is supported by the existence of the simple-designed and reliable transversely pumped CO_2 (TEA [3]) laser, with the wavelength directly getting into convenient atmospheric transparent window ($7.5 \mu\text{m} \leq \lambda \leq 10 \mu\text{m}$ [4]).

The most highly sensitive photodetectors, which based on lidars, are capable to detect single photons. First of all it is a classical PMT (photomultiplier photoemission-based tube) and APD (avalanche photodiode based on internal photoelectric effect). However, the work function of both external and internal photoelectric effect usually covers the region of the one electron volt, while in the discussed infrared range of $\lambda \approx 10 \mu\text{m}$ quantum of radiation carries only $\hbar\omega \approx 0.12$ eV.

In order to create a sensor which is able to work beyond the edge of the photoeffect as a photodetector, it was investigated the influence of infrared radiation ($\hbar\omega \approx 1.24$ eV) on GaAsP LED with two electronvolts bandgap ($\Delta E \approx 1.71$ eV), which was under the opening electric displacement. Current had decreased under the influence of the radiation, but in contrast to the effect of light influence on the CVC of the simple photodiode (Figure 1) current-voltage characteristics of the LED did not "drop", but the slope of our measured curve's reduced (Fig. 2). Apparently, the electrons transferred from n to p region are moved by radiation quanta above their placement in the n region and returned there, creating a "counter photocurrent" proportional to the electric current.

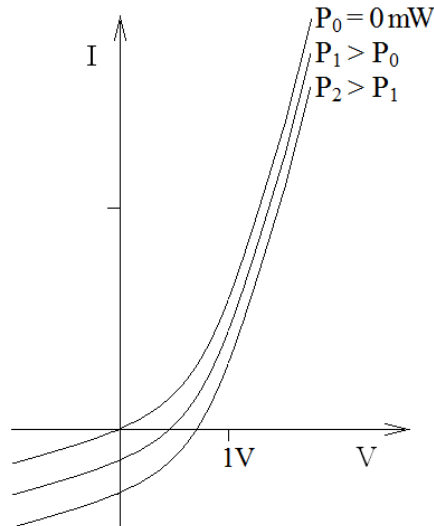


Fig. 1. Typical current-voltage curves of simple photodiode.

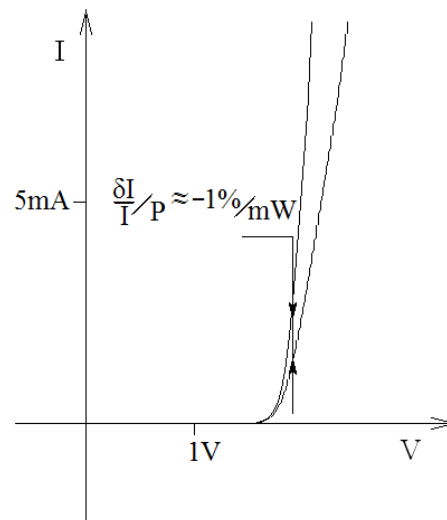


Fig. 2. Measured IU -curves of GaAsP LED.

The work was performed under the auspices of the grant RFBR № 13-08-01190 "Development and modeling method of high-precision positioning Space Telescope in orbit"

1. J. Strutt (Lord Rayleigh) "On the scattering of light by small particles". Philosophical Magazine, London **41** (4), pp.447-454, 1871.
2. V.V. Protopopov, N.D. Ustinov. "Infrared laser radar system" Voenizdat, Moscow, 1987 (in Russian).
3. O. Svelto. "Principles of Lasers". Plenum Press, 1976.
4. V.E. Zuev. "Transparency atmosphere for visible and infrared rays". Soviet Radio, Moscow, 1966 (in Russian).

Large Scale ($\sim 25 \text{ m}^2$) metal diffraction grating of submicron period as possible optoelectronic detector for short scalar gravitational waves

V.A. Zhukov

*St. Petersburg Institute of Information Science and Automation, Russian Academy of Sciences, St. Petersburg, Russia,
E-mail address: valery.zhukov2@gmail.com*

Currently in theoretical astrophysics the prevailing view is that in nature there are only two types of gravitational waves: tensor (quadrupole) and scalar [1]. In recent years, in the frames of LIGO projects, attempts were made, yet unsuccessful, to detect long-wavelength (with λ in interval $43 \div 10000 \text{ km}$) quadrupole radiation from the millisecond pulsars [2], synchronous with their electromagnetic radiation. It should be noted that the proposed hitherto antenna (detectors) of long wave gravitational radiation are massive pendulums, coupled with sensitive displacement sensor. At the same time there are powerful explosive processes associated with relativistic accretion of matter into a supermassive "black hole" (quasar), located in the center of our galaxy. The power of these processes is superior on the tens of orders the power of processes associated with the rotation of the non-axisymmetric pulsars [2, 3]. Processes of accretion in the quasar are accompanied by intense electromagnetic radiation in all observable spectral regions. As it follows from [1], the scalar gravitational waves should also be emitted at such accretion. Moreover, it must be in sync with electromagnetic bursts and in all regions of the spectrum, including the optical frequencies. In this paper we propose a detector of scalar gravitational wave with a length of $\lambda \sim 0.5 \text{ microns}$. It is a flat metal film with a thickness of the order of 2λ . The wave vector of the gravitational waves will lie in the plane of the film. Electrons in the conduction band of the metal are used in this detector as pendulums. By analogy with the Mossbauer effect we believe that the ion subsystem of metal at temperatures below the Debye temperature will not respond to the impact of short gravity waves. For reasons of symmetry the scalar gravitational wave is a longitudinal wave of vibrations of the gravitational potential gradient, such as a wave of longitudinal oscillations of the particles in an acoustic wave in the gas. Under the influence of gravitational waves, the electrons in the conduction band of the metal will due to the principle of equivalence of inertial and gravitational masses have oscillations along the direction of wave propagation with acceleration equal to the gradient of the potential in the wave. Synchronously with these oscillations the fluctuations of the electromagnetic field will occur, the electric vector of which will oscillate around zero along or against the direction of propagation of the gravitational wave. These oscillations of the field to be converted to electromagnetic waves emitted outside the metal film. For this purpose it is proposed to create the grating with a sinusoidal profile and of period λ on the surface of a metal. Profile height should be equal to $\lambda/2$ and strokes of grating must be parallel to the plane of a gravitational wave. Alternating electric field induced in the "negative" spatial half-cycles of the sine that correspond to grooves of grating at propagation normal to the plane of the grating at a distance of $\lambda/2$ changes sign. According to [4], two plane waves of TM-type with magnetic vector parallel to the grating grooves will arise in this case. They will be emitted by this grating at the same angles ($\sim 45^\circ$) to the normal. One of the resultant waves will need to be directed to a parabolic mirror of large optical telescope parallel to its axis and further need to be directed to its photo detector. By using a data on the ultimate sensitivity of optical telescopes, calculations were made to determine the conditions of reliability for registration of scalar gravitational waves with $\lambda \sim 0.5 \text{ }\mu\text{m}$ from the quasar. They showed that the amplitude of the alternating gradient of the gravitational potential in the source, at its Schwarzschild radius, should not be less $A_G = 1.4 \cdot 10^{17} \text{ m/s}^2$. According to an estimate by the special theory of relativity, the maximum possible value of this amplitude at a given frequency will be by 7 orders of magnitude greater. The following method can be proposed for manufacturing of the above-described diffraction grating with area of 25 m^2 . Take a square polished silicon wafer with size $200 \times 200 \text{ mm}^2$. Create the desired metal profile on it by photolithography and plasma-ion etching. And then to put together the 625 such plates on flat ground.

1. H. Sotani, "Scalar gravitational waves from relativistic stars in scalar-tensor gravity", arXiv:1402.5699v1.
2. <http://www.ligo.org/science/outreach.php>.
3. D. Majaess, "Concerning the Distance to the Center of the Milky Way and Its Structure" Acta Astronomica, **60**, pp. 55-74, 2010.
4. H.A. Haus, "Waves and Fields in Optoelectronics", Prentice-Hill, Ink., New Jersey, 1984.

Digital holography in 3D integral circuits and neo cortical columns

V.A. Zhukov

St. Petersburg Institute of Information Science and Automation, Russian Academy of Sciences, St. Petersburg, Russia,
E-mail address: valery.zhukov2@gmail.com

The ultimate goal of such sciences as the theory of artificial intelligence, neuro science, neuro computing and informatics is the creation of an artificial brain, with the ability to integrate all of human science and with the ability to withstand to all current and future global challenges and threats. Micro-and nano-electronics is designed to provide the element base and architecture (topology) of VLSI for such brain. According to experts, the nature of neo cortical columns (so called "mini columns") in the neocortex of the brain is currently the number one problem in the neurophysiology of the brain [1]. The researchers found that the neocortex of mammals is a mosaic, which is composed of columns of 2-3 mm in height and of about 0.5 mm in diameter, each containing about $10^4 \div 10^5$ neurons. Mini columns do not stand out morphologically, but each of them is connected to only one of the five analyzers (senses). The average length of axons that connect neurons does not exceed 1 mm, and there is no the specific coding of signals (pulses) from the various analyzers in the brain. Henry Markram, who is leading the project Blue Brain, has taken up this challenge in 2005 [2]. The European Commission represents to him a €1 billion investment over the 10 next years. Markram set out to create a model of object with the structures of type of the "mini columns" by means of supercomputer Blue Gene [3]. The essence of the computer experiment reduces to the specification of the experimental data on individual responses of neurons to stimulation of each neuron from about $10^4 \div 10^5$ neurons in ensemble with the number of interconnections of about 10^8 . This ensemble forms a topological equivalent of a multi-dimensional network (dimensionality about $10^3 \div 10^4$) embedded in our 3D space. Markram was sharply criticized by colleagues for his too narrow aim and lack of a priory model [4] and also for his potential inability to use the results that to be expected for an ensemble with the stochastic nature of interconnections, for building of organized regular models that are created by means of microelectronics. Thus the complete virtual model of the brain that is obtained in this simulation can be built only as the imaginary model within a supercomputer of gigantic scale. Or by means of the Internet with the number of active IP nodes ("neurons"), of about $10^{10} \div 10^{11}$. Since the pattern of "mini columns" resembles rather the nodes and antinodes of the standing wave in the resonator, we offer to return back to the idea of a "holographic metaphor" for the cerebral cortex that was suggested in the 60th years by Michael Arbib [5] and that has not been realized yet. According to this idea, the external analogy between associative memory of brain and holographic recording and reconstruction in optics should have the inner analogy in the form of the presence of the reference "waves" and the signal "waves". From the neurophysiology data it is known that in the brain, in fact, there are several distinct waves (rhythmes). Using this approach, we considered the problem of holographic recording and reconstruction of information in a multilayer 3D grid with a cubic unit cells and with microprocessors that are placed in grid nodes [6]. With this approach the condition of holographic recording signal is an implementation of the discrete Helmholtz equation at the grid. In this paper, we consider examples of realization of the device for recognition of visual images on such a cubic grid, on the 3D integrated circuits. Also an example of generalization of this approach to multi-dimensional holographic virtual network that is embedded in 3D multilayer integrated circuit with a cubic unit cell have been considered. Also the folding of multilayer 3D network in a spherical layer (in "two brain hemispheres") with deformed cubic cells was considered in order to produce the cyclic boundary conditions.

1. D.P. Buxhoeveden, "The minicolumn hypothesis in neuroscience", *Brain*, **125** (5), p. 935, 2002.
2. <http://bluebrain.epfl.ch/>
3. <http://www-03.ibm.com/ibm/history/ibm100/us/en/icons/bluegene/>
4. <http://www.neurofuture.eu/>
5. M.A. Arbib, "*The Metaphorical Brain*", Wiley Interscience, New York -London, 1972.
6. V.A. Zhukov, "Micro Systems Engineering and Digital Holographic Flash Memory", *Russian Microelectronics*, **43**, pp. 80–90, 2014.

The sensor of surface defects based on electrical impedance tomography technique

E. Ryndin, A. Isaeva

*Institute of Nanotechnology, Electronics and Electronic Equipment Engineering of Southern Federal University,
Taganrog, Russia, rymenator@gmail.com*

This paper describes the application of electrical impedance tomography (EIT) to development of the surface defect sensor that can be used for structural health monitoring (such structural as bridge bearing, airframe, etc.) [1]. Thin conductive film with electrodes along its boundaries, as a sensor skin, applied to structural surface. By using the corresponding boundary potential measurements and the value of applied current the both forward and inverse EIT problem were solved and method of defects detection in thin conductive film was created. This method allows to calculate two-dimensional distribution of conductivity in film and, indirectly, distribution of defects in it.

The reconstruction defect efficiency criteria and the method of its calculation were proposed. The influence of initial data disturbance (non-uniform conductivity of the film as its roughness) on reconstruction defect efficiency without using all the combinations of current electrodes was examined.

This approach is useful in the automatic defect sensors development field. This sensor can be applied to monitor appearance of crack and its evolution and acquire data about mechanical stress, humidity and pH (by using film that sensitive to these stimuli) by mapping the film conductivity [2, 3].

This study was supported by the Russian Foundation for Basic Research (projects 13-07-00274, 14-07-31234), and by the Ministry of Education and Science of Russian Federation (project 213.01–11/2014–12).

1. E.A. Ryndin, A.S. Isaeva, 'Method of construction surface defect's analysis using electrical impedance tomography'. Vestnik Yujnogo nauchnogo centra RAN, 9, №1, pp. 17-21, 2013.
2. T. Hou, K. J. Loh, J. P. Lynch, 'Spatial conductivity mapping of carbon nanotube composite thin films by electrical impedance tomography for sensing applications', Nanotechnology, pp. 1-9, 2007
3. Kenneth J. Loh, Tsung-Chin Hou, Jerome P. Lynch, Nicholas A. Kotov., Loh, K. J., 'Nanotube-based Sensing Skins for Crack Detection and Impact Monitoring of Structures'. Proceedings of the 6th International Workshop on Structural Health Monitoring, Stanford, CA, p.11-13, 2007.

Electrostatically actuated MEMS switch with resistive contact

I.V. Uvarov, V.V. Naumov, R.V. Selyukov

*Institute of Physics and Technology (Yaroslavl Branch), Russian Academy of Sciences,
Yaroslavl, Russia, ilnik88@mail.ru*

Electrostatically actuated MEMS switches have been used in various radiofrequency applications such as phased array radars and satellite communication systems. RF MEMS ohmic switches have shown lower insertion loss, higher isolation, greater linearity, and lower static power dissipation than solid state switches [1]. The main drawback of modern commercially available MEMS switches is the high actuation voltage [2]. In this paper a single-pole single-throw electrostatically actuated MEMS switch is presented. Moving electrode of the switch is the metal cantilever having nanoscale thickness and high length-to-thickness ratio (up to 400). Low actuation voltage of the switch is provided by low elasticity of the cantilever.

SEM image of the switch is shown in Fig. 1. Cantilever is located over the driving and signal electrodes. At the free end it has a contact dimple (Fig. 2). When actuation voltage is applied between the cantilever and the driving electrode, cantilever is attracted to the driving electrode by the electrostatic force and touches the signal electrode, opening the switch. When the actuation voltage is removed, the cantilever returns to its original position.

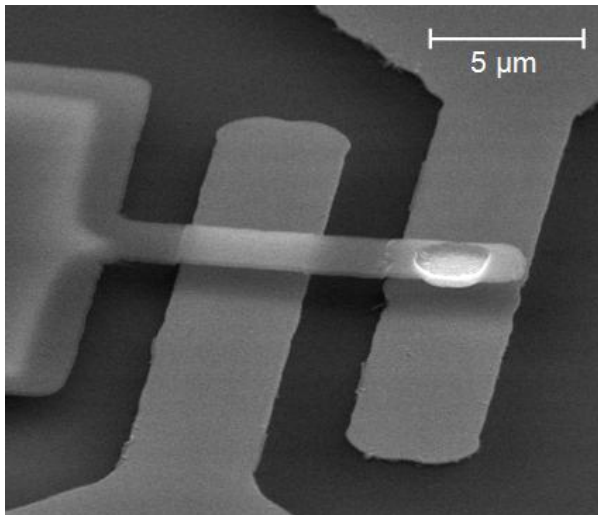


Fig. 1. SEM image of the switch.

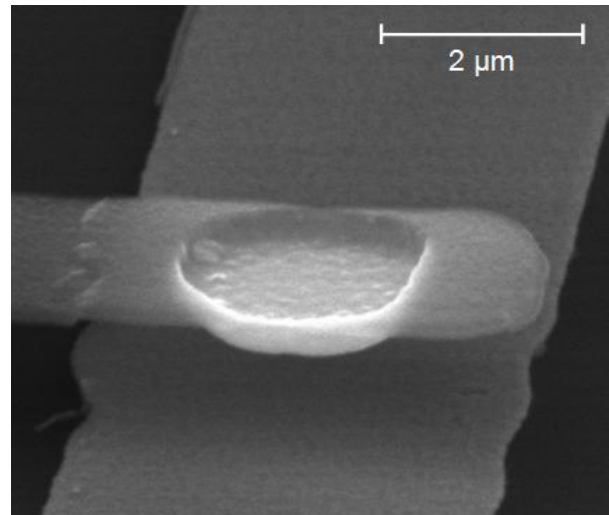


Fig. 2. SEM image of the free end of the cantilever.

Switches were fabricated by surface micromachining on thermally oxidized silicon wafers. Driving and signal electrodes had a thickness of 50 nm and were made of Pt. The cantilever had a three-layer Cr/Al/Cr structure with the layer thickness ratio of 1/6/1. Total cantilever thickness was 80, 120 and 160 nm. Cantilever had a length of 14-32 μm and width of 2-6 μm . Sacrificial layer was the amorphous Si layer of 1 μm thickness. Contact dimple had a diameter of 2 μm , a height of 100 nm and was made of Pt. So, the Pt-Pt contact was realized in the switch. Deposition of materials were performed by magnetron method, the sacrificial layer was removed by etching in SF_6 plasma.

Electromechanical parameters of the switch were calculated and experimentally determined. Lowest actuation voltage of 8.1 V was obtained. The contact resistance was 10-100 Ω . The switches held a DC current of 10 to 30 mA, depending on the geometry of the cantilever. The main problem lowering the reliability of the switch was stiction of the cantilever to the signal electrode under the adhesive forces.

This work was supported by FSC "Micro- and Nanostructures Diagnosis" and by RFBR, research project No. 14-07-31156 mol_a.

1. G.M. Rebeiz. *RF MEMS: Theory, Design, and Technology*. John Wiley & Sons, Hoboken, 2003.
2. M.-W. Kim, Y.-H. Song, H.-H. Yang, J.-B. Yoon. "An ultra-low voltage MEMS switch using stiction-recovery actuation". *J. Micromech. Microeng.*, **23**, p. 045022, 2013.

How to increase reliability of frameless PCB based on the organic substrates

Yu. Dolgovykh, A. Pogalov, G. Blinov, S. Timoshenkov, N. Korobova

National Research University of Electronic Technology (MIET), Bld. 5, Pas. 4806, Zelenograd, Moscow, Russia, 124498, E-mail: korobova3@mail.ru

Steady increase of the chips integration, general increase in the layout density of elements and devices for electronic equipment leads to the search for improved design and technological solutions by microminiaturization electronic products. Development of multichip modules based on the technology of assembly and mounting bare chips on flexible board (technology COF - Chip on Flex) is one of these decisions. Substrate flexibility allows to create three-dimensional spatial structure and to increase the layout density at times.

Determining processes in technological mounting route of multi-crystal micromodules (MCM) are the creation of wide high-precision double-side polyimide flexible boards with reliable mounting of switching levels of board opposite sides, mounting crystals ball pins on flexible boards, which have gone pre certification. Material of flexible switching boards for MCM primarily should have high specific volume and surface resistance, low dielectric constant to reduce the parasitic couplings between circuit elements.

Brand Kapton's foiled polyimide film with 25 microns thickness was used as a substrate for flexible switching board, due to the exceptional properties combination such as high dielectric strength, ability to maintain the stability of physical and chemical properties at high temperatures up to +260 °C, possibility of selective chemical processing. Contact pads on the flexible multilayer board have a hemispherical shape for crystal ball pins mounting to increase reliability, improve packing density, and performance in the manufacture of memory modules in large capacity. Such a decision [4] provides automatically positioning and crystal fixation on the board and allows facilitate alignment of IC ball pins with them and reduce the manufacture of modules complexity. Authors proposed a technology for creating multi-pins bare chips with ball pins that are formed directly on the crystal contact pads (CP). The crystal after attestation immediately mounted on a flexible board. Flexible multi-level switching polyimide board has hemispherical manual for mounting the crystal ball pins. Mounting ball pins from low-melting solder for soldering to a printed board were formed on the other board side in full-formed matrix. Pins with diameters from 50 to 100 microns were ranging, diameter of solder balls mounting on the back board side was from 250 to 350 microns. Presented technology provides increased packing density, increasing productivity by use group technology and automated installation ICs methods on flexible boards, increasing materials durability reliability, connections and design elements. This technology has originality and uniqueness that allows you to create ball pins on any VLSI wafers with their further appraisal and subsequent installation. IC mounting with ball pins on a flexible board was carried out using automatic installation mounting crystals FC 150, which is used for alignment and fixing one or more chips on the substrate, using one of several available technologies flip chip («flip-chip»), including thermo-compression, cold compression and compression along with curing the adhesive (see Fig. 1).

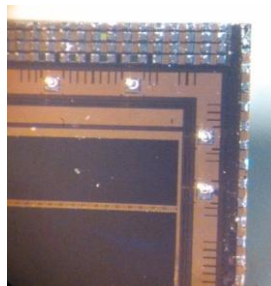


Fig. 1. Fragment of crystal with ball pins.

Main technical micro modules parameters were following: device structure - low weight and size - structure on a flexible substrate; delay time in switching ≤ 0.04 ns/cm; crystals number in construction is not less than 4; specific (per unit length) wire resistance ≤ 0.01 Ohm/cm.

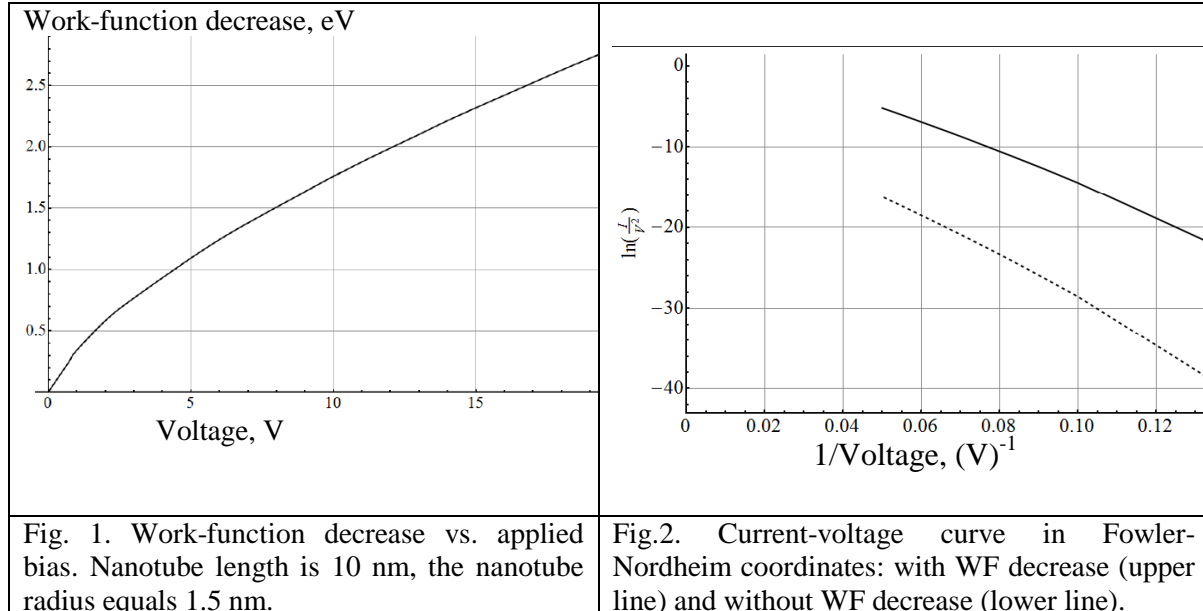
Work-function lowered upon field emission from nanotubes and graphene

G. Alymov, D. Svintsov, V. Vyurkov

Institute of Physics and Technology RAS, Moscow, Russia
Moscow Institute of Physics and Technology (State University) Moscow, Russia
svintcov.da@mipt.ru

Carbon materials (graphene and nanotubes) are widely regarded as potential candidates for cold field emission devices. Work-functions (WFs) measured in multiple experiments with field emission from nanotubes exhibit a noticeable diversity: from 0.2 eV up to 7.3 eV [1, 2], meanwhile, the graphite work-function equals 4.8 eV. The reasonable explanation is based on the microscopic phenomena at the nanotube edge. It could be a surface reconstruction or adsorption of atoms and molecules. Here we introduce a new explanation which could be called macroscopic. The essence is that a strong electric field near the nanotube tip results in a large electron density. This entails an essential growth of the Fermi energy, therefore, the corresponding decrease in the work function. It should be noted, that this effect is negligible for metallic injectors due to very large density of states at the Fermi level in metals. The density of states in graphene and metallic nanotubes is much smaller than that in common semiconductors, not to mention the metals. The low density of states leads to a pronounced effect of quantum capacitance.

The simulation involves an iterative procedure for the solution of the Poisson equation in the integral representation where the local charge density is related to the local potential through the local Fermi energy. After that the tunneling current was calculated via the Fowler-Nordheim theory adapted to low-dimensionality (1D and 2D). The substantial decrease in the work function at the nanotube tip is evident from Fig. 1. The applied bias is, in fact, the mean field between cathode and anode times the nanotube length. Fig. 2 manifests a considerable impact of a lowered WF on the emission current (by several orders of magnitude).



Similar effects were also simulated for field emission from graphene blades.

The research was supported by the grants of Russian Academy of Sciences and the Russian Foundation for Basic Research (# 14-07-00937, 14-07-31315).

1. Yu.V. Gulyaev et al. "Work function estimate for electrons emitted from nanotube carbon cluster films". *J. Vac. Sci. Technol. B*, **15**, pp. 422-424, 1997.
2. A.V. Eletskaa. "Carbon nanotube-based electron field emitters". *Phys. Usp.*, **53**, pp. 863-892, 2010.

Monte Carlo simulation of hot carrier transport in deep submicron SOI MOSFET

A.V. Borzdov¹, V.M. Borzdov¹, V.V. V'yurkov²

1. Belarusian State University, Minsk, Belarus, borzdov@bsu.by

2. Institute of Physics and Technology, Russian Academy of Sciences, Moscow, Russia, vvyurkov@gmail.com

Ensemble Monte Carlo method is a powerful tool for the simulation of carrier dynamics in deep submicron SOI MOSFETs and has been used to simulate electrophysical properties of the transistors for decades [1, 2]. One of the advantages of Monte Carlo simulation is the fact that mathematical models describing different physical processes can be incorporated into the simulation procedure. Current work is focused on the simulation of electron impact ionization process in the channel of deep submicron SOI MOSFET presented in Fig. 1 and is the extension of the previous simulations of common MOSFETs [3, 4].

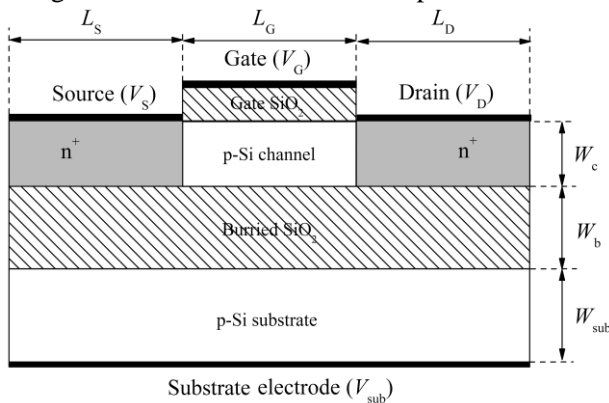


Fig. 1. The cross-section of the simulated SOI MOSFET

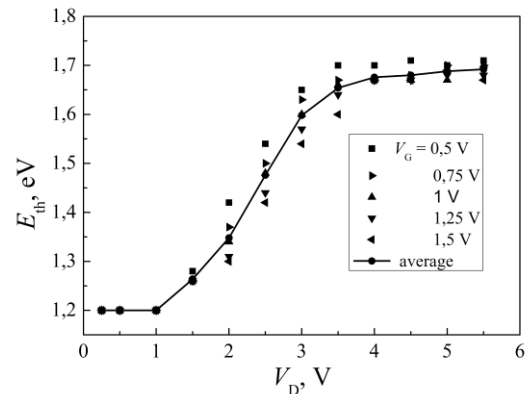


Fig. 2. Dependences of the impact ionization effective threshold energy on the drain bias

The transistor dimensions denoted in the Fig. 1 are as follows: $L_S = L_G = L_D = 100$ nm, $W_c = 30$ nm, $W_b = 100$ nm, $W_{sub} = 200$ nm. The gate oxide thickness is 5 nm. Simulation temperature is 300 K. Source and substrate electrodes are supposed short-circuited and the applied bias is zero. The doping levels of n^+ regions and p-Si are 10^{25} m^{-3} and $8 \cdot 10^{23} \text{ m}^{-3}$, respectively. Electron scattering processes are intravalley and intervalley acoustic and optic phonon scattering, plasmon scattering, ionized impurity scattering and impact ionization process. The latter process is treated in the framework of Keldysh model with "soft" threshold. Since impact ionization becomes sufficient at high drain biases, hole transport is also included. Scattering mechanisms for holes are inelastic optical and acoustic phonon, and ionized impurity scattering.

In Fig. 2 the dependences of the electron impact ionization effective threshold energy E_{th} versus the drain bias V_D are presented for several gate biases V_G as well as an averaged over all gate biases value of E_{th} (solid line). As can be seen from the figure, the behaviour of E_{th} resembles that of common MOSFET [3, 4]. I.e. when impact ionization starts and up to breakdown mode the effective threshold energy dependence on the drain bias is close to linear and does not depend considerably on the gate bias. The latter makes it possible to use an *a priori* known effective threshold energy while simulating impact ionization process.

1. K. Throngnumchai, K. Asada, T. Sugano. "Modeling of 0.1- μm MOSFET on SOI Structure Using Monte Carlo Simulation Technique". IEEE Trans. Electron Devices, **ED-33**, pp. 1005-1011, 1986.
2. R. Rengel, M.J. Martin, T. Gonzalez, J. Mateos, D. Pardo, G. Dambrine, J.-P. Raskin, F. Danneville. "A Microscopic Interpretation of the RF Noise Performance of Fabricated FDSOI MOSFETs". IEEE Trans. Electron Devices, **53**, pp. 523-532, 2006.
3. D. Speransky, A. Borzdov, V. Borzdov. "Impact Ionization Process in Deep Submicron MOSFET". Int. J. of Microelectronics and Computer Science, **3**, pp. 21-24, 2012.
4. V.M. Borzdov, A.V. Borzdov, D.S. Speransky, V.V. V'yurkov, A.A. Orlikovsky. "Evaluation of the Effective Threshold Energy of the Interband Impact Ionization in a Deep-Submicron Silicon n-Channel MOS Transistor". Russian Microelectronics, **43**, pp. 189-193, 2014.

Radiation-Induced Mismatch Enhancement in 65 nm CMOS SRAM for Space Applications

M. Gorbunov^{1,2}, P. Dolotov¹, A. Shnaider¹, G. Zebrev², A. Antonov¹, A. Lebedev²

1. Scientific Research Institute of System Analysis, Russian Academy of Sciences, Moscow, Russia, gorbunov@niisi.msk

2. National Research Nuclear Institute (MEPhI), Moscow, Russia, gizebrev@mephi.ru

Technology node scaling provides high performance and high density memory chips, which are very desirable for space applications. CMOS scaling implies supply V_{dd} and threshold V_{th} voltage reduction. Unfortunately, the threshold voltage reduction is much lower than that of supply voltage due to undesirably high leakage currents. The result of such disproportion is the reduced headroom: the designer can place only ~2-3 transistors between power rails V_{dd} and V_{ss} [1, 2]. Since transistor's dimensions decrease, the mismatch between a transistor pair becomes more and more important [2]. In particular, these factors lead to the read- and write margins degradation in SRAMs [2]. As a rule, thin gate oxides provide a high level of total ionizing dose (TID) hardness. However, due to the increase of gate leakage, the physical thickness of the gate oxide is not less than 1.2-3 nm depending on the dielectric material (SiON, High-K, etc.).

Although matching is a well studied subject, the publications on combined action of irradiation and inherent mismatch still lack. It is known that degradation imbalance in different transistors leads to drifts in offset parameters in bipolar technologies. We showed in [3] that enhancement of parameters mismatch can be due to various electrical regimes of transistors in CMOS ICs during irradiation.

In this work, we show the experimental and simulation results of radiation-induced mismatch enhancement (RIME) in a 65 nm CMOS SRAM. The results were obtained using X-ray and heavy ion irradiation.

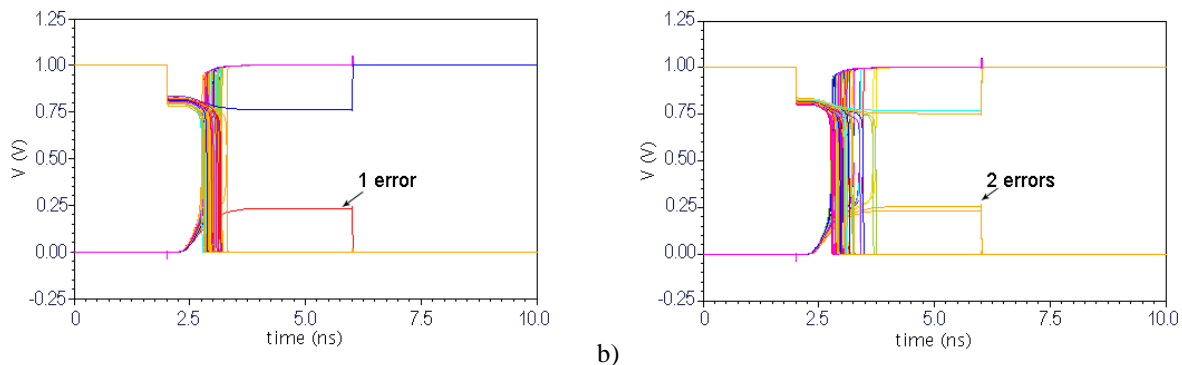


Fig. 1. Write operation at “FF” corner: a) without any changes, b) after the threshold voltage shift introduction.

We used the standard SPICE models provided by manufacturer for Monte Carlo mismatch simulations of write operations. Simulations were done at typical-typical (“TT”) and fast-fast (“FF”) technology corners at 27 °C. Fig. 1 shows the simulation results for “FF” corner. One can see that “before irradiation” (without any changes in model file) we obtain 1 error of 100 runs, which is in a good agreement with experiment (about 1% of 2K×64 cells). The introduction of the threshold voltage shift was made by assignment of 3 needed transistors to the modified models, in which we added a constant to the threshold voltage SPICE parameter “VTH0”. After the introduction of 11 mV threshold shift we obtain 2 errors of 100 runs, which is in a good agreement with experiments. Note that the shift is of the same order of magnitude with standard deviations of threshold voltage in sub-100 nm technologies [2]. There is no errors without threshold voltage shift and 1 error after introducing $\Delta V_T = 13$ mV for “TT” corner. Our experiments and modeling proved that local heavy ion strike to a single cell can cause the write error if the resulted threshold voltage shift is enough to enhance the mismatch.

1. G. Drake. “Dependence on Feature Size. The Factors That Limit Time Resolution in Photodetectors”. University of Chicago Workshop, 2011.
2. H. Iwai. “Technology Roadmap for 22nm CMOS and Beyond,” Presentation, IEDST 2009, Bombay, June 1, 2009.
3. M.S. Gorbunov, I.A. Danilov, G.I. Zebrev, P.N. Osipenko, “Verilog-A Modeling of Radiation-Induced Mismatch Enhancement,” IEEE Trans. on Nucl. Sci., vol. 58, no. 3, June 2011, pp. 785–792.

TCAD Calibration of Nanoscale SOI MOSFETs

E. Artamonova¹, A. Klyuchnikov², A. Krasnyukov¹, T. Krupkina¹

1. National Research University of Electronic Technology (MIET) Moscow, Russia, artamonova@org.miet.ru

2. JSC Molecular Electronics Research Institute, Russia, aklyuchnikov@mikron.ru

Technology Computer-Aided Design (TCAD) has widely used to develop and optimize semiconductor processing technologies and devices [1]. It helps to cut development costs and to speed up product cycles. However, because of the large number of models and the corresponding model parameters and their dependency on fabrication processes and device types, it is difficult to derive automatically a well-adjusted device simulation environment for specific simulation tasks. Therefore, selection of models and calibration of their parameter sets are necessary to obtain good agreement between measurements and simulations in reasonably time.

Due to the large number of parameters involved and the complex nature of the devices that are modeled a systematic approach to calibration is required for both process and device calibration. Often calibration begins with adjusting 1D and 2D impurity profiles from the process simulation to the secondary ion mass spectroscopy (SIMS) experimental data. Then device calibration is performed according to the next steps: CV calibration to extract effective impurity concentration in the gate and thickness of the gate dielectric; transport (mobility) model calibration using IdVg characteristics for low drain bias voltage (LDBV) and long-channel devices; for low drain bias voltage and short-channel devices; for high drain bias voltage (HDBV) and short-channel devices [2].

Final TCAD device calibration results of partially depleted SOI MOSFETs with 70 nm SOI layer and different gate lengths are shown in fig. 1. During calibration the next device and models parameters have been adjusting: impurity concentration in the gate $N_{poly} = 7 \times 10^{19} \text{ cm}^{-3}$, thickness of the gate dielectric $T_{ox} = 3.4 \text{ nm}$, mobility model parameters: $\delta = 2 \times 10^{19} \text{ V/s}$, $B = 4.2 \times 10^7 \text{ cm/s}$, $C = 1 \times 10^4 \text{ cm}^{5/3}/(\text{V}^{2/3} \times \text{s})$, $\beta_0 = 0.48$, $v_{sat0} = 5 \times 10^7 \text{ cm/s}$, contact resistance $R_{cont} = 77 \text{ Ohm}$.

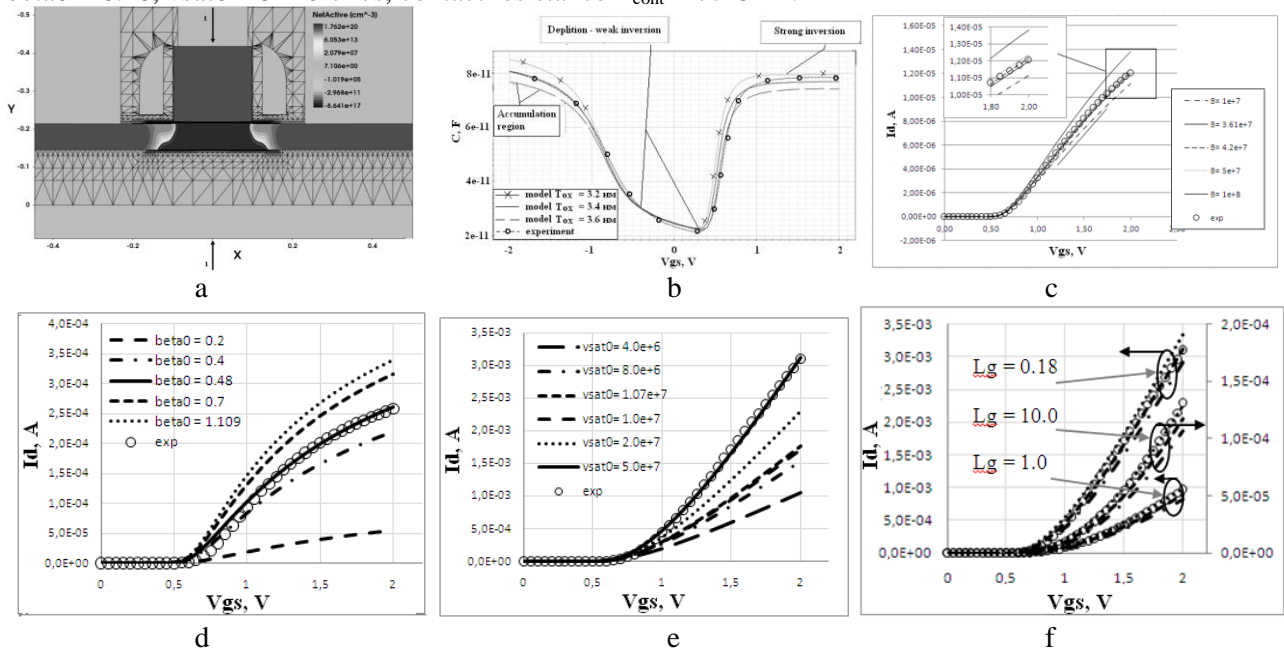


Fig.1 2D model of SOI MOSFET with $T_{box} = 150 \text{ nm}$ and $T_{si} = 70 \text{ nm}$ (a). Calibration T_{ox} : CV characteristics (b); calibration μ_{ac} : IdVg characteristics at LDBV (c); calibration μ_{HFS} at HDBV: β_0 variations for $L_g = 0.18 \text{ um}$ (d); v_{sat0} variations for $L_g = 0.18 \text{ um}$ (e); calibrated characteristics for different L_g and T_{ox} (dot - $T_{ox} = 3.2 \text{ nm}$, dash - $T_{ox} = 3.4 \text{ nm}$, dashdot - $T_{ox} = 3.6 \text{ nm}$, circle - experiment) (f).

1. <http://www.synopsys.com/tools/tcad/Pages/default.aspx>.

2. B. Cretu, C. Mourrain, P. Cottin, G. Ghibaudo. "New method for parameter extraction in deep submicrometer MOSFETS". IEEE, ICMTS 2000, pp. 181-186, 2000.

Modeling of single event gate rupture in power MOSFETs under heavy ion irradiation

R.G. Useinov^{1,2}, G.I. Zebrev¹, V.V. Emeliyanov², A.S. Vatuev²

1. National Research Nuclear University (MEPhI), Moscow, Russia, gizebrev@mephi.ru

2. Research Institute of Scientific Instruments, Lytkarino, Moscow, Russia

All power MOSFETs operated in the off-mode may be susceptible to single event gate rupture (SEGR), i.e. an electric breakdown of the gate oxide under impact of high-energy heavy ions typical for space environment [1]. Typically, the maximum of breakdown electric field of the SiO₂ gate oxide can be as large as $E_{bd}^{max} \sim 10^7$ V/cm. High energy heavy ions are capable to lower this value several times. An extent of such lowering depends in a complex way on ion's atomic number Z_{ion} , its energy, linear energy transfer (LET) etc. Complexity of the oxide breakdown mechanism in itself is additionally exacerbated by complexity of the physical processes under the ion impacts. SEGR is a destructive single event induced effect and, consequently, can be characterized quantitatively by the cross section concept [2, 3]. We measured experimentally the SEGR cross section of power MOSFETs (with gate oxide thickness 70 nm) with irradiation of them by ions of Bi ($Z=83$, LET = 102 MeV×cm²/mg), Xe ($Z=54$, LET = 73), Kr ($Z = 36$, LET = 43), Fe ($Z = 26$, LET = 28) as functions of the gate voltage (gate oxide electric field) [4]. As can be seen in Fig. 1 the experimental SEGR cross section dependencies (points) have a threshold form and drastically increases with a moderate change of gate voltage V_G by several (almost 5) orders. Maximum cross section corresponds approximately to the gate oxide area. We argued in this report that the SEGR effects belong to a

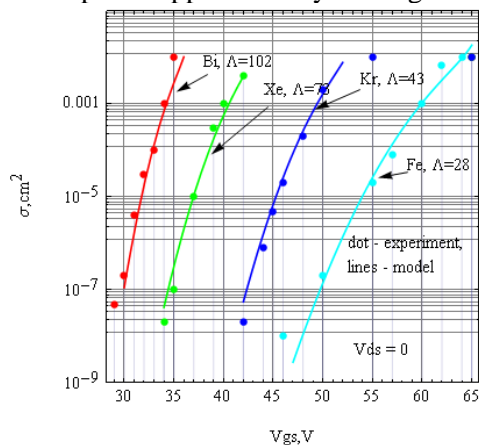


Fig.1. Comparison of experimental data (points) and simulation (lines) results for SEGR cross section vs gate voltage under irradiation for 4 kinds of ions with different LET

class of subthreshold effects which are very sensitive to fluctuations of energy deposition like as it takes place for soft error problem in digital memory ICs [5]. We found that the steepness of the cross section vs V_G curves is determined by secondary electron energy dispersion. We estimated this value as the Bohr straggling energy per a number of released release electron-hole pairs N : $\sigma_B^2/N^2 \propto v_E^4/Z_{ion}^2 d_{ox}$, where d_{ox} is oxide thickness, v_E is ion's velocity. As shown in Fig.1 the cumulative Bohr distribution with variance of secondary electron energy is well fitted for experimental data with different Z_{ion} . Lesser Z_{ion} corresponds to lesser steepness (larger variance) of cross section curves. Typical magnitudes of the variance are of order of tens electron-volts that is comparable with energies supplying by the electric fields in the gate oxides. Breakdown voltage $V_{bd}(Z)$ under irradiation by ions with Z_{ion} is determined by an empirical Titus relation [1] $V_{bd}(Z) \cong 10^7 d_{ox} / (1 + Z/Z_0)$, where $Z_0 \sim 45-55$. Exact mechanism of such dependence remains still unknown and concerns presumably with displacement effects and creation of chain of structural defects as precursor of breakdown. Detailed discussion and the model description would be presented in a final version of the report.

1. J.L. Titus, C. Wheatley, K. Van Tyne, J. Krieg, D. Burton, and A. Campbell, "Effect of ion energy upon dielectric breakdown of the capacitor response in vertical power MOSFETs," *Trans. Nucl. Sci.*, **45**, pp. 2492–2499, 1998.
2. G.H. Johnson, K.F. Galloway, R.D. Schrimpf, J.L. Titus, C.F. Wheatley, M. Allenspach, and C. Dachs, "A physical interpretation for the single-event-gate-rupture cross-section of n-channel power MOSFETs," *IEEE Trans. Nucl. Sci.*, **43**, pp. 2932–2937, 1996.
3. A. Javanainen, V. Ferlet-Cavrois, H. Kettunen, M. Muschitiello, F. Pintacuda, M. Rossi, J.R. Schwank, M.R. Shaneyfelt, and A. Virtanen, "Semi-empirical model for SEGR prediction," *IEEE Trans. Nucl. Sci.*, **60**, pp. 2660–2665, 2013.
4. V.V. Emeliyanov, A.S. Vatuev, V.S. Anashin, "SEGR cross-section analysis in gate oxides of power MOSFETs," Report in All-Russian Conference Stoykost, Lytkarino, June 2014 (in Russian).
5. G.I. Zebrev et al., "Methodology of Soft Error Rate Computation in Modern Microelectronics," *IEEE Trans. Nucl. Sci.*, **57**, pp. 3125–3733, 2010.

TCAD models for ETSOI FET with undoped body

Y. Chaplygin, A. Krasnyukov, T. Krupkina, D. Rodionov

National Research University of Electronic Technology (MIET), Moscow, Russia, ieem@miee.ru

The modern TCAD software [1] has a wide range of physical models for the main parameters of semiconductor devices. One of the most important parameters is the carrier mobility. The existing models take into account the temperature dependence of the mobility, the effect of impurity concentration, the electric field and others. For nanoscale MOSFETs predominance of quasi-ballistic transport mechanisms in the channel violates the classical relationship between the carrier mobility and the saturated drain current. SOI MOSFETs as a key element of various types of integrated circuits with nanoscale design rules needs a properly models for main physical parameters.

MOSFET with undoped fully depleted ultrathin gate region replace conventional CMOS structures on bulk silicon or partially depleted silicon-on-insulator layers at the transition to structures with channel length less than 10 nm. The lack of specific doping in the channel region suppresses the problems associated with the spread of the threshold voltage. The quasi-ballistic model was proposed by M. Lundstrom [2] for the transport processes in such structures. According to this model the drain current of the short-channel transistors at high voltages at the drain is proportional to the rate of carrier injection from the source. As a result, the current in the linear region is determined by the effective mobility, but the current in the saturation region is determined by the effective speed of the carriers. This model requires the special calibration efforts on the basis of I-V and C-V experimental curves for different lengths of the channel [3].

The structure of ETSOI FET with undoped body was investigated by means of TCAD software Synopsys Sentaurus. The simulated structure includes an intrinsic SOI body with thickness 6.1 nm, SiON gate oxide with thickness 1.1 nm. The effective channel length is 30 nm and 50 nm.

Calculations carried out in TCAD, show that the proposed model agrees well with the simulation results on condition that the effect of roughness of the interfaces on the carrier mobility is included [4] for thin layer mobility model [1].

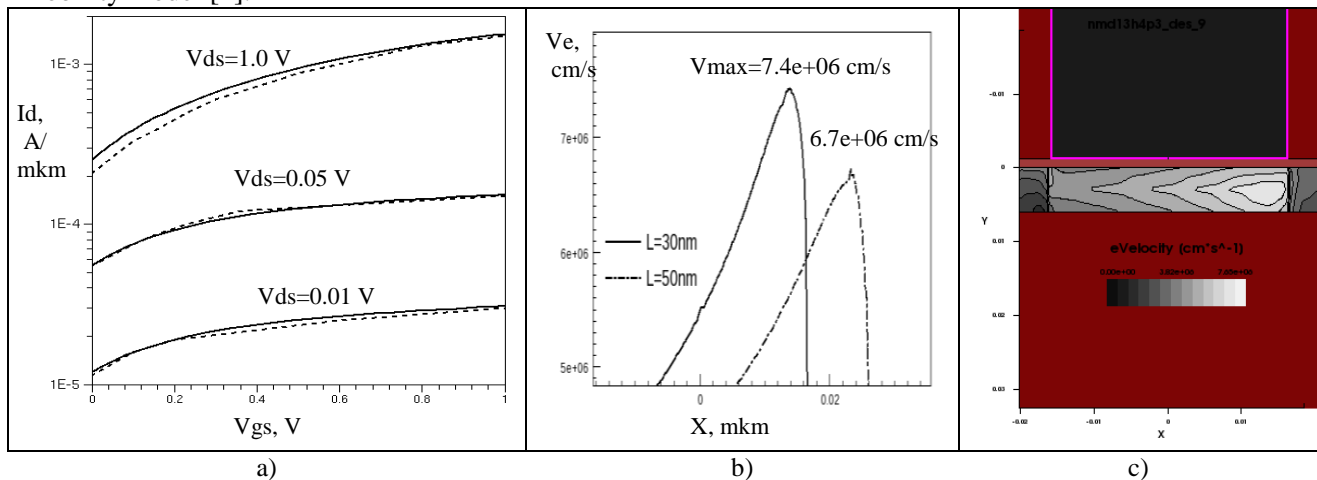


Fig. 1. The results of ETSOI FET TCAD simulation: a – I_d - V_{gs} characteristics, $L = 30$ nm (---experiment [3]); b - electron velocity V_e along the channel near the drain, V_{max} corresponds to V_{x0} [3] ($V_{x0} = 7.8 \times 10^6$ cm/s for $L = 30$ nm, $V_{x0} = 6.7 \times 10^6$ cm/s for $L = 50$ nm); c - the 2D distribution of electron velocity at $V_{gs} = 0.5$ V, $V_{ds} = 0.5$ V, $L = 30$ nm.

1. <http://www.synopsys.com>

2. Lundstrom M. “On the mobility versus drain current relation for a nanoscale MOSFET”. IEEE Electron Device Letters, **22**, pp. 293-295, 2005.

3. Majumdar A., Antoniadis D. “Analysis of carrier transport in short-channel MOSFETs”. IEEE Trans. Electron Devices, **61**, pp. 351-358, 2014.

4. Krupkina T., Rodionov D., Titova I., Shvetz A. “An account of the Si/SiO₂ interface roughness for simulation of nanoscale MOS transistors” Proc. Int. Conf. “Opto-, nanoelectronics, nanotechnology and Microsystems”. Ulyanovsk. 2011, pp. 454 – 455.

Modeling of mobility degradation in electron-irradiated SiGe p-type MOSFETs with different Ge concentration

E.V. Orekhov¹, L.M. Sambursky^{1,2}, R.A. Torgovnikov¹, A.A. Pugachev¹

1. Institute for Design Problems in Microelectronics, Moscow, Russia, eugene.orekhov@gmail.com

2. National Research University "Higher School of Economics," Moscow, Russia, lsambursky@hse.ru

A device-level model for mobility degradation in electron-irradiated SiGe p-type MOSFETs with different Ge concentration is developed in Synopsys Sentaurus TCAD. SiGe p-type MOSFET simulation was performed with account for the said effect; good correlation with measured data is obtained.

SiGe MOSFETs are promising devices for telecommunications, spacecraft electronics and other demanding applications due to their enhanced mobility, intrinsic radiation hardness [0, 0]. Many papers are devoted to simulation of strained MOSFETs [0, 0]; however, device models for SiGe MOSFETs with account for radiation-induced effects have not been proposed. In [0] SiGe p-type MOSFETs with gate dimensions $W/L = 10/0.3 \mu\text{m}$ and different Ge% (in the range 0—30%) were studied experimentally at 2-MeV electron radiation (with fluence in the range $0\text{—}5 \cdot 10^{17} \text{ e/cm}^2$) without bias voltage. Total ionizing dose (TID) effect in threshold voltage shift is very small because of the small oxide thickness; radiation-induced reduction in stress level, which reduces the strain-induced valence band shift [0] and compensates partly the effect of the TID charges is quantified in [0] with data for mobility degradation with increasing fluence.

The corresponding device structure was built in Synopsys Sentaurus TCAD tool. Three different values of Ge% were used for Source/Drain areas with the purpose of setting up the channel strain: 0%, 20%, 30%. Radiation-induced mobility degradation data [0] was linearized with respect to Ge concentration (with 10% maximum error); then relative change of mobility was reconstructed for each device with different Ge% with respect to their respective non-irradiated states (see symbols in Fig. 1). This dependency was approximated with a smooth analytical function of two variables: fluence and Ge% (see Eq. 1 and Fig. 1). Strain-induced mobility enhancement is already accounted for in the device simulation tool, thus this dependency only separately accounts for radiation-induced change:

$$\partial\mu(F, x) = -a_1(x)(1 - \exp(-F \cdot 0.693 \cdot 10^{-17})) - a_2(x)/(1 + \exp(-(F - 3.66 \cdot 10^{17})/0.49 \cdot 10^{17})), \quad (1)$$

where $a_1(x) = 0.067 - 0.1x$ and $a_2(x) = 0.138 + 1.3x - 2.97x^2$ are fitting factors, x is the Ge concentration, a. u., F is the electron fluence, e/cm^2 . Maximum fitting error is 4%. The function of Eq. 1 was introduced into TCAD, and transfer characteristics of a SiGe p-type MOSFET with Ge concentration of 30% were simulated with account for 2-MeV electron irradiation with values of fluence $1 \cdot 10^{17}$, $2 \cdot 10^{17}$, $5 \cdot 10^{17} \text{ e/cm}^2$ (Fig. 2).

This work was supported with Russian Foundation for Basic Research grant 13-07-01030 A.

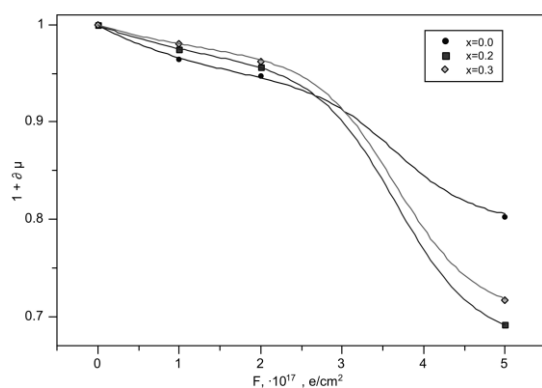


Fig. 1. Radiation-induced relative degradation of mobility for devices with different Ge concentration (symbols – experiment [0], lines – approximation)

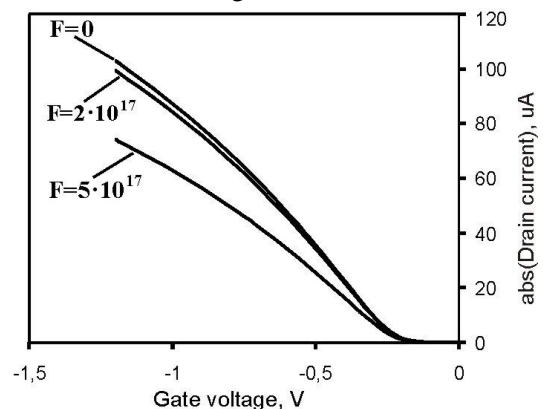


Fig. 2. Simulated transfer characteristics of electron-irradiated SiGe p-MOSFET with $x = 0.3$.

1. K. Rim et al. Electron Devices Meeting, 1995. IEDM'95., International. IEEE, 1995.
2. Kodera, Masako et al. Japanese Journal of Applied Physics, **47** (4S), p. 2506, 2008.
3. E.M. Bazizi et al. IEEE International Electron Devices Meeting (IEDM), pp. 15.1.1 - 15.1.4, 2010.
4. F.K. Khoshkbijari et al. IEEE Intl. Conf. on Semiconductor Electronics (ICSE), pp. 288–292, 2012.
5. T. Nakashima et al., Thin Solid Films **520** (8), pp. 3337–3340, 2012.
6. Claeys, Corneel et al., Solid-State Electronics **52** (8), pp. 1115–1126, 2008.

Modeling and simulation of dose effects in bipolar analog integrated circuits

G.I. Zebrev¹, M.G. Drosdetsky¹, A.M. Galimov¹, A.A. Lebedev¹, I.A. Danilov², V.O. Turin³

1. National Research Nuclear University (MEPhI), Moscow, Russia, gizebrev@mephi.ru

2. Scientific Research Institute of System Analysis, Russian Academy of Sciences, Moscow, Russia

3. State University ESPC, Orel, Russia, voturin@ostu.ru

Linear analog integrated circuits current ΔI_{in} , increases usually monotonically with ionizing dose D . Though, the non-monotonic dose curves $\Delta I_{in}(D)$ behavior is often observed [1, 2], which can not be explained in terms of a simple linear dose model. It was proposed in [3] that peak shaped non-monotonic dose curves are mainly due to circuit effects rather than physical effects occurring in the field isolation oxides. Circuit-related factors and aspects of dose rate degradation in linear ICs from radiation in space are also discussed in [4]. An alternative approach based on a system of non-linear rate equations for the accumulation and annealing of recombination centers and the charge trapped in the oxide ΔN_{ox} of the input bipolar transistor has been proposed in [5]. The system of the rate equations coupled through a dependence of the trapped charge and the oxide electric field E_{ox} has a form

$$\frac{d\Delta I_B}{dD} = F_{rt} \left(\frac{A_S \sigma_r \nu_t W_B}{A_E D_B} \right) \eta_{eff}(E_{ox}) K_g I_C d_{ox} - \frac{\Delta I_B}{P\tau_a}, \quad (1)$$

$$\frac{d\Delta N_{ox}}{dD} = F_{ot} \eta_{eff}(E_{ox}) K_g d_{ox} - \frac{\Delta N_{ox}}{P\tau_b}, \quad E_{ox}(D) = E_{ox0} - \frac{q\Delta N_{ox}(D)}{\epsilon_{ox}\epsilon_0}, \quad (3)$$

where η_{eff} is the effective charge yield, F_{rd} and F_{ot} are the dimensionless efficiencies of recombination center and charged oxide trap generation per a radiation-induced electron-hole pair, P is dose rate, A_S is the area of the base-oxide interface, A_E is the area of the emitter-base junction, D_B is the diffusivity of minority carriers in the base, W_B is the base width, ν_t is the carrier's thermal velocity ($\sim 10^7$ cm/s), σ_r ($\sim 10^{-15} - 10^{-16}$ cm²) is cross-section of carrier's capture on the recombination centers, τ_a (τ_b) is thermal annealing constant for recombination centers (oxide trapped charge), I_C is the dose-independent collector current at which measurements performed. Base input current saturates at $\Delta I_B^{SAT} \propto P\tau_a \eta_{eff}(E_{ox})$. Thereby, if $\tau_b \gg \tau_a$ then the trapped charge keeps increasing after the base current saturation and, consequently, E_{ox} and $\eta_{eff}(E_{ox})$ decreasing. This can lead to non-monotonic dependence of base current. Thus, non-monotonic behavior of dose degradation can be explained by different kinetics of buildup and annealing of recombination centers and oxide trapped charge. Discussion of alternative mechanisms of remarkable non-monotonic dose dependence of input currents of bipolar linear circuits would be presented in a final version of the report.

1. J. Boch, F. Saigne, S. Ducret, R.D. Schrimpf, D.M. Fleetwood, P. Iaconi, and L. Dusseau, "Total dose effects on bipolar integrated circuits: Characterization of the saturation region," IEEE Trans. Nucl. Sci., **51**, pp. 3225–3230, 2004.
2. R.D. Harris, S.S. McClure, B.G. Rax et al., "ELDRS Characterization for a Very High Dose Mission," IEEE Radiation Effects Data Workshop (REDW), 2010.
3. L. Dusseau et al. "Review and Analysis of the Radiation-Induced Degradation Observed for the Input Bias Current of Linear Integrated Circuits," IEEE Trans. Nucl. Sci., **55**, pp. 3174–3181, 2008.
4. H.J. Barnaby et al. "Identification of Degradation Mechanisms in a Bipolar Linear Voltage Comparator Through Correlation of Transistor and Circuit Response," IEEE Trans. Nucl. Sci., **46**, pp. 1666–1673, 1999.
5. G.I. Zebrev, A.S. Petrov et al., "Simulation of Bipolar Transistor Degradation at Various Dose Rates and Electrical Modes for High Dose Conditions," IEEE Trans. Nucl. Sci., **61**, No. 4 (June) 2014.

Estimation Technique for SET-tolerance of Combinational ICs

A. Balbekov¹, M. Gorbunov²

1. *Scientific Research Institute of System Analysis RAS, Moscow, Russia, balbekov@cs.niisi.ras.ru*

2. *Scientific Research Institute of System Analysis RAS, Moscow, Russia, gorbunov@cs.niisi.ras.ru*

Single Event Effects (SEE) caused by ionizing particles are the main source of soft errors in space applications. Ionizing particles induce Single Event Transients (SET) in combinational ICs. SETs become larger treat with scaling to the nanoscale technologies due to effects of single event multiple transients.

There are two approaches to simulate SET: using circuit or technology computer-aided design (CAD) tools. The former is less accurate but most suitable for circuit designer, the latter is the most accurate but also time and computational resources consuming. We describe a characterization technique of each node contribution to the overall SET tolerance of combinational circuit. The technique implies using the tools that are available to a circuit designer (UltraSim, Python, SKILL) and does not require technology CAD.

Characterization procedure requires calculation of the critical charge of each node with regard to SET occurrence and graphical representation of the obtained data. We provide SET simulation with double-exponential current source [1, 2].

SET detector consists of a model circuit, a test circuit and a comparison system. The model circuit and the test circuit have the same design. The comparison system includes XOR elements, RS Flip-Flops and reset signal.

Because of the same design, there is no difference in the output reaction to the same input pattern of the model and test circuits. If SET in the test circuit influences an output, XORs will detect it and write these data to the flip-flops. Characterization system automatically repeats simulation and SET injection for each node in different time points, automatically acquires and processes simulation data.

Input values for the technique are collected charge, pulse shape, SET occurrence time. Pulse shape is intrinsic for a given technology, so the characterization is conducted by varying collected charge and SET occurrence time.

Graphical representation of the characterization data is implemented by the means of custom developed SKILL tool for Cadence Virtuoso. Visualization system acquires characterization data and displays it in the circuit-level CAD. Data are displayed as colored markers near each device of the circuit; color represents arbitrary value of critical charge of the device. Designer can switch between time points (e.g. before/simultaneously/after clock signal) if critical charge varies in different time points marker color will change.

We used the presented technique for comparative study of different SET protection solutions: dual modular redundancy, triple modular redundancy with different types of voters. Description of advantages and disadvantages are also given. Above calculations were made for 0.25 μm SOI.

The developed technique provides an estimation of SET tolerance of combinational circuits. The technique is technology-independent; it can be applied to nanoscale technologies. Visualization system is integrated to the designer's tools and allows graphical representation of characterization data. A designer is able to estimate each node contribution to SET sensitivity and to find the optimal solutions to improve the SET tolerance of the design.

1. G.C. Messenger. "Collection of Charge on Junction Nodes from Ion Tracks", IEEE Tran. Nuclear Science, **29** (6), pp. 2024-2031, 1982.

2. I.A. Danilov, B.V. Vasilegin, P.N. Osipenko. "Method of the automated circuit simulation of effects of heavy charged particle action on the modern CMOS IC". VANT, Lytkarino, Vol. 4, pp. 13-16, 2011 (in Russian).

Simulation of Nanoelectronics Devices in Cognitive Nanoinformatics

V. Shakhnov, L. Zinchenko, E. Rezchikova

Bauman Moscow State Technical University, Moscow, Russia, shakhnov@mail.ru

Nanoelectronics is one of promising application areas in nanotechnology. While other nanotechnology areas are hindered by limitations of knowledge in physics, biology etc., a progress in nanoelectronics is obvious. However, till now nanodevices yield is below 10% [1]. To scalable nanomanufacturing novel approaches to information management in nanotechnology applications are required.

Nanoinformatics focus is on nanodevices simulation, data collection and curation for a comparison of nanomaterials and nanodevices [1-3]. Three categories of nanoinformatics tools have been specified in [2]. The first group is for data collection and curation. The second category is for analysis and simulation and the last group is used for data accessibility and information sharing. We review recent advances in nanoinformatics databases and software tools. We discuss the features of informatics applications in nanomanufacturing enhancement as well.

In [4] the theoretical framework of Cognitive Informatics has been elaborated. The Information (I) – Matter (M) – Energy (E) model has been proposed that it is in line with the design methods proposed by R. Koller [5]. It was shown that cognitive elements improve human-machine interaction because of adaptability and an effective information representation. In [6] the modified Information-Matter-Energy model for Cognitive Nanoinformatics has been proposed. This model takes into account the wave-particle duality and quantum mechanics. In general, the modified model is given as follows:

$$I = \psi(M, E), \quad (1)$$

$$E = f_5(M), \quad (2)$$

$$M = f_6(E), \quad (3)$$

where ψ , f_5 , and f_6 are generic functions. The model considers statistical models of nanodevices in a comparison of the Information-Matter-Energy model [4].

In the paper, we discuss the usage of Cognitive Nanoinformatics to advance manufacturing of nanoelectronics devices. We elaborate that Cognitive Nanoinformatics tools can be used in variation modeling, nanoelectronics devices design, and in metrology research. We propose a multiscale approach to data management to simplify simulation data management. In [7] features of knowledge representation for VLSI and MEMS have been discussed. In the paper, we outline the specific approaches to knowledge representation for nanoelectronics devices simulation based on the modeling with smart little people method [8].

Finally, we conclude that Cognitive Nanoinformatics is a promising area to enhance research in nanotechnology and to use the advantages of e-sciences to advance nanomanufacturing.

1. Q. Huang. "Integrated nanomanufacturing and nanoinformatics for quality improvement," *44th CIRP International Conference on Manufacturing Systems*, 2011.
2. *Nanoinformatics 2020 Roadmap*. Published by the National Nanomanufacturing Network, Amherst, 2011.
3. V.A. Shakhnov, L.A. Zinchenko, "Nanoinformatics: direction of development of information technologies". *Information Technologies and Computing Systems*, **3**, pp. 84 -89, 2012 (in Russian).
4. Y. Wang. "On the informatics laws and deductive semantics of software". *IEEE Transactions on Systems, Man, and Cybernetics (Part C)*, **36**(2), pp. 161-171, 2006.
5. A.I. Polovinkin. *Basics of engineering creativity*. Lan, Moscow, 2007 (in Russian).
6. V.A. Shakhnov, L.A. Zinchenko, E.V. Rezchikova, "Simulation and visualization in cognitive nanoinformatics". *International J. of Mathematics and Computers in Simulation*, **8**, pp. 141-147, 2014.
7. V. Shakhnov, V. Makarchuk, L. Zinchenko, V. Verstov, "Heterogeneous knowledge representation for VLSI systems and MEMS design," *Proc. IEEE CogInfoCom'13*, pp. 189-194, 2013.
8. A.V. Revenkov, E.V. Rezchikova. *The theory and practice of technical problems decision*. Forum, Moscow, 2009 (in Russian).

Optimization of the I-V characteristics of the multi-barrier heterostructures by band engineering method

V. Gergel, A. Verhovtseva, N. Gorshkova, V. Minkin
Kotelnikov Institute of Radio Engineering and Electronics of RAS, Moscow, Russia,
E-mail address: vgergel@mail.ru

The generalized model of electron drift in multi-barrier heterostructures with energy barriers of different heights is proposed. The model is based on quasi-hydrodynamic theory of electron drift in super lattices which was presented recently [1]. Similarly, the multi-barrier heterostructure is considered as a sequence of elementary unit cells which consist of two layers: a narrow-band (doped) layer and the adjacent wide band (undoped) layer [1]. Moreover, the values of the corresponding physical parameters can differ significantly in different elementary volume cells. If we examine the first elementary unit cells (with respect to the direction of electron drift) in the narrow bandgap contact layer (which is relatively extensive). Here the temperature of the electron gas is close to the steady-state value T_1 which corresponds to the local energy balance of Joule heating and thermo-relaxation at a given current density.

This numerical value of T_1 allows us to define the voltage drop across the narrow bandgap contact layer if we use the assumption based on the thermal injecting mechanism of electroconductivity on the heteroboundary with the first wide-band layer. This assumption allows us to define the voltage drop across the wide-band layer and the corresponding increment of the flux density of the electron temperature which enters into the narrow bandgap layer of the second unit cell. In turn, the heat flux flowing into the narrow bandgap layer of the second unit cell is a kind of boundary condition for the corresponding heat equation. The solution of this equation allows us to calculate the electron temperature on the heterojunction boundary of the second unit cell as well as the voltage drop on the second hetero-barrier and corresponding increment of the flux density of the electron temperature which enters into the narrow bandgap layer of the third unit cell, and so on up to the last unit cell. The resulting current-voltage characteristic (I-V curve) is simply obtained by summing up all of the partial voltages from all unit cells. The proposed algorithm realizes the well-known concept of the so-called "band engineering". This concept allows us to optimize the resulting I-V curve using purposeful variations of the physical parameters of the unit cells, which are required for the specific technical applications.

Then, the I-V characteristics of the GaAs/Al_xGa_{1-x}As double-barrier heterostructure are calculated using the proposed approach. Here the height of the second barrier Δ_2 is two times more than the height of the first barrier Δ_1 ($\Delta_2 = 2\Delta_1$, where $\Delta_1 = 0.25; 0.22; 0.2$ eV), and the doping level of the first narrow-band layer ($3 \times 10^{17} \text{ cm}^{-3}$) is three times smaller than it is in the second one (10^{18} cm^{-3}). So, that is clear that even such a simplified double-barrier heterostructure could be successfully used to generate a high frequency electromagnetic radiation when $\Delta_2 = 0.25$. When the values of Δ_2 are relatively small, i.e. Δ_2 is approximately equals to 0.18, then it could be seen that the negative differential resistance disappears, but the current increases dramatically. Such kind of asymmetric heterostructure (at moderately high barriers) could be very promising for the creation of so-called A_{III}B_V circuit technique, in particular for the high frequency rectifying diode elements. This method could be even used to create the transistor elements, but there are needed more complicated technologies for etching and metallization which would help to create an ohmic contact to GaAs layer of the second unit cell.

This work was partially supported by Russian Foundation for Basic Research (research projects No. 12-07-00063a and No. 12-07-00589a).

1. V.A. Gergel, I.V. Altukhov, A.V. Verkhovtseva, G.G. Galiev, N.M. Gorshkova, S.S. Zhigaltsov, A.P. Zelenyi, E.A. Il'ichev, V.S. Minkin, S.K. Paprotskij, M.N. Yakupov. "Analytical model of the electrical instability mechanism in multibarrier heterostructures with tunnel-opaque barriers". *Semiconductors*, **48**, pp. 465-470, 2014.

Effect of emitter spacer layer on high frequency response of resonant tunneling diode taking into account electro-electron interaction

M. Remnev

All-Russia Research Institute of Automatics (VNIIA) Moscow, Russia, m.remnev@yandex.ru.

Resonant tunneling diodes (RTD) are the fastest active semiconductor devices in nanoelectronics. They can be used as generators of the electromagnetic radiation and in super-fast logical devices in nano- and microelectronics. However, characteristics of the devices are still not sufficient for practical applications. The one of the ways of increasing device's characteristics are theoretical investigations and computer simulations.

The present work is devoted to research of the effect of emitter spacer layer size on the linear high-frequency response (the value characterizing the power of generation of electromagnetic radiation) of RTD. Spacer layers were originally grown between doped contacts and the active area (quantum well and barriers) of the device to prevent transfer of impurities into the active area. However, they can significantly affect the device's characteristics. Previously we have shown by means of numerical simulation that the width of spacer layer influences the peak current on I-V curves [1]. It increases when energy level in triangle quantum well, formed in the biased spacer layer, is the same as resonant level in the active area [2]. These works have explained deviations in experiments where increase of spacer width resulted in decrease of peak current [3] or peak current was growing and then decreasing [4]. Further, we showed that tuning of spacer width could extremely increase the response of RTD at resonant frequency [5]. The value we obtained was 70 times higher compared to the case of zero spacer width. These calculations were performed without electron-electron interactions. In [6] we showed that its inclusion suppresses this extreme growth of peak current but it still can be tuned by changing spacer width. We expect that electron-electron interaction will also influence high frequency response of RTD.

In present work we calculated dependencies of linear response on generation frequency at different spacer widths by self-consistent solution of one dimensional Schrödinger and Poisson equations. Electrons in left and right contacts have Fermi distribution and all computational parameters correspond to AlGaAs/GaAs system. It was shown that electron-electron interaction sufficiently decreases linear response and the drop in its value is proportion to suppression of peak current in I-V curves. But it is still possible to significantly increase the high-frequency response at resonant frequency (and consequently then power of generation) by careful tuning of emitter spacer width. We obtained increase by the factor of four of response compared to the case of zero spacer width. Moreover, at certain spacer widths we observed two peaks in frequency dependence of response. It is due to particular difference of energy levels in quantum well and spacer layer. The greatest increase of high-frequency response is achieved at spacer width when energy level in emitter spacer coincides with that in quantum well.

1. M. Remnev, I. Kateev, and V. Elesin. "Effect of spacer layers on current-voltage characteristics of resonant-tunneling diode". *Semiconductors*, **44**, pp. 1034-1039, 2010.
2. V. Elesin and M. Remnev. "Effect of the emitter spacer level on the peak current of resonant tunneling diode", *Nanotechnologies in Russia*, **8**, pp. 250-254, 2013.
3. Zang Yang et al. "Influence of space layer thickness on the current-voltage characteristics of pseudomorphic AlAs/In_{0.53}Ga_{0.47}As/InAs". *Chinese Physics B*, **17**, pp. 1472-1474, 2008.
4. T. Daniels-Race and S. Yu. "Effect of spacer layer thickness on tunneling characteristics in asymmetric AlAs/GaAs/AlAs double barrier structures". *Solid-State Electronics*, **38**, pp. 1347-1349, 1995.
5. M. Remnev, I. Kateev, and V. Elesin. "The effect of spacer layers thickness on high-frequency properties of resonant tunneling diode". *Nuclear Physics and Engineering*, **1**, pp. 560-565, 2010.
6. V. Elesin, M. Remnev, and I. Kateev. "Modelling of the influence of interelectronic interaction on the stationary characteristics of a resonant tunnel diode with spacer layers". *Russian Physics Journal*, **52**, pp. 1186-1192, 2009.

Resonant tunneling multiple quantum well structures in p-i-n photovoltaic element

M.P. Telenkov^{1,2}, Yu.A. Mityagin^{1,3}, G.N. Zhuchkov²

1. P.N. Lebedev Physical Institute, Moscow, Russia, maxim_telenkov@mail.ru

2. National University of Science and Technology (MISiS), Moscow, Russia, maxim_telenkov@mail.ru

3. National Research Nuclear University (MEPhI), Moscow, Russia, yumityagin@mail.ru

The embedding of the quantum confined structures into the active area of the semiconductor photovoltaic elements is one of the possible ways to increase a radiation-to-current conversion effectiveness by photo-excitation of the electrons and holes due to an additional intersubband absorption of the long wavelength part of the solar spectrum. A considerable expansion of the absorption spectrum can be achieved by the use of rather deep quantum wells, where the efficiency of the thermal ionization rapidly decreases. In this situation it is important to provide an effective mechanism of photoexcited carrier separation and their fast transfer from quantum wells to prevent their recombination.

Here a method is proposed of an effective separation of the photoexcited charge carriers based on the resonant tunneling effect in multiple quantum well structure embedded into the i-layer of the p-i-n photovoltaic element [1]. A specific design of a quantum well structure is developed providing the resonant tunneling transport channel not only for electrons but also for photoexcited holes in the intrinsic electric field of p-i-n junction.

A microscopic model of the resonant tunneling in quantum well structures is developed [1]. The model takes into account optical and acoustical phonon scattering processes as well as an interface roughness scattering. The kinetic tunneling times were calculated for $\text{Ga}_{1-x}\text{In}_x\text{As}$ and $\text{Ga}_{1-x}\text{Al}_x\text{As}$ based structures as a function of the structure parameters. A possibility was shown to achieve tunneling times of tens picoseconds - much shorter than recombination times (hundreds picoseconds), thus providing an effective transfer of the photoexcited electrons and holes from quantum wells into continuum and their contribution to a total photocurrent.

This work was supported by the RFBR (project 12-02-00564) and NUST «MISiS» (grant no. 3400022).

1. M.P. Telenkov, Yu.A. Mityagin, "Resonant tunneling multiple quantum well structures in p-i-n photovoltaic element", Bulletin of the Lebedev Physics Institute, **40** (12), pp.32-42, 2013.

Peculiarities of sub-THz wave rectification by resonant tunneling semiconductor nanostructures at zero bias voltage

V. Kapaev^{1,2}, V. Murzin¹, S. Savinov¹, V. Egorkin²

1. P.N. Lebedev Physical Institute of the Russian Academy of Sciences, Moscow, Russia, s.a.savinov@gmail.com

2. National Research University of Electronic Technology (MIET), Moscow, Zelenograd, Russia

The modern solid state electronics is in need of compact high-sensitivity room-temperature detectors for sub-THz and THz frequency range. The diode nonlinear elements, like a Schottky barrier diode, which are commonly used at present for direct wave rectification in microwave range, become to be less effective at higher frequencies. Rectification at zero bias is especially attractive due to circuit layouts simplification and shot noise reduction [1]. Resonant tunneling diode (RTD), which is characterized by electron transient times less than 1 ps, looks much promising as candidate for sub-THz zero-bias detector [2], in particular in a case of specially asymmetric RTD heterostructures that provide strongly nonlinear current-voltage characteristic.

The present work is devoted to detailed analysis of peculiarities of microwave rectification effect in RTD nanostructures at zero bias voltage with the purpose of increase the sensitivity of detector elements based on RTD in sub-THz frequency range. The investigations of RTD nonlinear properties are carried out on the base of coherent model of resonant-tunneling under external electromagnetic field and numerical solution of Schrödinger equation implying to $\text{In}_{0.53}\text{Ga}_{0.47}\text{As}/\text{AlAs}$ single-quantum-well double-barrier (DBRTS) and double-quantum-well triple-barrier (TBRTS) heterostructures [3]. In this paper we consider only the case that the photon energy $\hbar\omega$ is smaller than quantum-well resonant level width Γ , that means the time-dependent Schrödinger equation turns into stationary form and the rectification currents are fully determined by the stationary current-voltage curves $I_0(V_{dc})$. The calculations are performed for RTD structures with different configuration both for relatively low external AC field intensities, when the DC current changes ΔI_0 are proportional to the second derivative d^2I_0/dV_{dc}^2 , and for high AC amplitudes reaching the negative differential conductivity region. The issues of creation possibilities of DC current asymmetry in DBRTS and TBRTS are examined. The optimal DBRTS and TBRTS structural parameters in the view of highest curvature of RTD current-voltage characteristics at $V_{dc} = 0$ are evaluated. It is shown that the optimal TBRTS are by an order of magnitude more effective than DBRTS for detection of a weak sub-THz radiation.

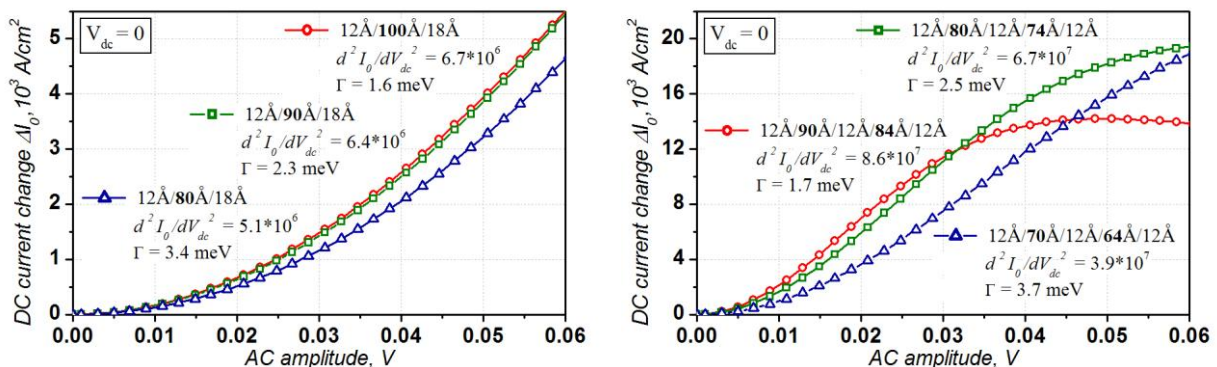


Figure 1. The calculated DC current changes ΔI_0 depending on AC amplitude for some optimal DBRTS (left) and TBRTS (right) at $V_{dc} = 0$ with the second derivatives d^2I_0/dV_{dc}^2 (in $\text{A} \cdot \text{V}^{-2} \text{cm}^{-2}$) and resonant level widths Γ showing.

The research was supported by RFBR (grant № 14-02-00658), MES of Russia (ass. № 2014/101).

1. L. Liu, J. Hesler, H. Xu, et al. "A Broadband Quasi-Optical Terahertz Detector Utilizing a Zero Bias Schottky Diode". IEEE Microw. Wireless Compon. Lett., **20**, pp. 504–506, 2010.
2. S. Takahagi, H. Shin-ya, K. Asakawa, et al. "Equivalent Circuit Model of Triple-Barrier Resonant Tunneling Diodes Monolithically Integrated with Bow-Tie Antennas and Analysis of Rectification Properties towards Ultra Wideband Terahertz Detections", Jpn. J. Appl. Phys., **50**, pp. 01BG01-1–01BG01-5, 2011.
3. V.V. Kapaev, Yu.V. Kopaev, S.A. Savinov, V.N. Murzin, "High-Frequency Response and the Possibilities of Frequency-Tunable Narrow-Band Terahertz Amplification in Resonant Tunneling Nanostructures", J. Exp. Theor. Phys., **116**, pp. 497–515, 2013.

Conducting media with spatial dispersion in a microwave field: eigenvalue problem for permittivity operator

M.A. Dresvyannikov¹, A.P. Chernyaev², A.L. Karuzskii¹, Yu.A. Mityagin¹, A.V. Perestoronin¹,
N.A. Volchkov¹

1. P. N. Lebedev Physical Institute of Russian Academy of Sciences, Moscow, Russia, karuz@sci.lebedev.ru

2. Moscow Institute of Physics and Technology (State University), Dolgoprudny, Moscow District, Russia

An increase of the mean free path length of the current carriers up to values greater than the penetration depth of electromagnetic field leads to domination of the spatial dispersion in the response of cooled conductors [1-3]. The effects that depend on spatial parameters, besides of the obvious interest to such effects especially in structures with small (micro and nano) sizes or low dimensionality and of the importance in simulation and modeling of micro- and nanoelectronic devices [4], open the possibility of investigation of conductivity in novel materials. Microwave effects of the spatial dispersion allow to study the properties of carriers and pairing mechanisms in superconductors, including high- T_c superconductors. To deduce this information a description of the surface impedance of conducting media should be in satisfactory agreement with experimental data. Complications in frames of the microscopic model are always arisen and in a large extent result from use of the constitutive equation that relates the current density and the field in metal, and is deduced on the rigorous base of the linearized Boltzmann equation [1-3]. Such sophistication of a theoretical description and absence of an illustrative and clear physical view of transport processes enhance a peril of losses of additional or novel solutions. So the fact that quantitative kinetics theory [1-3] has given an explanation of the results [5] does not ensure generally an explanation of the results obtained under slightly different experimental conditions [6, 7]. Microwave effects of the spatial dispersion have been considered recently in [8] and rather general relation has been established there between the eigenvalue $\tilde{\varepsilon}_a$ of the total permittivity operator $\hat{\varepsilon}_a$ and the surface impedance \tilde{Z} . It corresponds with the usual expression for a transverse wave propagating into a conductor without dispersion $\tilde{Z} = (\mu_0 / \tilde{\varepsilon}_a)^{1/2}$. Substitution of the eigenvalue of permittivity operator into the Maxwellian field-stress tensor, which determines the Abraham force [1, 2], results to conditions of spatial-type force resonances. The obtained resonances include a particular solution corresponding to anomalous skin effect value of the complex surface impedance $\tilde{Z} = R + iX$ with the phase of $\pi/3$.

The eigenvalue problem for permittivity operator is considered below generally. Conducting media with spatial dispersion may be described formally by the single operator - operator of dielectric permittivity, which completely defines the microwave response of conductors with spatial dispersion [1,2]. A wave problem is formulated to search the solutions, which correspond to the eigenvalues of permittivity operator, similar to the problem of wave propagation in hollow waveguides and resonators. Dispersion relations and general solutions are obtained. Significant role of the spatial-type force resonances is considered. Conditions for the spatial resonances are derived. The obtained resonances include particular solutions corresponding to surface impedance for anomalous skin effect, surface impedance of superconductor, as well as four novel solutions, obviously related to polarization, two of which correspond to the waves with amplitude increasing into the depth of conductor, and two else describe solutions with unusual properties.

This research was supported by Grants RFBR (14-02-00658), by Grants RAS (24, IV.12 and III.7).

[1] L.D. Landau and E.M. Lifshiz. *Theoretical Physics* Vol 8; Vol 10, Nauka, Moscow, 1992 [in Russian].

[2] V.P. Silin and A.A. Rukhadze. *Electromagnetic Properties of Plasma and Plasma-Like Media*. Gosatomizdat, Moscow, 1961 [in Russian].

[3] G.E.H. Reuter and E.H. Sondheimer. "The Theory of the Anomalous Skin Effect in Metals". Proc. Roy. Soc. A, **195**, pp. 336-364, 1948.

[4] A. Satou at al., "Theoretical study of terahertz plasma instability in asymmetric double-grating-gate transistor structures". ICMNE 2012, *Book of Abstracts*, p. O1-05, Moscow - Zvenigorod, Russia, 2012.

[5] A.B. Pippard. "The surface impedance of superconductors and normal metals at high frequencies. II. The anomalous skin effect in normal metals". Proc. Roy. Soc. A, **191**, pp. 385-399, 1947.

[6] A.S. Shcherbakov at al., "Giant absorption of high-frequency electromagnetic field power in high-temperature superconductors". Fiz. Met. Met., **64**, pp. 735-741; pp. 742-746, 1987 (in Russian).

[7] A.P. Chernyaev at al. "Retardation effect in microstrips and microwave detection of spatial dispersion in superconductors". J. Phys. Chem. of Solids, **69**, pp. 3313-3316, 2008; Physica C, **282**, pp. 1585-1586, 1997.

[8] N.A. Volchkov at al., "Additional microwave modes in systems with conductivity of metals and superconductors". JETP, **111** pp. 292-297, 2010; J. Phys.: Conf. Ser., **400** pp. 022048-1-022048-5, 2012.

Molecular dynamic simulations of free vibrations of metallic nanocantilever

A.N. Kupriyanov, O.S. Trushin, I.I. Amirov

Institute of Physics and Technology (Yaroslavl Branch), RAS, Yaroslavl, Russia, ildamirov@yandex.ru.

Nanocantilevers are widely used as sensor elements in MEMS and NEMS [1]. Frequencies of their free vibrations are located in the range of several GHz. Understanding of vibrational properties of these systems is important for achievement of the best performance characteristics in many applications. Theoretical studies of vibrations of nanocantilevers are usually done in the framework of continuum elastic media theory. However due to gradual shrinking of geometrical sizes of modern nanocantilevers it became important to achieve atomic level resolution in description of its vibrations. Natural choice for such studies is molecular dynamic simulation. This method allows one to simulate time evolution of systems containing up to several million atoms with femtosecond resolution using semiempirical potentials. Recently MD simulations of nanowires have attracted new interest in this area of research [2, 3].

In this work free vibrations of copper nanocantilevers ($l = 16.4$ nm, $t = 3.0$ nm) have been studied using molecular dynamics simulations with Embedded Atom Method [4] potentials. Geometry of our model is shown at fig.1a. Copper nanowire with cross section of $30 \times 30 \text{ \AA}^2$ and length of 164 \AA has been fixed from one side to the substrate with sizes $70 \times 70 \text{ \AA}^2$. Total number of atoms in the model was 22048. At the beginning all atoms had coordinates in space according to FCC(100) lattice.

Initial state of the system has been prepared by relaxation of the sample using MD cooling method. After minimal energy state has been achieved the nanorod was deflected as schematically shown in the fig. 1a with maximal amplitude of 5 \AA . Starting from that state the system was released to evolve according to classical Newton mechanics using NVE ensemble of molecular dynamics. To characterize free vibrations of the system several methods may be used: 1) by observing time evolution of potential energy of the system, 2) by observing time evolution of the spatial labels located in different places of the nanorod. While the first method of characterization is widely used in literature [2, 3], the second one (in our opinion) gives much more complete information about vibration modes. In Fig.1b we show typical dependence of X coordinates of the spatial labels on time.

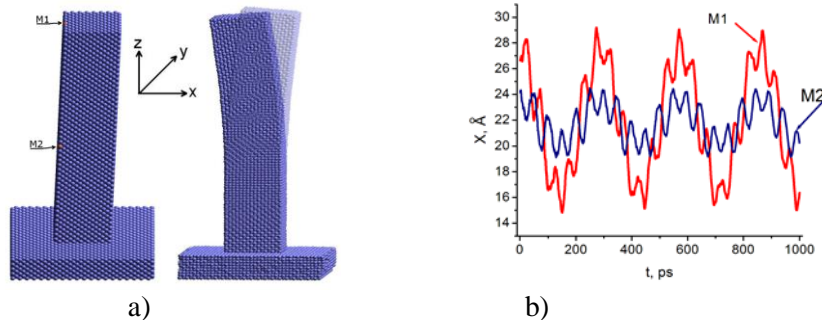


Fig.1 Typical geometry of nanocantilever used in the simulations (a) and time dependence of X coordinates of spatial labels (M1 –located at free end of the nanowire, M2 – in the middle of it) (b).

In conclusion we presented the results of MD simulations of free vibrations of copper nanocantilever. Our study showed complex character of vibration of such system where mixture of different vibrational modes takes place. This study might be useful for interpretations of experimental observations for nanoresonators.

1. K. Eom, H.S. Park, D.S. Yoon, T. Kwon. “Nanomechanical resonators and their applications in biological/chemical detection: Nanomechanics principles”, *Physics Reports*, **503**, pp. 115–163, 2011.
2. S.Y. Kim, Y.S. Park “Utilizing mechanical strain to mitigate the intrinsic loss mechanisms in oscillating metal nanowires”, *Phys. Rev. Lett.*, **101**, pp. 215502(1-4), 2008.
3. H.F. Zhan, Y. Gu. “A fundamental numerical and theoretical study for the vibrational properties of nanowires”, *J. Appl. Phys.*, **111**, pp. 124303(1-9), 2012.
4. S.M. Foils, M.I. Baskes, M.S. Daw. “Embedded-atom-method functions for the fcc metals Cu, Ag, Au, Ni, Pd, Pt, and their alloys”, *Phys. Rev. B*, **33**, pp. 7983-7990, 1986.

Simulation of eigen frequencies and MEMS switches voltage in response to changes in their geometric dimensions and parameters of the material

K.V. Lebedev, V.F. Lukichev

Institute of Physics and Technology, Moscow, Russia; E-mail: kiriklebov@gmail.com

Cantilever (a beam one end of which is attached) is one of the main moving elements of micro- and nanoelectromechanical systems (MEMS and NEMS). A wide class of MEMS/NEMS is switches among which the most widespread device is one with an electrostatic actuation mechanism. One of the disadvantages of electromechanical keys is high voltage operation. Therefore, the development of MEMS/NEMS switches with low voltage operation is an important task.

The aim of this study is the modeling of the eigen frequencies of silicon and tungsten cantilevers depending on the change of the geometrical dimensions and electrostatic analysis to improve performance MEMS switches, to increase the reliability of MEMS switches, and to reduce their energy consumption.

Modeling of the cantilever and the MEMS switches was performed in the program COMSOL Multiphysics 3.5a. The built-in MEMS module, specially designed for simulation of various MEMS/NEMS finite elements was used.

This report presents the results of modeling of changes in natural frequencies of oscillation of the MEMS cantilevers made from polycrystalline silicon and tungsten depending on changes in their geometric dimensions such as length (in the range of 1 μm -500 nm), the width (in the range from 100 to 200 nm), and height (in the range from 100 to 500 nm). Simulation of eigen frequencies of oscillation when the change of Young's modulus of polycrystalline silicon (in the range 140 to 190 GPa) and tungsten (in the range 300 to 500 GPa) was also carried out.

Four vibrational modes of the cantilever, the resonance frequency, the calculated quality factor of the cantilever were identified. Also this report presents the results of modeling of the actuation of polysilicon and tungsten MEMS switches, the optimal voltage actuation of the switches depending on changes in their geometric dimensions such as length cantilever (in the range 1 μm to 3 μm), the height of the epitaxial layer (in the range 500 nm to 1 μm), the size of the control electrode.

It is the author's opinion that the data presented are of interest to improve the performance of MEMS switches, to increase the reliability of MEMS switches, and to reduce their energy consumption.

References

1. T.-H. Lee, S. Bhunia, M. Mehregany. "Electromechanical Computing at 500°C with Silicon Carbide", *Science* **329**, pp. 1315-1319, 2010.

An Estimation of the Thermal Distribution in Silicon Field Emitter

A. Levitskiy

Siberian Federal University, Krasnoyarsk, Russia, ALevitskiy@sfu-kras.ru

The testimony of the undiminished interest to applications of a field emission in microelectronics is creation of new vacuum microelectronic devices [1-4]. However one of the most important questions still has reliability of field emitters. Big density of current in the emitter (to 10^6 A/cm² and more) can lead to damages because of a strong heating. It is confirmed by that the failed emitters often have "thawing" signs. In many cases of damage of field emitters remain badly predicted [5].

In this work the thermal effects in silicon field emitters are analyzed. A traditional version of semiconductor field emission structure, based on silicon cone was analyzed (Figs. 1, 2).

The results of modeling correspond to the general ideas of temperature distribution in the field emitter. The greatest heating is observed at emitter top owing to the high density of current. Since some value of current the sharp growth of temperature of the emitter is observed (Fig. 2).

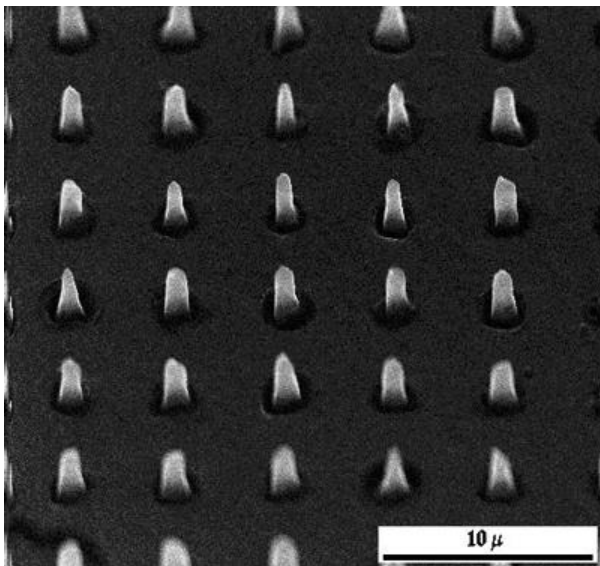


Fig. 1. Scanning electron micrographs emitters [6].

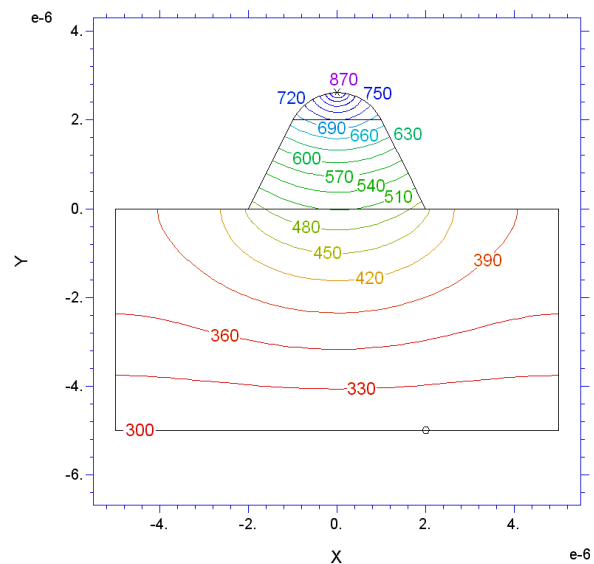


Fig. 2. Thermal Distribution in the emitter cone.

The accounting of Nottingham effect, heterogeneity of electric field and volume charge static distributions in the semiconductor, and dependences of kinetic characteristics of charge carriers on them bring noticeable specifications.

1. G.N. Fursey. *Field Emission in Vacuum Microelectronics*. Kluwert Academic / Plenum Publishers, 2005.
2. Cho, et al. "Vacuum field transistor". US Patent № 6437360 B1, 2002.
3. L.D. Karpov. "Karpov's vacuum transistor". Patent 2089004 RU, 1997.
4. J.-W. Han, J. S. Oh, and M. Meyyappan. "Vacuum nanoelectronics: Back to the future?—Gate insulated nanoscale vacuum channel transistor". *Appl. Phys. Lett.* **100**, 213505 (pp.1-4), 2012.
5. M.G. Ancona. "Modeling of thermal effects in silicon field emitters. Technical Digest of 8th Int. Vacuum Microelectronics Conference, Portland, OR, 61 (pp.1-5), 1995.
6. A.P. Genelev, A.A. Levitskiy, V.S. Zasevskov. "Field Emission Structure with Schottky-Barrier Electrode". *Mat. Res. Soc. Symp. Proc.* **621**, R.5.6 (pp. 1-4), 2000.

Software package for the modeling of quantum circuits in terms of quantum operations

Yu.I. Bogdanov^{1,2,3}, A.Yu. Chernyavskiy^{1,4}, D.V. Fastovets^{1,2}

1. Institute of Physics and Technology RAS, Moscow, Russia.

2. National Research University of Electronic Technology (MIET), Moscow, Russia.

3. National Nuclear Research University (MEPhI), Moscow, Russia.

4. Lomonosov Moscow State University, Moscow, Russia.

The modeling of noisy quantum gates is an important task for quantum computing. The next step is to simulate not only the single gates, but also whole quantum circuits, and this work is devoted to the software package that solves this task in terms of quantum operations.

Different mathematical representations of quantum operations are used: Kraus operators, Choi-Jamiolkowski isomorphism and evolution matrix. This approach leads to the speed-up of computations and more effective memory usage. Another feature of the package is the separation of big algebraic computations, which will be helpful for the future supercomputer realization.

The implemented software was used to simulate and analyze some simple error correction codes and QFT (Quantum Fourier Transform).

This work was supported in part by Russian Foundation of Basic Research (projects, 13-07-00711, 14-01-00557), and by the Program of the Russian Academy of Sciences in fundamental research.

The analysis of the accuracy of quantum tomography protocols

Bogdanov Yu.I.^{1,2,3}, Chernyavskiy A.Yu.^{1,4}, Gavrichenko A.K.¹, Somova M.I.⁴

1. Institute of Physics and Technology RAS, Moscow, Russia

2. National Research University of Electronic Technology (MIET), Moscow, Russia

3. National Nuclear Research University (MEPhI), Moscow, Russia

4. Lomonosov Moscow State University, Moscow, Russia

Quantum tomography is the main method to estimate the quality of quantum information technologies. In this work, on the basis of the universal statistical distribution we analyze the accuracy of the statistical reconstruction of arbitrary quantum states. Using the random mutations algorithm and supercomputer “Lomonosov” we calculate the maximal losses for the wide range of quantum tomography protocols.

This work was supported in part by Russian Foundation of Basic Research (projects, 13-07-00711, 14-01-00557), and by the Program of the Russian Academy of Sciences in fundamental research.

Comparison of different methods of quantum tomography based on photon registration

Yu. I. Bogdanov^{1,2,3}, G.V. Avosopyants², T.V. Shepitko³

1. Institute of Physics and Technology, Russian Academy of Sciences, 117218, Moscow, Russia

2. National Research University of Electronic Technology (MIET), 124498, Moscow, Russia

3. National Research Nuclear University (MEPhI), 115409 Moscow, Russia

In present paper, we consider the problem of finding a method to effectively plan and execute statistical reconstruction of quantum states by collecting and analyzing photon count data. It is demonstrated that the inverse Radon transform while being important from a historical standpoint is not completely rigorous and reliable for the reconstruction of quantum states. We have developed an alternative method of reconstruction based on the root approach to the problem. Tomography based on the root approach suggests that instead of evaluating the density matrix of a quantum state, we consider the square root of it (hence the name of the method). We have shown that the new approach includes strict quantitative criteria of adequacy and completeness of the statistical inverse problem, and provides a simple and reliable way to estimate the error of the reconstructed quantum state.

This work was supported in part by Russian Foundation of Basic Research (project 13-07-00711), and by the Program of the Russian Academy of Sciences in fundamental research.

Continuous-time fermionic quantum walks

A. Melnikov¹, L. Fedichkin^{1,2,3}

1. *Institute of Physics and Technology, Russian Academy of Sciences, Moscow, Russia, melnikov@phystech.edu.*

2. *Moscow Institute of Physics and Technology (State University), Dolgoprudny, Russia, leonid@phystech.edu.*

3. *NIX, Moscow, Russia, leonid@nix.ru.*

We study quantum walks of identical particles on graphs. Due to numerous advantages for the quantum information processing purposes, the interest to quantum walks have been increased recently [1]. Apart from quantum information applications, quantum walks may explain the energy transfer within photosynthetic systems [2] and provide the speedup to active learning agents [3].

There are several ways to specify quantum walks, in this work the walks under consideration are continuous-time that are governed by the time-independent Hamiltonian

$$H = \Omega \sum_{i=0}^{N-1} (|x_{i+1}\rangle\langle x_i| + |x_i\rangle\langle x_{i+1}|),$$

where x_i is the coordinate of the node i with the total number of nodes N and Ω is the hopping amplitude. It was shown that one-particle continuous-time quantum walk of the described form could perform any quantum computation and the necessary gates were provided [4].

In universal quantum computation implementation by one-particle quantum walk the number of components scales exponentially with the number of encoded qubits. One can reduce the number of components by using two particles in the quantum walk. One way of realizing the two-particle quantum walk is by two electrons tunneling between the coupled quantum dots in Si or SiGe [5]. Semiconductor quantum dots are promising elements for quantum computation, but decoherence is a significant obstacle. The decoherence process of a one-particle state in this system was studied in [6] and we study it further by considering two interacting fermions. The interaction causes the quantum correlations between the electrons, i.e. qudits become entangled. We investigate the entanglement dynamics in the realistic scenario of decoherence presence. The proposed scheme for two-particle quantum walk could be used for entangling gates construction.

1. S.E. Venegas-Andraca. *Quantum Information Processing* **11**, pp. 1015-1106, 2012.

2. G.S. Engel et al. *Nature* **446**, pp. 782-786, 2007.

3. G.D. Paparo, V. Dunjko, A. Makmal, M.A. Martin-Delgado, H.-J. Briegel. *Phys. Rev. X* **4**, 031002, 2014.

4. A.M. Childs. *Phys. Rev. Lett.* **102**, 180501, 2009.

5. A.Yu. Vasiliev and L. Fedichkin. *Quantum Information Processing* **13**, pp. 1893-1905, 2014.

6. D. Solenov and L. Fedichkin, *Phys. Rev. A* **73**, 012313, 2006.

Author Index

Ablayev F.	qL1-02	Belova N.	O2-08
Ablayev M.	qL1-02	Berdnikov A.E.	P2-06
Abramov I.I.	O3-09	Beterov I.I.	q1-03
Adelmann C.	L1-01	Blagov E.V.	P1-12
Agafonov V.V.	O3-11	Blanc W.	P1-18
Akhmedova N.	P1-20	Blinov G.	p2-17
Ala-Nissila T.	O3-16	Bogdanov Yu.I.	q3-01, q3-02, q3-03, q3-04, q3-05, P2-36, P2-37, P2-38
Aleshin A.N.	O1-04	Bogdanova N.A.	q3-03, q3-05
Alexeev A.N.	S1-05, O1-05	Bogoyavlenskaya E.	P1-01, P1-02
Alimov G.	P2-18	Boltalin A.I.	P1-22
Allman D.D.J.	O2-08	Bömmel J.	L1-01
Alvarez-Hérault J.	O1-07	Borgardt N.I.	P1-04
Amirov I.I.	P2-33	Borgardt V.	P1-11
Amitonov S.V.	O1-23, P2-02	Borshchevskaya N.	q2-09
Andreeva C.	q1-03	Borzdov A.V.	P2-19
Antonenko A.H.	O1-22, O2-09, P1-13	Borzdov V.M.	P2-19
Antonov A.	P2-20	Borzenkova O.	O3-04
Antonov V.N.	O1-20	Boyko A.	O1-10
Aristov V.V.	q3-09	Bozhjev I.V.	P1-33, P1-34, P2-05
Artamonova E.	P2-21	Bruk M.A.	P1-26
Arzhanova N.	P1-35	Burlakov A.V.	O1-21
Asadov M.	P1-19, P1-20	Burmistrova A.V.	O1-19
Avosopyants G.V.	P2-38	Bykov V.A.	S1-06
Babich A.	O2-01	Byrnes T.	q2-05
Baklanov M.R.	O1-11, O1-12	Chaly V.P.	S1-05, O1-05
Bakurskiy C.B.	O1-16, O1-17, O1-18	Chaplygin Yu.A.	P1-32, P2-23
Balbekov A.	P2-26	Cherkov A.G.	O2-09
Bantysh B.I.	q3-01, q3-02	Cherkova S.	O1-22
Barabanenkov M.Yu.	O2-10	Chernikh A.V.	O1-06, O1-21
Barabanenkov Yu.N.	O2-10	Chernomordick V.D.	P2-06
Barabanova N.	P2-08	Chernyaev A.P.	P2-32
Belinsky L.V.	q3-04	Chernyavskiy A.Yu.	q3-01, q3-02, P2-36,
Belov A.N.	P1-24, P1-25		

Author Index

	P2-37	Entin V.M.	q1-03
Choutov D.	O1-07	Exarchos M.	O1-20
Chuev M.	L2-05	Fastovets D.V.	P2-36
Constantinian K.I.	P1-23	Fedichkin L.	P2-39
Croes K.	L1-01	Fel'dman E.B.	q1-01, q2-03, q2-04
Dagesyan S.A.	P2-01, P2-02	Filippov S.	q1-05, q2-02
Danilkin E.	O1-07	Fomin L.	O1-06
Danilov I.A.	P2-25	Francois-Saint-Cyr H.	P1-18
Denisenko M.	O3-10	Friman A.	P1-16
Denisenko Yu.	P1-01, P1-02	Galiev G.B.	O1-04
Devyatov I.A.	O1-19	Galimov A.M.	P2-25
Divochiy A.	q3-10	Galkov M.S.	P1-13
Dolgovykh Yu.	P2-17	Gavrichenko A.K.	P2-37
Dolotov P.	P2-20	Gavrilin I.	P1-15
Doncova A.	P1-11	Gavrilov S.A.	O1-02, O2-11, P1-17, P1-24, P1-25
Doronin S.I.	q2-04	Gavrushina M.L.	O1-08
Dresvyannikov M.	P2-12, P2-32	Genkin M.	O1-07
Dronov A.	P1-15, P1-17	Gerasimenko A.Y.	P1-12
Drovosekov A.	P1-10	Gergel V.	P2-28
Drozdetsky M.G.	P2-25	Gismatulin A.A.	O1-22, O2-09
Dubkov S.	P1-11	Goldstein R.V.	P1-37
Ducruet C.	O1-07	Goltsman G.	q3-10
Dudin A.A.	P1-07	Golubov A.A.	O1-16, O1-18
Dutta S.	L1-01	Gorbatsevich A.A.	O3-03
Dyakonov I.	q2-09	Gorbunov M.	P2-20, P2-26
Dyakonova N.	O2-04	Gorshkova N.	P2-28
Efremov A.	P1-27	Granato E.	O3-16
Egorkin V.	P2-31	Greenwood B.	O2-08
Egorov K.	O2-06	Grishina Y.S.	P1-04, P1-11
Elezov M.	q3-10	Gromov D.G.	O2-02, O2-11, P1-04, P1-07, P1-11
Elshocht S. van	L1-01	Guillermier C.	P1-18
Emeliyanov V.V.	P2-22	Gurtovoi V.L.	O1-20, O1-21, q3-07
Emelyanov A.	O2-03		

Author Index

Gusev V.N.	P2-06	Kitsuk E.P.	P1-12
Gushin O.	O3-04	Klenov N.V.	O1-16, O1-17, O1-18, P2-09
Haase M.	L1-02	Klimenko O.A.	O2-04
Holevo A.S.	qL1-01, q3-01	Klyuchnikov A.	P2-21
Hombourger C.	P1-18	Knap W.	L2-04, O2-04
Hübner M.	L1-02	Kochubey S.A.	P1-13
Ichkitidze L.P.	O1-08, P1-12	Köhler N.	L1-02
Ignatiev F.Yu.	q3-05	Kokin A.A.	q1-02
Il'ichev E.	O1-17	Kokin V.A.	q1-02
Ilin A.I.	O1-21	Kolomejtseva N.V.	O3-09
Il'nitsky M.A.	L2-02	Konoplev B.	O3-10
Iñiguez B.	O3-01	Korobova N.	P1-03, P2-17
Isaeva A.	P2-15	Koroleva O.M.	P2-07
Iskakov R.	P1-03	Kovalyuk V.	q3-10
Ivanenko I.P.	O1-13	Kovyrkin P.	O1-10
Ji Y.	q2-05	Kozyukhin S.	O2-01, O2-02
Kalnov V.A.	O1-13, P1-08, P1-26	Krasyukov A.Yu.	P2-21, P2-23
Kamaev G.N.	O1-22, O2-09, P1-13, P1-14	Krasnoborodko S.Y.	S1-06, P1-32
Kapaev V.	P2-31	Krasovitsky D.M.	S1-05, O1-05
Kapelnitsky S.	P1-10	Kravtsov K.S.	qL1-04
Karminskaya T.Yu.	O1-16	Kravtsova V.	P1-03
Karuzskii A.	P2-11, P2-12, P2-32	Kreines N.	P1-10
Kataeva T.S.	O3-03	Kremer E.	S1-04
Katamadze K.	q2-09	Krishtab M.	O1-11, O1-12
Kateev I.Yu.	q1-04	Krivelevich S.	O3-17
Kelm E.	O3-13, O3-14	Krupenin V.A.	O1-23, P1-33, P1-34, P2-02, P2-05
Ketov S.V.	P1-21	Krupkina T.Yu.	P2-21, P2-23
Khaydukov Yu.	P1-23	Krynin A.	S1-01
Khorin I.	P1-08	Kucherov M.M.	q2-07
Kim C.-H.	O3-01	Kudrya V.P.	O3-07
Kirilenko E.P.	P1-07, P1-11	Kukhtyaeva V.R.	P1-06
Kislinskii Yu.V.	P1-23	Kulik S.P.	qL1-04, q2-09

Author Index

Kulko D.Yu.	q3-05		P2-34
Kupreenko S.	P1-30	Lysenko I.	O3-02
Kupriyanov A.N.	P2-33	Machnev A.A.	O2-11
Kupriyanov M.Yu.	O1-16, O1-18	Mackay K.	O1-07
Kurochkin V.L.	q3-10	Magonov S.M.	S1-06
Kurochkin Y.	q3-10	Maidanchuk I.Yu.	O2-09, P1-14
Kutsevol A.A.	O3-11	Maishev Yu.P.	O3-07
Kuzmin L.S.	O1-17	Makarchuk V.	O1-25
Kuznetsov A.V.	P2-09	Makarov S.	O3-01
Kuznetsov D.	O1-10	Makhviladze T.M.	P1-36, P1-37
Kuznetsov V.I.	P2-10	Malikov I.	O1-06
Kuznetsova E.I.	q2-04	Mamaev V.V.	S1-05, O1-05
Kwon K.-H.	P1-27	Mammadov A.	P1-19
Labunov V.A.	O3-09	Markeev A.	O2-06
Lang N.	L1-02	Markin A.	O1-01
Larson D.J.	P1-18	Martin I.	P1-18
Lavrukhin D.V.	O1-04	Matveyev Yu.	O2-06
Lazarenko P.	O2-02	Matyukhin S.	O3-01
Lazzarino F.	O1-11, O1-12	Meixner T.	O2-08
LeCoustumer P.	P1-18	Melnikov A.	P2-39
Lebedev A.A.	P2-20, P2-25	Melnikov I.V.	O2-11
Lebedev E.A.	P1-07	Merkulov A.	S1-07
Lebedev K.V.	P2-34	Merkulova A.I.	P1-29
Lee J.	P1-27	Miakonkikh A.V.	O1-13, O1-14, O1-15, O3-08, P1-28, P1-31, P1-33
Levitskiy A.	P2-35	Mikhailov G.M.	O1-06, O1-21
Lisovskyy I.P.	O2-09, P1-14	Mikhailova M.S.	P1-06, P1-29
Litovchenko V.G.	O2-09, P1-14	Milovanov R.	O3-13, O3-14
Liu M.	P1-22	Minkin V.	P2-28
Lomov A.	P1-31	Mironenko A.A.	P2-06, P2-07
Lopotov V.S.	O1-04	Mironov S.	O2-01
Lotkhov S.V.	O1-23	Mischenko I.	L2-05
Louzguine-Luzgin D.V.	P1-21	Mitin D.	O1-01
Lukichev V.F.	O3-08, q3-01, q3-02,		

Author Index

Mitin V.	L2-03	Pankratov A.L.	O1-17
Mityagin Yu.A.	O2-04, O3-11, P2-30, P2-32	Paterova A.	q2-09
Moiseev E.S.	qL1-03	Pavlov A.A.	P1-12
Moiseev S.A.	qL1-03	Pavlov G.	O3-05, O3-06
Molchanova A.	P1-05	Pavlova L.M.	P1-04
Molchanova L.	O3-02	Peres P.	S1-07
Molodtsova G.	O3-13, O3-14	Perestoronin A.	P2-11, P2-12, P2-32
Montes L.	L1-03	Peter A.P.	L1-01
Morozov I.V.	P1-22	Petrosyan S.	O2-07
Murzin V.	P2-31	Petrov S.I.	S1-05, O1-05
Mustafaeva S.	P1-19	Petrov V.	P1-09
Naumov V.V.	P2-07, P2-16	Petrzhik A.M.	P1-23
Naumova O.V.	L2-02	Petukhov I.N.	P1-06
Nazarkin M.Yu.	O2-11	Petukhov V.	O2-03
Neizvestniy I.G.	O2-09, P1-14	Podtserkovsky M.A.	q3-05
Nersesyan S.	O2-07	Pogalov A.	P2-17
Neuville D.	P1-18	Popov A.A.	P2-06
Nikulov A.V.	O1-20, O1-21, q3-07, q3-09	Popov V.P.	L2-02
Norman E.	S1-07, P1-18	Popov V.V.	L2-04
Odinokov V.	O3-05	Popova E.	P1-17
Ogryzko V.	q3-08	Popovici M.	L1-01
Orekhov E.V.	P2-24	Portemont C.	O1-07
Orlikovsky N.A.	O1-13, q1-04, P1-08, P1-30	Pourtois G.	L1-01
Orlikovsky A.A.	O1-15, q1-04, q1-05, L2-01, O2-05, q3-01, q3-02	Preobrazhensky R.Y.	O1-08
Otsuji T.	L2-03, L2-04	Presnov D.E.	O1-23, P1-22, P1-33, P1-34, P2-02, P2-05
Ovchenkov Y.A.	P1-22	Presnova G.	P2-05
Ovsyannikov G.A.	P1-23	Presnukhina A.A.	P1-17
Ozhegov R.	q3-10	Prikhodko O.	P1-03
Ozhigov Yu.I.	q3-06, q3-08	Prischepa S.L.	O1-16
Panin V.	O3-05	Pristupchik N.	O3-02
		Prokaznikov A.	P1-35
		Prokaznikov M.	P1-35

Author Index

Prosa T.J.	P1-18	Safonov S.O.	O3-15
Pugach N.G.	O1-16	Safronova N.A.	P1-13
Pugachev A.A.	P2-24	Sambursky L.M.	P2-24
Pushkarev S.S.	O1-04	Sankaran K.	L1-01
Pyatilova O.	O1-02, P1-25	Sapkov I.V.	P1-34, P2-03
Pyrkov A.N.	q2-05	Sarychev M.E.	P1-36, P1-37
Radchenko I.V.	qL1-04	Savinov S.A.	P2-31
Rakhmanova N.V.	P1-29	Savitskiy A.I.	P1-04
Rakitin A.	P2-04	Schulz S.E.	L1-02
Rakitin V.	P2-04	Selishchev S.V.	P1-12
Raschinsky V.	O3-05	Selyukov R.V.	P2-16
Rau E.	P1-30	Semenikhin I.	O3-12, q3-01
Redichev E.	O2-02	Serdobintsev A.	O1-01
Remnev M.	P2-29	Shadrin A.V.	P1-23
Rezchikova E.	P2-27	Shahsenov I.	P1-28
Rjevskiy A.V.	P1-34	Shaikhaidarov R.	O1-20
Rodionov D.	P2-23	Shakhnov V.	P2-27
Rogozhin A.	O1-14, O3-08, P1-05, P1-08	Shalimov A.	O1-10
Romanova I.A.	O3-09	Shaman Yu.P.	P1-07, P1-12
Röpcke J.	L1-02	Shauro V.	q2-08
Roschin V.M.	P1-06	Shcherbakova A.V.	P1-25
Rozanov R.	P1-25	Shepitko T.V.	P2-38
Rubtsova M.	P2-05	Sherchenkov A.	O2-01, O2-02
Rudakov V.I.	O1-23, O3-08, P1-01, P1-02, P1-33	Shevchuk S.L.	O3-07
Rudenko K.	O1-14, O1-15, O3-08, P1-28	Shevyakov V.I.	P1-24, P1-25, P1-32
Rudenko M.	q1-05, O2-05	Sheyerman A.E.	P1-23
Ryabtsev I.I.	q1-03	Shilyaeva Yu.I.	P1-07, P1-29
Rylkov V.	P1-10	Shklyayev A.A.	O1-03
Ryndin E.	O3-10, P2-15	Shluger A.	P1-21
Ryzhii M.	L2-03	Shnaider A.	P2-20
Ryzhii V.	L2-03	Shorokhov V.V.	P2-02
		Shpakov A.	O3-05
		Shtern M.	O2-02

Author Index

Shtern Y.	O2-01	Trifonov A.S.	P1-21, P1-22, P1-33
Shubnikov A.	O3-05	Trifonov A.Y.	P1-04
Shuliatyev A.S.	O2-11, P1-07	Trushin O.S.	O3-16, P2-07, P2-08, P2-33
Shur M.S.	L2-03, O3-01	Tskhovrebov A.	P2-11, P2-12
Siew Y.K.	L1-01	Tsukanov A.V.	q1-04
Skovoroda N.A.	q3-06	Tugushev V.	P1-10
Smirnov D.I.	P1-07	Tulin V.A.	O1-20, O1-21
Smirnov E.	O1-07	Turin V.O.	O3-01, P2-25
Smirnov K.	q3-10	Umersakova M.	P1-03
Sokolov L.	O1-09	Useinov R.G.	P2-22
Soldatov E.S.	P2-01, P2-03	Uvarov I.V.	P2-16
Soloviev I.I.	O1-16, O1-17, O1-18, P2-09	Vachtomin Y.	q3-10
Somova M.I.	P2-37	Vagin M.S.	P1-06
Spirin A.V.	P1-26	Vasiliev A.N.	P1-22
Stepanov A.S.	P2-01	Vatuev A.S.	P2-22
Straupe S.S.	qL1-04	Venig S.	O1-01
Streltsov D.R.	P1-26	Verhovtseva A.	P2-28
Struchalin G.I.	qL1-04	Verstov V.	O1-25
Suchkov E.	S1-03	Vertyanov D.	P1-09
Sudin V.	S1-02	Vinnichenko V.	O1-06
Svintsov D.	L2-01, O2-05, P2-18	Volchkov N.A.	P2-32
Swerts J.	L1-01	Volodin V.A.	O1-22, O2-09, P1-13, P1-14
Tagachenkov A.	P1-30	Vorobiev M.I.	P1-24
Tatarintsev A.A.	O1-13, P1-30	Vyurkov V.	q1-05, L2-10, O2-05, q2-02, P2-18, P2-19
Telenkov M.P.	O3-11, P2-30	Wen L.G.	L1-01
Tikhonova O.V.	P2-09	Yakshina E.A.	q1-03
Timina N.M.	P2-07	Yesayan A.	O2-07
Timoshenkov S.	O1-02, O2-02, O2-03, P1-09, O1-10, P2-17	Ying S.-C.	O3-16
Tókei Z.	L1-01	Yurischev M.A.	q2-01
Tombet S.B.	L2-04	Zanuccoli M.	O3-12
Torgovnokov R.A.	P2-24	Zaytsev S.	O3-04
Tretyakov D.B.	q1-03		

Author Index

Zebrev G.I.	O1-24, O3-01, P2-20, P2-22, P2-25
Zenchuk A.I.	q2-03
Zenkevich A.	O2-06
Zharik G.	P2-01
Zheleznyakova A.V.	P1-15, P1-17, P1-25
Zherikhina L.	P2-11, P2-12
Zhigalov V.	O1-02, O2-03
Zhikharev E.N.	P1-26
Zhou S.	P1-10
Zhuchkov G.N.	P2-30
Zhukov V.A.	P2-13, P2-14
Zhuravlev M.N.	O3-03
Zimmermann S.	L1-02
Zinchenko L.A.	O1-25, P2-27
Zlobin S.A.	P1-14
Zobov V.E.	q2-06
Zorin A.B.	O1-23
Zotovich A.	O1-11, O1-12
Zubov D.	O3-13, O3-14